Refinement of the Inverted T-Beam Bridge System for Virginia

Ezra B. Arif Edwin

Thesis submitted to the faculty of the Virginia Polytechnic Institute and State University in partial fulfillment of the requirements for the degree of

Master of Science
In
Civil Engineering

Carin L. Roberts-Wollmann ,Chair
Matthew H. Hebdon
Ioannis Koutromanos

June 9th 2017
Blacksburg, VA

Keywords: Inverted T-Beam, Poutre Dalle, Accelerated Bridge Construction, Reflective Cracking, Subassemblage,

Refinement of the Inverted T-Beam Bridge System for Virginia

Ezra B. Arif Edwin

ABSTRACT

The inverted T-beam bridge system is a bridge construction technique that follows accelerated bridge construction processes. The system was discovered in France and first adopted in the U.S. by the Minnesota Department of Transportation. In 2012 the system was modified and adopted by Virginia, with research being carried out at Virginia Polytechnic Institute and State University (Virginia Tech). The research focused on multiple items involving the system, but the most relevant one is that regarding the transverse bending behavior of the system for different geometries, and joint types between adjacent precast beam members. The study found that using a joint system without any mechanical connection between adjacent beams was most efficient, and gave adequate performance under monotonic loading. The study recommended cyclic load testing be carried out on this joint type, as well as a welded joint similar to those found in decked bulb-T systems

The research contained herein presents the setup and results of this testing. From the work it was found that the no-connection joint behaves adequately under cyclic loading at service loads, however surface roughening between precast and cast-in-place concrete must be adequate. The welded connection behaves well, granted the surfaces to be welded are properly prepared. From these results it is recommended to evaluate different surface roughening techniques, and repeat the cyclic testing using the best. The surface roughening technique chosen should be used to provide guidance on this aspect of construction with inverted T-beams.

Refinement of the Inverted T-Beam Bridge System for Virginia

Ezra B. Arif Edwin

GENERAL AUDIENCE ABSTRACT

The inverted T-beam bridge system is a new type of bridge system intended for use in short to medium length bridges. The system was discovered in France in 2004, where a similar type was being used. It was first modified slightly, and adopted in the in Minnesota. In 2012, the system was again modified to increase its strength and its construction speed, and was then adopted in Virginia. The modifications to the system in Virginia focused on the connections between the individual units making up the bridge, and the geometry of each of these units.

The focus of this research was to quantify the long-term performance of two of the connection types currently used on bridges in Virginia. This was achieved by subjecting a test specimen to repeated loads in the laboratory at Virginia Tech. The loading used in the laboratory represented the conditions that a real bridge of this type would be subjected to.

The research showed that the two connection types performed well under the repeated loading conditions. However, it was concluded that the concrete surfaces which are in contact with one another must be properly roughened, so that the system maintains its strength.

The importance of this research is due to the fact that the large costs associated with maintaining the nation's bridge infrastructure can be substantially reduced due to this system's quick and simple construction. In addition to this, road users experience less disruption because of the shortened construction times.

ACKNOWLEDGEMENTS

I would firstly like to thank Dr. Carin Roberts-Wollmann for the opportunity to work on this project. Her experience and guidance have been instrumental to my progress with this thesis, and with the completion of this project. In addition to this, my progress as a graduate student would not have been possible without my interactions with her. I would also like to extend my thanks to Dr. Matthew Hebdon, and Dr. Ioannis Koutromanos for agreeing to serve on my committee, and for their assistance and contributions to this work.

I would like to thank David Mokarem, Brett Farmer, and Dennis Huffmann, for all of their help, and guidance in the structures lab – none of the experimental work for this project would have been possible without their contributions to testing setup, concrete orders and placements, and so much more.

I would like to extend my thanks to James J. Reilly, a former Master's student at Virginia Tech who assisted with the design and construction of the formwork, and the construction of the no-connection specimen, during his final semester at Virginia Tech. In addition, I would like to extend my gratitude to Carrie S. Field, for putting in the initial leg-work on the preliminary design tables, and for a smooth handover of the project. I am also grateful to Vijaykanth Pulumati and all of the other graduate students who helped with the numerous concrete placements and concrete cylinder making that went on over the course of this work.

Last, but not least, I would like to thank my friends (near and far) and family for all of your support and encouragement. Being on the other side of the world has been challenging, but thanks to all of you it has been a rewarding experience, and more importantly, a ton of fun!

CONTENTS

LIST OF FIGURES

LIST OF TABLES

INTRODUCTION

Background and Motivation

Due to continually increasing demands on the transportation network, there is a need for new construction, replacement, and rehabilitation of bridge infrastructure. Shutting down road networks for extended periods of time is costly, and diminishing resources give rise to Accelerated Bridge Construction (ABC) practices. The basis of ABC relies on the ability to prefabricate as many bridge elements as possible, minimize on-site formwork, and therefore speed up the construction process. Current examples of ABC systems used in the United States include adjacent box-beam and voided-slab systems.

In April 2004, the Federal Highway Administration (FHWA) and the American Association of State Highway and Transportation Officials (AASHTO) sent representatives to Europe and Japan to observe bridge construction practices that could be adapted to ABC in the United States. The Poutre-Dalle (meaning beam-slab) system was found in France. The system consisted of precast, prestressed inverted T-beam units placed side-by-side, connected by a longitudinal joint, with a cast-in-place topping subsequently applied over the entire system (Ralls et al. 2005). Minnesota was the first to adopt a system based on this concept, and between 2005 and 2011 a number of studies were carried out at the University of Minnesota related to the inverted T-beams. Also during this period, twelve bridges were constructed in Minnesota using their own modifications to the Poutre-Dalle system (Menkulasi 2014). In 2015 the construction of two bridges in Virginia was completed using a modification to Minnesota's inverted T-beam system. One of these was a high-volume highway bridge located near Richmond, VA along U.S. Route 360, and the other a low-volume bridge on Towlston Road over Rocky Run in Fairfax, VA. The two bridges differed in their longitudinal connection detail between beams (Roberts-Wollmann et al. 2016). Refer to Figure 1 below for a visual depiction of three systems described.

(a)

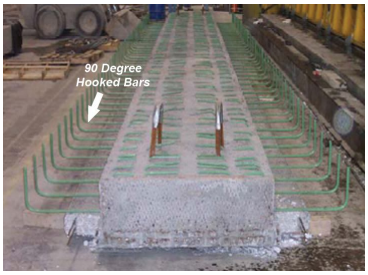

(b)

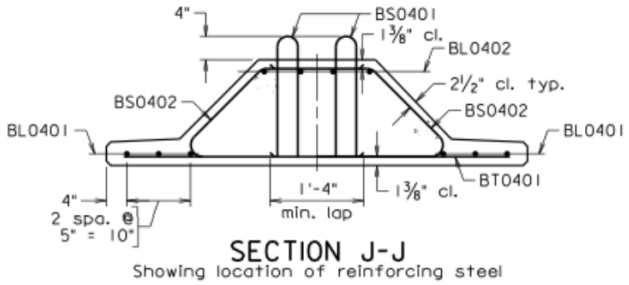

(c)

Figure 1 Development of inverted T-beam System. (a) Original Poutre-Dalle system obtained from (Ralls et al. 2005). (b) MnDOT system obtained from (Mercer 2012). (c) Virginia Inverted T-Beam system obtained from (Roberts-Wollmann et al.).

The inverted T-beam system offers advantages over traditional ABC systems such as adjacent box-beams and voided slabs, by way of improved longitudinal joint details. In traditional systems, these joints are formed by a shear key filled with a non-shrink grout. The grout must resist shear and tensile stresses generated by the transverse distribution of loads when vehicles cross the bridge, which eventually leads to cracking in the joint. On high volume roads in Virginia – defined by the Virginia Department of Transportation (VDOT) as roads which have more than 200 Average Daily Truck Traffic (ADTT) and more than 4000 Average Daily Traffic (ADT) - these systems are required to have a constant 7.5-inch-thick cast-in-place topping, and cracks open up in the topping directly above the cracked joint. This type of cracking is termed reflective cracking, and results in the ingress of water and chlorides into the joint which leads to deterioration of reinforcement in the superstructure. Inverted T-beams provide a solution to this issue by using a thicker cast-in-place topping over the joints, and by providing reinforcement in the joint region capable of resisting transverse bending stresses. This prevents the propagation of cracks to the surface of the deck, thereby reducing deterioration of the superstructure due to reflective cracking. Additionally, the profile of Virginia's inverted T-beam system allows for transverse bending stresses to be transferred through a combination of tensile bond, and shear stresses developed at the interface of the precast and cast-in-place components, as well as via a non-contact lap splice between reinforcement in the precast and cast-in-place components. This provides improved strength when compared to joints which, as a result of their shape, can only transfer these stresses via tensile bond between components. This profile also provides a more gradual change in shape at re-entrant corners, reducing stress concentrations at these locations.

Previous research involving Virginia's inverted T-beam system has been carried out by researchers at Virginia Polytechnic Institute and State University. Mercer (2012) and Menkulasi

(2014) carried out monotonic testing on subassemblage specimens, and finite element modeling to investigate the longitudinal joint between adjacent beams to address the constructability issues faced with the Minnesota Department of Transportation (MnDOT) detail. Three different connection details were investigated as shown in Figure 2 below. Menkulasi (2014) additionally carried out investigations involving time dependent and temperature effects on inverted T-beams, deck cracking in composite bridge systems, end-zone stresses in inverted T-beams with tapered webs, composite action in precast inverted T-beams with a cast-in-place topping, and live load distribution factors used in the design of inverted T-beam bridges. The results of these investigations led to recommendations to investigate the behavior of the longitudinal connections under cyclic loading, carry out further analytical and experimental work regarding time-dependent and temperature effects, include the Hoyer effect and the effect of prestressing strand slippage in the investigation of end-zone stresses, and extend the bridge system to accommodate spans longer than 65 feet (the current system is intended for use in bridges with spans ranging between 20-65 feet).

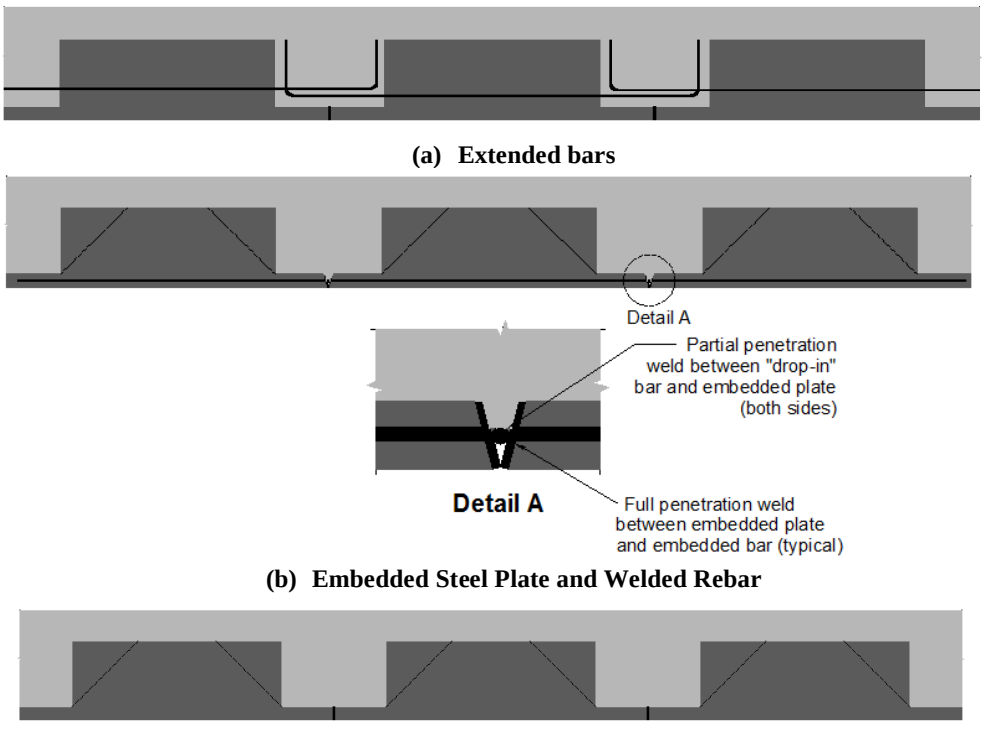

Figure 2 Previous Testing of Three Transverse Connection Details. Obtained from (Menkulasi et al. 2015).

Scope and Objectives

The scope of this research is limited to the refinement of Virginia's inverted T-beam system. This includes the development of preliminary design tables for the inverted T-beam system, the extension of the system to longer spans, and the experimental investigation of the longitudinal connections between adjacent beams under cyclic loading.

The primary objectives of this research are to:

- Develop a standard set of design tables for the inverted T-beam system, similar to those currently produced by VDOT for the adjacent box-beam and voided slab systems, that can be subsequently used by bridge designers in preliminary design.
- Validate the use of the system with no mechanical connection (shown in Figure 2 above) on high-volume bridges through cyclic load testing.

Organization

The next section of this thesis covers a review of literature regarding accelerated and prefabricated bridge construction, precast bridges with transverse joints, and the development of the inverted T-beam bridge concept from its identification in France, to the adoption of the concept by Minnesota, and finally the modification and adoptions by Virginia. Succeeding the literature review is a chapter describing the development of the preliminary design tables to their current stage. After the preliminary design tables, is a chapter describing the test specimens to be used during the experimental work, and the construction of these specimens. A chapter on analytical methods and modelling carried out as a precursor to the experimental work follows the construction of the specimens. Note that the results from the analytical work are presented in this chapter, rather than with the remainder of the results. The experimental methodology is then presented. This is followed by a chapter presenting the results obtained from the experimental work. The results are expanded on and the implications of these results described in the discussions. These lead to the conclusions drawn from the research, and finally the implications and recommendations made for future work with these inverted T-beams. A list of all references cited in the text, and appendices are then added as the back-end matter of this thesis.

LITERATURE REVIEW

This chapter presents the results of a review of literature regarding prefabricated bridge construction systems. Specifically, the literature search focuses on those topics most relevant to the current testing regime of the inverted T-beam system. Based on the development of this system up until this time, this involves the topics of accelerated bridge construction and prefabricated bridge construction, bridges with longitudinal joint systems, and the Minnesota inverted T-beam system. It also includes the results of previous testing carried out on the inverted T-beam system developed for use in Virginia.

Accelerated Bridge Construction & Prefabricated Bridge Construction

Due to increasing demands on the traffic network, and the large costs associated with traffic management during construction procedures, a need for quicker bridge construction methodologies has developed. According to FHWA (2017), approximately one-quarter of the bridges in the United States requires rehabilitation, repair, or replacement. Traffic management involving detours, lane closures (whether partial or full), and traffic control creates additional work on projects that is not directly related to the replacement of the bridge system, but amounts to a large proportion of the cost. Costs are not limited to the amount of project spending; business time lost by commuters, as well as the safety risks posed to construction workers are additional costs which increase as project time increases (Hällmark et al. 2012).

Accelerated Bridge Construction (ABC) is a bridge construction technique that utilizes a basic concept of prefabricating as many elements (or even systems) of a bridge as possible, and/or, using innovative methods to lift and place structural members (FHWA 2017). The result of this is a reduction in the on-site time required to construct a bridge and therefore reduces the negative impacts that bridge maintenance and construction has on a traffic network.

Prefabricated bridge construction involves building as many bridge elements off-alignment as possible and then moving these pieces into their final alignment position (FHWA). Prefabricated bridge construction in the United States is split into three technical levels. The first involves prefabrication techniques that have become standard practice, the second are techniques that have been found to be practical to use but are not standardized, and the third level involves techniques that have not been used in-field before (Hällmark et al. 2012). Hällmark et al. (2012)

acknowledges that in the United States, the most common type of concrete prefabrication involves prestressed girders.

Other advantages associated with prefabricated bridge construction includes better working environments and quality control measures that can be undertaken since the work is carried out in precast plants rather than on-site; by the time precast girders are ready to be transported and lifted into place, they would have usually reached their 28-day specified compressive strength and so there is less – if any – formwork required to place the girders on-site; and better worker safety as there is both less required formwork construction and casting processes that need to be undertaken, and there is less time spent on-site which decreases the potential for mishaps to occur (Mercer 2012).

As noted by Ralls et al. (2005) when it comes to Prefabricated Bridge Elements and Systems (PBES) there are many options. As mentioned previously the most common in the United States for concrete construction projects are precast prestressed girders. Concrete can also be used to prefabricate deck panels, pier caps, and in some cases, columns, abutments, footings and retaining walls. PBES is not limited to concrete. Other systems that fall into the category of PBES are steel girder bridges where the steel girders are prefabricated welded girders, steel deck forms that support the deck reinforcement and concrete are also by definition PBES systems, steel deck systems, and fiber reinforced polymer deck systems. In the deck systems, the deck is fabricated in units in a fabrication (precasting or steel fabrication) plant and then transported to site ready to be placed. The focus of this literature search involves PBES systems related to precast prestressed concrete girders as this is the category of systems into which the inverted T-beam system falls.

Precast Bridges with Transverse Joints

Bridges constructed using methods involving precast prestressed girders are usually constructed by placing the precast girders adjacent to each other on top of their supports (abutments or piers), and then using a joint system between the girders to tie the girders together and get the individual girders to act as a single bridge unit. In other words, the connections must allow the bridge to do what is described by the FHWA as emulating cast-in-place detailing (Culmo 2011). The transverse joint system used to connect prefabricated bridge elements varies in type between states in the United States. Many places prefer to use a grouted shear key and

transverse post-tensioning systems to tie the girders together and prevent cracks opening up in the shear keys between girders. However, in some cases, non-post-tensioned systems have been used such as dowel bar connections filled with grout or in more recent cases Ultra-High Performance Concrete (UHPC) (Hällmark et al. 2012). Some examples of the use of adjacent beam bridges with different types of transverse joint systems are adjacent box beam bridges, voided slab bridges, and decked bulb tee bridges.

Figure 3 shows the transverse joint system used in a typical voided slab system. As can be seen, the joint consists of a shear key running the length of the bridge, which is filled with a high-strength, non-shrink grout. The grout serves the dual purpose of sealing the joint to prevent water or other runoff from entering the joint region, and creating bond between the two precast units. In addition to this, this joint is also responsible for distributing loads between the members and transferring vertical shear forces. The depth of the shear key in the voided slab systems can either be partial depth (as shown here), or full depth (Joyce 2014).

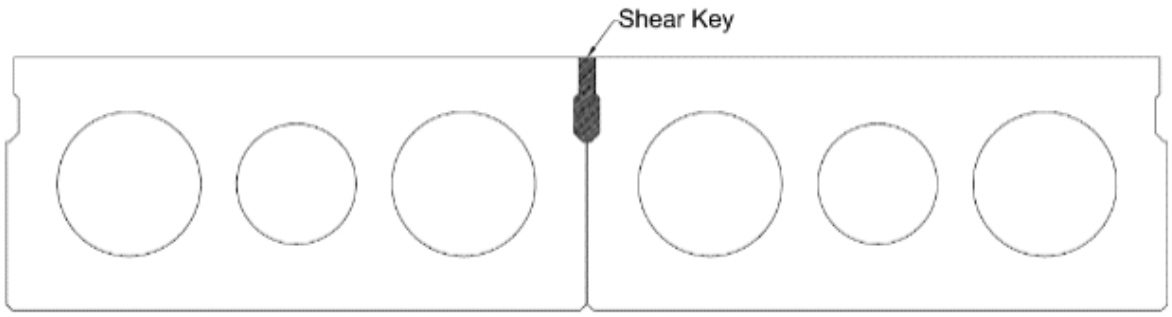

Figure 3 Adjacent voided slab with partial depth grouted shear key. Obtained from (Joyce 2014)

An example of a transverse joint connection in adjacent box-beam systems as described by Russell (2011) can be seen in the figure obtained from Grace et al. (2011) (refer to Figure 4). Typically, the system consists of a grouted shear key similar to that found in the voided slab joint system, used in conjunction with transverse post-tensioning. Again, the grout used is typically a high-strength, non-shrink grout and is responsible for sealing the joint, bonding the adjacent units, and distributing loads laterally between the members of the bridge through vertical shear transfer. Note that the jointing system shown in Figure 4 is somewhat unique, but demonstrates the use of a full depth keyway with transverse post-tensioning.

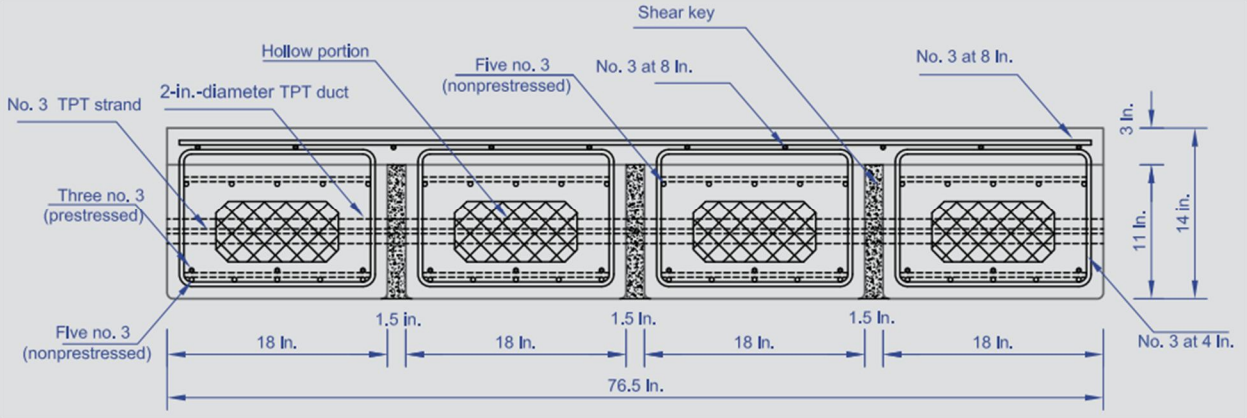

Figure 4 Shear key and transverse post-tensioning in adjacent box-beams. Obtained from (Grace et al. 2011)

The Decked Bulb Tee (DBT) bridge unit is a commonly used type of bridging system in the Pacific Northwestern states of the United States. The system consists of tee beam units that have a widened top flange. The wider flange serves as the riding surface and no cast-in-place topping is placed over these. Joints are formed between the top flanges of each adjacent tee beam unit to emulate monolithic action of the bridge. The concept of the DBT system can be seen in Figure 5. The joint system used in decked bulb-tee bridges can be seen in Figure 6. As the figure shows, the joint consists of a connector plate embedded into either side of the top flange of the DBT unit. Once the units are placed adjacently in the field, a piece of smooth connector rod is dropped into the gap formed between the connector plates, and the remaining space is filled with weld material (FHWA 2015). This forms a mechanical tie between the adjacent units which is again capable of transferring vertical shear forces to distribute loads laterally between the adjacent members making up the bridge.

Figure 5 DBT bridge system. Obtained from (Li et al. 2010)

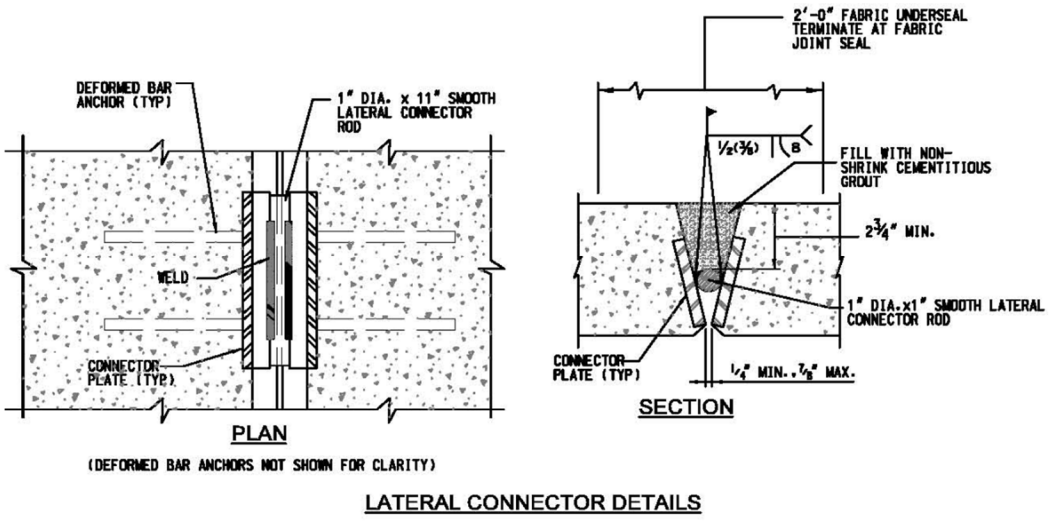

Figure 6 Connection detail for DBT bridge units. Obtained from (FHWA 2015)

The most common, and most problematic, issue that arises with these types of bridge systems which using transverse joints is the long-term performance of the joint. The joint is subjected to normal and transverse stresses during the operation of the bridge and eventually cracks open up in the joint. Over time, this can lead to reflective cracking opening up in the deck surface over the joint. A study on different types of grout mixes by Issa et al. (2003) noted that over time, the cracking allows foreign materials – which is described by Russell (2011) as "chloride-laden water" – to make its way into the sides and bottom of the beam. This can lead to corrosion of the transverse post-tensioning, which reduces the pre-compression of the joint region further opening up cracks, and resulting in a loss of monolithic action and the lateral load sharing ability of the bridge (Joyce 2014). Overall this results in a loss of bridge performance, reduced life time and ultimately large maintenance and/or replacement costs. Li et al. (2010) also notes that the welded tie connection in DBT systems are subject to cracking due to applied loads as well. The welded tie connections, being spaced relatively far apart cannot control crack widths, and water ingress into these joints corrodes the welded connection leading to the same issues mentioned previously.

Poutre Dalle

In 2004 the American Association of State Highway and Transportation Officials (AASHTO) sent a team of representatives on a scanning tour of PBES in Japan and Europe. The

purpose of this tour was to identify overseas practices that could be brought back and used in the United States to maintain and repair the nations aging bridge infrastructure.

In France, a system called the Poutre Dalle (which means beam slab) was found. The system consists of shallow, inverted tee-beams made from precast prestressed concrete, placed in an adjacent member configuration. A single unit can be seen in Figure 7. Once placed, the beams and longitudinal joints are covered with Cast-In-Place (C.I.P.) concrete which forms the riding surface. The joint region (as shown in Figure 7) has hooked reinforcement passing through which overlaps with the reinforcement from the adjacent beam. The hooked reinforcement provides continuity in the joint region. The advantage of this system lies in its ease of construction, once the precast units have been formed, no additional on-site formwork is required, the precast units are simply placed and the C.I.P. topping poured over it (Mary Lou Ralls et al. 2005). The system also does not require a grouted shear connection, or transverse post-tensioning. Another advantage that the system provides lies in its increased resistance to reflective cracking due to a thicker concrete section over the joint, and reinforcement passing through the joint which can help arrest cracks before they propagate to the surface of the deck (Menkulasi 2014).

Figure 7 Poutre Dalle beam unit. Obtained from (Mary Lou Ralls et al. 2005)

Minnesota Inverted T-Beam

The first place in the United States to adopt the concept of the Poutre Dalle was Minnesota in 2005 (French et al. 2011). It was adopted here for the efficient replacement of short to medium span bridges (Piccinin and Schultz 2012). According to Piccinin and Schultz (2012) the preliminary design of the Minnesota inverted T was created by using the cross-section of a

typical I-beam, but widening the bottom flange to 6 ft and incorporating the top flanges into the C.I.P. topping. Additionally, the section was made shallower. As can be seen in Figure 8, the most obvious difference between the Poutre Dalle, and the Minnesota inverted-T is the use of a 90 degree hook on the reinforcement passing through the joint, as opposed to the 180 degree hooks used in the Poutre Dalle. The primary reason for this difference was to allow the use of a drop-in reinforcing cage in the joint region on-site to provide additional crack control and crack resistance through the joint region (Menkulasi 2014).

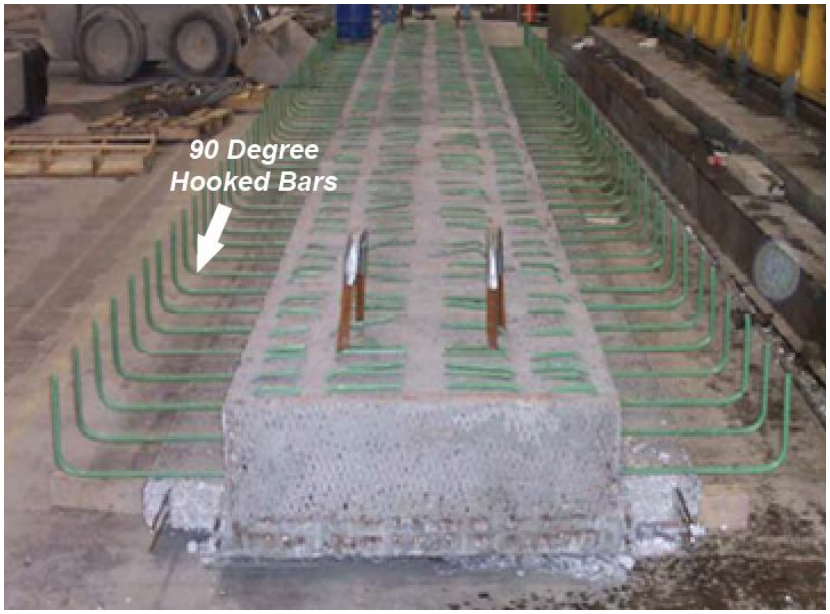

Figure 8 Minnesota inverted T-beam. Obtained from (Mercer 2012)

Research was carried out by the University of Minnesota that involved an attempt to optimize the transverse reinforcement passing through the joint region. The methodology and results for this testing is described in French et al. (2011). It was found that using larger bars, at smaller spacing and less additional drop-in cage reinforcement represented the most efficient combination of reinforcement for these systems. During this scheme of testing, seven subassemblage specimens were constructed in the laboratory, with each specimen having a single deviation from the original system (e.g. reinforcement size, spacing, specimen depth etc.) to investigate the effect this would have on the performance of the system. The laboratory testing program for these subassemblages involved incrementally loading the specimen whilst loading and unloading at a quasi-static rate three times and then cycling the specimen 1000 times at each load increment prior to progressing to the next increment. A loading frequency of 0.7 Hz was

used for these cycles in a displacement-controlled test. Once a crack was identified, the load was recorded as the cracking load, and the specimen was subjected to 5000 cycles of load, and then another 2000 cycles at what was termed the "base load" taken as 55 percent of the cracking load. Metrics of interest from the testing were visual observations of cracking, strains due to shrinkage measured by embedded strain gauges, width of opening of the joint measured using LVDT's, and core samples taken to investigate the vertical and horizontal reflective cracking that may have occurred within the specimen. The results of testing were organized into a design guide, and were summarized by Mercer (2012) who noted two items: first, reflective cracking can be controlled using a drop-in reinforcing cage, and second, reinforcement spacing is defined as the maximum spacing between any pieces of reinforcement crossing the joint – whether from the extended transverse bars or the drop-in cage does not matter.

Virginia Inverted T-Beam

The development of the inverted T-beam system in Virginia is described briefly in Roberts-Wollmann et al. (2016). During 2014-2015, two bridges were constructed in Virginia using modifications to the Minnesota inverted T-beam concept. The modifications made to the system in Virginia aim to make fabrication and construction simpler, and to reduce stress concentrations. The Virginia detail (shown in Figure 9) utilizes tapered webs rather than vertical webs to reduce stresses at the reentrant corners. The tapered web also allowed for a combination of tensile bond and shear stresses to develop at the interface between the precast beam and C.I.P. concrete. The ability to develop shear stresses improves stress transfer at the interface location (Menkulasi 2014). The detailing in Virginia eases fabrication through modification of the joint. Two options were selected: the first being a welded continuous tension connection between adjacent beam flanges (similar to those used on DBT bridges), and the second having no mechanical connection between adjacent members. This second connection was coined the "no-connection connection" system. Both options eliminated the need for the horizontal reinforcement penetrating the sides of the beams that was present in the Poutre Dalle and Minnesota design (Roberts-Wollmann et al. 2016). One structure was completed on a high volume bridge – U.S. Rte. 360 over the Chickahominy River – and another was constructed on a low volume road – Towlston Road over Rocky Run in Fairfax, Virginia. The high volume bridge

was constructed using the welded tie connection detail, while the low volume bridge was constructed using “no-connection connection” system.

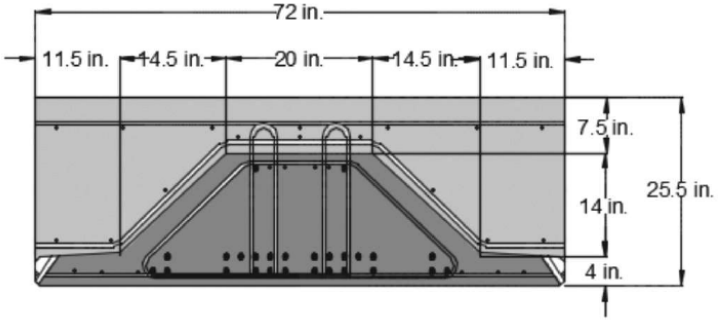

Figure 9 Virginia inverted T-beam Concept. Obtained from (Roberts-Wollmann et al. 2016)

Testing on these modified inverted T-beam systems was carried out by researchers at Virginia Polytechnic Institute and State University (Virginia Tech), from 2012-2014 (Menkulasi 2014) (Mercer 2012). The objective of the research carried out was to compare the different geometries and joint types (Mercer 2012), make recommendations to reduce differential shrinkage effects, identify a C.I.P. mix that would result in low amounts of restrained shrinkage cracking, investigate stresses in the pre-tensioned anchorage zones for these uniquely shaped sections, investigate the capability of the section to develop composite action, and determine suitable live load distribution factors to be used when designing a bridge using this system (Menkulasi 2014). Ultimately the testing carried out at Virginia Tech was used to influence the design of the two bridges constructed in Virginia in 2015.

During the testing, the researchers tested five subassemblage specimens using different combinations of tapered or straight web geometry, and a selection of either the extruded reinforcing bar, welded tie connection, or no-connection connection joint detail. They subjected each subassemblage to monotonic loading, increasing the loads incrementally to failure. The increment was 10 kips until the first crack; this was reduced to 5 kips after first cracking. When a crack appeared (or appeared to propagate), the specimen was cycled at that increment until the crack stabilized (stopped propagating), at which point the load was taken to the next increment.

The results of the testing showed all systems to perform well under these conditions. Overall the tapered web systems were found to perform better due to the increased interface resistance thanks to the ability of a shear bond to be developed. The no-connection connection system with tapered webs was found to be the most efficient to construct due to the lack of

mechanical tie between adjacent beams and the ease of creating forms for these beams. This overall performance in terms of load-carrying capacity of other systems was higher than this system, however it was still seen to perform more than adequately. It was recommended that cyclic load testing be carried out to verify the performance of the no-connection connection system with tapered webs under long-term repeated load effects.

DEVELOPMENT OF PRELIMINARY DESIGN TABLE(S)

This chapter presents the development of the preliminary design tables. The first portion of the chapter will focus on the tables as they currently stand, their implementation, the aspects of design considered during the development of these tables, and the limiting factors for the span lengths. The second part of this chapter discusses the iterations undertaken in order to arrive at the current state of the design tables.

Current Preliminary Design Table(s)

Implementation

The preliminary design tables in their current configuration can be seen in Table 1 below. The tables are intended to be used as an initial design aid for bridge engineers. Knowing the required span lengths of a bridge, designers are able to look at the table for the inverted T-beams and pick out a strand arrangement for their beam. In this sense, the preliminary design tables can also be used during conceptual design phases for cost comparisons with other adjacent bridge beam systems such as adjacent box-beams and voided slabs.

Note the following diagram (Figure 10) and footnotes (Table 2), that apply to the final preliminary design tables:

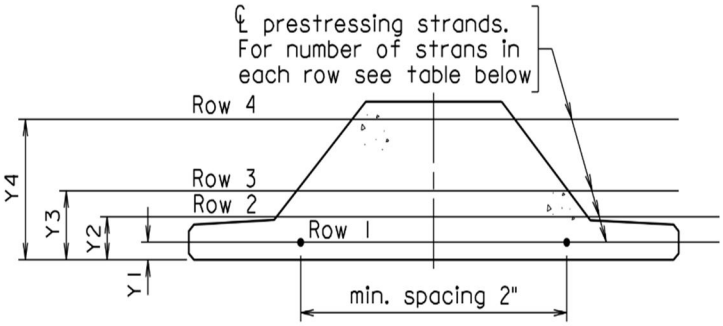

Figure 10 Prestressing strand arrangement for preliminary design tables

Table 1 Final preliminary design tables

Span Length (ft)	**Normal Weight Concrete**				
	Prestressing arrangement				
	Row 1	**Row 2**	**Row 3**	**Row 4**	**Debonded**
30	10	0	0	2	0
35	11	0	0	2	0
40	20	0	0	4	2
45	23	5	0	4	6
50	23	16	0	5	10
55[a]	23	21	0	3	14
60[a]	23	21	6	2	16
65[b]	23	21	12	2	21
70[b,c]	23	21	19	3	24
Span Length (ft)	**Light Weight Deck**				
	Prestressing arrangement				
	Row 1	**Row 2**	**Row 3**	**Row 4**	**Debonded**
30	10	0	0	2	0
35	11	0	0	2	0
40	15	0	0	2	4
45	23	4	0	4	6
50	23	14	0	4	8
55[a]	23	21	0	3	17
60[a]	23	21	6	2	16
65[b]	23	21	7	2	17
70[b,c]	23	21	19	3	24
Span Length (ft)	**Light Weight Deck & Beam**				
	Prestressing arrangement				
	Row 1	**Row 2**	**Row 3**	**Row 4**	**Debonded**
30	10	0	0	2	0
35	10	0	0	2	0
40	16	0	0	3	2
45	23	2	0	4	4
50	23	12	0	4	8
55[a]	23	9	0	2	12
60[a]	23	19	0	2	16
65[b]	23	21	13	1	22
70[b,c]	23	21	19	6	24

Table 2 Footnotes for Preliminary Design Tables

Footnotes for Preliminary Design Tables
a. This span can be reached by staging construction - pouring a third of the deck located near midspan prior to completing the deck pour
b. This span can be reached using temporary shoring at mid span - shore for approximately 10 days for topping to reach about 75% of 28-day f`c for composite action to be achieved
c. To reach this span, all of the strands in Row 4 need to be cut prior to pouring the cast-in-place topping concrete

Design Aspects Covered by the Preliminary Design Table(s)

In their current iteration, the strand arrangements for each span length presented in the preliminary design tables have been selected based on design considerations including flexural strength, deflections and camber, and allowable stresses at the ends and midspan of the member. It is important to note that partial debonding of strands at the ends of the member has been included in order to meet allowable stress limits at these locations. Numbers of partially debonded strands adhered to the limits set out in the AASHTO LRFD Bridge Design Specifications Section 5.11.4.3 (AASHTO 2014).

Flexural strength of the member was calculated as per the AASHTO LRFD Bridge Design Specifications (AASHTO 2014) Section 5.7 for prestressed concrete members assuming rectangular section behavior. Required flexural strength was calculated at midspan which was assumed to be the location of critical flexural demand for the preliminary design of a simply supported beam. Applied loads consisted of combinations of permanent loads and live loads in accordance with the Strength I Limit State in AASHTO Table 3.4.1-1 (AASHTO 2014). Permanent loads included self-weights of the beams and topping concrete, prestressing forces (including allowances for loss of prestress), and allowances for the weights of barriers, medians and future wearing surfaces. Live loads were applied as per AASHTO Section 3.6 (AASHTO 2014) and consisted of the design lane load and the design truck or tandem. Live load distribution factors were determined as per AASHTO Section 4.6.2.2 (AASHTO 2014) for a bridge of cross-section type f (precast beam with shear keys with a cast-in-place concrete overlay). This cross-section type was determined to be appropriate based on a previous study carried out by Menkulasi (2014). The distribution factors were used to determine the fraction of the total bridge live load force that would be carried by a single beam in the system. The worst-

case beam was the one having the highest distribution factor, and was used conservatively for all design calculations.

Deflections and camber were calculated using the well-known equation for the elastic displacement at midspan for a simply supported member which has been repeated below.

$$\delta_{mid} = {5wL^4}/{384EI}$$

The calculation of deflections included the effects of self-weight of the precast and cast-in-place components, as well as the effects of service level live loads acting on a single girder, calculated using the distribution factor method. The cambers were calculated as the upwards deflections of the girder due to the effects of prestressing. Deflections due to prestressing were calculated using the equation below. Note that in the following equation, P_i is the prestressing force at the time of transfer, E_{ci} and $I_{g.precast}$ are the gross, uncracked section properties of the precast beam at the time of transfer, and e_{pg} is the eccentricity of the prestressing from the centroid of the precast beam.

$$\delta_{prestress} = \frac{-P_i}{E_{ci}I_{g.precast}}\left[\frac{e_{pg}L^2}{8}\right]$$

The difference between the upwards deflections and downwards deflections was taken to be the final deflection, and was compared to a limit of L/800, provided by AASHTO Section 2.5.2.6 (AASHTO 2014). It is important to note that long term deflections due to creep and shrinkage were not included in these calculations.

Allowable stresses were checked in accordance with the limits set out in AASHTO Section 5.9.4 (AASHTO 2014). The stress at the extreme tensile and compressive fibers of the section were calculated assuming linearly elastic behavior. Stresses were checked against these limits at three stages during the lifetime of the structure, first at transfer of the prestressing force into the concrete, then at the time of deck placement, and finally during service life once all long term prestress losses had occurred. In the first stage, prestress forces, and the self-weight of the beam section were considered to act on the beam section alone since the cast-in-place topping had not been constructed at this time. During the second stage, prestress forces, the self-weight of the beams, and the weight of the wet cast-in-place topping concrete was assumed to act on the beam section alone as composite action could not yet be assumed to have been achieved. In the final stage, it was assumed that the stresses resulting from the first two stages of the structure's life were locked-in. Additional stresses due to the self-weight of overlays, barriers, medians, and

stresses resulting from live loads were assumed to act on the composite section, and the final stress state was calculated as the sum of the locked-in stresses and these additional stresses acting on the composite section.

Limiting Factors in the Development of the Preliminary Design Table(s)

The main factor limiting the span lengths was determined to be the midspan allowable stress checks for the final in-service condition, specifically the compressive stress. The largest components of compressive stresses result from the effects of prestressing and self-weights of the beam plus cast-in-place topping, acting on the bare beam section alone during the first two stages of the structure's life. Reducing the magnitudes of these stresses by aiming to get a portion of the self-weight components to act on the composite section, increases the possible span length of the inverted T-beam. A couple of ways in which this can be achieved are through the use of temporary shoring at midspan, or a staged deck pour construction sequence where the center portion of the cast-in-place topping is placed first. Once some of the topping concrete has been allowed to gain sufficient strength to ensure composite action at midspan, the remainder of the self-weight can be placed on the section. As can be seen from the tables, this allows the maximum span length to be increased from 53 ft to 73 ft.

Development of Current Iteration of Preliminary Design Table(s)

The preliminary design tables went through a number of iterations before arriving at their final stage. These iterations are further discussed in this section.

Iteration 1 – Based on work plan & previous research recommendations

Upon conclusion of his doctoral work, Menkulasi recommended that the system be extended to spans longer than 40 ft. Menkulasi et al. (2015) decided that a suitable way of doing this would be to provide additional cross-sectional geometries. Two additional geometries were suggested, one for shorter spans from 20 ft – 40 ft, and a larger one for spans above 40 ft. Figure 11 to Figure 13 show the three geometries. Using this information, the first iteration of the preliminary design tables was developed and can be seen in Table 3. This iteration included the following design considerations: flexural strength, deflection and camber, and allowable stress checks at three critical stages of the beam's life (at transfer of prestressing force into the

concrete, at deck placement, and at final service after all prestress losses have occurred). The iteration did not include the effects of strand debonding, or shear strength.

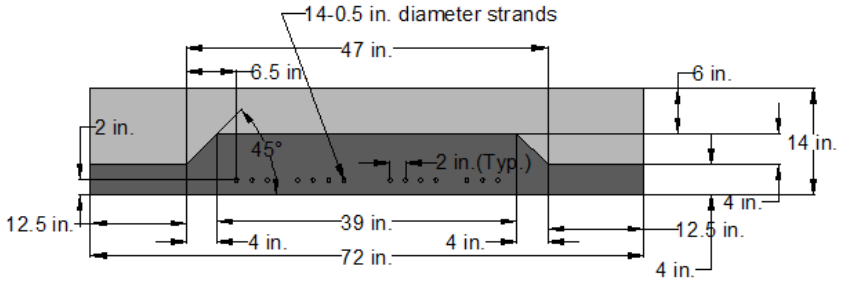

Figure 11 Inverted T-beam system. Small section geometry as obtained from Menkulasi et al. (2015)

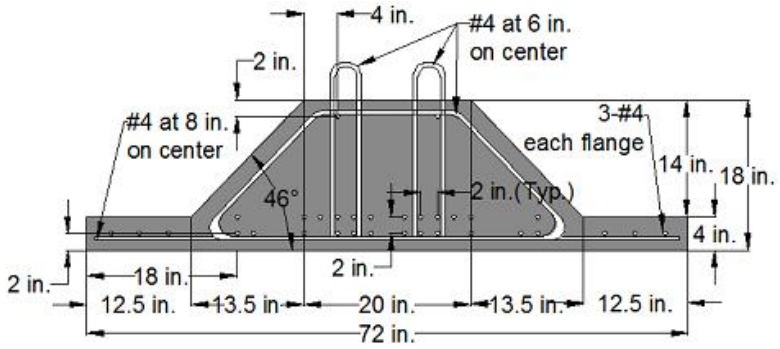

Figure 12 Inverted T-beam system. Medium section geometry as obtained from Menkulasi et al. (2015)

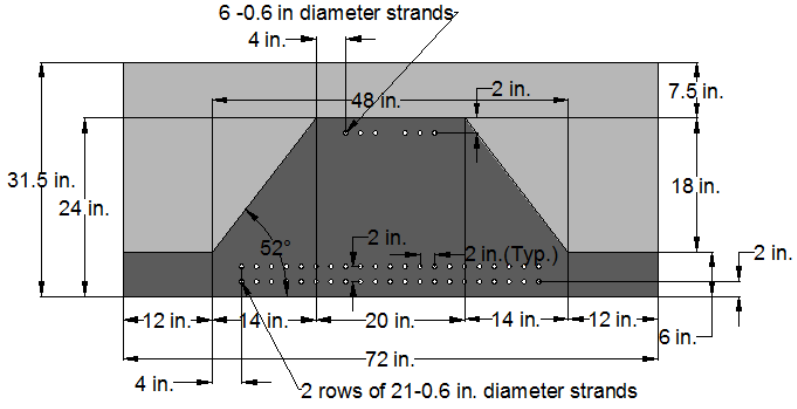

Figure 13 Inverted T-beam system. Large section geometry as obtained from Menkulasi et al. (2015)

Table 3 Inverted T-beam Preliminary Design Tables Iteration 1

L (ft)	Small			
	Row 1	**Row 2**	**Row 3**	**Row 4**
10	10	0	0	1
15	10	0	0	1
20	10	0	0	1
25	11	0	0	1
L (ft)	**Medium**			
	Row 1	**Row 2**	**Row 3**	**Row 4**
30	10	0	0	2
35	11	0	0	2
40	17	0	0	4
45	23	0	0	5
L (ft)	**Large**			
	Row 1	**Row 2**	**Row 3**	**Row 4**
50	23	1	0	6
55	23	8	0	7

Iteration 2 – Including the effects of strand debonding and strand layout optimization

Limitations on span lengths in iteration 1 were caused by tensile and compressive allowable stresses being exceeded at the ends of the member. This was happening both at the time of release, and at service. A solution to this issue was the debonding of strands at the ends of the member. The maximum limits set by AASHTO Section 5.11.4.3 (AASHTO 2014) were adhered to.

In addition to this it was realized that by altering the geometric layout of the strands in the precast section, the centroid of the location of prestressing could be changed. This would in turn affect the stresses on the section possibly reducing the overall stresses in the section.

With these two effects being accounted for in the MATLAB algorithm (Appendix A – MATLAB Code for Preliminary Design Tables), the maximum span lengths for each section were able to be increased by 5 ft each, and the resulting set of tables are shown in Table 4.

The limiting design consideration now changed to the midspan service stress check for all of the sections.

Table 4 Inverted T-beam Preliminary Design Tables Iteration 2

Small										
L (ft)	**Debonding**					**Debonding & Strand Geometry Optimized**				
	Row 1	**Row 2**	**Row 3**	**Row 4**	**No. Debonded**	**Row 1**	**Row 2**	**Row 3**	**Row 4**	**No. Debonded**
10	10	0	0	2	0	8	2	0	0	0
15	10	0	0	2	0	10	0	0	2	0
20	10	0	0	2	0	10	0	0	2	0
25	11	0	0	2	0	12	1	0	0	2
30	19	0	0	2	2	17	2	0	0	2

Medium										
L (ft)	**Debonding**					**Debonding & Strand Geometry Optimized**				
	Row 1	**Row 2**	**Row 3**	**Row 4**	**No. Debonded**	**Row 1**	**Row 2**	**Row 3**	**Row 4**	**No. Debonded**
30	10	0	0	2	0	10	0	0	2	0
35	11	0	0	2	0	8	4	2	2	0
40	20	0	0	4	2	10	6	6	2	0
45	23	5	0	4	6	13	9	9	2	2

Large										
L (ft)	**Debonding**					**Debonding & Strand Geometry Optimized**				
	Row 1	**Row 2**	**Row 3**	**Row 4**	**No. Debonded**	**Row 1**	**Row 2**	**Row 3**	**Row 4**	**No. Debonded**
50	23	6	0	5	6	12	8	6	2	6
55	23	14	0	5	10	15	12	12	3	8
60	23	23	2	6	12	21	17	15	4	14

Iteration 3 – Using light-weight concrete

In order to reduce the midspan stresses at service, the possibility of using light-weight concrete was investigated. Two options were considered; the first used light-weight concrete for the cast-in-place topping, while using a normal weight precast girder (LW Option 1); and the second option used both a light-weight topping and girder (LW Option 2). The resulting tables for both of these options can be seen in Table 5 and Table 6 respectively.

From the tables it can be seen that LW Option 1 did not reduce stresses significantly enough to be able to increase the span lengths, however, the amount of prestressing required for each cross-section could be reduced in most instances. Using LW Option 2, the span lengths for

the largest section were able to increase, but the other sections remained at the same span with less prestressing required.

In this case, the limiting design consideration was the sustained compressive stress limits at the midspan of the beam, and the midspan tensile stresses under service conditions. It was found that removing strands from the top of the beam reduced these stresses, however removing too many top strands reduced the total number of strands that could be debonded which shifted the issue back to the end zones.

Table 5 Inverted T-beam LW Option 1 Preliminary Design Tables

Small - NW Beam, LW Deck										
L (ft)	Debonding					Debonding & Strand Geometry Optimized				
	Row 1	Row 2	Row 3	Row 4	No. Debonded	Row 1	Row 2	Row 3	Row 4	No. Debonded
10	10	0	0	2	0	8	2	0	0	0
15	10	0	0	2	0	10	0	0	2	0
20	10	0	0	2	0	10	0	0	2	0
25	10	0	0	2	0	11	1	0	0	2
30	18	0	0	2	2	16	2	0	0	2

Medium - NW Beam, LW Deck										
L (ft)	Debonding					Debonding & Strand Geometry Optimized				
	Row 1	Row 2	Row 3	Row 4	No. Debonded	Row 1	Row 2	Row 3	Row 4	No. Debonded
30	10	0	0	2	0	10	0	0	2	0
35	11	0	0	2	0	7	4	2	2	0
40	15	0	0	2	4	8	6	4	2	0
45	23	4	0	4	6	11	8	8	2	0
50	23	14	0	4	8	15	11	11	2	6

Large - NW Beam, LW Deck										
L (ft)	Debonding					Debonding & Strand Geometry Optimized				
	Row 1	Row 2	Row 3	Row 4	No. Debonded	Row 1	Row 2	Row 3	Row 4	No. Debonded
50	23	4	0	5	4	11	7	7	2	6
55	23	13	0	5	10	15	11	11	3	8
60	23	23	0	6	12	19	16	16	4	12

Table 6 Inverted T-beams LW Option 2 Preliminary Design Tables

Small - LW Beam, LW Deck										
L (ft)	Debonding					Debonding & Strand Geometry Optimized				
	Row 1	Row 2	Row 3	Row 4	No. Debonded	Row 1	Row 2	Row 3	Row 4	No. Debonded
10	10	0	0	2	0	8	2	0	0	0
15	10	0	0	2	0	10	0	0	2	0
20	10	0	0	2	0	10	0	0	2	0
25	10	0	0	2	0	11	0	0	2	0
30	17	0	0	2	0	15	2	0	0	0

Medium - LW Beam, LW Deck										
L (ft)	Debonding					Debonding & Strand Geometry Optimized				
	Row 1	Row 2	Row 3	Row 4	No. Debonded	Row 1	Row 2	Row 3	Row 4	No. Debonded
30	10	0	0	2	0	10	0	0	2	0
35	10	0	0	2	0	10	0	0	2	0
40	16	0	0	3	2	9	4	4	2	0
45	23	2	0	4	4	10	8	6	2	0
50	23	12	0	4	8	15	11	9	2	4

Large - LW Beam, LW Deck										
L (ft)	Debonding					Debonding & Strand Geometry Optimized				
	Row 1	Row 2	Row 3	Row 4	No. Debonded	Row 1	Row 2	Row 3	Row 4	No. Debonded
50	23	1	0	4	6	9	8	6	2	4
55	23	10	0	5	8	15	11	9	3	8
60	23	21	0	6	10	18	15	13	4	10
65	23	23	9	7	14	23	23	9	7	14

Iteration 4 – Based on conclusions from meeting with VDOT representatives

On 9/28/2016, four VDOT representatives, and four representatives from Virginia Tech's inverted T-beam project team met at the Thomas M. Murray Structural Engineering Lab at Virginia Tech. During the meeting the geometry of the precast sections was discussed, along with ideal outcomes for the beams regarding span lengths. In addition to this, possible methods of achieving these outcomes was discussed.

Based on the conclusions drawn from the meeting, it was decided to postpone the investigation of the smaller and larger cross-sections until the current (mid-sized) section had

been sufficiently investigated. The ideal situation would be to get the medium sized section to span around 75 ft. Possible methods of achieving this mentioned during the meeting included the addition of mild reinforcement to the section, using higher strength concrete, or debonding the top strands during the construction operation (the idea of cutting the top strands prior to pouring the deck was suggested). This formed the basis of the investigation carried out during this design iteration.

It was discovered that the limiting design consideration were the midspan stresses under the final in-service load configuration. As a result of this, no method regarding altering the stressing sequence would affect the final condition enough. Increasing the concrete strength to f'_c = 10 ksi was attempted, however this did not sufficiently increase the allowable stress limits under the midspan in-service condition to validate this approach. Top strands were removed completely from the analysis as their primary reason for placement was to control stresses during transfer and deck placement, but the issue was with in-service stresses, and so the idea of cutting top strands prior to deck placement was made redundant.

Two additional options were then proposed and investigated. Since the largest components of stresses on the beam were due to the prestressing and concrete self-weights acting on the bare beam section alone, it followed that by achieving some composite action at the midspan of the beam prior to application of all of these loads, the stresses would reduce. Therefore, the possibility of a staged deck placement where part of the midspan section was placed first, allowed to harden sufficiently to achieve composite action and then the remainder of the deck placed, was investigated. In addition to this, the idea of using temporary shoring at midspan was studied. Design spreadsheets (Appendix B – Design Spreadsheets for Preliminary Design Tables) were created plotting the stresses along the length of the beam against AASHTO's allowable stresses.

Using the staged deck placement option, the maximum span length of the beam was able to be increased to 63.5 ft using normal weight concrete, 65 ft using a light-weight topping, and 67 ft using a light-weight beam and topping. Providing temporary shoring at midspan, the maximum span length of the beam was able to be increased to 72 ft for the normal weight concrete and for LW Option 1, and 73 ft for LW Option 2.

The limiting stresses in both of these situations were the midspan in-service stresses with compressive stresses governing the staged deck pour option, and tensile stresses governing the temporary shoring option.

TEST SPECIMENS

In order to carry out the cyclic testing in this research, two specimens were constructed to represent the transverse bending behavior of the bridge. Both specimens had geometry similar to the geometry of the test specimens used in the previous testing carried out by Menkulasi (2014) and Mercer (2012). One of the specimens used the no-connection connection, while the other used the welded connection. The purpose of creating a specimen with the welded connection was so that there would be a 'control' against which the performance of the no-connection connection could be compared, when subjected to the same laboratory and loading conditions.

Geometry

The purpose of testing was to determine the behavior of the connections between adjacent girders when subjected to cyclic loads in the transverse bending direction in a real bridge. Therefore, the test specimens represented two inverted T-beam girders placed adjacent to each other over a 4 ft length of the bridge in the longitudinal direction. Figure 14 shows the overall dimensions of the test specimen. As can be seen, each specimen is 12 ft wide by 4 ft long by 25.5 in. tall. According to Menkulasi (2014), 4 ft was chosen as the "slice" of the bridge to be constructed because this was a multiple of the welded connection spacing, and a multiple of the spacing of the original MnDOT extended bar connection. Mercer (2012) additionally noted that this would give good behavior and connection alignment, while meeting the constraints of Virginia Tech's laboratory cranes. The Thomas M. Murray Structural Engineering Laboratory at Virginia Tech has two overhead cranes, each with a capacity of 5 tons. With the selected dimensions, each specimen weighs approximately 7.8 tons and could be lifted using both cranes simultaneously.

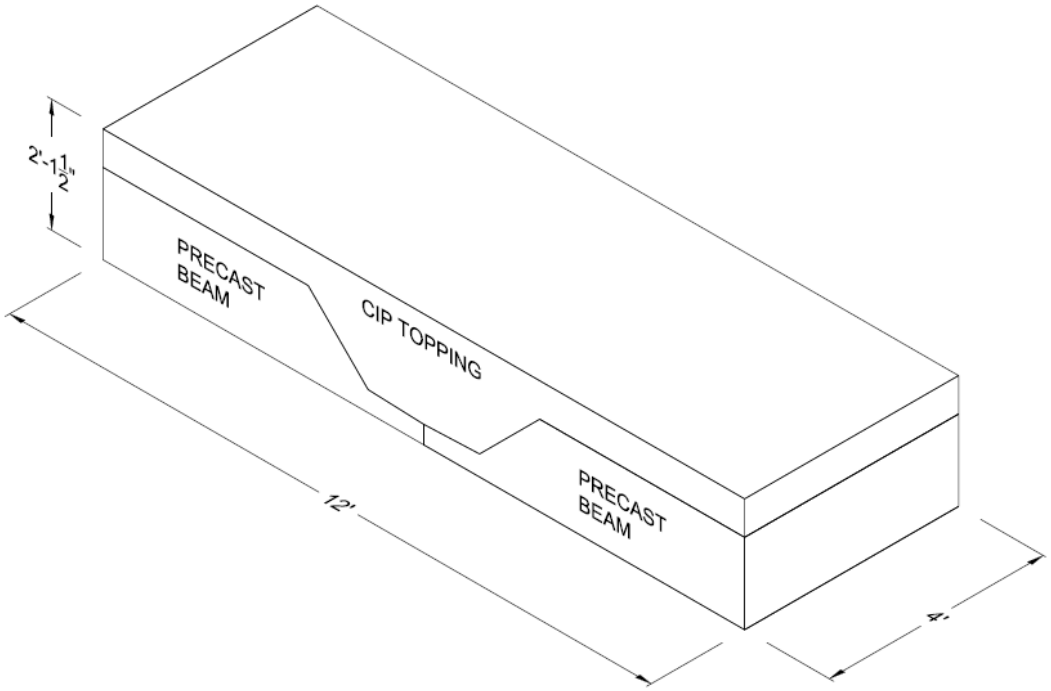

Figure 14 Test specimen overall geometry

A more detailed cross-sectional geometry of each of the test specimens is shown in Figure 15 and Figure 16. As can be seen from the figure, the specimens have the same dimensions with the only difference being at the location between the tips of the flanges of the precast section. The reason for this difference is due to the construction procedure for each of the connections (for more information regarding this, refer to the section on connections below).

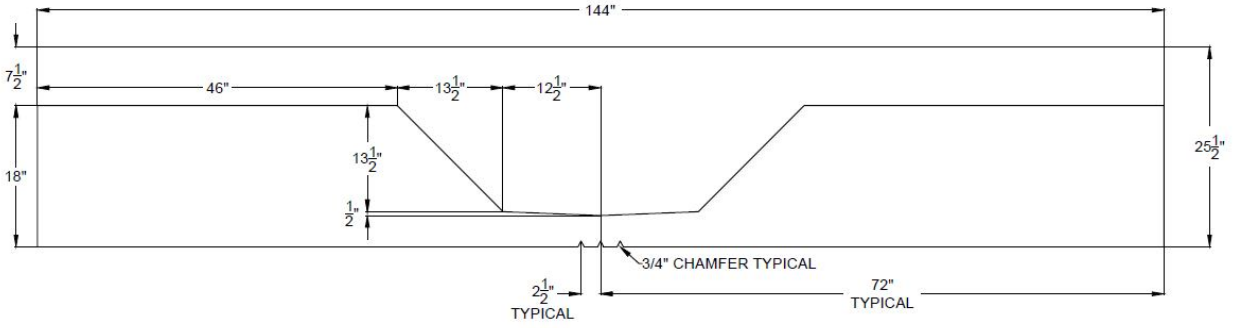

Figure 15 Cross-sectional geometry of No-Connection Connection Test Specimen

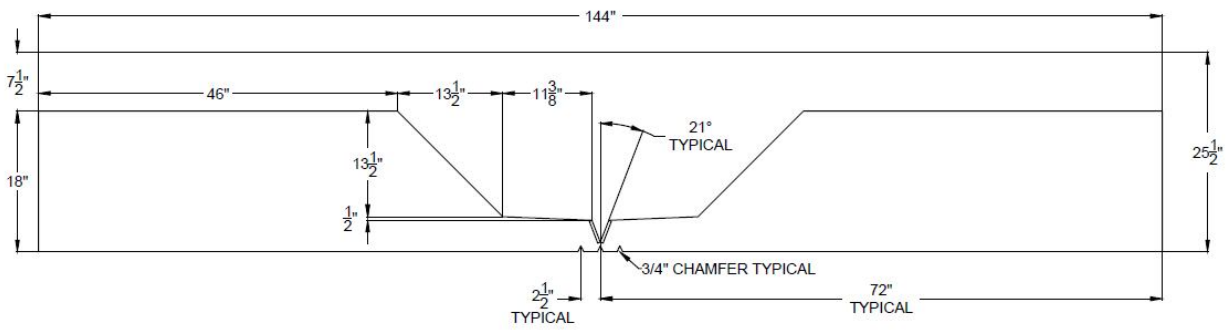

Figure 16 Cross-sectional geometry of Welded Connection Test Specimen

Comparing the geometry of the test specimens in Figure 15 and Figure 16 to the geometry of an inverted T-beam that was used in the Rte. 360 bridge shown in Figure 17, it can be seen that the outside flange of each of the specimens was replaced by an extended web. This was first done by Menkulasi (2014) during his testing as he noted that the extended web region would create a better bearing condition at the supports, reducing the chance of any unforeseen failure mode near the supports. As the purpose of this testing was to examine the behavior at the midspan of the test specimens – where the longitudinal joint was located - rather than near the supports, the same extended web region was used.

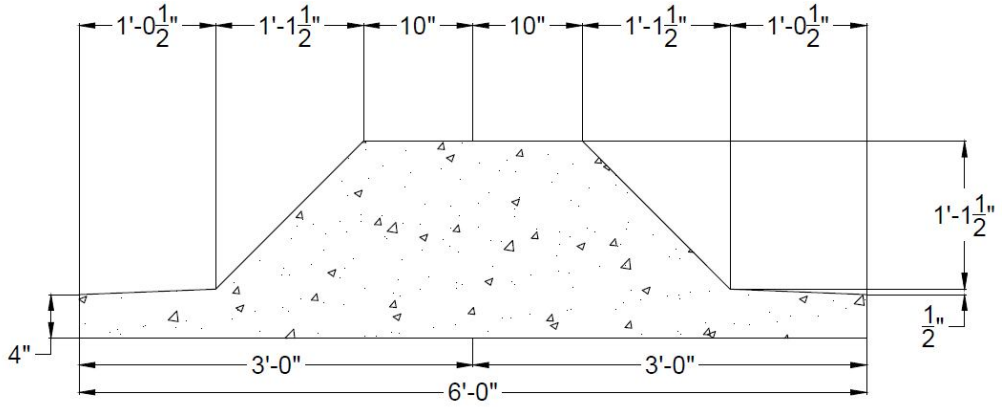

Figure 17 Inverted T-beam on U.S. Rte. 360 Bridge Over Chickahominy River

Connections

Each of the specimens used a different type of connection. The first specimen constructed used the no-connection connection shown in Figure 2. The connection is shown in Figure 18 in this section diagrammatically for convenience. It was mentioned in the Introduction that two

bridges were built in Virginia using the inverted T-beam system, one being on U.S. Rte. 360 over the Chickahominy River near Richmond, and the other on Towlston Road over Rocky Run in Fairfax. The no-connection connection is the one which was used on the Towlston Road bridge, and is the main focus of this research. The second specimen constructed used the welded connection shown in Figure 2 and again shown diagrammatically in Figure 19 and Figure 20. As a result of the previous work carried out by Menkulasi (2014) and Mercer (2012), this connection type was deemed suitable for high volume bridges, and is the one being used on the U.S. Rte. 360 bridge over the Chickahominy River. The second specimen was considered a control for the purposes of this testing – since it is already being used on a high volume bridge, its performance is a useful standard to be compared against.

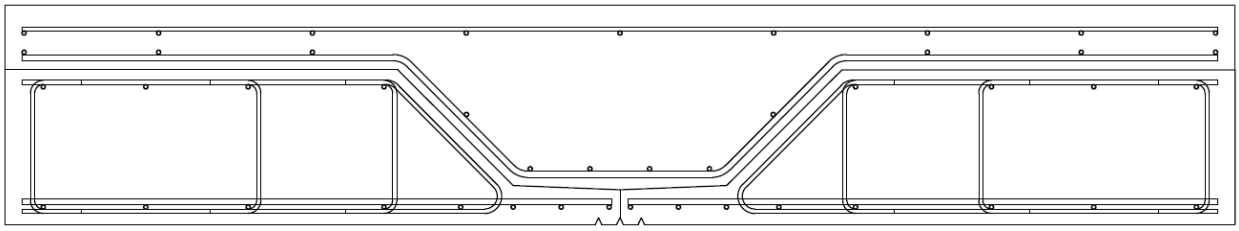

Figure 18 Test specimen with no-connection connection

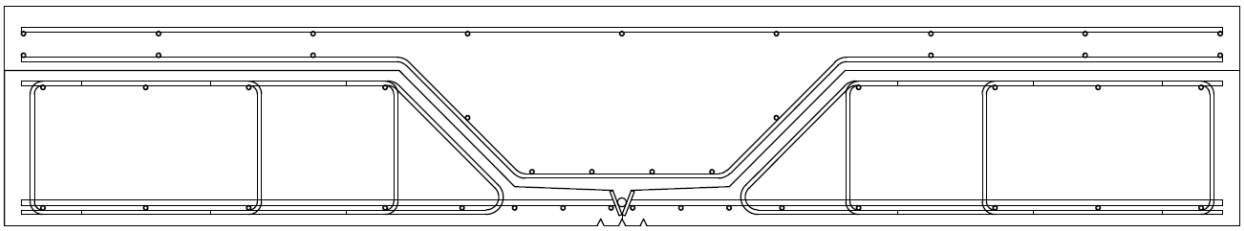

Figure 19 Test specimen with welded connection

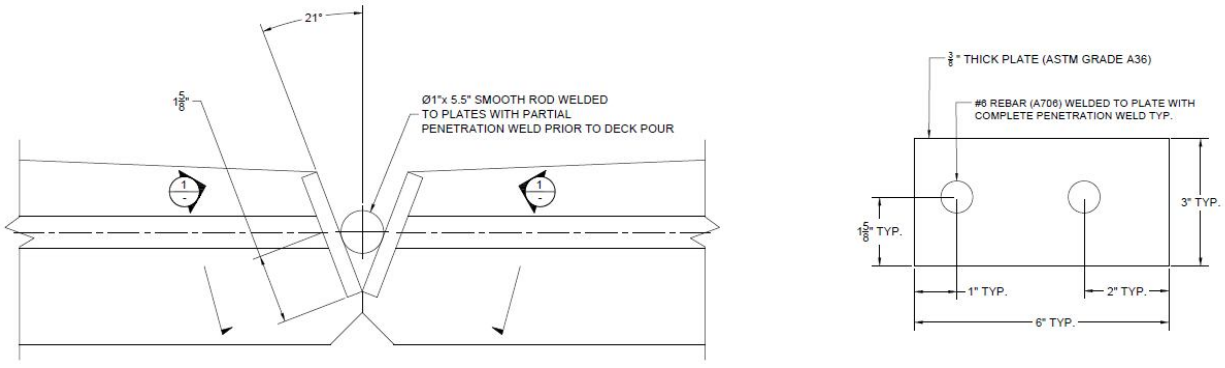

Figure 20 Welded connection details

The two connections transfer transverse bending forces between adjacent members through different mechanisms. In order to transfer the transverse bending forces between the two girders, the no-connection connection type relies on a non-contact lap splice between the longitudinal reinforcement in the bottom of the flanges and the longitudinal reinforcement following the shape of the cast-in-place topping (refer to Figure 18 and the section on Reinforcing Steel for a better illustration of the aforementioned reinforcement). In addition to this, friction between the precast beam and the cast-in-place topping, aided by roughening of the surfaces of the two components in contact with each other, allows the system to act as a monolithic beam. In the welded connection, under positive bending conditions, the reinforcement in the flange of the section is in tension. The tension force is transferred through the reinforcement, into the embedded plate via the complete joint penetration weld, and then into the smooth rod field welded to the plate with a partial joint penetration weld. This is the mechanism by which forces are transferred between the adjacent girders.

Construction of the specimen without connection was significantly more straightforward compared to the specimen with the welded connection. This was a major driving factor for the further testing of the no-connection connection – if it could be validated for use in higher volume bridges, its ease of construction will benefit the ABC process much more than the current use of the welded connections. In order to build the no-connection connection specimen, the formwork was constructed to conform the geometry shown in Figure 15. No special allowances for the connection were needed as the reinforcement for each precast beam was self-contained within the beam and to form the connection the two beams were simply positioned with their flanges touching each other. For the welded connection, however, the 3/8 in. thick embedded plates were first welded to the No. 6 A706 reinforcing bars in the bottom flange. The embedded plates were at an angle of 21 degrees to the vertical, and the plate formed the tip of the flange of the precast section. This would allow the smooth rod to be dropped into place and welded to the embedded plates to form the connection, prior to casting the topping concrete.

It is significant to note that in a real bridge, the plates would be exposed to the environment at the beam soffit, and therefore may not be suitable, for example, in marine environments where wetting/drying of the underside of the bridge could lead to corrosion of the connection itself. In cases like this, the plates would need to be made corrosion resistant. This

would be another instance where using the no-connection connection would provide advantages over the welded connection.

Reinforcing Steel

The reinforcement layout is shown in Figure 21 and Figure 22. All reinforcing steel, with the exception of the No. 6 bars in the flange of the welded connection, used A615 Grade 60 reinforcement. The No. 6 bars in the flange of the welded connection were A706 Grade 60 weldable reinforcement. This was required so that the reinforcement could be welded to the plates used in the welded connection. Further details and a schedule of quantities of the reinforcement is provided in (Appendix C – Reinforcement Details and Schedule of Quantities).

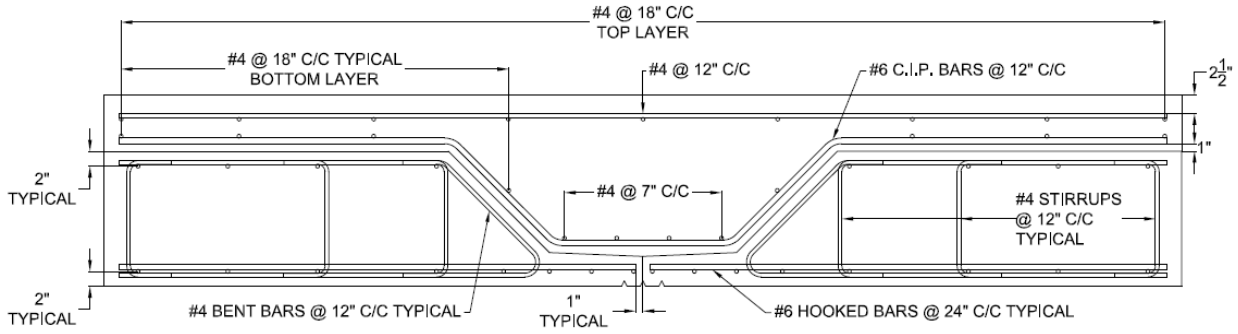

Figure 21 No-Connection Connection Reinforcement Layout

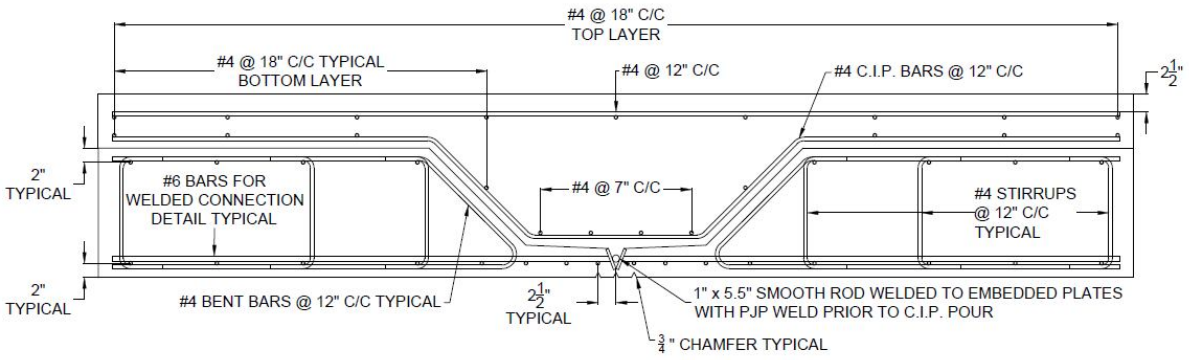

Figure 22 Welded Connection Reinforcement Layout

In the real bridge, substantial amounts of longitudinal prestressing are provided in each of the inverted T-beam girders. However, in the subassemblage specimens this prestressing steel is not provided. During the previous study of the inverted T-beams carried out by Menkulasi (2014) and Mercer (2012), it was decided that the presence of longitudinal prestressing does not

affect the transverse bending behavior greatly, and as such these researchers provided strands that were not prestressed. Additionally, the procedure of prestressing is dangerous due to the large amounts of potential energy stored in the strands during the stressing procedure, and difficult to achieve in the constrained laboratory environment. All things considered it was decided this time, to forgo entirely the presence of longitudinal prestressing.

The design of the reinforcement in the test specimens was based on work carried out by Menkulasi (2014). For the welded connection specimen, the reinforcement in the flanges of the beam was based an allowable stress design using the service live load moments. Menkulasi used his analytical models to quantify the transverse bending moments resulting from the two-way plate bending behavior of the real bridge. Using an allowable stress in the transverse reinforcement of 30 ksi he was then able to size this reinforcement. This resulted in the No. 6 weldable bars in the precast flange. The reinforcement in the deck was originally designed as shrinkage and temperature reinforcement and not relied on for flexural strength. For the no-connection connection, the reinforcement in the flanges was initially designed to resist the weight of the wet concrete topping, however, this was subsequently increased to the No. 6 bars used in the current specimen because it was found that the original design created a weak link in the system and a largely reduced flexural capacity. The bent reinforcement in the bottom of the cast-in-place topping for this specimen was sized based on the transverse live load moments at service, similar to the welded connection bottom flange steel. The remainder of the steel in the specimen was designed as shrinkage and temperature reinforcement, or as part of the cage to allow top bars to be tied.

Three bent bars were provided in each specimen that acted as lifting points once the specimen had been cast. The location of these bars was selected so that the weight of the specimen would be well distributed between the pick locations. This served two purposes, the first being that it reduced the stresses imposed on the longitudinal joint region during the lifting procedure, and the second being that it made it easier to lift the specimen using the two cranes simultaneously as the load was evenly distributed.

SPECIMEN CONSTRUCTION

The purpose of the experimental work that was carried out was to validate the use of the no-connection connection in high volume bridges. Using this connection as opposed to the

welded connection that is currently in use on the Rte. 360 bridge over the Chickahominy River would simplify construction, and eliminate the time needed to carry out field welding. In addition to this, precasters would be able to use formwork that did not require any reinforcement to protrude from them as with the Poutre-Dalle or Minnesota inverted T-beam designs.

Surface Roughening

In order to ensure monolithic action would be achieved between the two concretes cast at different times, the surfaces of the concrete in contact were required to be roughened to a ¼ in. minimum amplitude. This requirement is set out in AASHTO (2014). Surface roughening was carried out via two methods for different locations for this study.

Above the extended web region, the surface of the concrete was not covered by formwork and the surface was raked to a ¼ in. amplitude once the concrete had been placed (refer to Figure 23).

Figure 23 Raked surface finish above extended web region

Surface roughening on the angled web, and the flange sections of the specimen was achieved by roughening the formwork that was used on these surfaces. During the previous study carried out by Menkulasi (2014) it was noted that roughening the formwork by creating indentations in the forms resulted in some pieces of the timber formwork becoming stuck to the concrete surface when it came time to remove the forms. As a result of this, other methods were looked into. Three methods of creating a roughened surface were investigated in a preliminary concrete pour on a small test specimen using Quickcrete (ready mix concrete).

The first method that was considered involved roughening the forms by creating indentations in the plywood, then covering the forms with a sheet of 3.5 mil thick painter's plastic. The hydrostatic pressure created from the casting process on the formwork would be

sufficient to push the plastic into the indentations allowing the surface roughening to be achieved. The advantage of this method was that the plastic created a separation barrier between the wooden formwork and the concrete and the forms were then able to be easily removed. The disadvantage of this was that due to the presence of the plastic, the undulations in the finished concrete surface were not as angular as would have been ideal (refer to Figure 24).

Figure 24 Indented formwork covered with 3.5mil thickness plastic sheet (left). Outcome from trial specimen with this roughening method (right)

Another method that was investigated to allow for easy removal of the formwork was roughening the plywood by gluing pieces of ¼ in. by ¼ in. dowels onto the form. The advantage of this method was that it resulted in sufficiently angular undulations that were guaranteed to have at least a ¼ in. amplitude. The disadvantage was similar to what was observed by Menkulasi (2014) where the glued on pieces would become stuck to the concrete when the forms were removed and then have to be chipped out of the concrete (see Figure 25).

Figure 25 Formwork indentation by glued on dowel pieces (left). Outcome from this surface roughening method on trial specimen (right)

The third method that was investigated was similar to the second method described, with the exception that instead of gluing ¼ in. by ¼ in. wood dowels onto the form, small pieces of hard Styrofoam that had a depth of ¼ in. was glued to the form (refer to Figure 26). The advantage of this method was that it was more efficient to construct the form with the Styrofoam as opposed to the wood dowels because instead of having to cut individual pieces, a large piece of Styrofoam could be obtained, and then the required pattern simply cut into the foam using a craft knife. The disadvantage was that the Styrofoam at a ¼ in. thickness was prone to breaking just from handling it, and upon casting of the concrete the foam became stuck to the concrete surface and was more difficult to remove than the wood dowels.

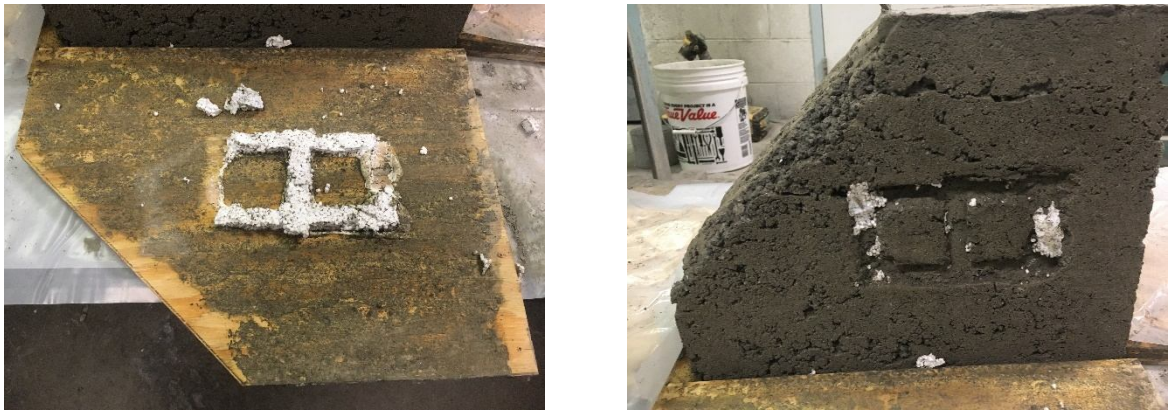

Figure 26 Formwork indentation by attaching styrofoam to surface of forms (left). Outcome using this method of surface roughening (right)

In the end, it was decided to create the surface roughening by indenting the forms and covering them with a thin sheet of painter's plastic as this was the most efficient for construction, and provided a sufficiently roughened surface while being easy to remove and reuse once the concrete had aged enough to remove the formwork.

Formwork Design and Construction

Design of the formwork to resist the hydrostatic pressures exerted on it during the concrete placement process was carried out by James Reilly - a Master of Science in Civil Engineering student at Virginia Tech. Previous formwork designs for these inverted T-beams by Mercer (2012) were used as the basis for the design of the formwork. Images of the formwork can be seen in Figure 27 and full AutoCAD and Sketchup drawings are provided in (Appendix D – Formwork AutoCAD and Google Sketchup Drawings).

Figure 27 Inverted T-beam formwork (left). Inverted T-beam C.I.P. Topping formwork (right)

The most significant part of this formwork design was the use of 1/4 in. diameter pencil rod that passed through the formwork in both the longitudinal and transverse directions. This was pretensioned as much as was possible without pulling the formwork out of line using a one-ton hand pretensioning system (shown in Figure 28). The purpose of doing this was to prevent the forms from bowing outwards during the casting process as hydrostatic pressures built up inside them.

Figure 28 Pencil rod (left). Hand pretensioning system (right)

The formwork was constructed using ¾ in. thick plywood boards, and 2 in. by 4 in. pieces of timber. Coarse thread drywall screws were used to connect timber members. Two different lengths of screw were used; the longer screws being 2 ½ inches long, and the second set of screws being 1 5/8 in. x 8 gauge screws.

As described in the previous section, indentations were created in the formwork at the web and flange locations to provide a roughened concrete surface. The indentations were created

using a wood router with a 1 in. wide square bit, to a depth of just over ¼ in. Providing a slightly deeper groove allowed the minimum ¼ in. amplitude to be achieved even after the thin sheet of painter's plastic was placed over the plywood form. The indentations were specified to have a spacing between them of 2 in. clear. The indented formwork is shown in Figure 29. It is noted in the Discussions regarding the failure mode of the no-connection specimen, that for one of the precast beams the indentations were spaced at 3 in. clear rather than 2 in. clear, which may have contributed to the observed failure mode for that specimen.

Figure 29 Indented formwork on precast beam flange

Concrete Casting

Casting of the concrete for each specimen was carried out in two stages. The first stage was to cast the precast beam, and the second involved placing the cast-in-place topping. For each placement that was carried out a slump test was done prior to the concrete being placed into the specimen formwork. For the cast-in-place topping of both specimens, and the beam concrete for the second specimen, air content and unit weights were also tested prior to placement. The beam concrete in the first specimen did not reach its specified 28-day strength. This is described more in the Issues Faced During Construction section of this document. It was realized at the 7-day break that this would happen and so the air content and unit weight was tested at this stage where it was revealed that the concrete had twice the air, and a lower unit weight than was specified. As a result, for all pours subsequent to this first one air contents and unit weights were tested in addition to slump prior to casting the specimen. The slumps, air contents, and unit weights of the concrete mix for each pour can be seen in Table 7.

Table 7 Characteristics of concrete cast for each specimen

Specimen	Pour	Slump	Unit Weight	Air Content
No-connection	Beam	8.5 in.	130 pcf	12.00%
	Topping	4.75 in.	-	5.50%
Welded Connection	Beam	5.0 in.	147.5 pcf	5.00%
	Topping	4 in.	-	4.50%

The specimens were moist-cured for a minimum of 7 days, and this was facilitated by placing wet burlap over the exposed concrete surfaces, and then covering this with sheets of plastic to retain the heat developed during the exothermic reaction taking place. Formwork was left in place for the entire moist-cure period where it was not required to be removed.

The precast beam concrete had a required 28-day compressive strength of 8000 psi, while the cast-in-place topping had a required 28-day compressive strength of 4000 psi. All concrete was sourced from Conrock based in Blacksburg, Virginia. The mix designs for the beam and topping concretes are provided in Table 8 below. These mix designs are the ones used by Conrock in previous placements on Menkulasi and Mercer's specimens. These differ only slightly from the mix designs shown for the inverted T-beams in Menkulasi et al. (2012). The differences were deemed insignificant enough to maintain the required properties of each of the respective pours. Conrock already has records of these mix designs under the following mix design numbers: 80003 for the 8000 psi beam concrete, and 2010-02-10 for the cast-in-place topping mix. For the mixes developed by Menkulasi, refer to Menkulasi et al. (2012).

Table 8 Concrete mix designs

Component	Beam Concrete Mix (per yd^3)	Cast-in-place Topping Mix (per yd^3)
	f`c = 8000 psi	**f`c = 4000 psi**
Cement	675 lbs	536 lbs
Microsilica	53 lbs	-
Fly Ash	-	134 lbs
#78 Stone (coarse aggregate)	1544 lbs	-
#57 Stone (coarse aggregate)	-	1773 lbs
Wythe NAT (fine aggregate)	1444 lbs	1177 lbs
Water	31 gal	35 gal
Air %	5.50%	6.50%
AEA 15	0.2 per cwt	Varies
Plastiment (retarder)	3.5 per cwt	Varies
SIKA 2100 (HRWR)	4 per cwt	Varies
W/C Ratio	0.35	0.44

The first placement carried out was for the beam portion of the no-connection connection specimen. This was cast on December 15th, 2016. When Menkulasi cast his specimens as part of his research, he noted during his first placement that the concrete was unable to flow all the way to the edges of the flanges due to there being no way to relieve the air pressure that built up as the concrete flowed into the flanges. For subsequent placement, an air pressure relief strip was provided to allow the concrete to flow all the way to the edge of the flanges (Menkulasi 2014). In order to eliminate the need for an air pressure relief strip during this series of testing, it was decided to initially leave the flange uncovered and place concrete directly into the flanges. The flange formwork piece was then screwed into position, and the remainder of the beam specimen cast. This also allowed the pressure created by the rest of the beam specimen to push the concrete in the flanges into the indentations in the formwork. During this placement, concrete cylinders were created for the 7, 14, 21, and 28 day breaks that would allow the concrete's strength gain over time to be monitored.

Casting of the topping concrete for the no-connection connection specimen was carried out on January 16th, 2017. The top surface of the concrete was smoothed and flattened using a

screed board. Concrete cylinders were again made at the time of casting the topping, for the purposes of monitoring the strength gain of the topping concrete with time.

The beam portion of the welded connection specimen was cast on March 20th, 2017. Again, the process of placing concrete directly into the flanges was done first to allow concrete to flow all the way to the tips of the flange. The flange was then covered and the remainder of the concrete was cast. Cylinders were once again made to monitor the concrete's strength gain with time.

The final cast-in-place portion for the welded connection was placed on April 20th, 2017, with compressive strength cylinders being cast similar to previous pours.

Welded Connection

The embedded plate welded connection was constructed by cutting out the tip of the flange of the formwork and placing the steel plate in this cutout. This allowed the concrete to be placed around the cutout at the flange, with the plate protruding. This can be seen in Figure 30. After this, the two precast beams were placed adjacent to each other with the flanges, and embedded plates, making contact with each other as shown in Figure 31.

A piece of 1 in. diameter smooth A36 steel rod was then dropped into the gap between the two embedded steel plates, and the gap was filled with weld material. This can be seen in Figure 32. The welding electrode used was an E7018 electrode, and a Gas Metal Arc Welding (GMAW) process was used. This was selected based upon the inverted T-beams that were previously constructed by Mercer (2012).

Figure 30 Embedded plate prior to placing adjacent beam and welding

Figure 31 Embedded plate connection prior to welding

Figure 32 Welded connection after welding completed

Moving Specimens

Both specimens (the no-connection, and the welded connection) used approximately 4.3 cubic yards of concrete and weighed 8.67 tons. Therefore, moving a single specimen took the use of both laboratory cranes – each crane having a 5 ton capacity. Lifting hooks were provided in

the specimen as can be seen in Figure 33 below. These lifting hooks were constructed from pieces of No. 4 deformed reinforcement bent in the shape of a stirrup, anchored in the bottom of the precast beam and protruding through the surface of the cast-in-place topping.

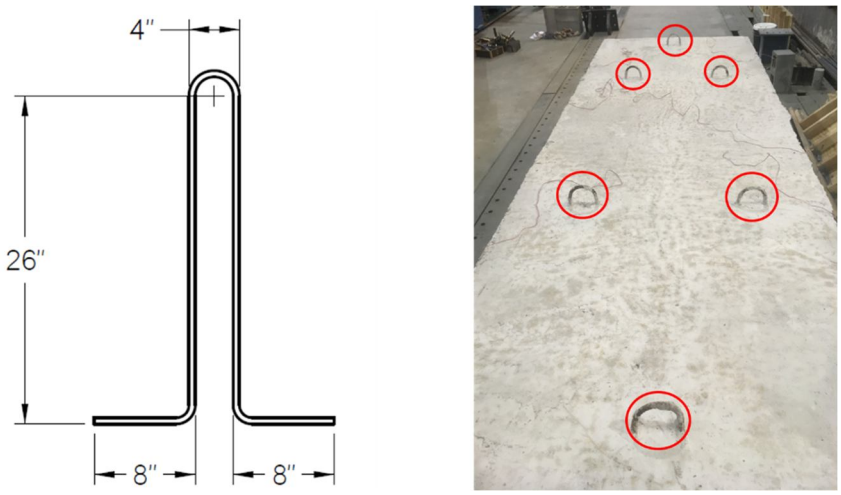

Figure 33 Lifting hooks for moving specimen

Issues Faced During Construction

While carrying out the 7-day concrete cylinder break for the precast beam concrete of the no-connection connection, it was discovered that the concrete had only attained a strength of 3200 psi. This was approximately half of what was expected at 7 days. Upon the subsequent comparison of the scale sheet provided by Conrock, and the scale sheet provided during the concrete placement carried out by Menkulasi, it was observed that for the same batch size of concrete, the air entrainment content had almost doubled, and more water had been added. The reasons for this being done by Conrock were unknown. The beam concrete for this specimen ultimately reached a strength of approximately 4530 psi – half of what was originally intended for the specimen.

Due to budget and time constraints, it was deemed infeasible to completely re-construct the specimen, and instead it was decided to proceed with the experiments using the weakened beam concrete. The decision to proceed in-spite of the weak concrete was made after due consideration of the loading to be applied, and the loads at which cracking and then failure occurred during the testing carried out by Menkulasi (2014). During the testing carried out by Menkulasi (2014) first cracking initiated at an actuator load of 60 kips, double the load at which the specimen was intended to be cycled. In addition to this it was determined that the first crack

initiated in the cast-in-place topping concrete (in the joint region) rather than the beam concrete. At ultimate loads the compression stress block was expected to remain within the cast-in-place topping, and, though the beam concrete was expected to crack at lower loads, the steel reinforcement in the precast beam would take the tensile forces generated. This steel reinforcement had not reduced since previous tests. Development and lap lengths of the reinforcement in the beams increased significantly, however, it was expected that the behavior of the specimens at service level loads – the primary focus of this series of testing - would not be substantially compromised.

Another issue faced during the construction process involved the steel reinforcement not being bent correctly by the steel fabricator. This was the case for both test specimens. In the precast beams, some of the smaller reinforcement was able to be bent back into place using a hand bender available in Virginia Tech's laboratory. However, in the cast-in-place topping, the No. 6 bars were bent in too awkward of a shape to allow them to be bent using a simple hand bending tool. As a result of this, in the cast-in-place topping the reinforcement did not "sit" properly on the beams. In extreme cases the bottom mat of reinforcement clashed with the top mat of reinforcement. However, in the vicinity of the longitudinal joint, the reinforcement was able to be adequately placed. All of this can be seen in the images in Figure 34.

Figure 34 Challenges with reinforcement placement. (Top-left) Inadequate cover at the tapered web-flange interface. (Top-right) Too much cover at extended web-tapered web region. (Bottom-left) Bottom mat of reinforcement clashing with top mat. (Bottom-right) Reinforcement placement within joint region.

ANALYTICAL METHODS

Prior to testing, finite element analysis was carried out using ABAQUS software. The intention of carrying out this analysis was to determine the loads needed to be applied to the test specimen in the laboratory, that would create a stress state in the vicinity of the longitudinal joint representative of that which would occur in a real bridge. Two models were created; the first was a full scale model of the U.S. Rte. 360 Over Chickahominy River bridge. This bridge was the first in Virginia to be constructed using the inverted T-beam system. The second model that was developed was a direct representation of the subassemblage specimen that was constructed and tested in the laboratory.

Model of the U.S. Rte. 360 Bridge Over the Chickahominy River

The finite element analysis model representing the full bridge can be seen in Figure 35.

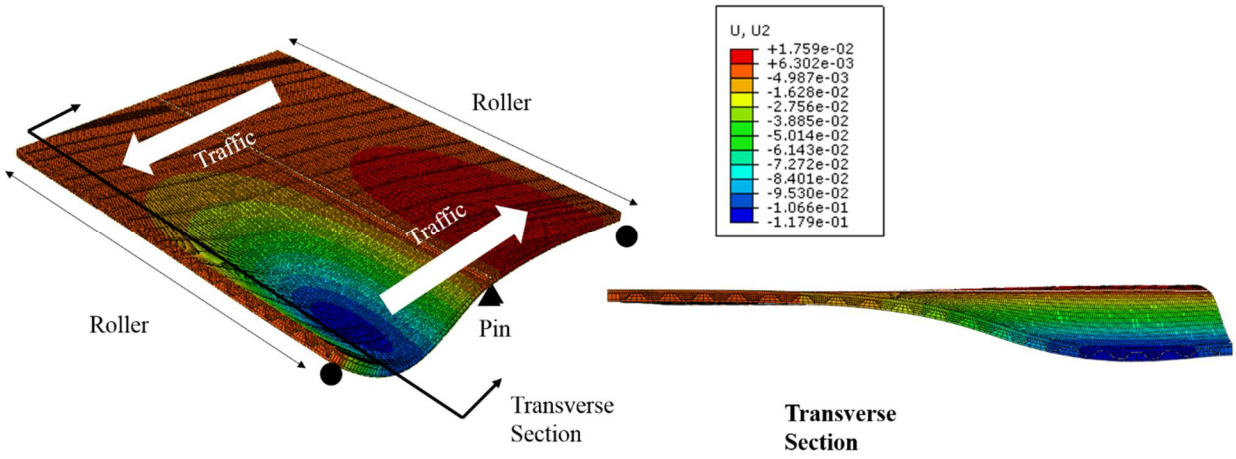

Figure 35 ABAQUS Model of the Full U.S. Rte. 360 Bridge Over the Chickahominy River

The model geometry is based on the design drawings of the U.S. Rte. 360 Bridge Over the Chickahominy River, provided to Virginia Tech by VDOT. These drawings are attached in (Appendix E – U.S. Route 360 Bridge Over the Chickahominy River Drawings). Elements of the bridge were modelled using three-dimensional solid elements. The cross-section of the bridge consists of two parts, the precast inverted T-beam, and the C.I.P. topping. The cross-sectional dimensions of each of these parts, for an individual inverted T-beam element can be seen in Figure 36. This cross-section is very similar to the one used in the development of the preliminary design tables discussed above. In the model, the C.I.P. topping was not created

element-by-element as the precast beam members were. Instead, the topping for the entire transverse width and longitudinal span of the bridge was defined as a single part. This is because during construction, the topping for the whole bridge would be cast in a continuous pour, rather than pouring 6 ft wide sections.

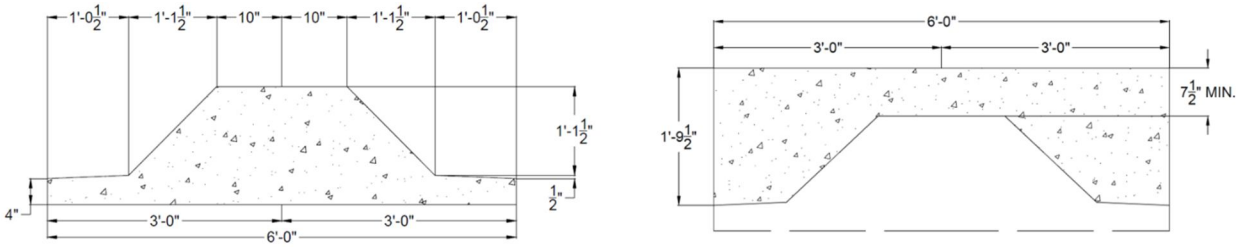

Figure 36 (Left) Inverted T-beam Cross-Section Geometry (obtained from design drawings of the Rte. 360 Bridge Over Chickahominy River). (Right) Cast-in-place topping cross-sectional geometry.

In the longitudinal direction the model consists of two simply supported spans. Span lengths are 40 ft - 9 in. from the center of the abutment, to the center of the bearing pad at the pier bent. At the pier bent, between the ends of each of the spans, is a 1 ft – 4 in. wide continuity pour that runs the full width of the bridge. Note that the 4 in., between the center of the bearing pad at the pier bent and the end of the precast beam at the pier bent, was not included in the model. Including this short distance (less than 1% of the span length) does not alter results significantly. In the transverse direction the model is 112 ft – 4 in. wide. This width is made up of 18 ea. 6 ft wide precast inverted T-beams, and two rectangular precast edge beams which are each 2 ft – 2 in. wide (refer to full bridge drawings in Appendix E – U.S. Route 360 Bridge Over the Chickahominy River Drawings for more details).

Both, the precast beam and the C.I.P. topping, were defined as elastic, isotropic materials. Based on the specified 28-day concrete strength of each of these components, equation 5.4.2.4-1 from AASHTO (2014) was used to calculate the respective Young's Modulus values. The Young's Modulus and Poisson's Ratio for the precast beam was defined as 5422 ksi and 0.2 respectively – for a concrete with a specified 28-day strength of 8000 psi. For the C.I.P. topping, with a specified 28-day strength of 4000 psi, these respective values were specified as 3834 ksi, and 0.2. Based on the finite element work carried out by Menkulasi (2014), the expected maximum stresses during the testing remained within the linear-elastic range of concrete behavior, therefore simplification of the model using elastic material properties was deemed to be sufficient.

The support conditions for the model were specified as a roller along the bottom edge of the end of the beams located at an abutment, and a pinned support along the bottom edge of each beam at the central bent. The bottom face of the C.I.P. topping was constrained to deform with the top faces of the precast beams using the tie constraint in ABAQUS. In this case, the beam surfaces were chosen to deform independently (master surface) and the C.I.P. surface was selected to deform correspondingly (slave surface). Another tie constraint was included to force the face of the continuity diaphragm to deform corresponding to the deformation of the end-face of the precast beam and C.I.P. topping. Here, the face of the precast beam and C.I.P. topping was selected as the master surface, and the face of the continuity diaphragm the slave surface. In doing both of these things, there is an implied assumption of perfect bond between the precast beam concrete and the C.I.P. concrete, as well as between the face of the continuity diaphragm and the end-face of the precast beams and C.I.P. topping.

Loads were applied in accordance with the HL-93 design loading described in AASHTO (2014). This consisted of a design lane load uniformly distributed across the width of the 12 ft wide design lane, and the design truck or tandem. The applied loading is shown diagrammatically in Figure 37. The loads were applied to each lane individually, and then in combinations to give the worst case transverse stress at the location of the joint between the girders. The configuration of loading most closely representing the loaded lanes on the U.S. Rte. 360 bridge, and giving the worst case transverse bending is shown in Figure 38. Although AASHTO (2014) states that the design lane load should be applied over a 10 ft width within the 12 ft wide design lane, in the model it was decided to apply an equivalent magnitude lane load over the full 12 ft width. The reason for this was that it does not alter the results significantly and, as each beam was 6 ft wide, it prevented the need to create further section partitions on the C.I.P. topping thereby simplifying the model. This approach was used in previous work by Menkulasi (2014). It is also important to note that for the U.S. Rte. 360 bridge, the design tandem created the worst-case bending stresses in the joint region as compared to the design truck. Self-weights were not included in the analysis of the full bridge. This is because Mercer (2012) makes the point that in the real bridge situation, the beam units are precast, and then placed and the C.I.P. topping subsequently poured. Transverse bending stresses do not develop until composite action has been achieved. Therefore, the only dead loads contributing to the transverse bending stresses at the joints are the self-weights of superimposed dead loads (future

wearing surfaces, and barriers). The weight of the future wearing surface - 0.025 ksf - and barrier weight – 0.3 k/ft distributed across the full lane width – were added to the design lane load to get the distributed load applied in the model. The values for the magnitude of the future wearing surface, and barrier weights were taken from the design calculations for the U.S. Rte. 360 Bridge Over the Chickahominy River, carried out by Mercer (2012) and Menkulasi (2014).

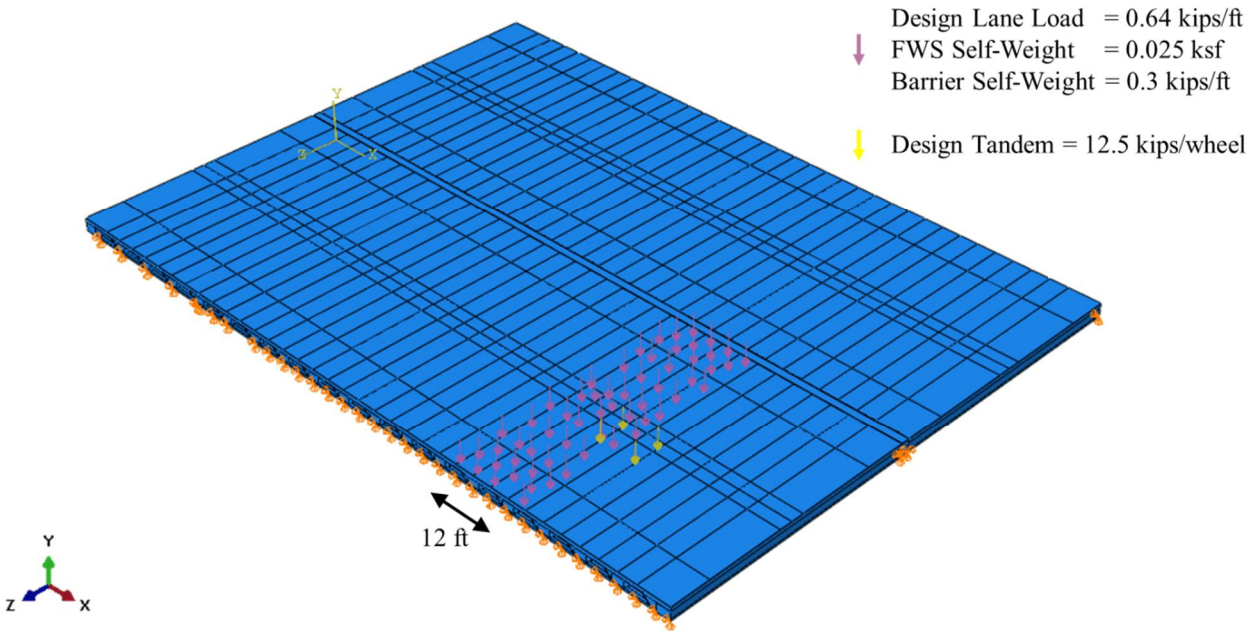

Figure 37 AASHTO HL-93 Loading Applied to a Single Design Lane

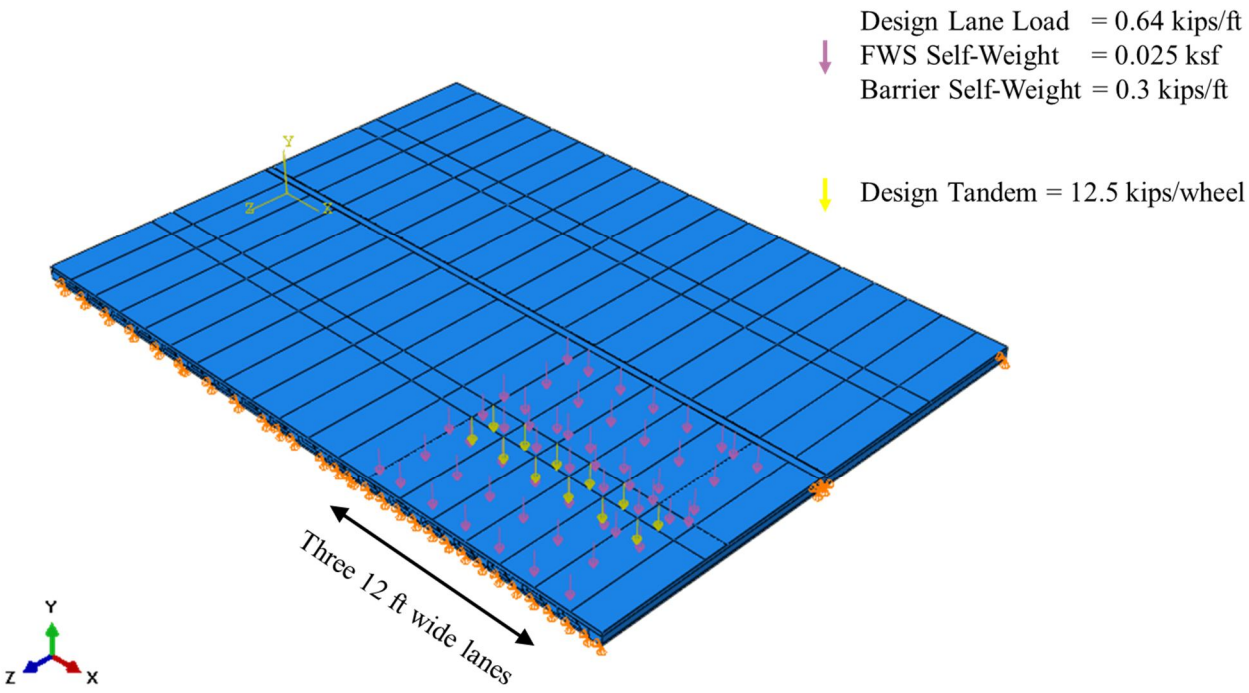

Figure 38 AASHTO HL-93 Loading Applied to 3 Design Lanes to Give Worst Case Transverse Bending Stress

A linear-elastic analysis was run on this model using gross section properties. As noted by Menkulasi (2014) this is appropriate up to the initiation of cracking. Since the aim of this research was to validate the performance of the bridge under service loads – where no cracking is expected – the use of such an analysis is justified.

Subassemblage Model

A finite element model representing the specimen that was to be tested in the laboratory at Virginia Tech was created. The model can be seen in Figure 39.

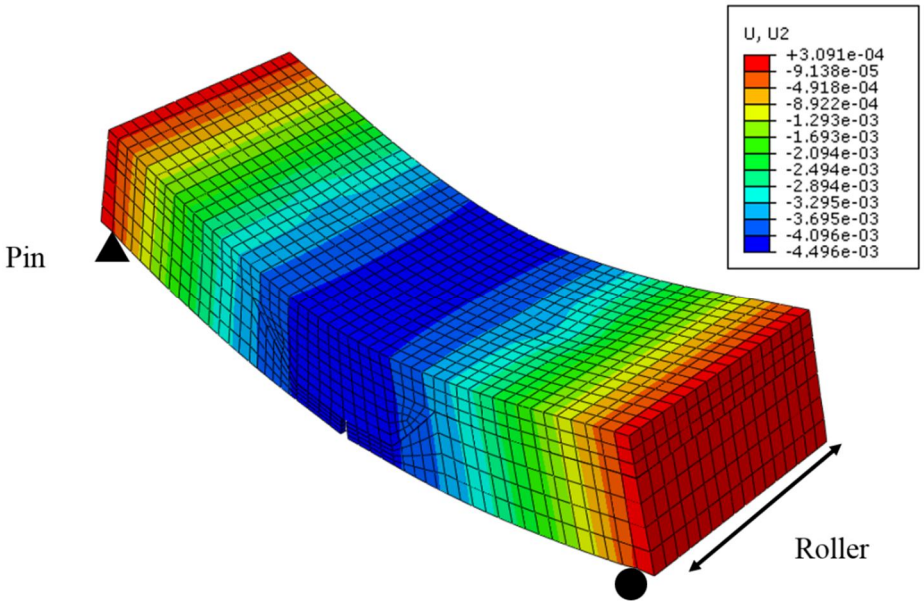

Figure 39 ABAQUS model of the subassemblage specimen. Deflections shown in units of in.

The cross-sectional geometry of the test specimen can be seen in Figure 14 and Figure 15. This geometry follows that of the inverted T-beams on the Rte. 360 bridge but with a modification to the flanges above the supports. The reasoning behind this modification is discussed more in the section on Test Specimen Geometry.

The beam portion of the subassemblage specimen was intended to be cast using an 8000 psi concrete mix. As a result, the material properties chosen to represent this concrete was an isotropic elastic material with a Young's Modulus of 5422 ksi, and a Poisson's Ratio of 0.2. The C.I.P. topping concrete would be cast using a 4000 psi concrete mix and therefore a Young's Modulus of 3834 ksi, and a Poission's Ratio of 0.2 was selected for this concrete. These properties are identical to the material properties in the full bridge model discussed above. As discussed previously, since the behavior of the specimen under application of service loads was expected to remain within the range of linear-elastic concrete behavior, elastic material properties were deemed sufficient for this analysis. For the no-connection specimen, as discussed further in the section of this thesis regarding Issues Faced During Construction, the concrete strength at 28 days was found to be around 4000 psi. For this reason, the model of the no-connection specimen used a Young's Modulus of 3834 ksi for both, the precast beam concrete and C.I.P. topping concrete.

Boundary conditions for the subassemblage model can be seen in Figure 39 and consisted of a pin type connection along the bottom edge of one end of the beam, and a roller type connection at the opposite end. The pin and roller supports were positioned at the center of the bearing pads used in the Testing Setup. Furthermore, the surfaces of the beam and C.I.P. topping concretes that were in contact with one-another were constrained to move together using ABAQUS's tie constraint. The beam surface was selected to move independently as the master surface, and the C.I.P. topping was constrained to move with respect to the beam surface therefore being the slave surface. Note that this is the same as in the full bridge model, and again there is an implied assumption of perfect bond between the surfaces of the two concretes.

The loading configuration for the subassemblage specimen represents the test setup in the laboratory. For the subassemblage specimen, self-weight of the specimen was included in the loadings applied to the finite element models. This is because, under laboratory conditions, the precast beam is cast, then the C.I.P. topping is cast, and composite action is gained prior to the specimen being lifted into position. In this case, unlike in the real bridge situation, by the time the specimen has to carry its own self-weight, composite action has been achieved and transverse bending stresses are able to develop. In addition to the self-weight of the specimen, Figure 40 shows that the specimen is loaded via two, 9 in. by 18 in. uniformly distributed loads, centered over its quarter points. The two point loads represent the wheel loads applied by the design truck or tandem in the real bridge. The magnitude of the applied loads was altered until the magnitude of stresses in the cast-in-place topping at the location of the longitudinal joint between the precast beams was similar to the stresses in the same location in the full bridge model. This confirmed the loading that was required to be applied to the test specimen in the lab setup.

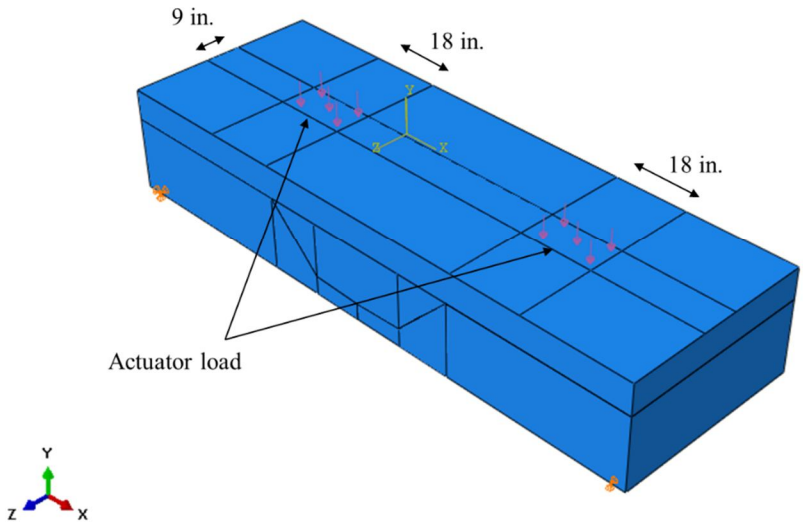

Figure 40 ABAQUS subassemblage model loading

Similar to the full bridge model, a linear-elastic analysis was run using gross section and un-cracked material properties. Prior testing carried out by Menkulasi (2014) indicated that the test specimen would remain un-cracked at service loads and thus this type of analysis would be suitable.

Results from Modeling

Figure 41 shows the results from the finite element model of the full U.S. Rte. 360 Bridge over the Chickahominy River. The area of interest in these models is around the joint region under transverse bending. The results show that the stresses in the real bridge occurring in the vicinity of the joint, sum to around 0.17 ksi from the self-weight of superimposed dead loads (future wearing surfaces and barrier weights transformed into a distributed load), and the HL-93 design loading (design lane loads and design tandem acting together).

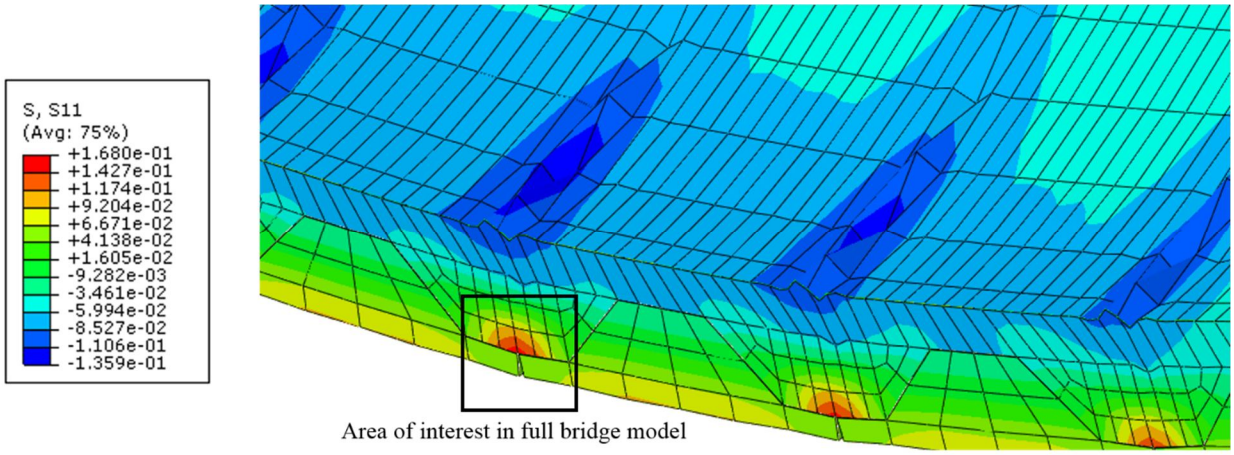

Figure 41 Stress contours around joint region in full U.S. Rte. 360 Bridge model for HL-93 load conditions and weights of future wearing surface and barriers. Units of S, S11 stresses shown are ksi

Figure 42, shows the results from the model of the subassemblage specimen required to be tested in the lab. The actuator load, $P_{actuator}$, that was applied to the model had a magnitude of 27 kips. This was applied through two bearing pads located approximately at the locations shown in Figure 42 (more detailed information regarding the locations of the applied loading is provided in the section on Experimental methods - Testing Setup). The results of the model show that under this 27 kip load, the stress at the critical location near the joint attains a value of 0.17 ksi. This loading of 27 kips to represent the service stresses in the full bridge is identical to what was attained in previous modeling by Menkulasi (2014), who obtained a value of 27 kips. It is noted that although the self-weight of the specimen increases the stresses in the critical region around the joint, the 96 psi increase would still result in stresses well below the modulus of rupture of the concrete. Thus it was concluded that self-weight of the specimen would not negatively impact the test specimen, and would allow for a conservative testing regimen. In addition, this would allow testing to closely follow that carried out by Menkulasi and Mercer.

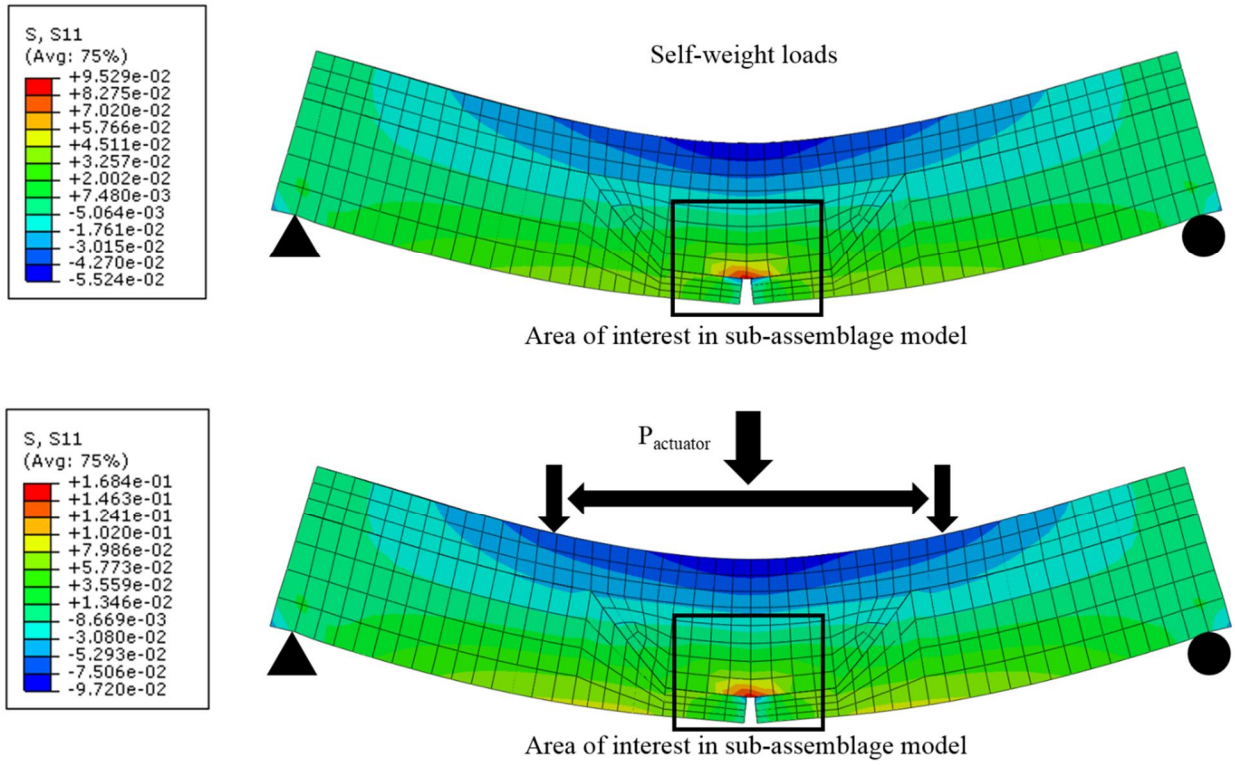

Figure 42 Stress contours around joint region in subassemblage model for self-weight and actuator loads. All S, S11 stresses provided have units of ksi

As can be seen in Table 9, reducing the Young's Modulus of the precast beam concrete for the subassemblage model representing the no-connection specimen reduced the stresses in the longitudinal joint region. However, the reduction in stress was small (8 psi) and so it was deemed that the low strength concrete in the beam of the no-connection specimen would not have a significant effect on the performance of this subassemblage specimen under service loading. As a result of the modeling that was carried out, and by comparison of the results from these models, to those created during the testing of Menkulasi (2014) and Mercer (2012), the loading range that was decided to be applied to the subassemblage specimen during lab testing was 30 kips. This load would create a stress condition in the vicinity of the longitudinal joint, similar to those that would be seen in the real bridge under service conditions. The stresses resulting from the application of self-weight and a 30 kip actuator load to the subassemblage model can also be seen in Table 9, and in Figure 43.

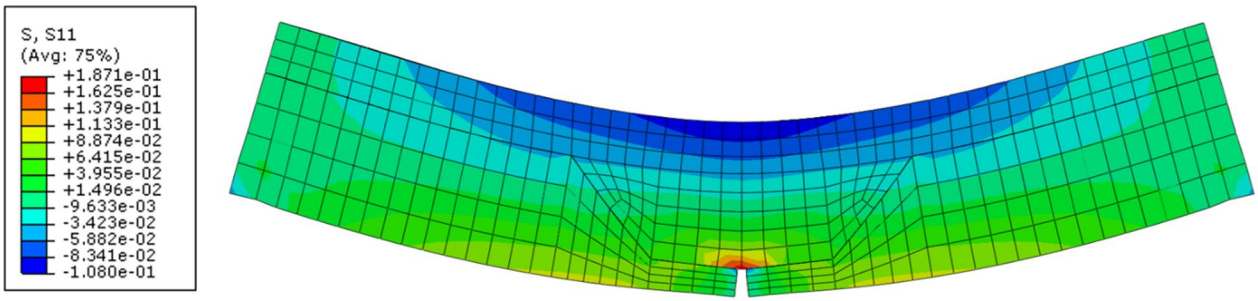

Figure 43 Subassemblage model with applied 30 kip actuator load. All stresses given in units of ksi

Table 9 Comparison of S11 stresses from model, for low strength precast beam concrete

Comparison of S11 Stresses at Critical Location of Subassemblage Specimen. All Values in ksi.		
Load Condition	**Precast Beam Young's Modulus, E**	
	E = 5422 ksi	**E = 3834 ksi**
Self-weight	0.095	0.091
27 kip Actuator	0.168	0.161
30 kip Actuator	0.187	0.178
Total (27 kip Actuator + Self-weight)	0.263	0.252
Total (30 kip Actuator + Self-weight)	0.282	0.269

EXPERIMENTAL METHODS

This chapter describes the experimental methods used to conduct the cyclic testing of the subassemblage specimens in the laboratory. In addition to this, a description of the method used to test the specimen's ultimate capacity is also provided. The test setup is first described, along with an explanation of the loading procedures for the cyclic and then ultimate load tests respectively. A discussion of the instrumentation systems used and their layout, follows the test setup discussion.

Testing Setup

The purpose of the experimental testing regime was to replicate the transverse bending behavior of the inverted T-beam system in a scaled laboratory setting. The ultimate goal of the testing was to validate the performance of the no-connection inverted T-beam system under repeated loading conditions. In order to achieve this, a reaction frame was required to be

constructed in the laboratory, and an actuator capable of providing a cyclic loading was then attached to the loading frame and test specimen.

The test frame setup can be seen in Figure 44 and Figure 45. The setup used is similar to that used in the testing of Mercer (2012) and Menkulasi (2014). The frame was constructed using two W21x62 steel columns mounted to the laboratory strong-floor using four 1 in. diameter A325 bolts per column. Spanning between the two columns, on either side of the columns, were two W21x62 crossbeams. The crossbeams had part of their flange cut away to allow the web of the section to be bolted to the column flange using six 7/8 in. diameter A325 bolts per connection. A custom steel mount was attached to the center of the two crossbeams using eight 7/8 in. diameter A325 bolts per side. An MTS Series 244.51 actuator was attached to the custom steel mount and was responsible for providing the vertical loading to the test specimen. The actuator applied load to a W12x50 spreader beam that was supported on top of the test specimen by two 9 in. x 18 in. x 2 ½ in. thick bearing pads spaced at 6 ft center to center. The plan dimensions and spacing of these bearing pads are a close representation of the wheel dimension and spacing of a single axle of the typical design truck, specified in Sections 3.6.1.2.5 (for the tire contact area) and 3.6.1.2.2 (for the wheel spacing) of the AASHTO LRFD Bridge Design Specifications (AASHTO 2014) respectively. The test specimen then sat, simply supported, on bearing pads measuring 10 in. x 48 in. x 2 in. thick. These bearing pads were placed at the edge of the top flanges of two W14x90 support beams (one at each end of the test specimen). These support beams were bolted to the laboratory strong-floor using four 1 in. diameter A325 bolts.

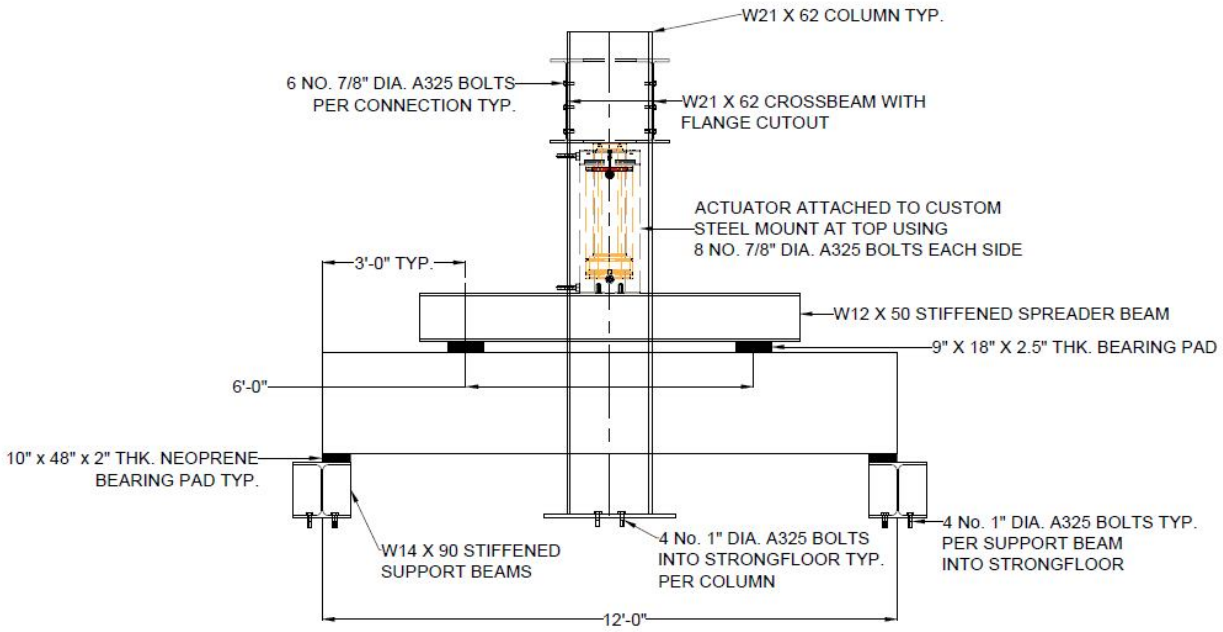

Figure 44 Test frame setup

Figure 45 Test frame

In order to conduct the monotonic load test to failure of the specimen, the W12x50 spreader beam needed to be switched to a larger section to facilitate the large loads that were expected to be required. The section chosen to replace this W12x50 spreader was a W14x120 section. Calculations for the capacity of the test frame are provided in (Appendix F – Testing Frame Capacity Calculations).

Load Protocol

Two different stages of loadings were applied to the test specimen. The first was the application of a cyclic load, and the second stage a monotonic loading to failure of the specimen

The cyclic load which was applied had a 30 kip peak amplitude and a frequency of 2 Hz. The loading amplitude ranged from 10 kips to 30 kips. The reason for having a residual 10 kip load as the lowest amplitude was to reduce the vibrations of the test frame which could have resulted in the loosening of the bolts holding the frame together, and also potentially resulted in the actuator sliding off of the spreader beam. The 2 Hz frequency of loading was chosen primarily to allow for a realistic timeline for the testing to be carried out, while minimizing any dynamic effects that would invalidate the purpose of the test. The specimen was cycled at this load magnitude and rate for a total of 3,650,000 cycles. This represents an ADTT of 200 over a 50-year design life. 200 ADTT is the minimum limit at which VDOT requires a bridge to have a 7.5 in. thick topping over the beams (VDOT, 2015). At certain intervals, the cyclic test was stopped, and the load was completely removed from the specimen. Then, a monotonic load test was carried out from 0 kips to 30 kips, and it was only during this time that instrumentation recordings were taken. The increments at which the cycling was halted were once the test had reached 10 cycles, 100 cycles, 1000 cycles, 100000 cycles, and then every 200000 cycles until the total number was reached – one more monotonic test being conducted at the end of all cycling. During the cyclic loading, the actuator was set to be load-controlled.

Upon completion of the 3,650,000 cycles of loading, a monotonic test to specimen failure was carried out. The purpose of this was to determine the failure load, crack propagation, and failure mechanism at the ultimate capacity of the section. The control for the actuator was switched to displacement-controlled, and the manual scroll setting was enabled so that the load could be slowly increased manually. The load was first taken to 30 kips, and then was increased at 10 kip increments. After each load increment, the specimen was inspected for cracks which

were marked and mapped prior to subsequently continuing with the next load increment. This process was repeated until failure of the specimen occurred. All instrumentation continuously recorded during this stage of testing.

Instrumentation Plan

The goal of this research was to confirm that the no-connection specimen would perform adequately under repeated loading conditions. In order to do this a combination of instrumentation was used which included Celesco PT101 Series String Potentiometers (String Pot), Trans-Tek Series 0354-0000 Linear Variable Displacement Transducers (LVDT), and Vishay Precision Group (VPG) Series C2A-06-250LW-350 Embedded Strain Gauges (Strain Gauge). Six of each type instrument was used. Data were recorded at a frequency of 1 Hz using a VPG System 5000 system, and StrainSmart software. In addition to these instruments, cracks were visually observed and mapped using a permanent marker on the specimen. The general layout of instrumentation can be seen in Figure 46 to Figure 49 below.

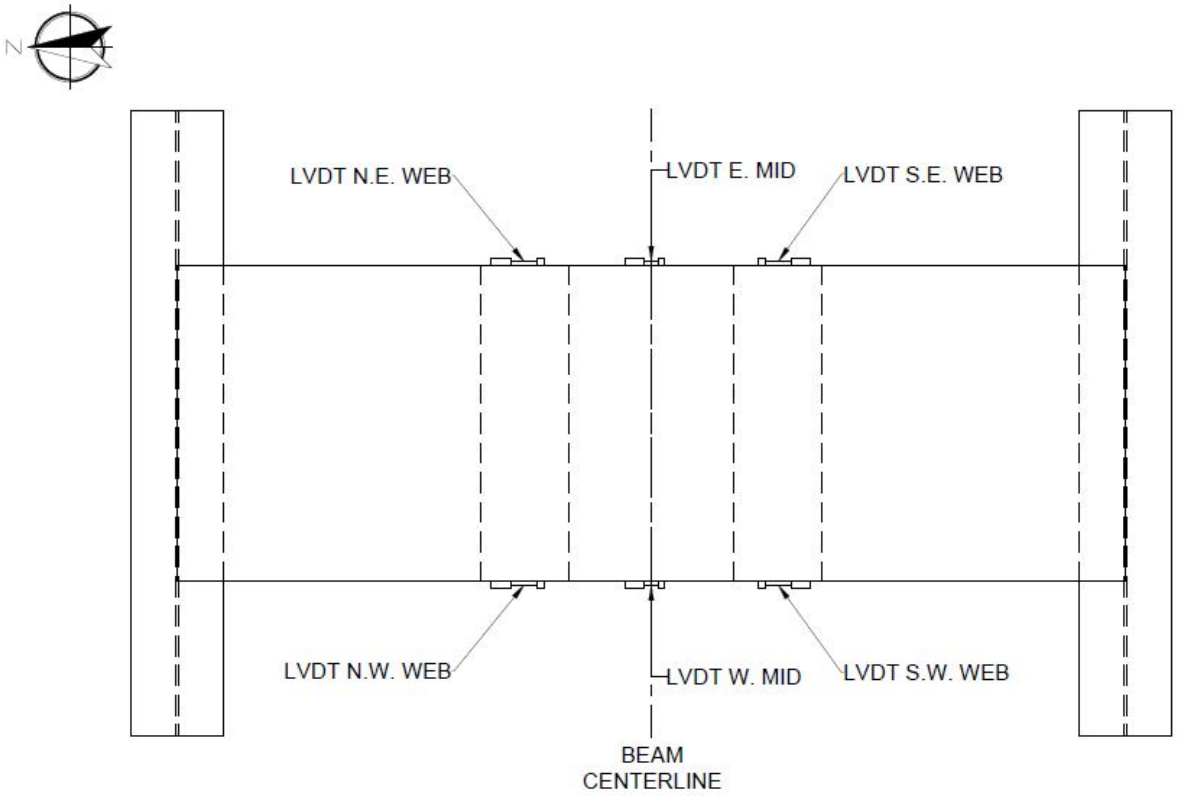

Figure 46 Plan view on inverted T-beam subassemblage specimen, showing arrangement and naming convention of LVDT's

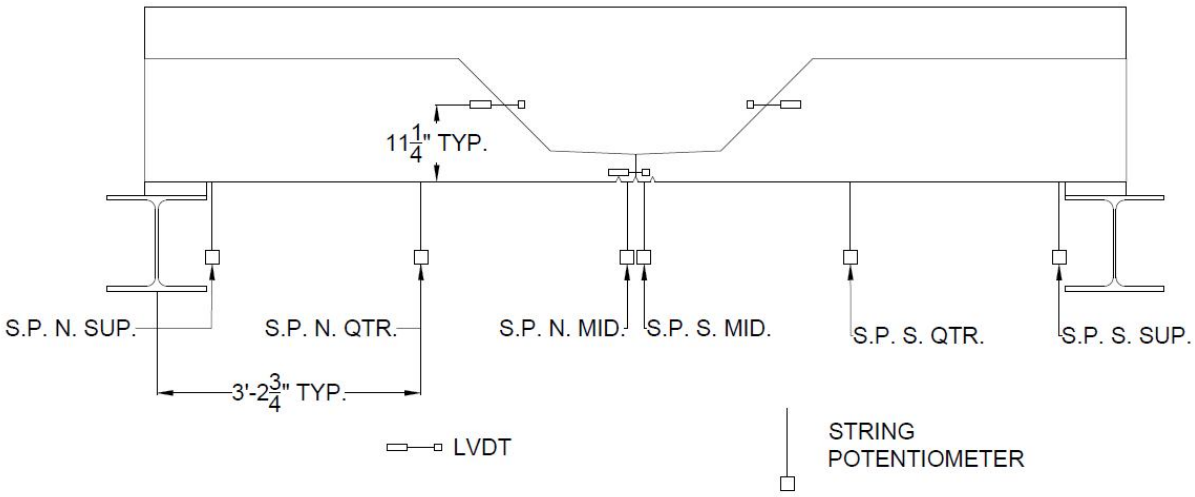

Figure 47 Elevation on inverted T-beam subassemblage specimen, showing arrangement and naming convention for string pots

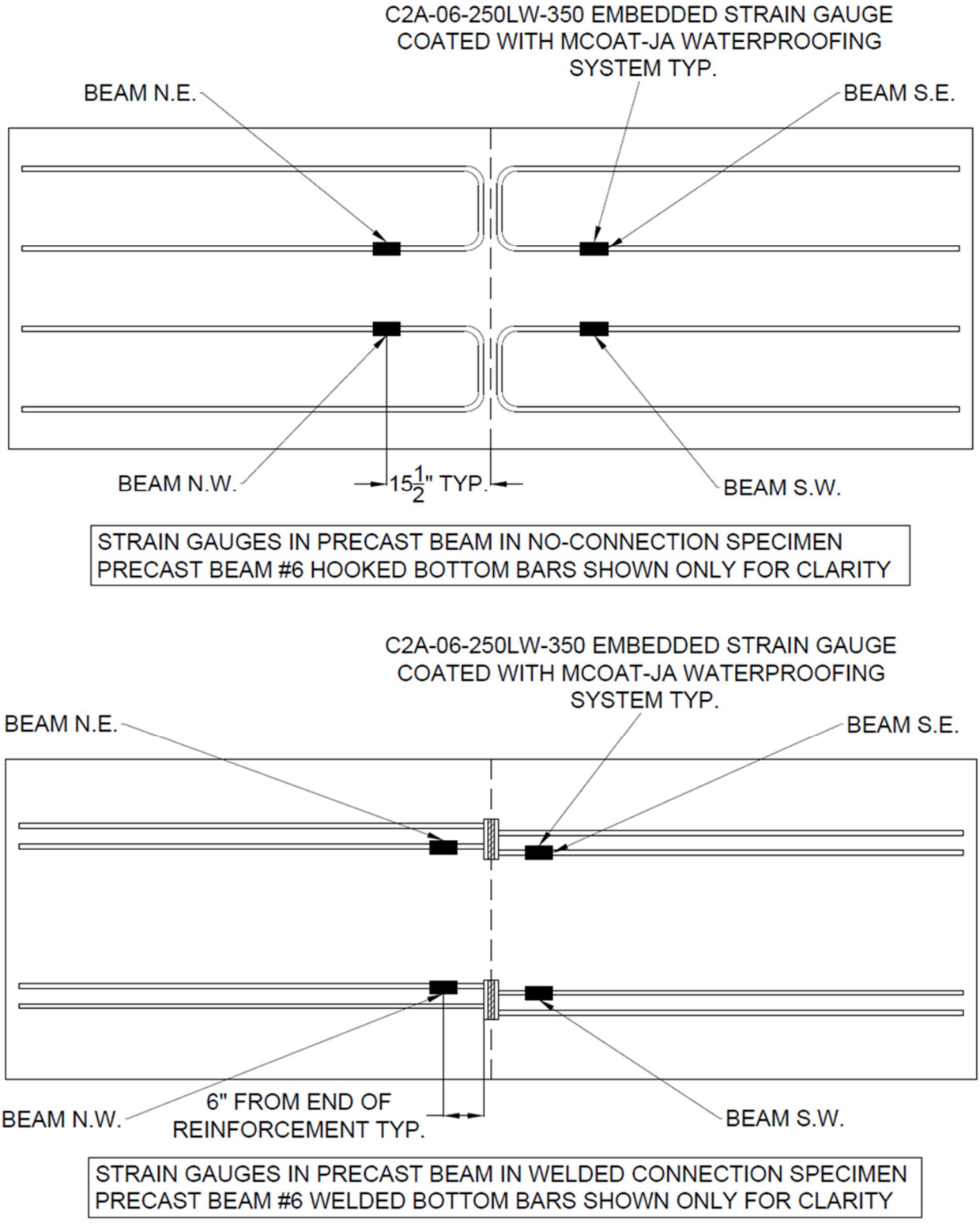

Figure 48 Plan view on precast beam portion of subassemblage, showing embedded strain gauge locations

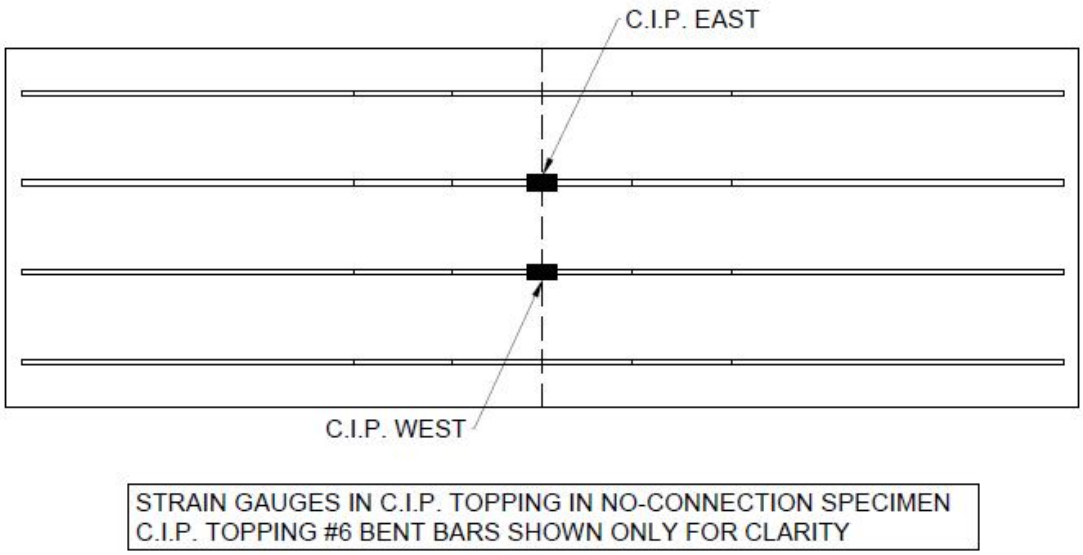

Figure 49 Plan view on C.I.P. topping portion of subassemblage, showing location of embedded strain gauges

The string pots were centered underneath the specimen and located at the supports, quarter points, and midspan of the beam. The string pots were attached to a steel plate using duct tape to provide a zero-reference point. The string was then extended and hooked to a screw with a circular magnetic base. This magnetic base was then attached to a thin piece of cold-formed steel that was glued to the underside of the test specimen using a Loctite 480 Instant Adhesive and Accelerator. This can be seen in Figure 50. The purpose of the string pots was to measure the displacements of the bearing pads at the supports, and the specimen displacements at the other locations. This was used to verify that composite action was achieved between the precast beam and the cast-in-place topping, and that the beam behaves monolithically rather than as two rigid bodies connected by a midspan pin joint. Figure 47 shows the locations and layout of the string pots.

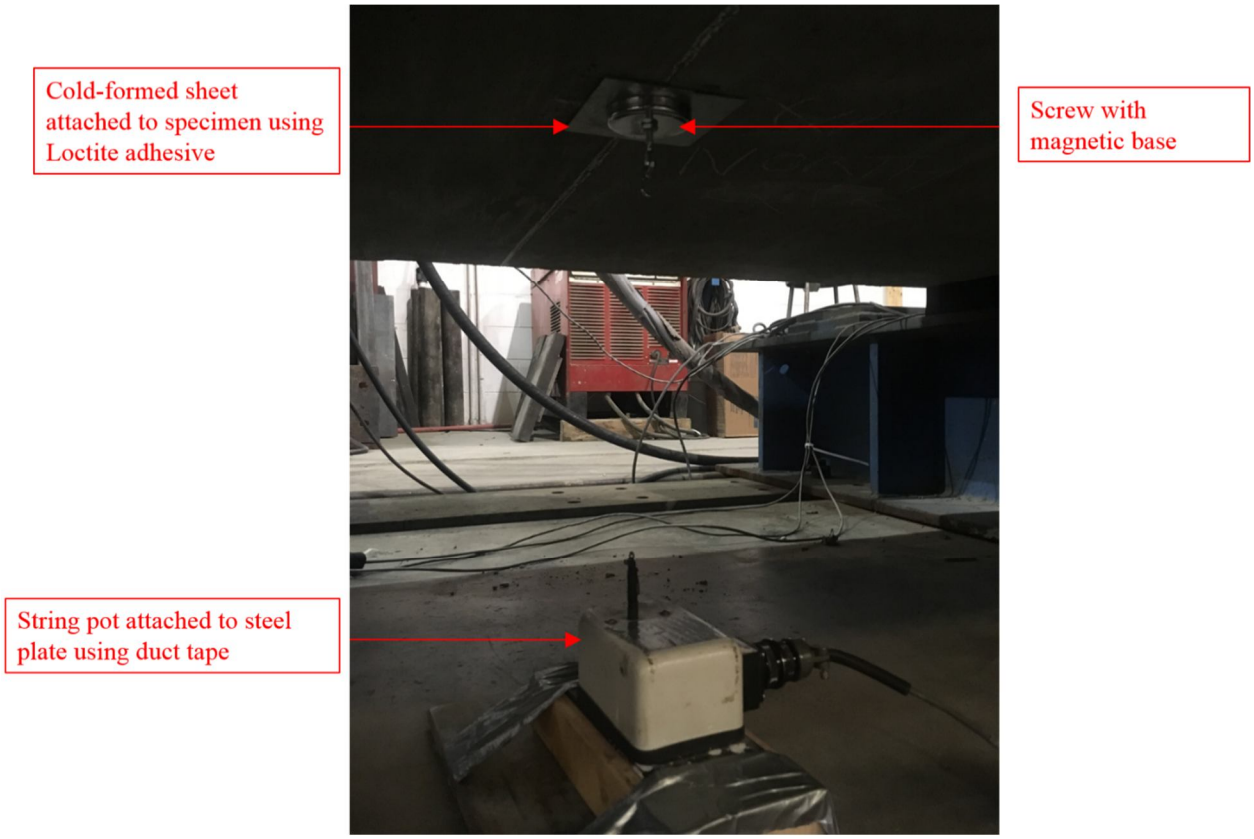

Figure 50 Typical string potentiometer set up

The LVDT's were placed on the tapered web portions of the specimen, and at the location of the joint between the two precast beams. A cylindrical pipe and steel collar setup was used to hold each LVDT. The pipe was attached to the concrete of the test specimen using the same adhesive mentioned in the previous paragraph. The LVDT was initially depressed using a small wooden block which was also glued to the specimen. Figure 51 shows the LVDT and wooden block in their final positions, ready for recording. The LVDT's attached to the joint region of the specimen measured the width of opening, if any, for the joint, while the LVDT's attached to the tapered web section measured slip along the interface between the two concretes. Opening of the joint during service loading would create cracks in the cast-in-place topping directly above the joint, while slip along the concrete surface interfaces would indicate inadequate surface roughening and result in a loss of composite action. Figure 46 shows the layout of the LVDT's on each side of the beam.

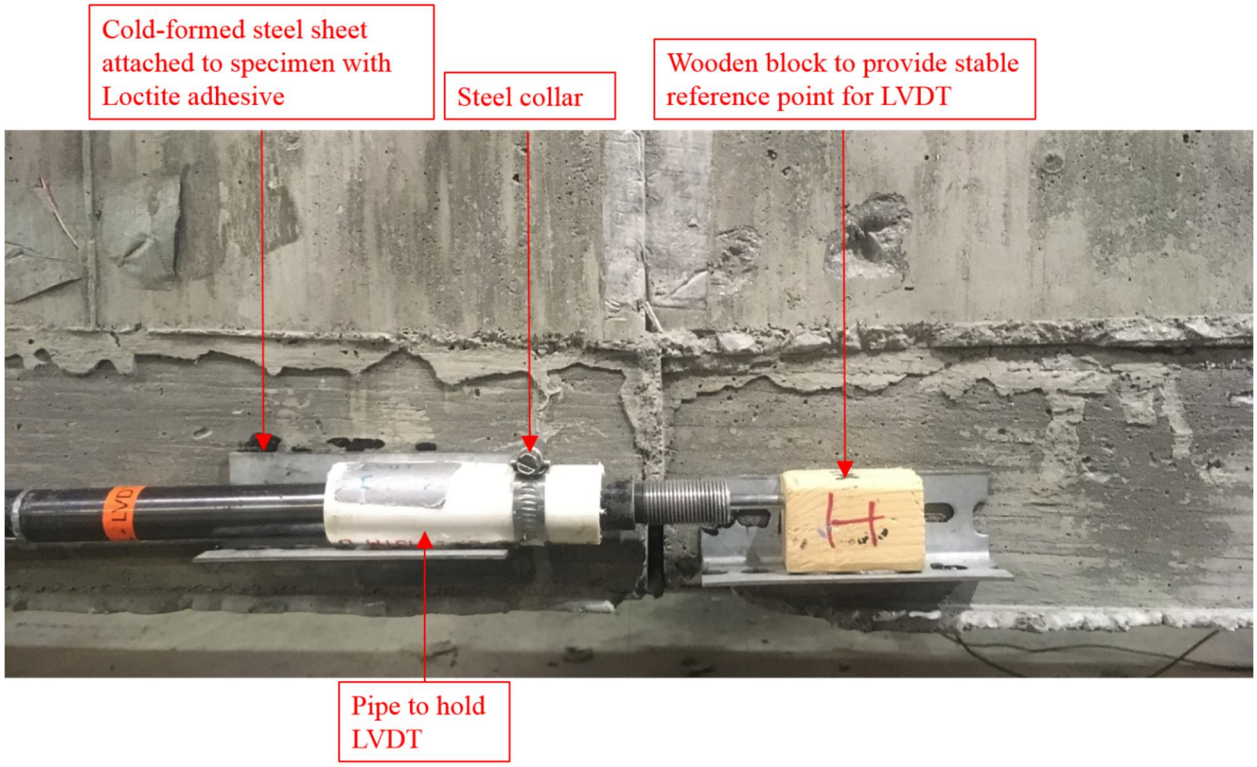

Figure 51 Typical LVDT setup

Embedded strain gauges were placed on the reinforcement in the precast beam, and on the bent reinforcement in the cast-in-place topping as shown in Figure 52. The strain gauges were placed using the VPG MBOND-200 adhesive and catalyst system, and waterproofed using the VPG MCOAT-JA coating system, and then covered with aluminum tape for additional protection. For the no-connection specimen this was important as the primary load transfer mechanism is via a non-contact lap splice between the bars in the precast beam, and the bent bars in the topping. For the welded connection, the importance of these gauges arises from an interest in the weld performance under cyclic loading. The locations of the strain gauges on their respective pieces of reinforcement can be seen in Figure 48 and Figure 49.

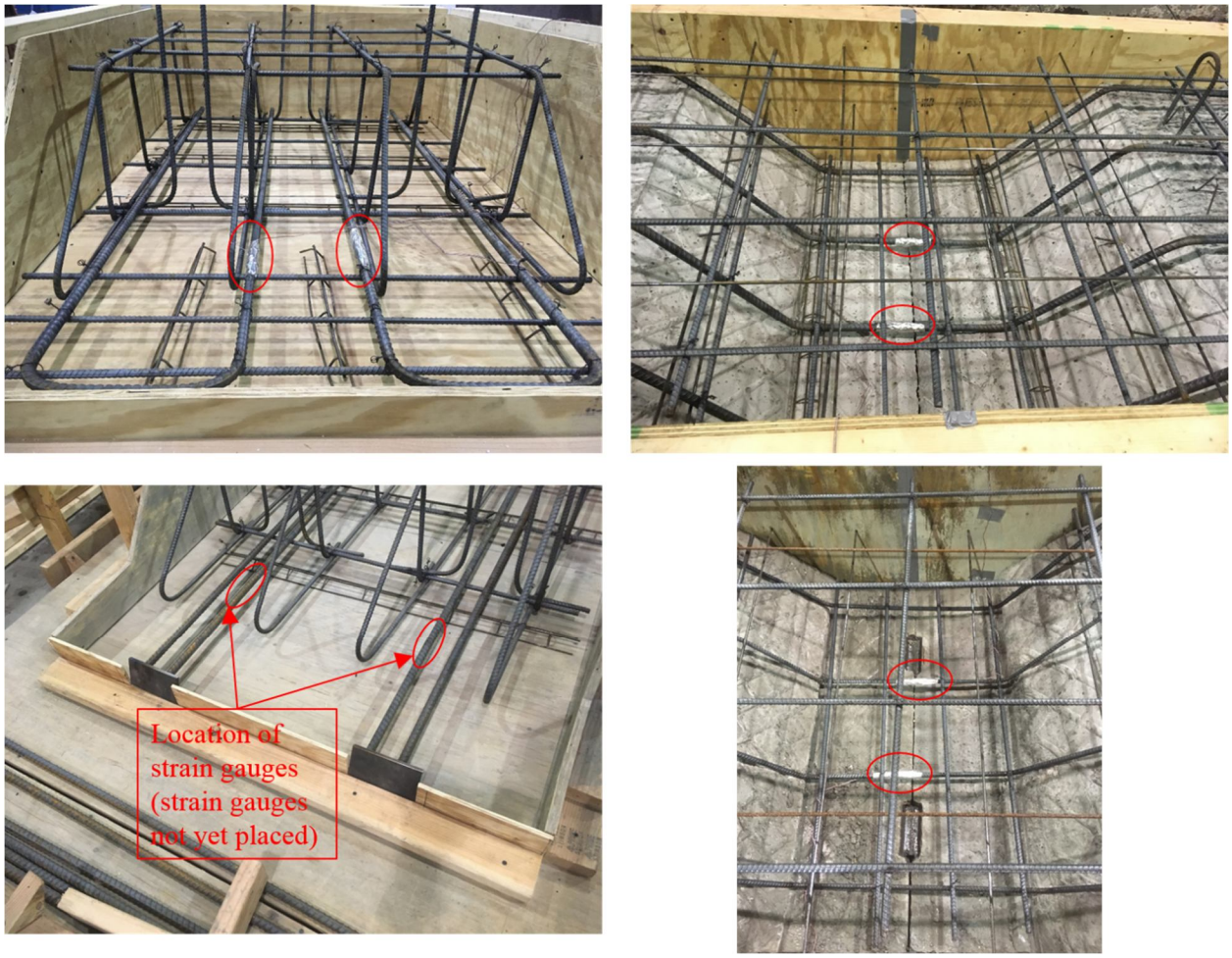

Figure 52 Strain gauges on no-connection beam reinforcement (top left), no-connection C.I.P. topping reinforcement (top right), welded connection beam reinforcement (bottom left), welded connection C.I.P. reinforcement (bottom right)

RESULTS

This chapter presents the results from the laboratory tests on the subassemblage specimens. The first part of this chapter presents the results of material testing on the concrete cylinders cast when concrete placements were carried out. Then the chapter describes the results from the two specimens which were tested; the first was the no-connection specimen, and the second was the specimen with the welded connection. Both specimens were fully instrumented, with the instrumentation discussed in the previous chapter.

Material Testing

During casting of the concrete for each of the specimens, concrete compressive strength cylinders were also made so that the strength gain over time of the concrete could be measured.

Figure 53, shows the strength gain over time of the concrete cast for the no-connection specimen precast beam. As can be seen, the concrete did not reach its specified 28-day compressive strength even after 53 days. The maximum strength attained by this concrete is equal to 4530 psi. This is described more in the section of this thesis entitled Issues Faced During Construction.

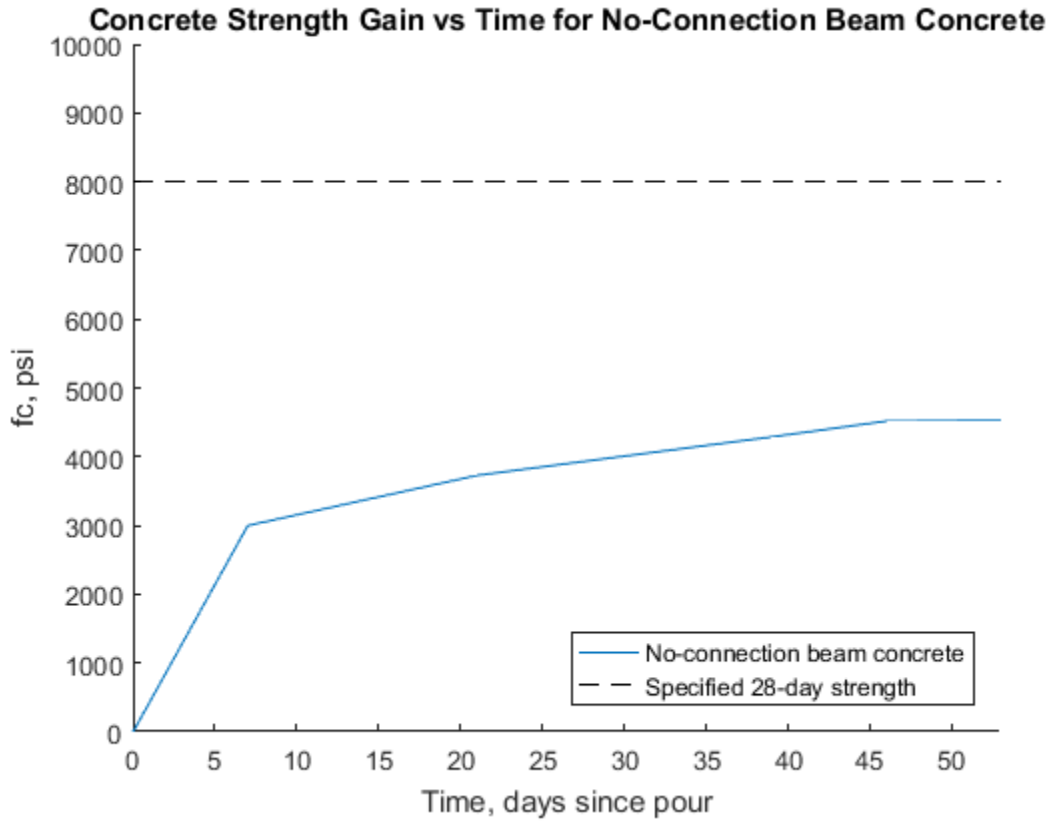

Figure 53 Plot showing concrete strength gain over time for the no-connection specimen, precast beam concrete

As can be seen in Figure 54, the C.I.P. topping concrete for the no-connection specimen reached its specified 28-day compressive strength after approximately 15 days. The maximum strength attained by the concrete based on the last compressive strength test carried out at 101 days was 6200 psi. It is important to note that the compressive strength of the C.I.P. topping is much greater than that of the precast beam concrete for the no-connection specimen.

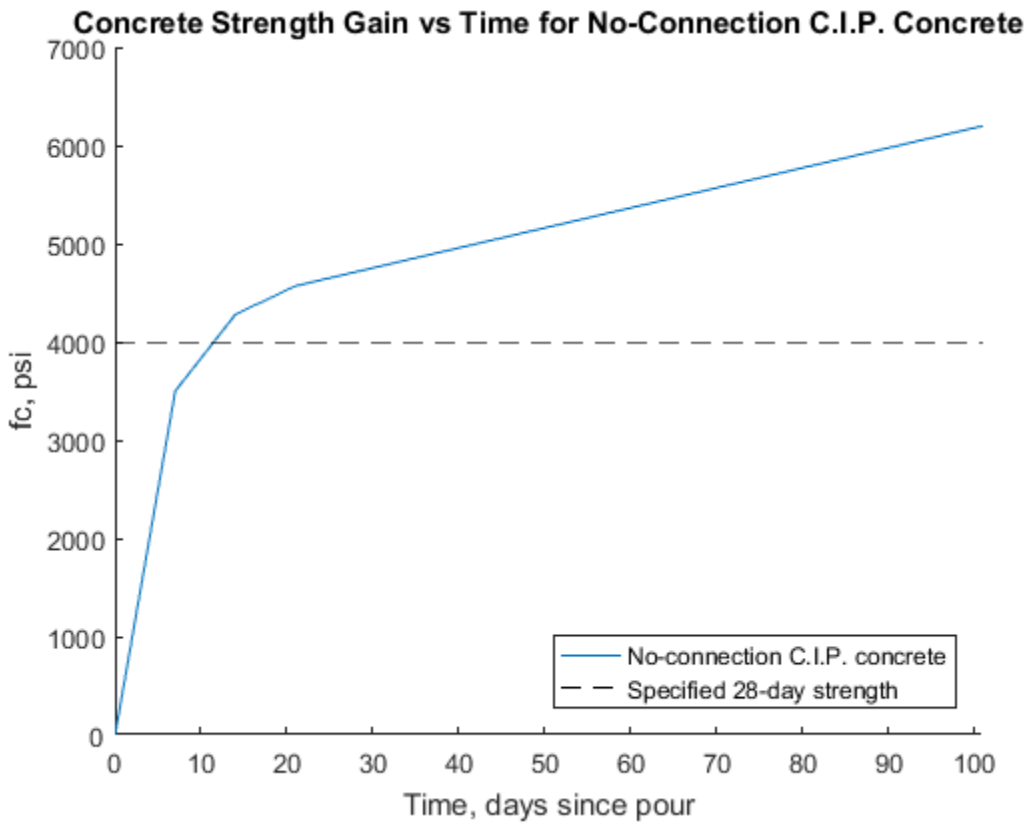

Figure 54 Plot showing concrete strength gain over time for the no-connection specimen, C.I.P. topping concrete

Figure 55 shows the concrete strength gain over time for the precast beam concrete of the welded connection specimen. The figure shows that the specimen had a specified 28-day concrete compressive strength of 8000 psi. It reached this value after 35 days – the time at which the final cylinders were tested to determine the strength of the concrete. The plot shows that at 28 days the actual strength of the concrete was close to, but had not quite reached, 8000 psi.

The same mix design number was specified for this concrete, as for the concrete used in the no-connection precast beam concrete (refer to Figure 53). However, it can be seen that for this concrete, the required strength was gained while this was not case for the no-connection precast beam concrete.

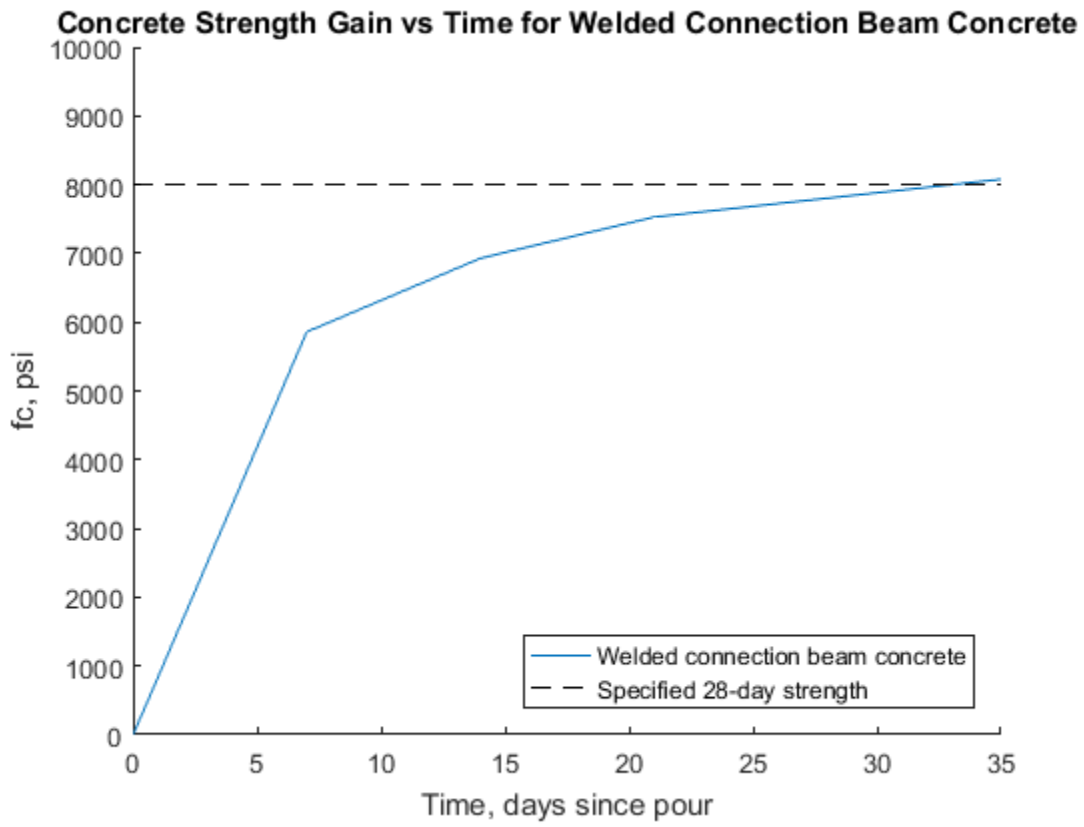

Figure 55 Plot showing concrete strength gain over time for the welded connection specimen, precast beam concrete

Figure 56 shows how the concrete placed for the welded connection specimen C.I.P. topping gained strength over time. It can be seen that the specified 28-day compressive strength for this batch of concrete was 4000 psi, and the concrete actually attained a value of almost 4500 psi after 28 days. The maximum compressive strength of the concrete measured based on cylinder breaks at 30 days was 4560 psi.

The same mix design number for this batch was provided to Conrock as for the concrete used in the no-connection specimen C.I.P. topping concrete. This batch of concrete did not reach the strength that was reached for the no-connection specimen, however it still surpassed the required 4000 psi compressive strength.

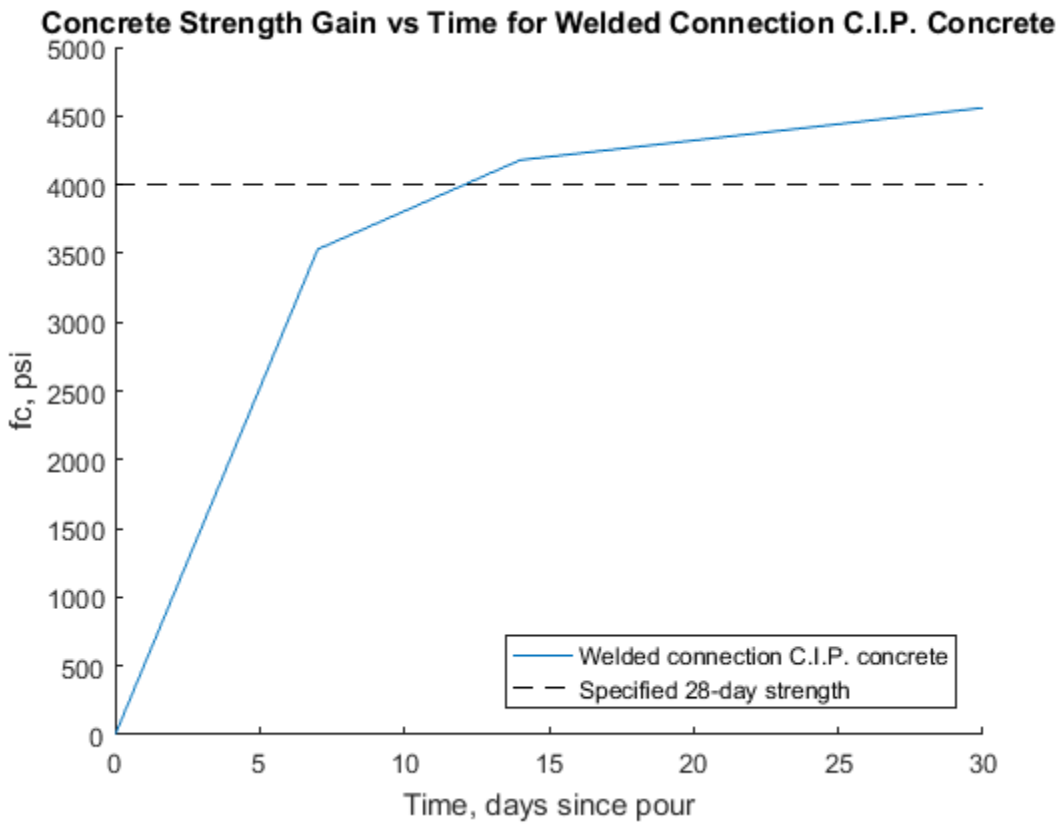

Figure 56 Plot showing concrete strength gain over time for the welded connection specimen, C.I.P. topping concrete

No-Connection Specimen

Results from Cyclic Load Test

Based on the static tests carried out at 200000 cycle intervals during the cyclic testing, no deterioration in performance of the specimen was observed. No visible cracks were formed, and all instrumentation results were consistent. The complete results of each piece of instrumentation can be seen in the tables provided in (Appendix G – Results Tables for No-Connection Specimen).

Table 10, shows that for each test over the total number of cycles, the range of values recorded by each string pot was relatively small (within 1/20 in.) except for the range of values recorded by the string pot located at the north support which reached a value of 0.12 in. Note that in Table 10, because more negative values indicate more displacement, the label maximum displacement occurs with the minimum recorded value and vice-versa. Therefore, the table indicates that the maximum recorded displacement occurred at the north midspan string pot, and had a magnitude of 0.048 in. Additionally, between 0.02 in. and 0.04 in. of the measured

displacement occurred at the support locations. At the midspan location, the difference in deflections between the south and north beam was only 0.006 in. which falls within the string pots accuracy (explained more in Discussions). Figure 57 shows a plot of the deflection recorded at maximum load during the static test, versus the position along the beam overlaid for every monotonic test. As can be seen, for every static test the results do not vary greatly, except for the deflection measured at the north support which reaches a positive 0.08 in. value. This occurred during the static test after the 2900000 cycle. Additionally, for tests after 300000 cycles, the values at the south quarter span point do not follow the expected deflected shape of the beam and instead show deflection in the opposite direction. Upon inspection of the string pots at these locations (south quarter, and north support), it became clear that these results were due to a physical malfunction of the string pot. The figure shows a maximum deflection of approximately 0.048 in. occurring at midspan. This equates to approximately L/36000. The graph also shows that near midspan, the deflections on the two sides of the joint are similar; the precast beam on one side does not deflect significantly more than the beam on the other side. Additionally, Figure 57 indicates that most of the service level deflections occurred at the supports (up to approximately 0.03 in.), and the shape of the plot generally follows the shape of the elastic curve of a simply supported beam subjected to two point loads at its quarter point locations.

Table 10 Maximum, minimum and range of string pot displacements at maximum load, for all static load tests

String Pot Displacements at Maximum Load, in.						
	S. Sup	**S. Qtr**	**S. Mid**	**N. Mid**	**N. Qtr**	**N. Sup**
Maximum	-0.024	-0.013	-0.028	-0.029	-0.027	0.082
Minimum	-0.032	-0.038	-0.042	-0.048	-0.043	-0.040
Range	0.008	0.025	0.013	0.018	0.016	0.122

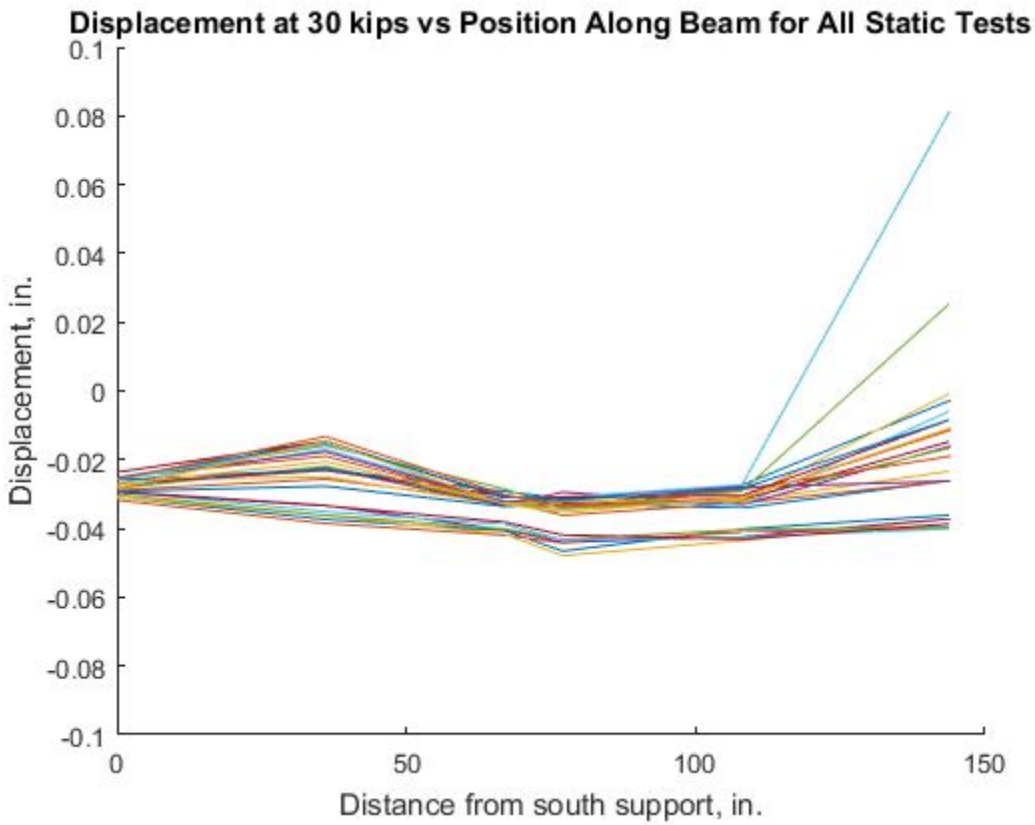

Figure 57 Plot of displacement vs position along beam for all static load tests for no-connection specimen

Figure 58 shows a plot of the load applied to the test specimen by the actuator, against the midspan deflection values recorded by the north midspan string pot at the initial static load test prior to cycling. Figure 59 shows the same plot, at the final static load test after completing 3650000 cycles. For both of these plots, the average of the displacements recorded at each support has been subtracted out. As can be seen in both figures, the behavior of the specimen is approximately linear elastic and can be approximated by the linear best fit lines shown in both figures. Additionally, it can be observed that the stiffness of the specimen seems to have deteriorated over time, demonstrated by the fact that the slope of the best fit line at 3650000 cycles, is lower than the value at 0 cycles. This apparent loss of stiffness is addressed more in the Discussions section of this thesis.

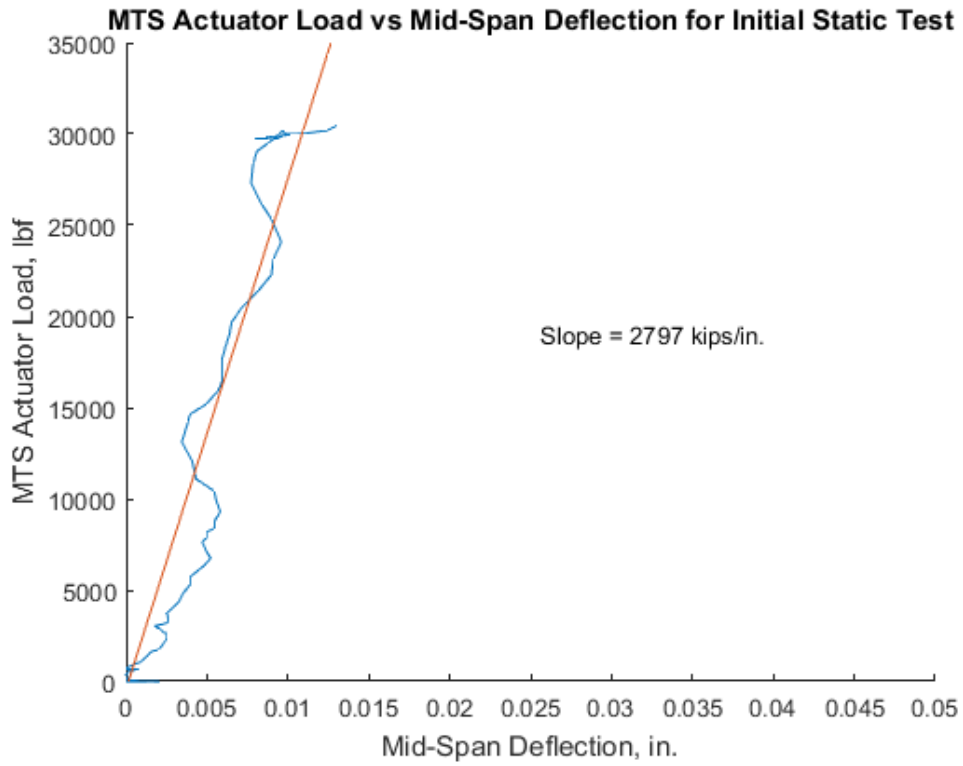

Figure 58 Plot of MTS actuator load versus midspan deflection (north midspan string pot) for the initial static test at 0 cycles

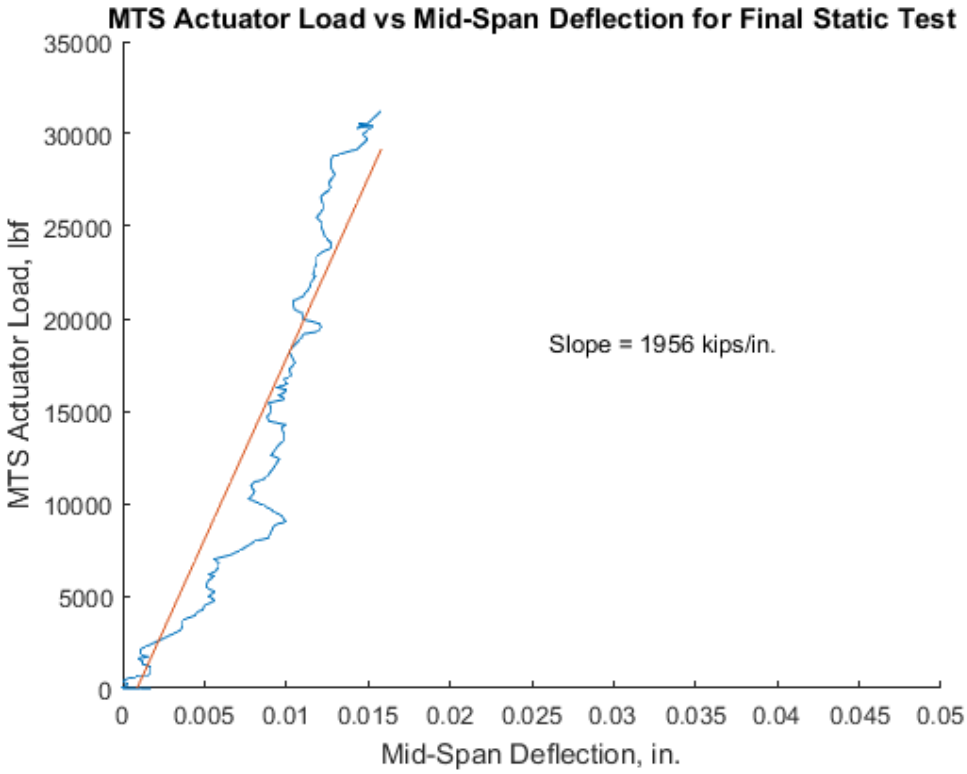

Figure 59 Plot of MTS actuator load versus midspan deflection (north midspan string pot) for the final static test at 3650000 cycles

The maximum, minimum, and range of values of LVDT readings over all of the static load tests for each of the LVDT locations can be seen in Table 11. The results show the same maximum and minimum values for all static tests. The range of readings for each LVDT recording data was zero, indicating no cracking or slipping of the interface during cycling. Figure 60 and Figure 61 show the applied loads graphed against the LVDT measurements at the east and west joint locations during the first and final static load tests. Both of the plots indicate that the magnitude of joint opening at the service level loading is insignificant (less than 1/1000 in.). Although the plots do indicate that there is more opening during the final static test, this difference is negligible due to the minute magnitudes of the measurements. Additionally, both plots indicate that upon unloading of the specimen, there are negligible residual joint openings – they effectively return to zero. Comparison of the two figures also indicates that the largest opening occurred in the west web location rather than the east.

Table 11 Maximum, Minimum, and Ranges of LVDT Slip Readings During Cyclic Testing

LVDT Reading, in.						
	Northeast Web	**East Web**	**Southeast Web**	**Northwest Web**	**West Web**	**Southwest Web**
Maximum	0.002	0.012	0.004	0.004	0.750	0.002
Minimum	0.001	0.011	0.003	0.003	0.750	0.002
Range	0.000	0.001	0.000	0.000	0.000	0.000

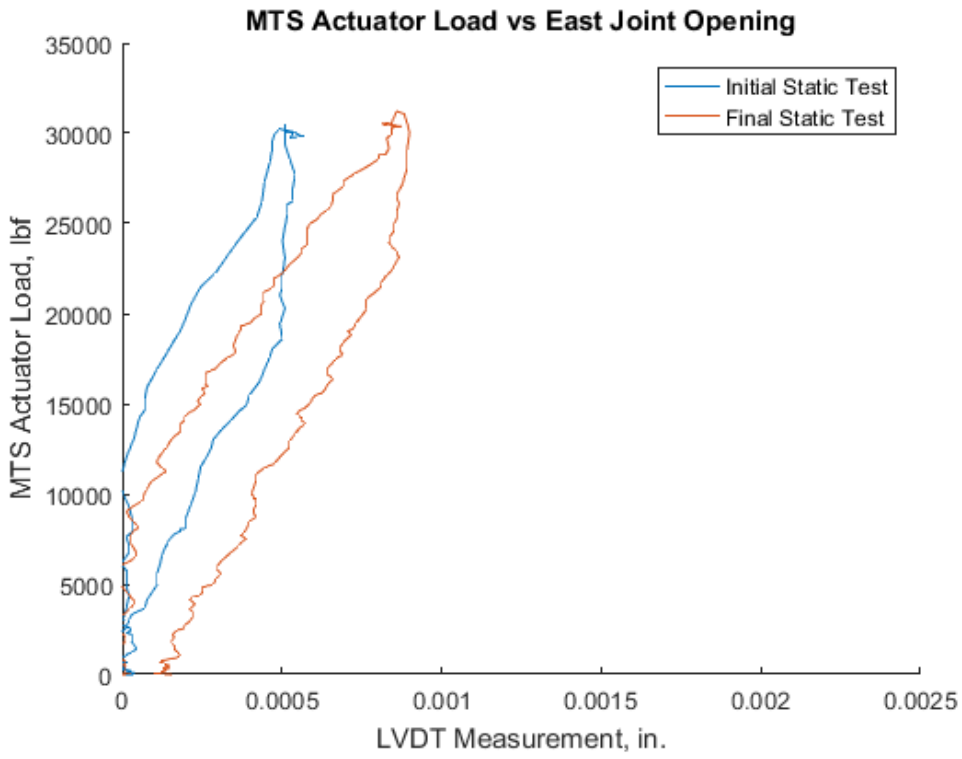

Figure 60 Plot of applied MTS actuator load against recorded LVDT measurements at the eastern joint location for the static load test at 0 cycles (initial) and at 3650000 cycles (final) for the no-connection specimen

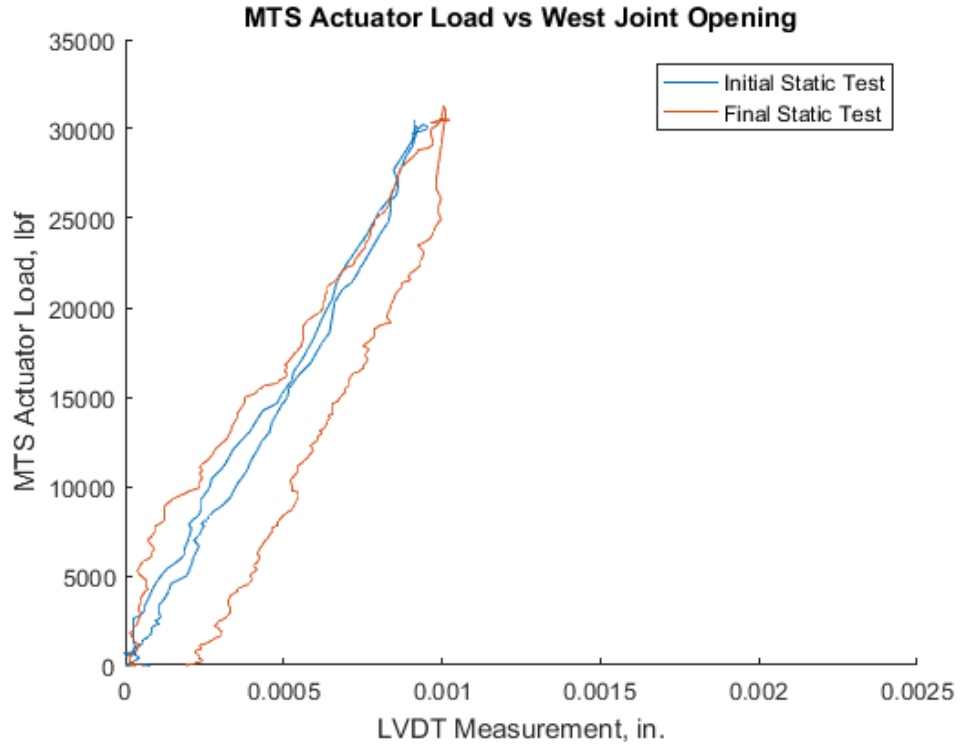

Figure 61 Plot of applied MTS actuator load against recorded LVDT measurements at the western joint location for the static load test at 0 cycles (initial) and at 3650000 cycles (final) for the no-connection specimen

The maximum, minimum, and range of values for strain gauge readings for all of the static load tests carried out can be seen in Table 12 below. It should be noted that the C.I.P. west strain gauge failed to record any information and is therefore not displayed in the following tables or figures. The maximum range of strain readings occurred in the C.I.P. topping rebar and was only 5 με. The maximum recorded strain was 44 με which occurred in the C.I.P. topping rebar. Figure 62 and Figure 63 plots actuator loads against strains for the strain gauges in the east side of the specimen. The plots show that for any applied load, the strain in the C.I.P. topping reinforcement is significantly higher than the strain in the precast beam reinforcing bars on either side of it. Additionally, it shows that the strains in the beam reinforcement differ by insignificant amounts. Figure 64 overlays the plots in Figure 62 and Figure 63. It shows that between the initial test and the final test, the strain gauge readings do not vary significantly.

The results in Table 12 and Figure 62 to Figure 64 also show that the observable strains during cyclic testing remain below the strain which would cause cracking in a linear-elastic concrete material. This relates well to the visual observations carried out during cyclic testing as no cracking was observed. This is described more in the Discussions section of this thesis.

Table 12 Maximum, minimum, and range of strain values for maximum loading during static test

Strains, με					
	Northeast Beam	**C.I.P. East**	**Southeast Beam**	**Northwest Beam**	**Southwest Beam**
Maximum	24	44	21	24	19
Minimum	21	39	19	20	16
Range	3	5	2	4	3

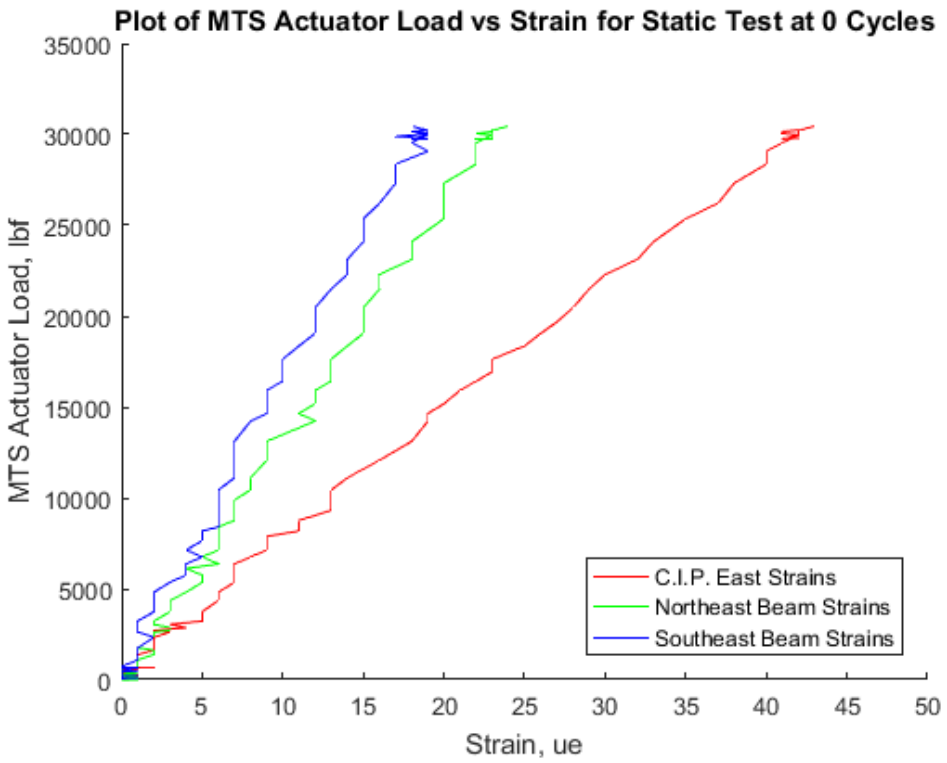

Figure 62 Plot of strain versus MTS actuator load for the initial static test, for the strains in the C.I.P. east side rebar, and the precast beam east side rebar

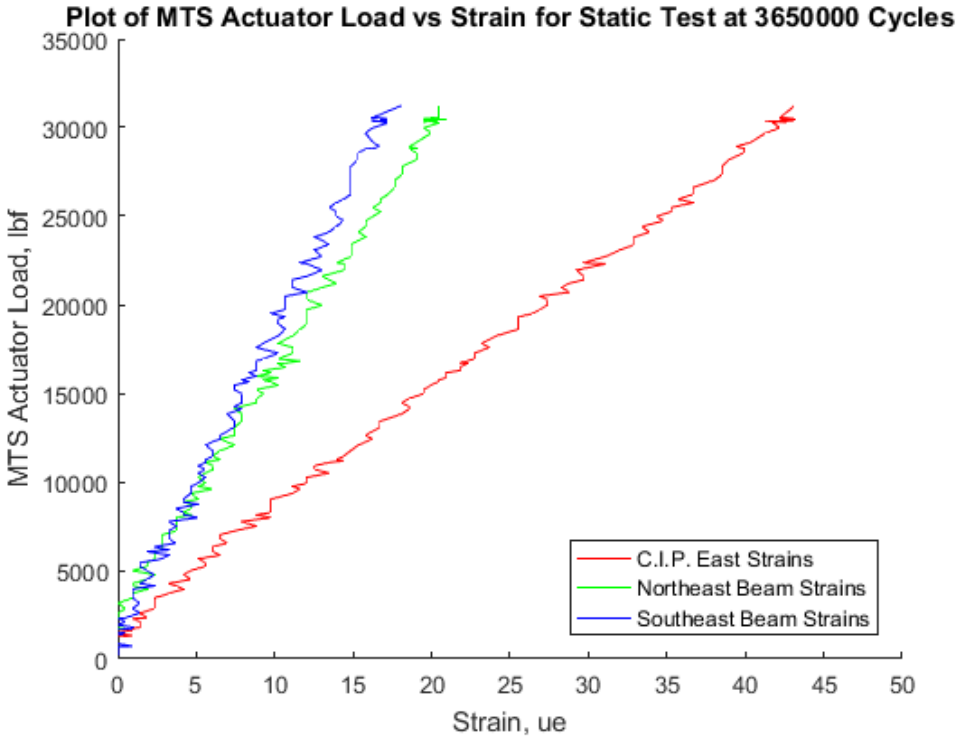

Figure 63 Plot of strains versus MTS actuator load for the final static load test, for the C.I.P. east side rebar, and the precast beam east side rebar

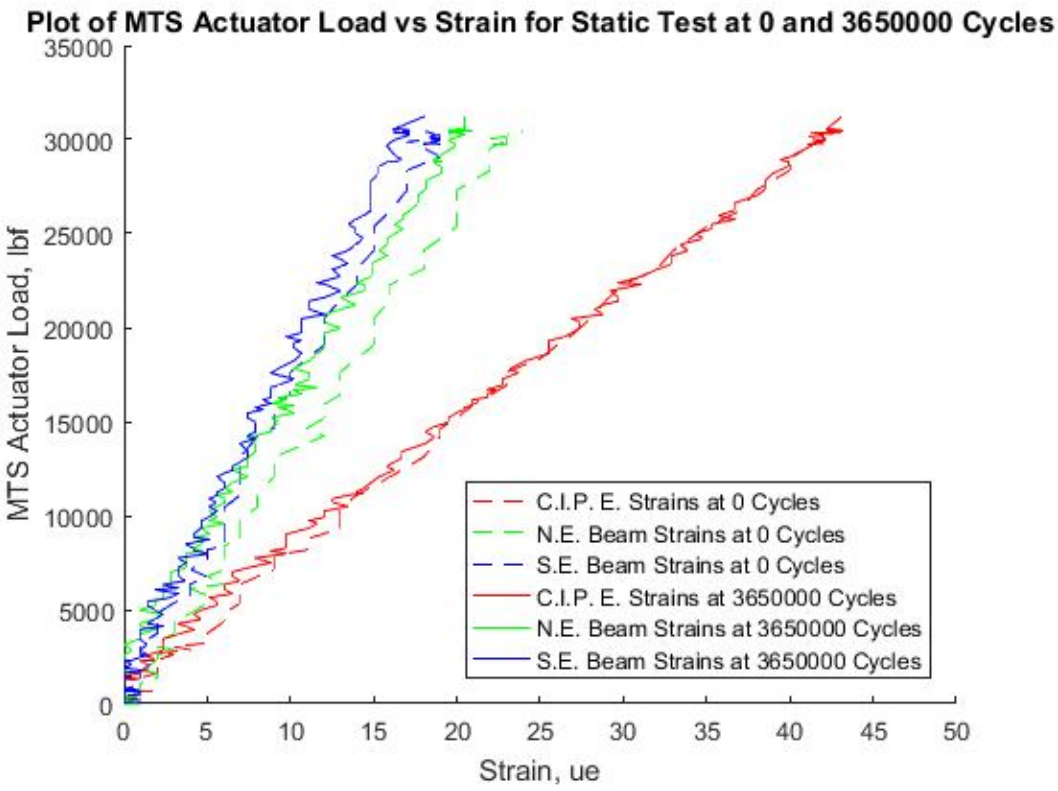

Figure 64 Plot of strain against MTS actuator load for the initial and final static tests for strain gauges in the C.I.P. topping and precast beams on the east side of the specimen

Results from Monotonic Test to Failure

During the monotonic test, at every load increment the specimen was inspected visually and cracks were noted and mapped. As can be seen in Figure 65, the first cracks were observed at a load of 40 kips and occurred at the interface between the two concretes cast at different times. These cracks began on the interface located on the “south” beam. Cracking at this load was small (less than 0.005 in.), and no flexural cracks were observed in the beam concrete (only cracks at the surface interface formed).

Figure 65 Monotonic load test to failure - cracking at 40 kips actuator load

Figure 66 shows the results of visual observations when the load increment was taken to 50 kips. At this level of loading, the images show that cracking at the surface interface between the two concretes propagated. In addition to this, flexural cracks began to become noticeable in the precast beam concrete. At this stage there was still no flexural cracking occurring in the cast-in-place concrete section in the joint region.

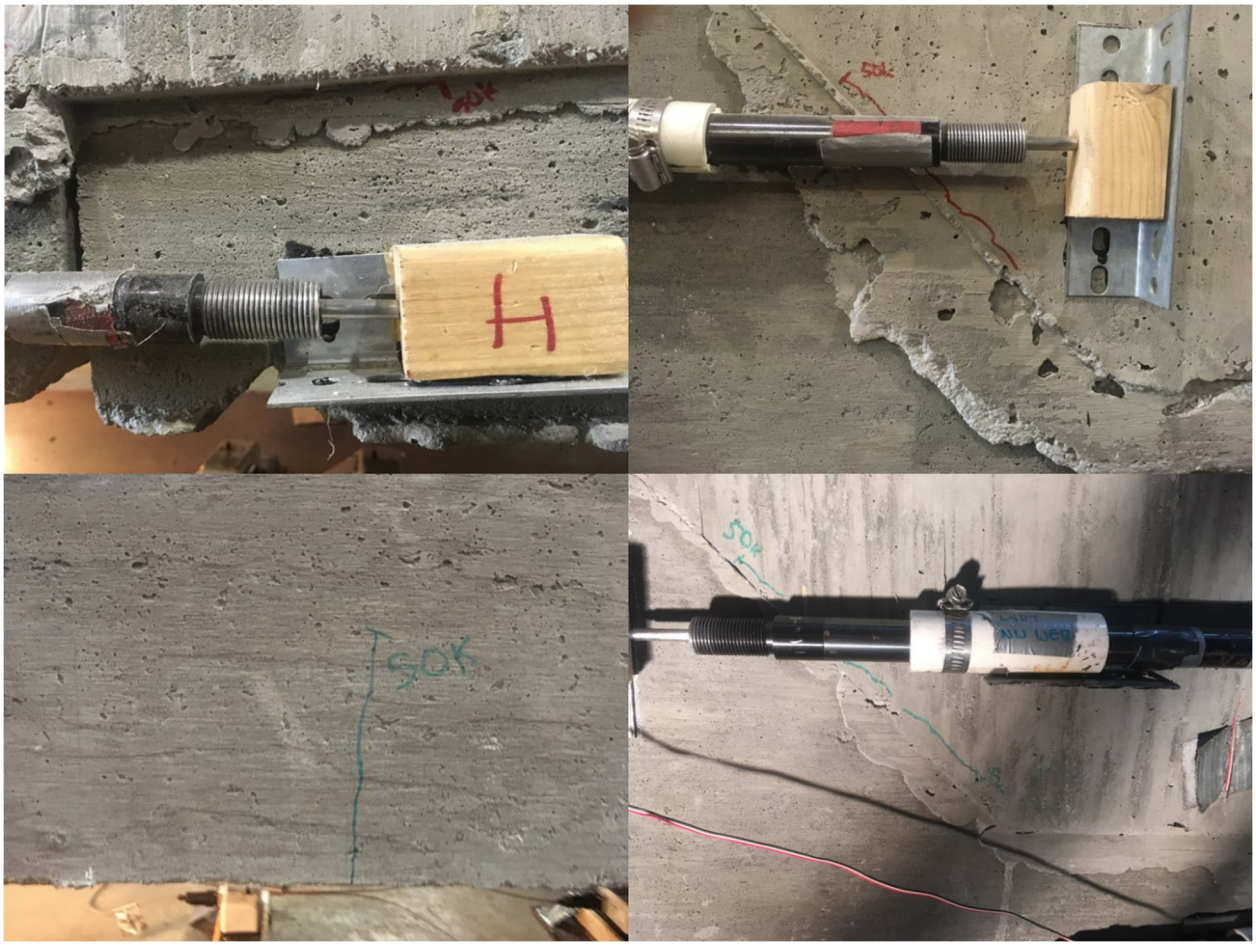

Figure 66 Monotonic load test to failure - cracking at 50 kip actuator load

Figure 67 shows results of the visual observation taken at a 60 kip load increment. As can be seen, the cracking at the surface interface of the two concretes, near the joint location propagated and increased in length. Additionally, at this level of load, cracking began to occur at the surface interface between the two concretes at the top of the extended web region, and at the tapered web location in these subassemblages. In addition to this, cracks in the C.I.P. topping concrete became observable near the region of the joint. The cracking in the C.I.P. topping propagated upwards through approximately ½ of the depth of the topping.

Figure 67 Monotonic load test to failure - cracking at 60 kip actuator load

At an actuator load of 63 kips, the specimen failed. The plane of failure was along the surface interface between the precast beam and C.I.P. topping concrete at the south beam location on both the east and western side. Crack openings were large. At the top of the tapered web region, rather than continuing along the surface interface plane at the extended web region, the crack turned up into the C.I.P. topping and went through over ½ depth of the 7.5 in. thick overlay. This failure can be seen in Figure 68.

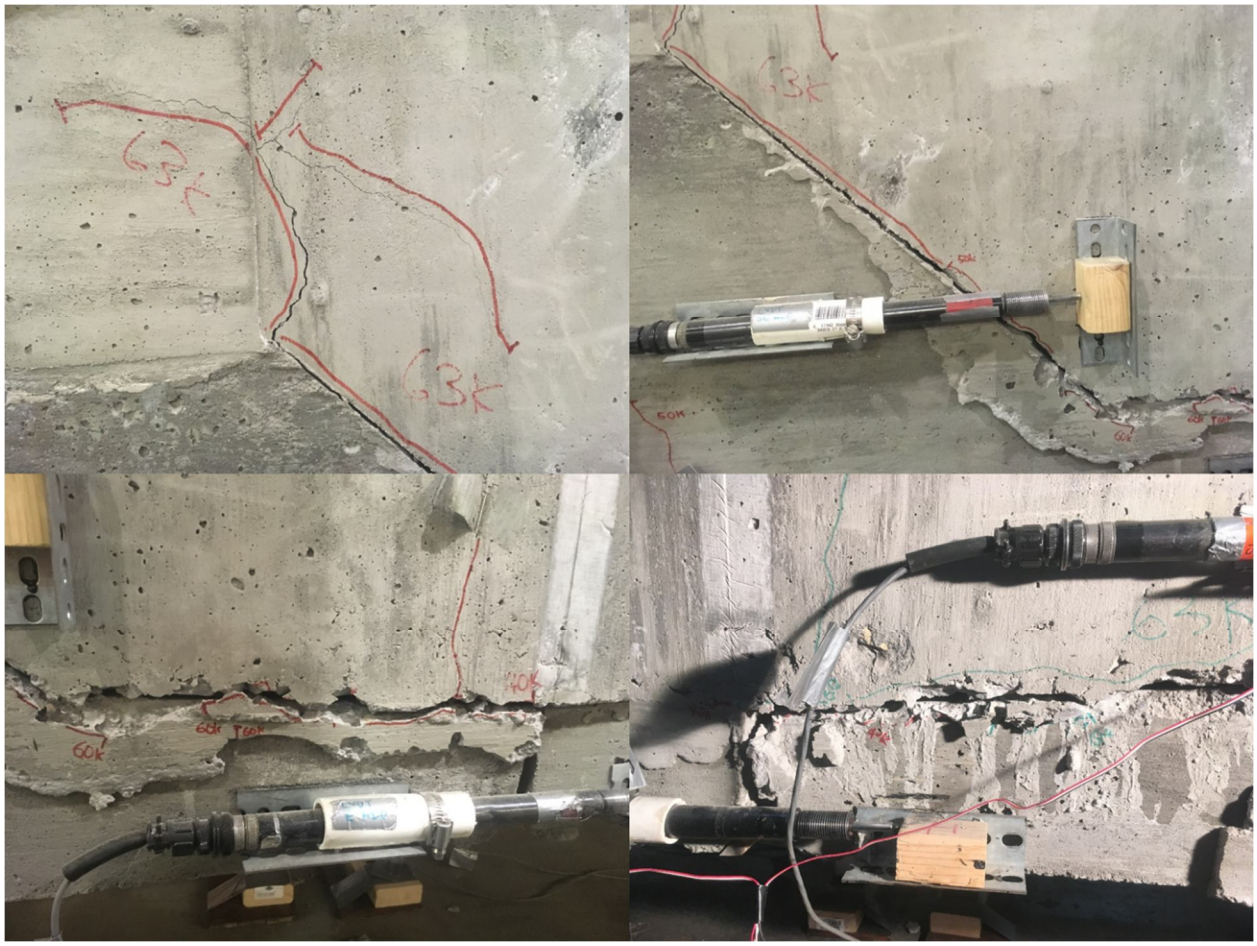

Figure 68 Monotonic load test to failure - cracking at 63 kip actuator load (failure)

Figure 69 shows the result of deflections within the span at each of the load increments. The plots clearly show a trend of increasing deflections up until the failure of the specimen. In addition to this, the figure shows that the deflections of the string pots on either side of the centerline of the member are approximately equal to each other. It should be noted that upon completion of the testing, and inspection of the string pot at the south quarter point, it was noted that the string pot was not functioning properly. Therefore, in the plots shown, the false data from the south quarter point string pot (36 in. away from the southern edge of the beam) are not shown.

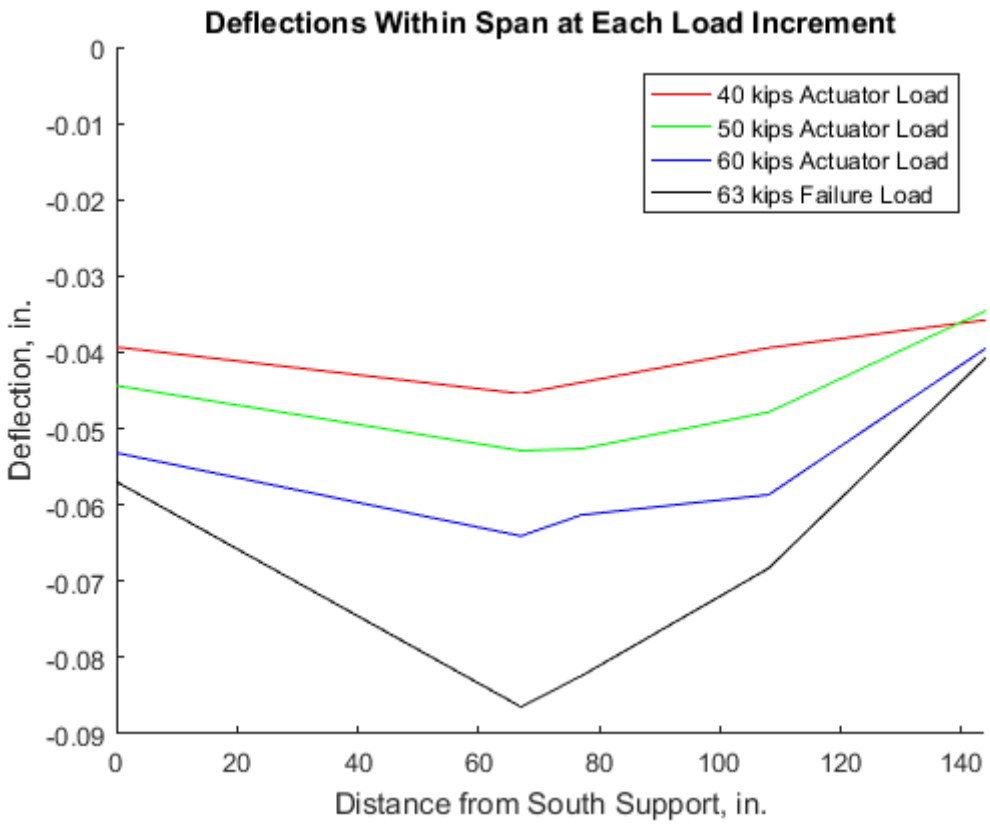

Figure 69 String pot deflection recordings against position within span for each load increment during monotonic load test to failure

Figure 70, shows the relationship between the MTS actuator load and midspan displacements recorded by the north midspan string pot during monotonic testing to failure. For this figure, an average of the displacements at each support has been subtracted from the midspan deflection value. As can be seen, displacements increase linearly with load until failure occurs at 63 kips. The maximum displacement recorded at this load attains a value of 0.031 in. downwards. This value is confirmed in Figure 69 as well if the support deflections are subtracted from the midspan deflection. The behavior of the specimen, its failure mode and lack of ductile response indicated by the load-displacement curve is described more in the Discussions section of this thesis.

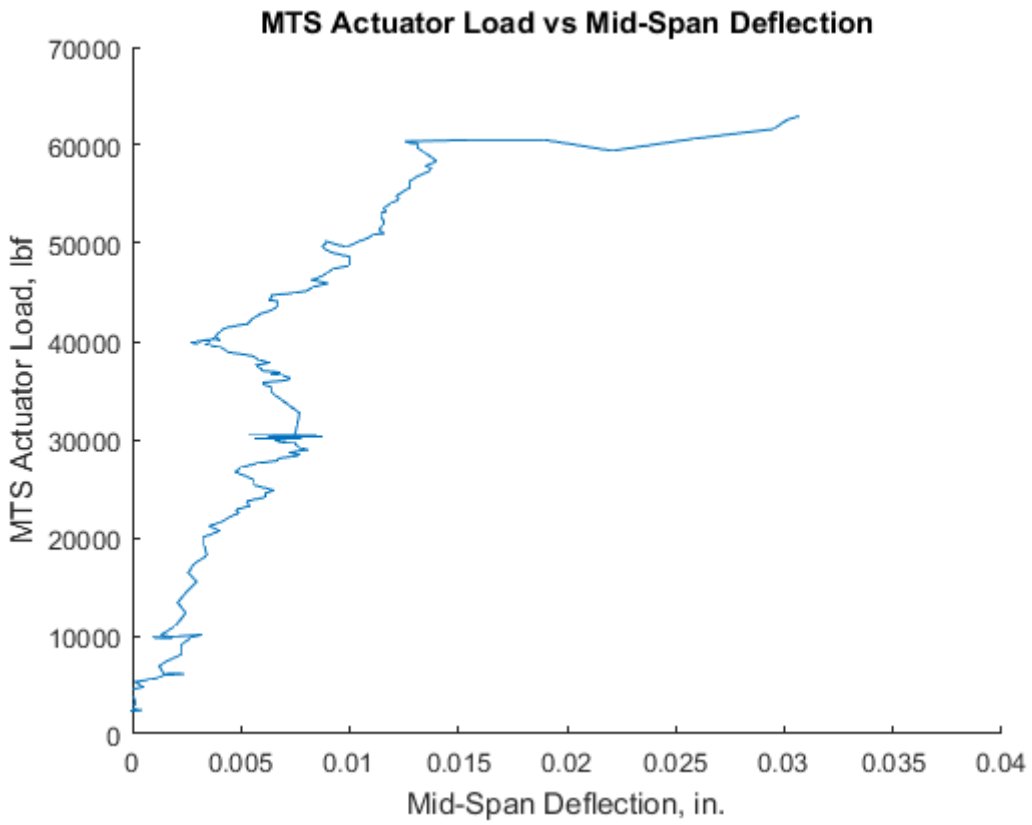

Figure 70 Plot of MTS actuator load vs midspan deflection during failure testing

The recorded strain values during the failure test for each load increment are shown in Table 13 below. The results show a trend of increasing strain at every location up until the failure load of 63 kips.

Both Table 13 and Figure 71 show a large jump in the values of strain in the C.I.P. topping when specimen failure is reached. Additionally, Table 13 shows that between 50 kips and 60 kips of load, there is a significant increase in the strain reading in the C.I.P. strain gauge and a smaller increment in the strain gauges in the precast beams on the east side of the specimen. This is discussed more in the Discussions section of this thesis.

It is important to note that at a load of 60 kips, where there is a significant increase in the values of strain, first cracking in the C.I.P. topping appears as is shown in the visual results described above.

At the failure load of 63 kips, it is noted that cracking, but not yielding, is indicated by the strains in the reinforcement being less than the yield strain of 2070 με.

Table 13 Recorded values of strain for each load increment during monotonic test to failure

Target Load for Increment, kips	Recorded Load, kips	Strains, με				
		Beam Northwest	Beam Southwest	C.I.P. East	Beam Northeast	Beam Southeast
40	40.3	32	27	60	31	25
50	50.2	39	31	85	38	30
60	60.5	47	35	141	44	31
70	63.0	50	26	1075	46	23

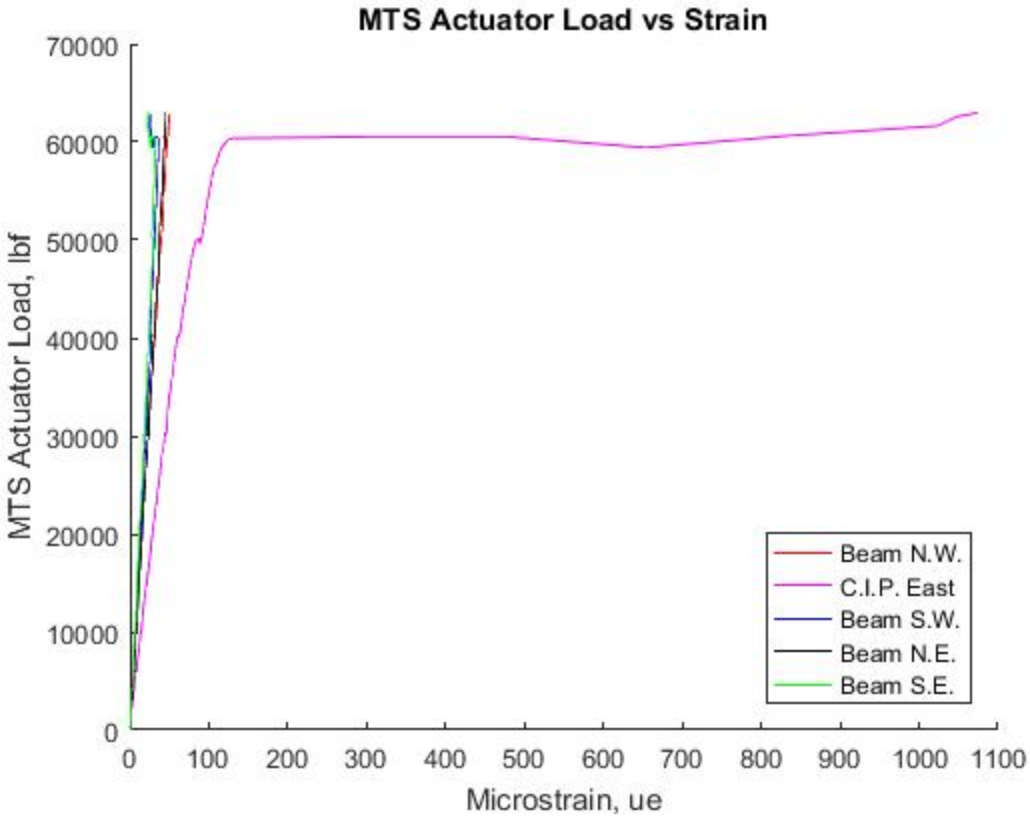

Figure 71 Plot showing MTS actuator load versus strains at different locations during failure test

Figure 72 to Figure 74 show the MTS actuator load plotted against corresponding LVDT measurements for the south tapered web, the midspan joint, and the north tapered web locations correspondingly. All of the data below is presented up to the failure load of 63 kips, at which point the interface between the precast beam and C.I.P. topping at the south end of the beam debonded. Past this point, LVDT data became incoherent and therefore is not presented here.

Looking at Figure 72 we see that at a load of 40 kips, the southwest beam-topping interface begins to slip. This is coincident with the first cracks appearing at this interface location. At 50 kips, there is more slippage occurring which also agrees with visual observations of crack propagation along the interface between the two concretes. At 60 kips of load, the southeast interface undergoes additional slip, while the southwest interface reduces in slip up to the failure load of 63 kips. A possible explanation of this behavior is included in the Discussions on LVDT results.

Figure 73 shows that as load increases on the specimen, the east and west joint show similar behavior up to a load of 40 kips, where first cracking occurs and slippage at the surface interface is noted in the southwest beam-topping tapered web location. From zero load up to 40 kips, both joints behave linearly, and open approximately 0.001 in. At 40 kips, the figure shows approximately 0.001 in. of additional opening in the east joint, while the west joint does not undergo any significant additional deformation. The behavior of both joints then goes back to being linear until 50 kips, where both joints undergo an additional small amount of opening. Their behavior is then linear again, up to 60 kips, where both joints begin to open significantly until failure at which point the west joint has opened by 0.014 in. and the east joint by 0.018 in.

Figure 74 shows that as applied load increases, the LVDT at the interface between the two concretes on the northeast side of the beam records a slowly but steadily increasing interface slip. No significant jumps in slip are noted by this LVDT. On the northwest side of the beam however, there is a large amount of slip occurring at a load of 50 kips – approximately 0.002 in. The slip at this surface then stabilizes until 60 kips, and between 60 and 60 kips, there is a slight increase in the amount of slip.

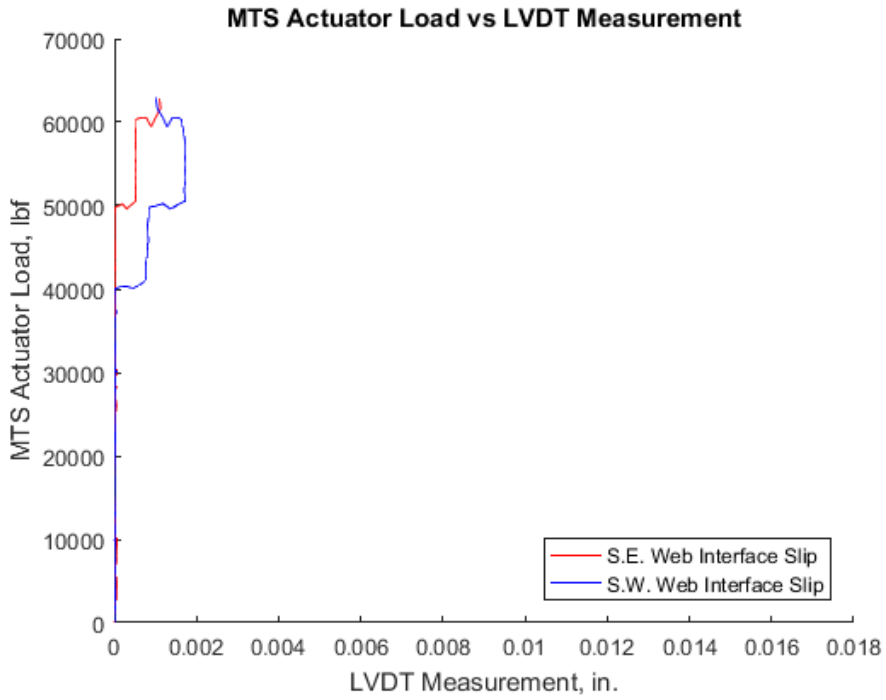

Figure 72 Plot of load versus LVDT slip measured at the southeast and southwest precast beam-C.I.P. topping interface for the no-connection specimen

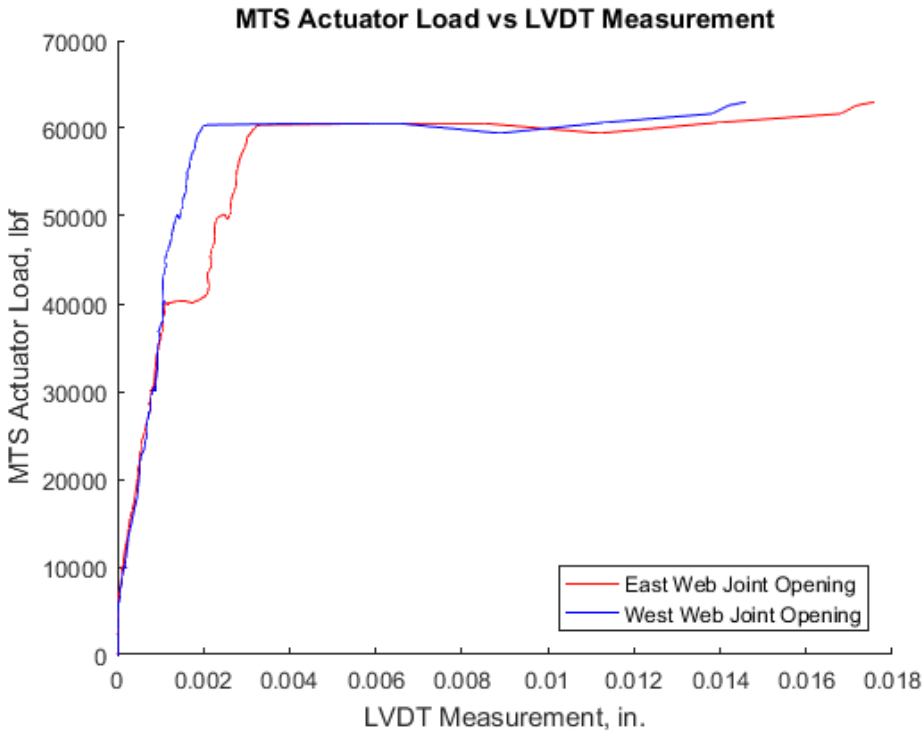

Figure 73 Plot of load versus joint opening measured by LVDT's at the east and west joint for the no-connection specimen

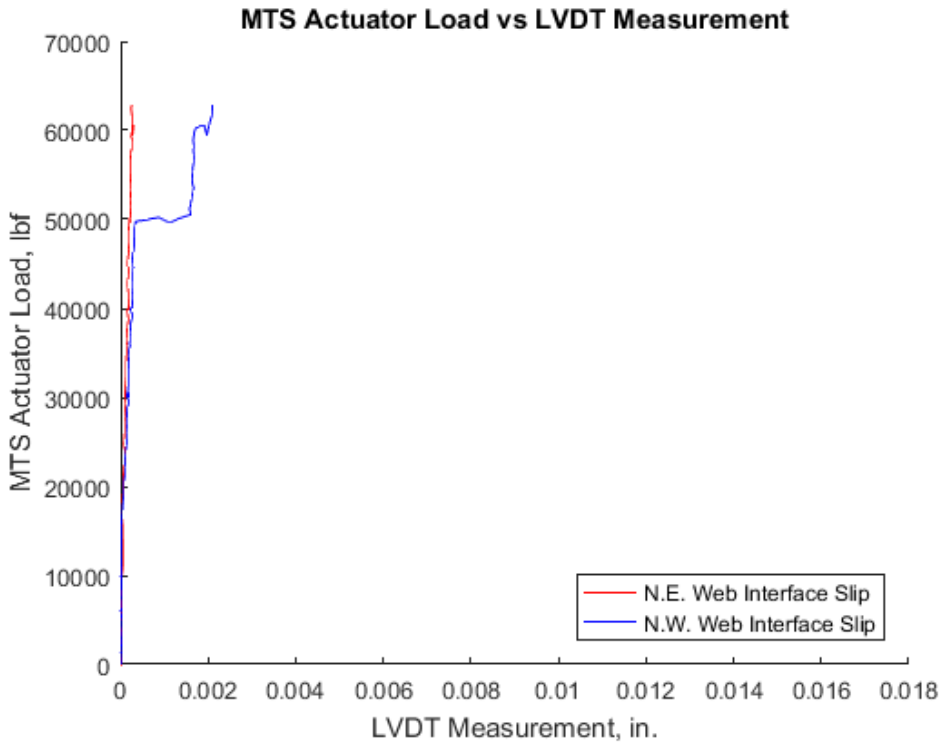

Figure 74 Plot of load versus LVDT slip measured at the northeast and northwest precast beam-C.I.P. topping interface for the no-connection specimen

Welded Connection Specimen

Results from Cyclic Load Test

For the welded connection specimen, no deterioration in performance of the specimen was observed visually during the period of cyclic testing. Over the entire 3650000 cycles, no visible cracking formed, and for each of the static load tests performed, the instrumentation recorded consistent values. The complete results of each piece of instrumentation is provided in the tables in (Appendix H – Results Tables for Welded Connection Specimen).

During each static load test, displacements were measured using string pots. As can be seen in Figure 76 and Figure 77, the maximum displacement during service loading occurs at the maximum load (30 kips). For each static load test, the displacement occurring at 30 kips was recorded. The maximum, minimum, and range of these values over all of the static load tests are shown in Table 14. It is important to note that, as with Table 10 for the no-connection system, more negative values in Table 14 indicate more displacement. Therefore, the maximum displacement actually occurs with the minimum recorded value in the table and vice-versa. As can be seen, the range of string pot displacements are relatively small – only up to 12/100 in. –

which demonstrates that between static tests, displacement results do not vary significantly. Table 14 also shows that the maximum amount of displacement occurs at the south midspan string pot, which attains a magnitude of 0.032 in. (approximately L/54000). The table also indicates that the displacements at the north midspan and south midspan string pots are essentially identical, differing only by 1/1000 in. These characteristics can be seen in Figure 75. Figure 75 shows the displacement against the string pot location (with 0 in. being at the south support, and 144 in. at the north support), for every static test overlaid on the same graph. The small vertical bandwidth in the plot at any location along the beam again shows that displacement results do not vary significantly between static tests. Figure 75 also shows that a significant proportion of the deflections occur near the supports with between 0.02 to 0.03 in. occurring at this location. Additionally, the plot shows that for all static load tests carried out, the displaced shape follows that of the elastic curve of a simply supported beam.

Table 14 Maximum, minimum and range of string pot displacements at maximum load, for all static load tests for the welded connection specimen

String Pot Displacements at Maximum Load, in.						
	S. Sup	**S. Qtr**	**S. Mid**	**N. Mid**	**N. Qtr**	**N. Sup**
Maximum	-0.022	-0.021	-0.028	-0.026	-0.025	-0.018
Minimum	-0.031	-0.031	-0.032	-0.033	-0.032	-0.026
Range	0.009	0.010	0.005	0.007	0.007	0.008

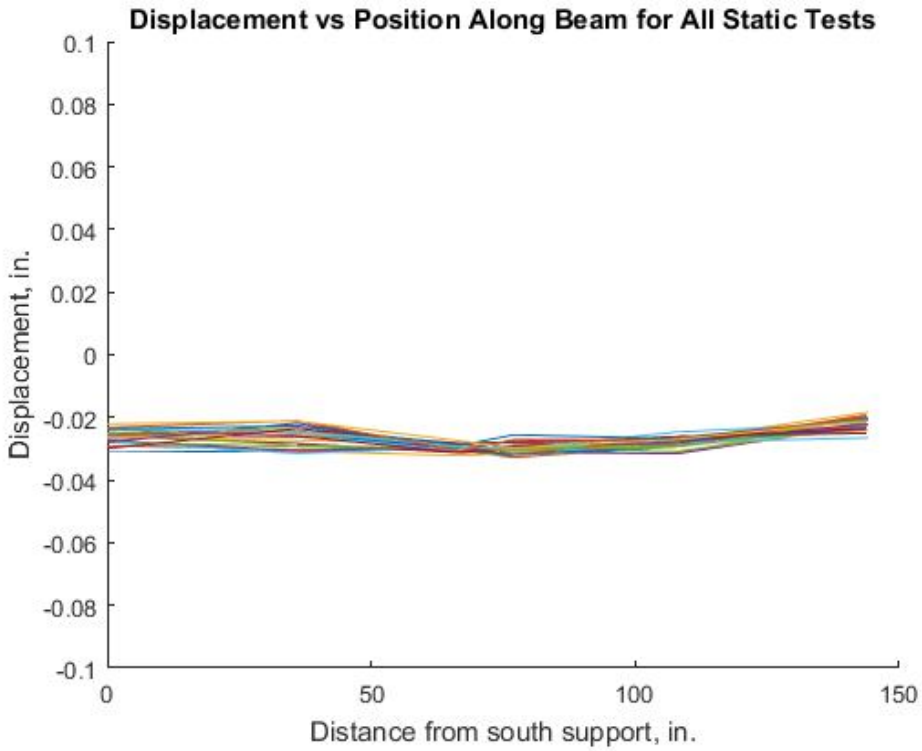

Figure 75 Welded connection specimen - plot of displacement vs position along beam for all static load tests

Figure 76 and Figure 77 both show plots of MTS actuator load versus displacement recorded by the string pot located at the north midspan support. Figure 76 shows this plot for records during the initial static load test, and Figure 77 shows the plot after the completion of 3650000 cycles of service loading. For both of these plots, the average of the displacements recorded at each support has been subtracted out. Both figures show a trend of linearly increasing displacement with load, with the maximum displacement being reached at application of maximum load. The figures also show that the behavior of the specimen is linear-elastic, and that a line of best fit can be drawn to gain an idea of the effective stiffness of the specimen in four-point bending. The slope of the best fit line during the initial static test is 2595 kips/in. and during the final test is 3073 kips/in. indicating that the specimen has not reduced in stiffness, rather, it has increased. This increase is addressed more in the Discussions section.

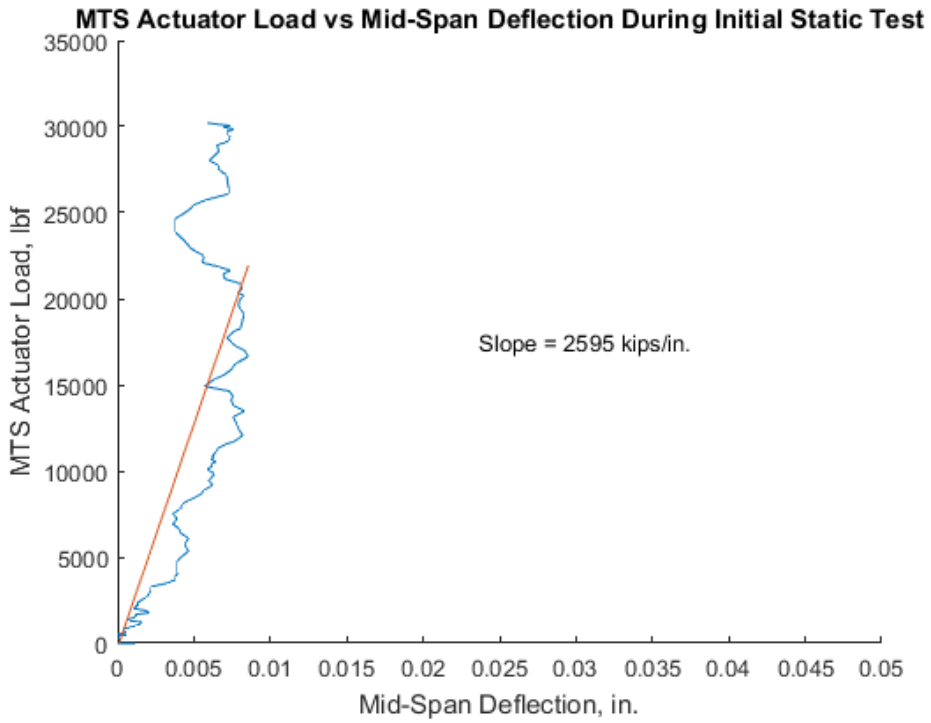

Figure 76 Plot of MTS actuator load versus midspan deflection (north midspan string pot) for welded connection during initial static test at 0 cycles

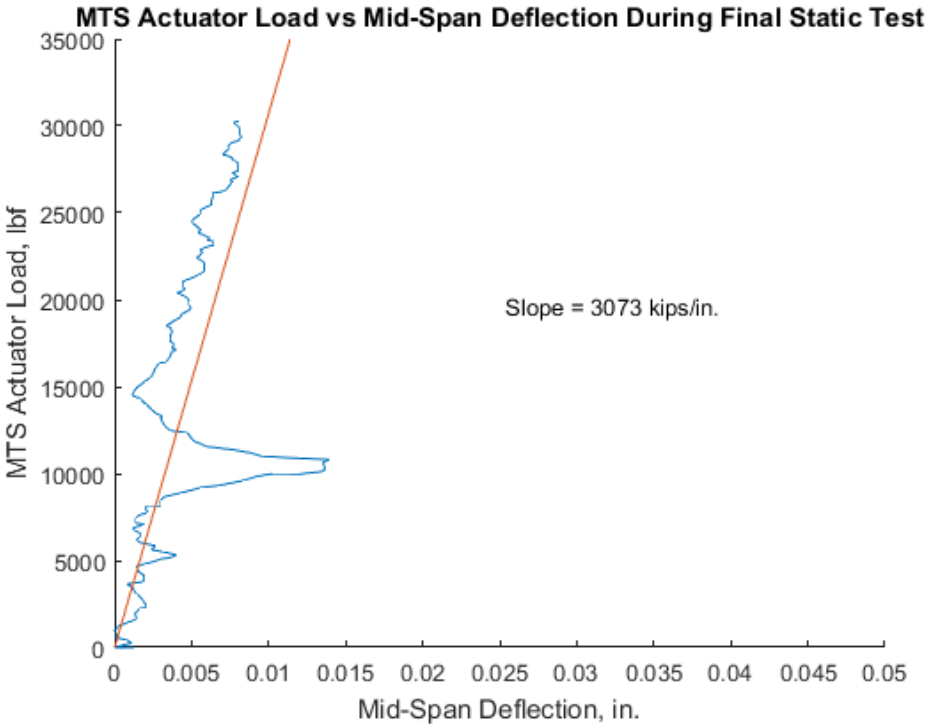

Figure 77 Plot of MTS actuator load versus midspan deflection (north midspan string pot) for welded connection during final static test at 3650000 cycles

For all of the static load tests carried out, the LVDT readings at the point of application of maximum load were recorded. The maximum, minimum and range of these values for all of the static load tests are reported in Table 15. As can be seen from the table, for all of the static load tests carried out during cyclic testing at service loading, the maximum and minimum LVDT readings were identical, giving a range of values of zero. This indicated no cracking or slipping of the interface during cycling. This also shows consistency in the recordings between all static tests. Figure 78 and Figure 79 show plots of applied load against joint openings during the initial and final static load tests. These plots are shown for the east web and west web location respectively. As can be seen from both plots, the magnitude of joint opening at the maximum applied service load of 30 kips is minute. The largest opening occurs in the west web during the final static test, but this still has a magnitude less than 5/10000 in. In addition to this, both plots show that upon unloading of the specimen, no significant residual joint opening remains. Finally, the plots show that between the initial test, and the final static test, the results do not vary significantly.

Table 15 Maximum, minimum, and ranges of LVDT slip readings during cyclic testing of welded connection specimen

LVDT Reading in.						
	Northeast Web	**East Web**	**Southeast Web**	**Northwest Web**	**West Web**	**Southwest Web**
Maximum	0.002	0.012	0.004	0.004	0.751	0.002
Minimum	0.002	0.012	0.004	0.004	0.750	0.002
Range	0.000	0.000	0.000	0.000	0.000	0.000

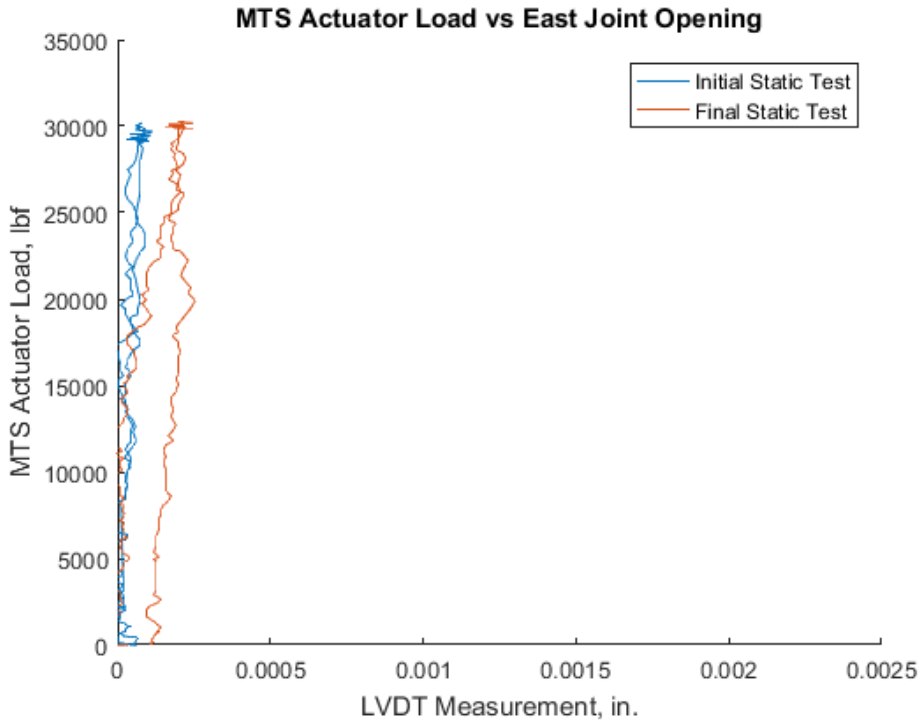

Figure 78 Plot of applied MTS actuator load against recorded LVDT measurements at the eastern joint location for the static load test at 0 cycles (initial) and at 3650000 cycles (final) for the welded connection specimen

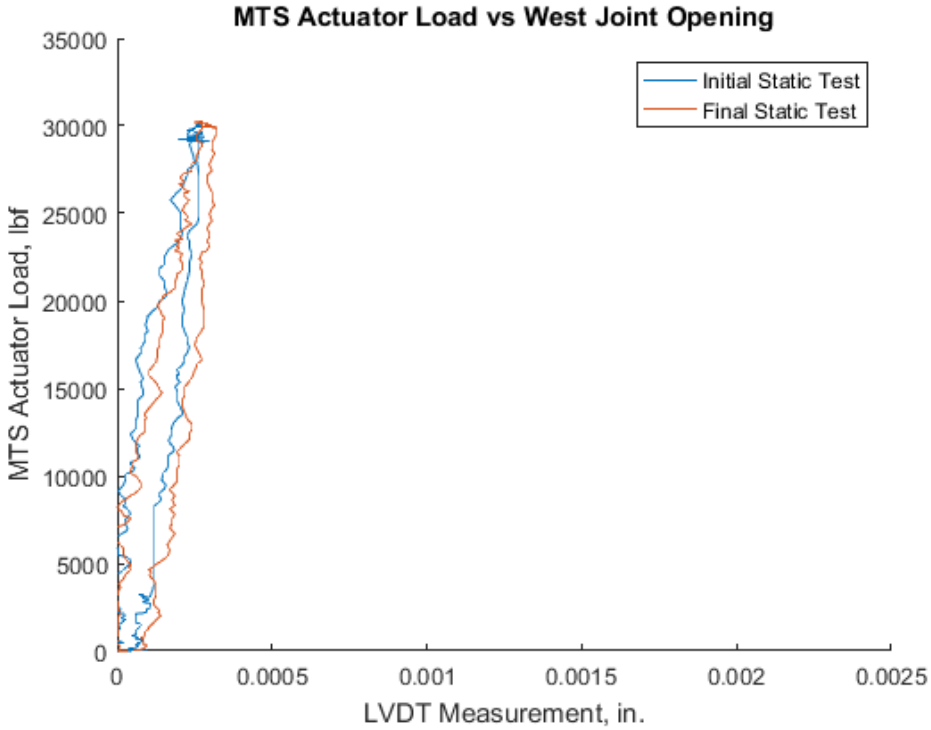

Figure 79 Plot of applied MTS actuator load against recorded LVDT measurements at the western joint location for the static load test at 0 cycles (initial) and at 3650000 cycles (final) for the welded connection specimen

Table 16 shows the maximum, minimum, and range of values recorded at maximum load by the strain gauges in each location, over all of the static load tests. The table shows all values in microstrain. As can be seen, between the static load tests, results do not vary greatly. The maximum range of results is in the C.I.P. East strain gauge which varies by 11 με, with the rest of the strain gauges recording results within 5 με of each other. The table also shows that the maximum recorded strain magnitude was 26 με and occurred in the C.I.P. topping reinforcement. The reinforcement in the precast beams had similar strains in each location that strain was recorded. Figure 80, Figure 81, and Figure 82 show the applied actuator load plotted against the strains for the initial static test, final static test, and initial and final test together, respectively. All figures show trends of linearly proportional strain increases with increasing load. Figure 82 additionally shows that between the first and last static load tests, the trend and magnitudes of recorded strains do not differ significantly.

The results shown in Table 16, and Figure 80 to Figure 82 indicate that strains in the C.I.P. topping, and in the precast beams remain below the strain which would cause cracking in a linear-elastic concrete material. This is in accordance with the visual observations during cyclic testing as no cracking was observed. This is described more in the Discussions chapter of this thesis.

Table 16 Welded connection - maximum, minimum, and range of strain values for maximum loading during static test

Strains, με					
	Northeast Beam	**C.I.P. East**	**Southeast Beam**	**Northwest Beam**	**Southwest Beam**
Maximum	16	26	15	15	17
Minimum	13	14	13	12	15
Range	3	11	2	3	3

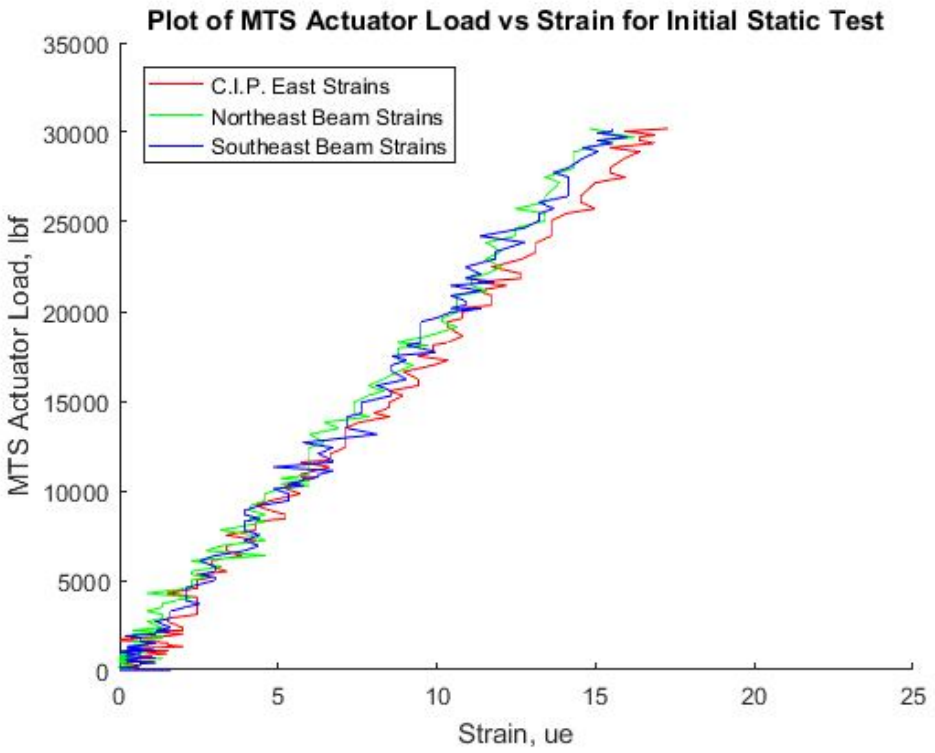

Figure 80 Welded connection - plot of MTS actuator load versus strain for the initial static test, for the strains in the C.I.P. east side reinforcement, and the precast beam east side reinforcement

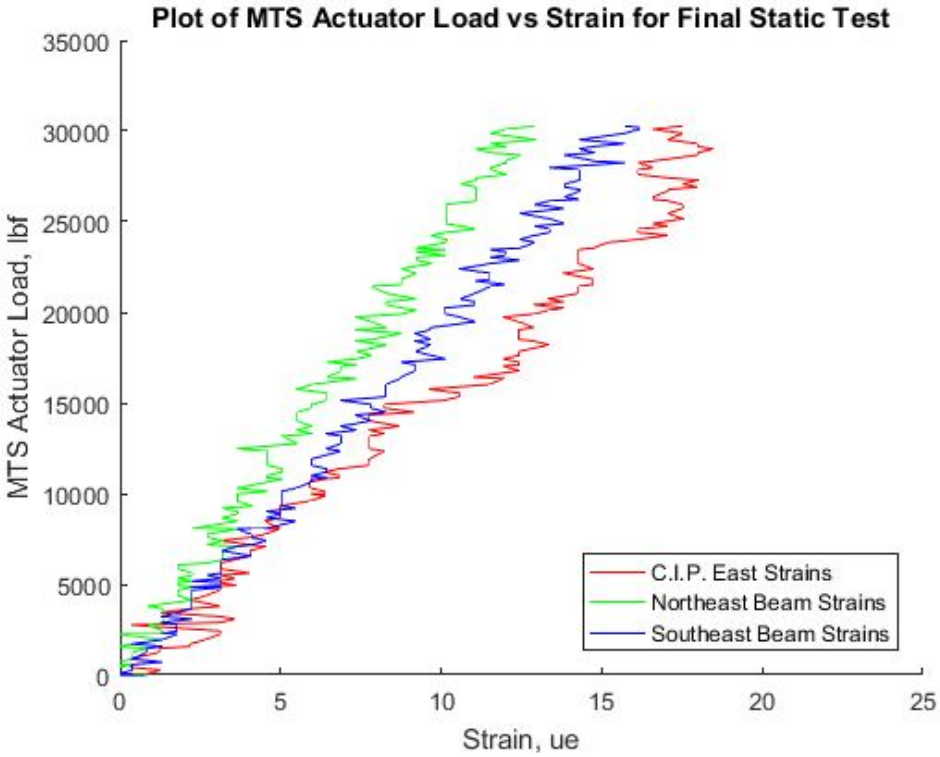

Figure 81 Welded connection - plot of MTS actuator load versus strain for the final static test, for the strains in the C.I.P. east side rebar, and the precast beam east side rebar

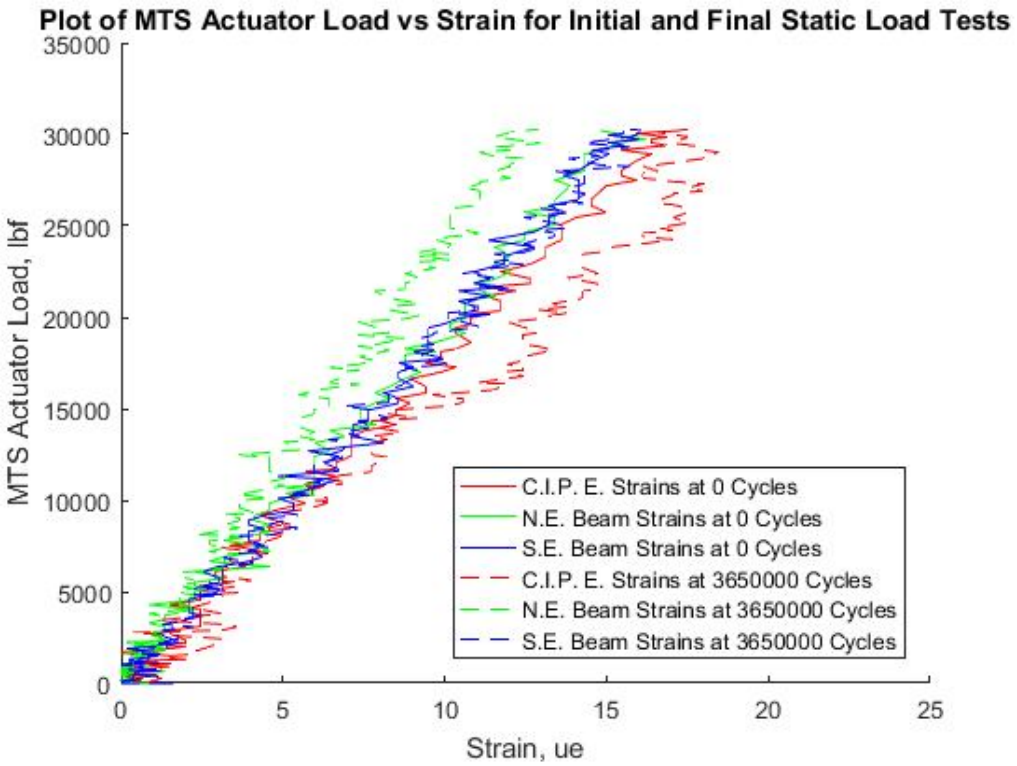

Figure 82 Welded connection - plot of MTS actuator load versus strain for the initial and final static test, for the strains in the C.I.P. east side rebar, and the precast beam east side rebar

Results from Monotonic Test to Failure

Monotonic load testing for the welded connection specimen was carried out over the course of two days due to the equipment setup required to fail this specimen. With the setup used for the cyclic testing, the MTS actuator could only apply a maximum load of 130 kips as it was limited by the calibration settings used for the cyclic testing. Due to time restrictions, it was decided to load the specimen to the 130 kips using the setup already in place in order to get initial results, and then to switch the MTS actuator with an Enerpac 200 ton actuator to complete the failure testing. Thus results are presented for both of the days of loading. Day 1 is defined as loading to 130 kips using the MTS actuator, while day 2 uses the Enerpac actuator to take the specimen to failure.

During the monotonic test, the specimen was visually inspected at each load increment, and cracks were noted and mapped. The beginning and end of cracks at that load increment were noted. As can be seen in Figure 83, the first cracks appeared as hairline cracks in the precast beam section, approximately 26 in. from the joint between the two adjacent beams. At this load,

there was no cracking in the C.I.P. topping, and no cracks could be observed at the interface between the precast beam and C.I.P. topping concrete. Additionally, at this load level, hairline cracks were observed at the location where the strain gauge wires ran vertically, embedded within the beam very close to its side face. However, upon subsequent loading, these cracks did not appear to propagate or widen and so at this stage it was acknowledged that these cracks were on the surface of the concrete specimen.

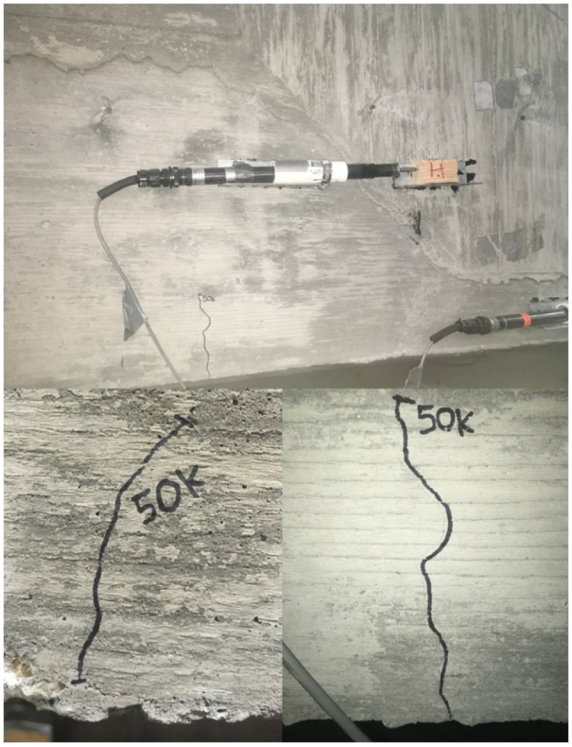

Figure 83 Welded connection failure test - first cracking at 50 kips

The first cracks to appear in the C.I.P. topping concrete were observable at an applied load of 100 kips. This can be seen in Figure 84. Also shown in Figure 84 is distributed cracking occurring at a load of 110 kips. At 100 kips and at 110 kips, any cracking that occurred in the C.I.P. topping, occurred directly over the joint between the two precast beams. Cracking at this load was still less than 0.005 in. wide. At this stage, cracking in the precast beams had propagated, but no new crack locations were observed in the precast beams. Additionally, no surface interface cracks appeared.

Figure 84 Welded connection failure test - C.I.P. cracking at 110 kips

Figure 85 shows the crack propagation in the beams that had occurred up to a load increment of 180 kips. In addition to the propagation of previous cracks in the precast beam, cracking in a new location occurred. This hairline crack was observed to form approximately 20 in. away from the joint between the adjacent beams. As can be seen in Figure 85, the initial crack which formed, propagated vertically through the section to the point where the tapered web of the inverted T-beam reached its full height. This is the typical crack pattern on all faces of the precast beams, and the cracks were noted to form at similar magnitudes of load – within 10 kips of each other. At this load, there was still no indication of slippage between the concretes which were cast at different times. At this stage, the cracks which formed initially in the precast beam at 50 kips had widened to 0.01 in. and had propagated vertically in the section. Additionally, cracks in the C.I.P. topping concrete had widened to 0.06 in.

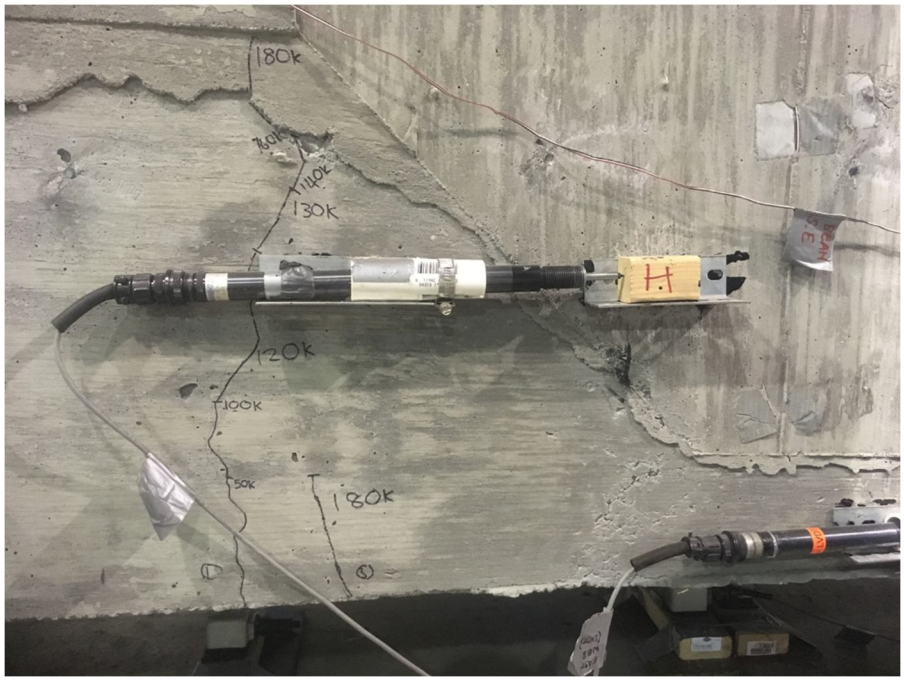

Figure 85 Welded connection failure test - crack propagation and new crack location at 180 kips

In Figure 86 once the magnitude of loading reached a value of 190 kips, cracking occurred along the interface between the precast beam and C.I.P. topping concrete in the northwest face of the subassemblage specimen. Cracks at this location were hairline in terms of width, but were relatively long and followed the profile of the inverted T-beam's tapered web. At this load, it was noted that the initial cracks in the precast beams had attained a width ranging between 0.01 in. and 0.02 in. The cracking in the precast beams closer to the joint were approximately 0.01 in. wide and had propagated vertically in the section. Also, the cracking in the C.I.P. topping reached a width of 0.08 in. on both sides of the specimen. Additionally, the cracks formed by the location of the strain gauges began to widen at this load, and so it was assumed that these cracks were no longer simply surface imperfections.

Figure 86 Welded connection failure test - interface cracking at 190 kips

Failure of the specimen occurred at a load of 194 kips. At this load, a large crack occurred in the C.I.P. topping directly above the joint between the two precast beams. The crack propagated upwards through the specimen. This can be seen in Figure 87. In addition, Figure 87 shows that the cracking that had initiated in the precast beams at 50 kips, had fully propagated through the beam section and had made its way into the C.I.P. topping. The cracking which was at 50 kips noted to be surface cracking, had by this stage propagated through the majority of the precast beam section. At failure, no slippage could be easily seen at the interfaces between the two concretes, and the cracking which occurred at the northwest interface at 190 kips did not further propagate.

Upon further inspection of the section, it was shown that failure of the weld metal near drop-in steel rod occurred. This is also shown in Figure 88. This failure is described in more detail in the Discussions section.

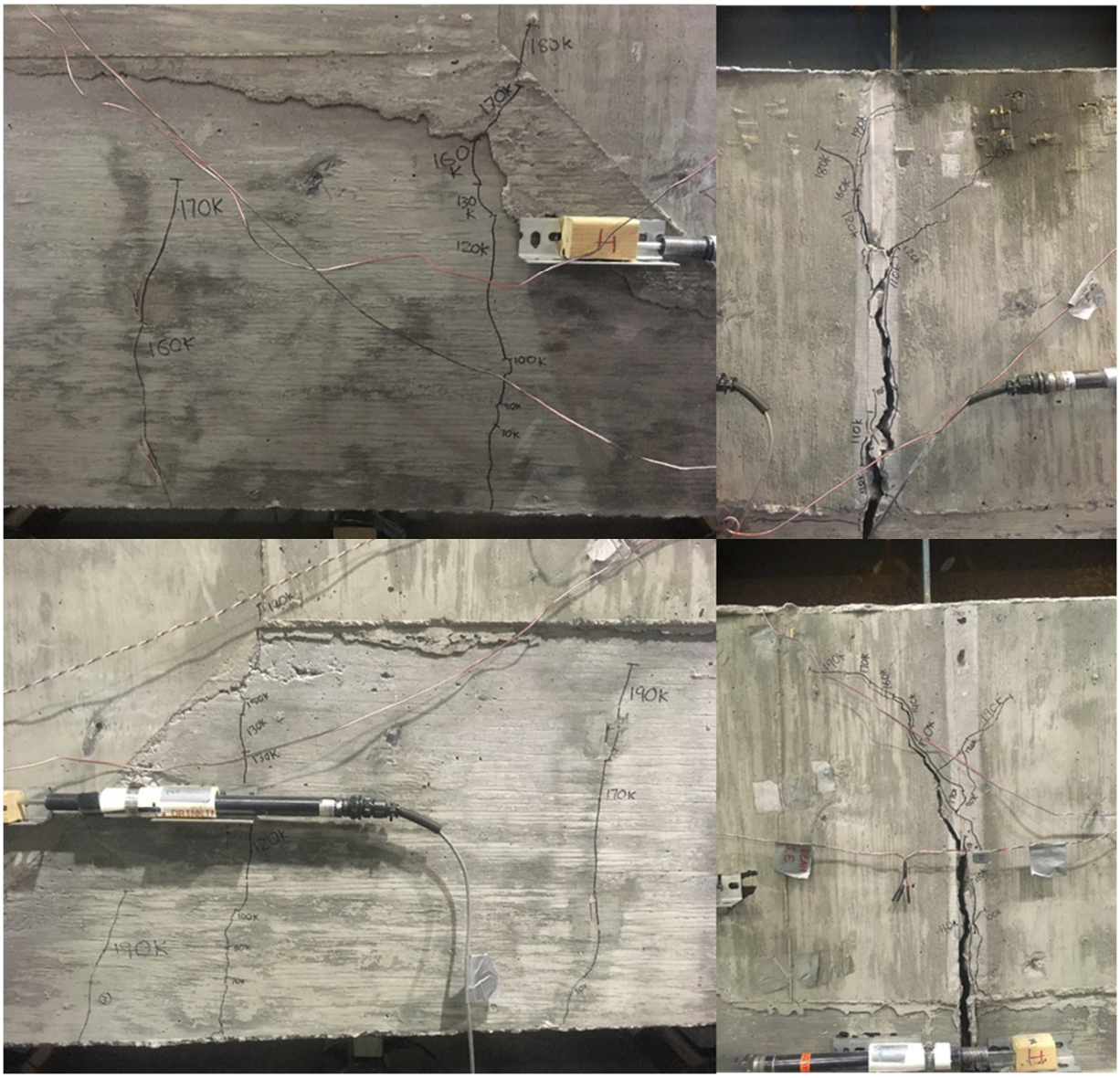

Figure 87 Welded connection specimen failure test - failure at 194 kips

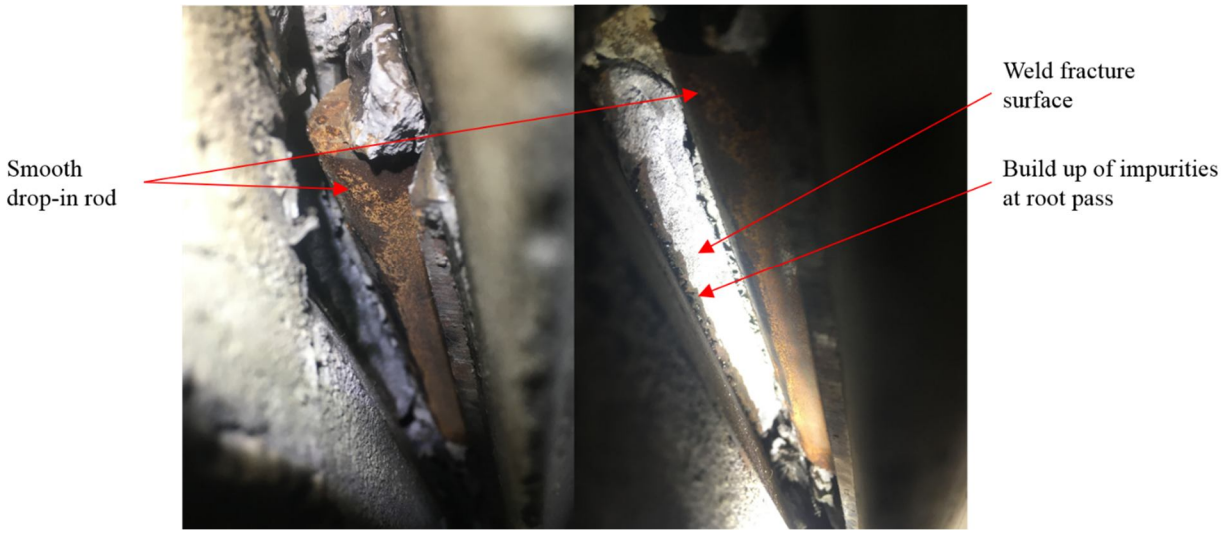

Figure 88 Welded connection failure test day 2 - weld failure at 194 kips

Figure 89 shows the deflection at each string pot for four different values of loading. As can be seen in the plot, at a load of 50 kips – the load at which the first cracks in the precast beam occurred – the beam still behaves as a monolithic beam, exhibiting small amounts of bending behavior. At this load, deflections were still small, reaching a value significantly less than 0.025 in. once the support deflections were subtracted out. At 110 kips, significant amounts of cracking occurred in the C.I.P. topping directly above the joint. The stiffness of the beam decreased and deflections increased significantly. As can be seen from the plot, the beam at this stage still exhibits obvious bending behavior as opposed to hinging. At a load increment of 180 kips, a hinge begins to form in the south precast beam. This is seen by the near triangular shape of the deflection plot up to 67 in. away from the south support. The north half of the subassemblage, however, continues to exhibit bending behavior. Finally, at the failure load of 194 kips, the figure shows that the hinge in the south precast beam has fully formed, and the beginning of a hinge is forming in the north half of the beam, noted as the plotted deflection diagram becomes more triangular. At the failure load, Figure 89 shows a deflection of 0.33 in. once the support displacements have been subtracted.

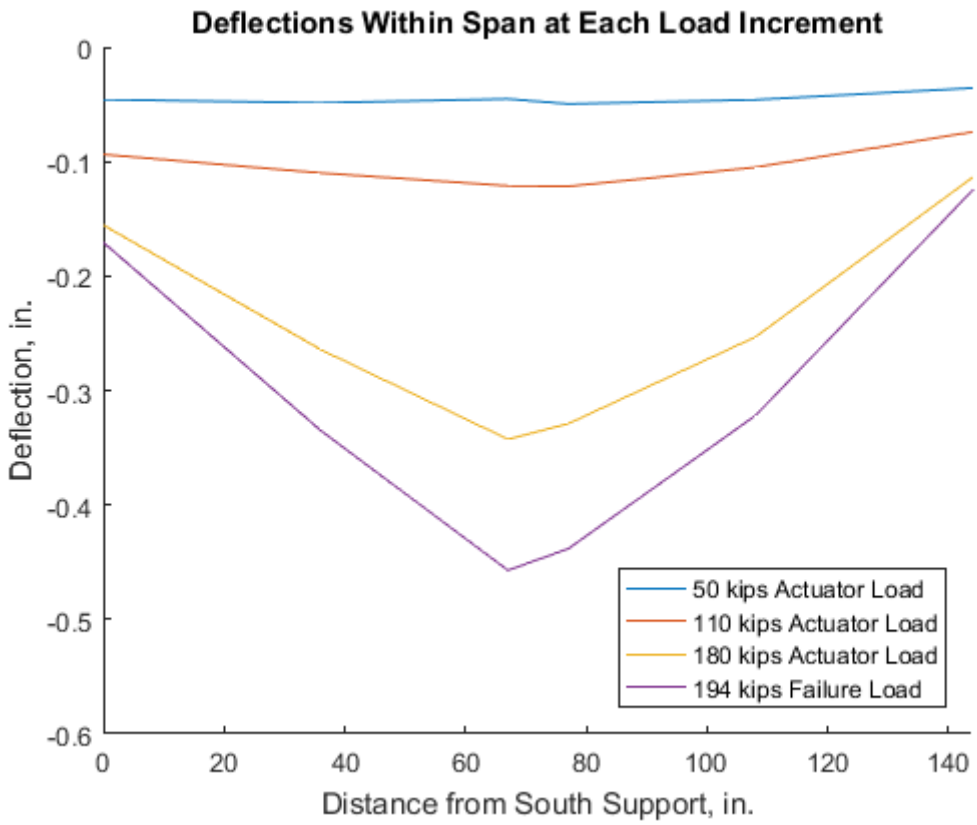

Figure 89 Welded connection failure test - deflections versus position within span

Figure 90 shows the applied load from the actuator plotted against the midspan deflection recorded by the north midspan string pot. Since the first day of testing of the specimen caused cracking, the full plots for both days of testing are shown. As can be seen, on the first day of testing prior to cracking the specimen shows a higher initial stiffness indicated by the steeper slope of the blue line. At 110 kips, significant amounts of cracking occur and the plot showing the load-displacement for the first day of testing begins to exhibit a lower stiffness, however soon after this loss of stiffness, testing had to be stopped. On the second day of testing, the load-displacement behavior shows that the specimen exhibits a cracked stiffness, lower than its initial stiffness up until 140 kips, at which point inelastic behavior becomes observable. At 140 kips, the specimen has displaced 0.06 in. Between 140 kips and 194 kips, the specimen undergoes significant deformation. The figure shows that the deflection increases from 0.06 in. to the final value of 0.33 in. Consequently, it is observed that 82% of the total midspan deflection of the specimen occurred within the final 28% of loading.

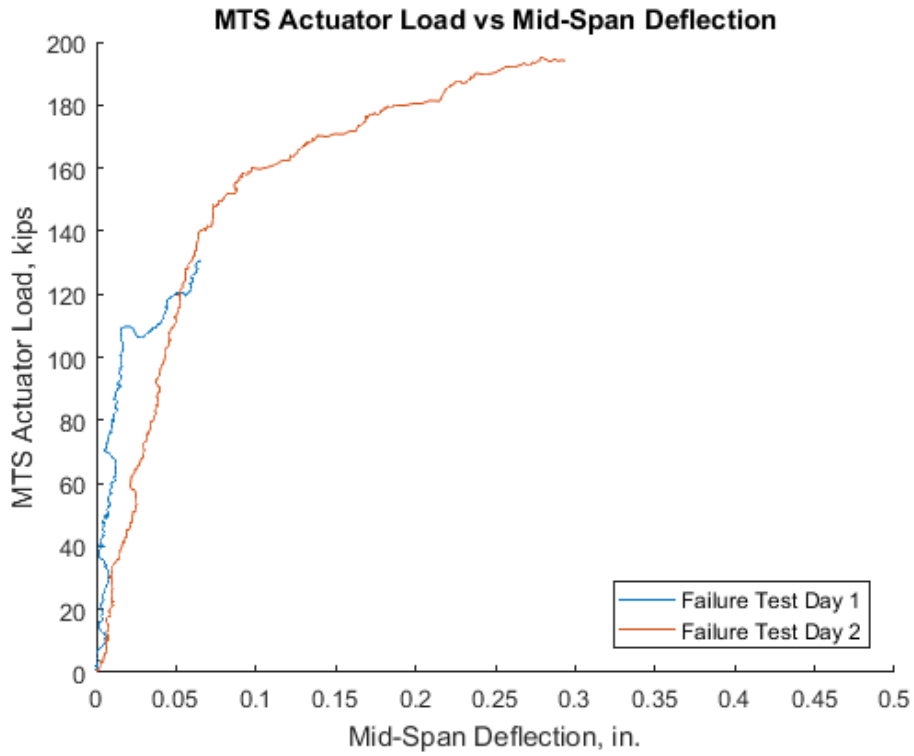

Figure 90 Welded connection failure test - load versus midspan deflection plot

The strains recorded during both days of testing are presented in Table 17 and Table 18. These strains are plotted with corresponding values of load in Figure 91 and Figure 92. It should be noted that on the second day of testing, the strain gauges attached to the C.I.P. east reinforcement, and the southwest beam reinforcement malfunctioned. It is thought that during unloading of the specimen on the first day of testing, the bond between the strain gauge and the reinforcement was compromised. As a result, these specific gauges did not produce intelligible results during the second day of testing, and are therefore not presented in the figures or table.

On the first day of testing it can be seen that reinforcement strains in all locations increase proportionally with load, and remain close to each other in terms of magnitudes, until a load of 100 kips. At this point, there is a small jump in strain of the reinforcement in the C.I.P. topping. At 110 kips, all of the strain gauges experience a significant jump in strains before continuing to increase linearly to 120 kips, at which point the beam reinforcement strain gauges experience another, smaller jump in strains. Interestingly, the strain in the C.I.P. topping reinforcement seems to then reduce slightly, before continuing to increase linearly to 130 kips. The sudden increases in strains are explained further in the Discussions chapter.

On the second day of testing, as shown in Figure 92, the strains in the beam reinforcement increase at a reduced stiffness until they reach the point at which loading was stopped during the first day of testing. At this point, and upon subsequent increases in load, the strains in the reinforcement continue to increase linearly, however they increase at a lower rate, and small jumps in strain occur. At the failure load of 194 kips, the maximum recorded strains can be seen in Table 18. It should be noted that these maximum strains are lower than the yield strain for mild steel reinforcement (2070 με), however it could be inferred that the more highly strained C.I.P. reinforcement has reached yield.

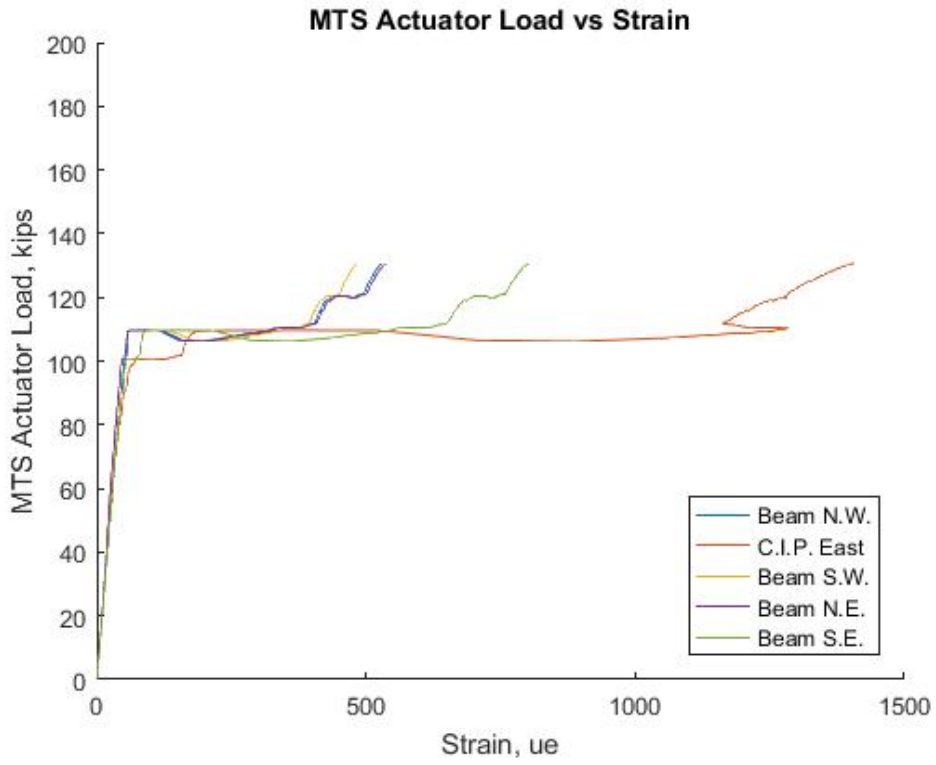

Figure 91 Welded connection failure test day 1 - actuator load versus strain

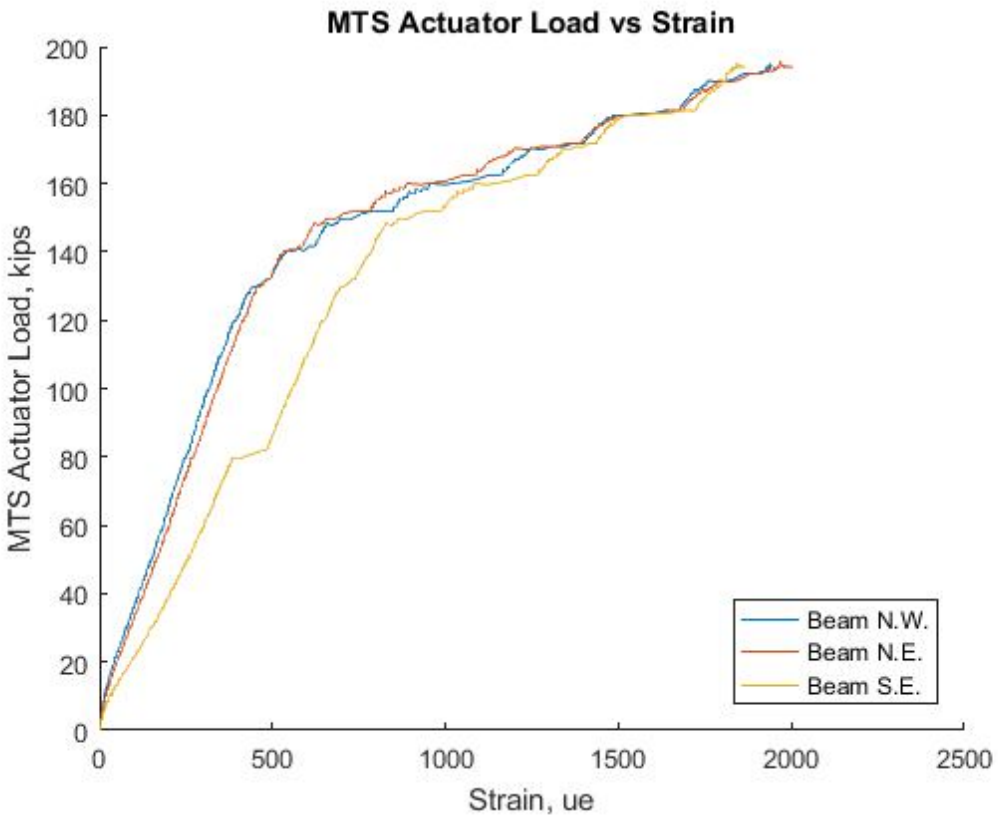

Figure 92 Welded connection failure test day 2 - actuator load versus strain

Table 17 Welded connection failure testing day 1 - Table of strains recorded at each load increment

Strains on Day 1 of Testing - up to 130 kips					
Load	**Beam N.W.**	**C.I.P. East**	**Beam S.W.**	**Beam N.E.**	**Beam S.E.**
30.6	16	13	15	14	16
40.5	20	17	19	19	19
50.6	25	22	24	22	25
60.3	30	27	25	26	30
70.5	35	33	31	30	35
80.5	41	40	37	36	40
90.6	46	51	41	41	45
100.7	52	77	47	47	55
110.5	335	1294	351	340	565
120.5	440	1279	427	445	702
130.6	531	1405	481	538	802

Table 18 Welded connection failure testing day 2 - Table of strains recorded at each load increment

Strains on Day 2 of Testing - up to Failure			
Load	**Beam N.W.**	**Beam N.E.**	**Beam S.E.**
30.4	79	91	154
40.8	116	130	208
50.9	151	167	259
60.3	182	200	301
71.1	215	236	346
80.4	247	268	387
90.3	282	306	515
100.4	315	339	556
110.0	349	374	599
120.3	392	416	648
130.4	445	460	702
141.0	550	539	795
151.1	705	664	874
160.3	970	903	1095
170.9	1255	1214	1347
180.4	1499	1526	1530
190.4	1771	1802	1809
194.0	1924	2003	1866

Figure 93 and Figure 94 show the actuator load plotted against LVDT measurements for the joint openings, and the LVDT's at the tapered webs respectively. These two figures show the data recorded by the LVDT's during the first day of testing. As can be seen from Figure 93, the joints open by essentially the same magnitudes. Joint opening is very small up to a load of 110 kips – the load at which cracking in the C.I.P. topping above the joint occurs. At this load, joint opening increases significantly from 0.002 in. to 0.026 in. In Figure 94, it can be observed that all of the LVDT's show insignificant amounts of displacements, indicating no cracking or slippage occurring at the interface surface on the tapered webs. However, at a load of 60 kips, the LVDT recording at the southwest web recorded a large increase in displacement. Upon further inspection of the section, a lengthy hairline crack was discovered along this interface surface. This is described more in the Discussions chapter.

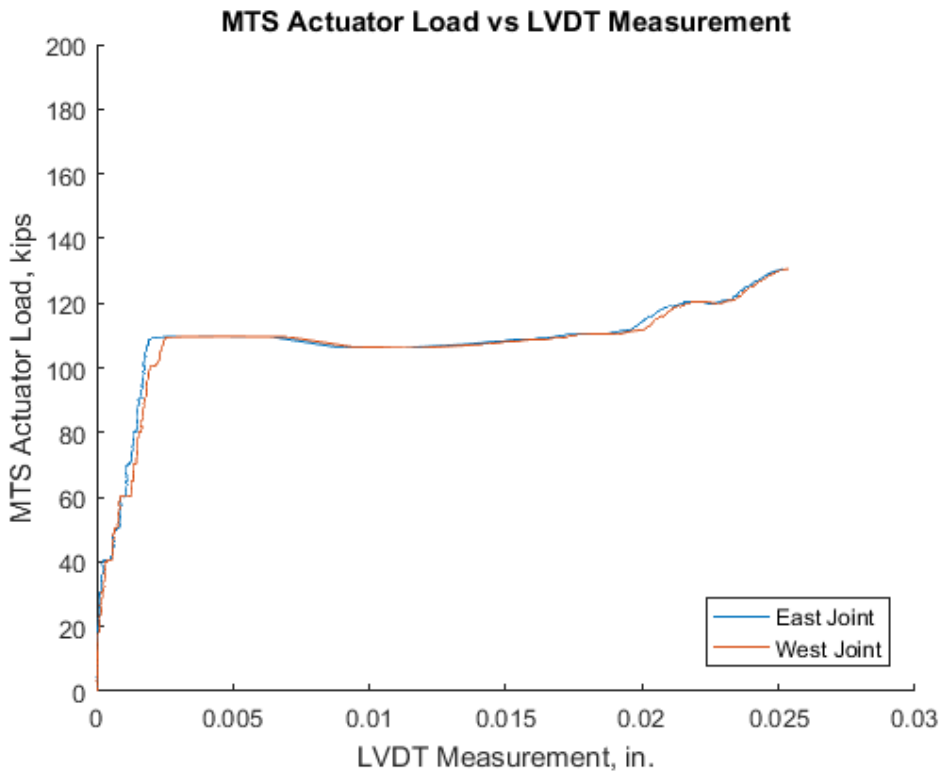

Figure 93 Welded connection failure test day 1 - actuator load vs LVDT measurements at the east and west joints

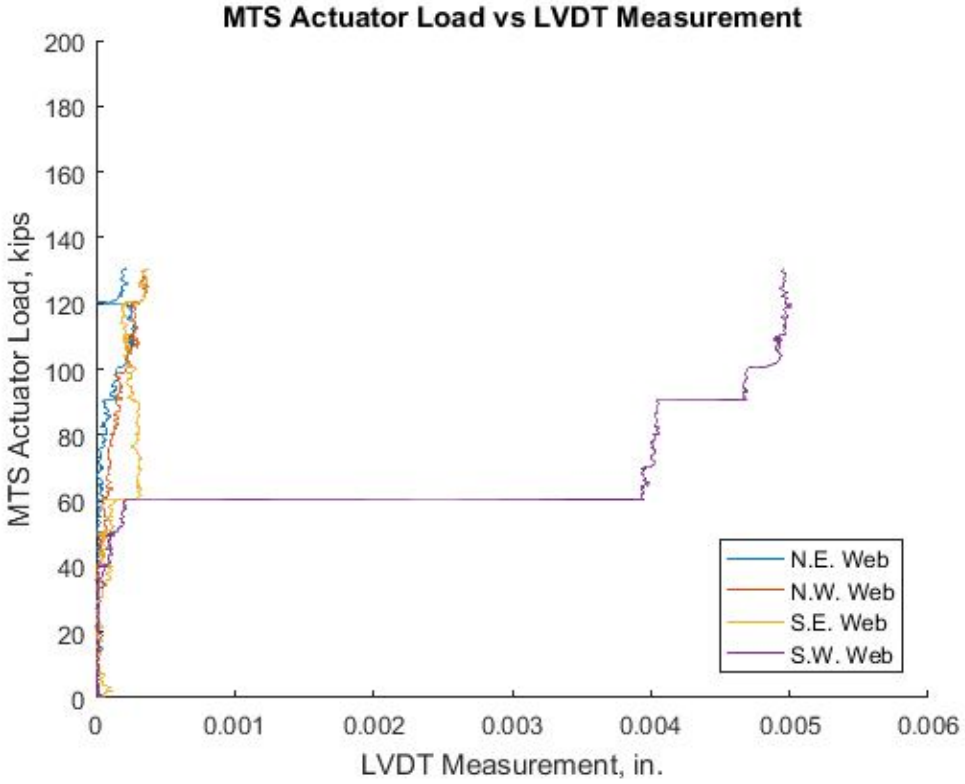

Figure 94 Welded connection failure test day 1 - actuator load vs LVDT measurements at the webs

Figure 95 and Figure 96 show the actuator load plotted against the LVDT results for the second day of testing. Figure 95 shows the joint openings, while Figure 96 shows the results at the interface between the tapered web precast beam and C.I.P. topping. Comparing the joint opening when loading the specimen from 0 kips to 130 kips, it is noted that rather than having a sharp increase in joint opening at 130 kips, the joints now have a reduced stiffness and the opening between them increases linearly at this reduced stiffness to reach a value of 0.025 in. at 130 kips – the same value recorded at the end of testing the previous day. After this value, the joints exhibit non-linear behavior up to the failure load at which the joint opening on both sides of the subassemblage are approximately 0.16 in. As can be seen in Figure 96, negligible slippage occurs at the interface between the precast beam and C.I.P. topping concrete at the tapered web locations. However, at 190 kips, a large jump in the recorded values at the northwest LVDT occurs. This occurred coincidentally with the cracking between the two concrete interfaces at this location.

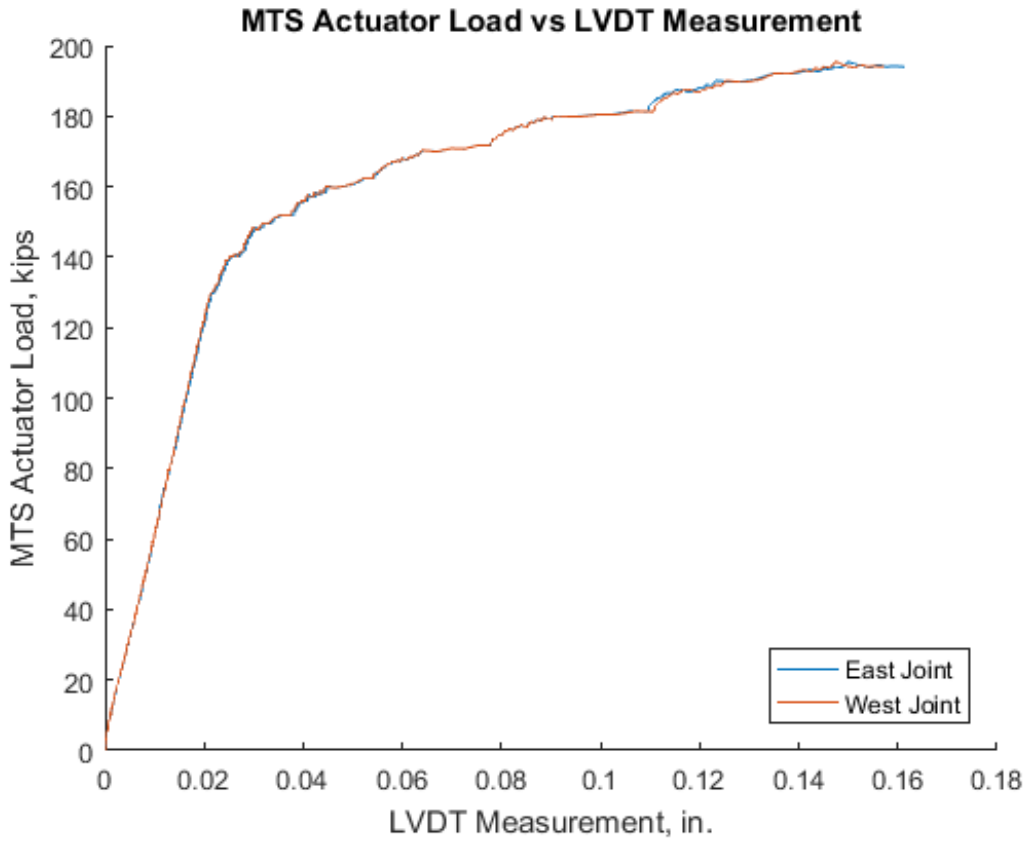

Figure 95 Welded connection failure test day 2 - actuator load versus LVDT measurement at the east and west joints

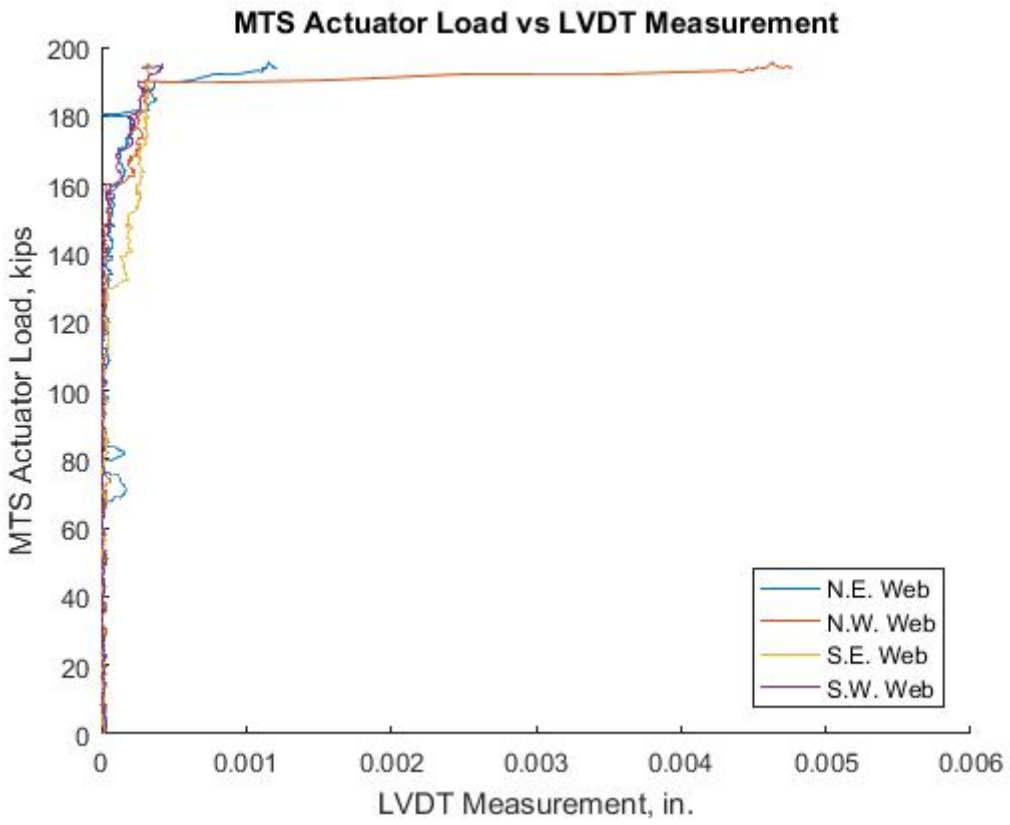

Figure 96 Welded connection failure test day 2 - actuator load versus LVDT measurement at the webs

Table 19 to Table 22 shows the values recorded by the LVDT's for joint openings and slip at the interface between the precast beam and C.I.P. topping concrete, at "interesting" load points. These "interesting" values correspond to sudden increases in LVDT measurements observed in the plots above (Figure 93 to Figure 96).

Table 19 Welded connection - loads and LVDT measurements at the joints for the first day of failure testing

LVDT Measurements at Joints - Day 1 of Testing		
Load, kips	**East Joint Deflection, in.**	**West Joint Deflection, in.**
40.5	0.000	0.000
60.3	0.001	0.001
110.5	0.018	0.019
120.5	0.022	0.022
130.6	0.025	0.025

Table 20 Welded connection - loads and LVDT measurements at tapered web locations on first day of failure testing

LVDT Measurements at Webs - Day 1 of Testing				
Load, kips	**N.E. Web, in.**	**N.W. Web, in.**	**S.E. Web, in.**	**S.W. Web, in.**
40.5	0.000	0.000	0.000	0.000
60.3	0.000	0.000	0.000	0.004
90.6	0.000	0.000	0.000	0.005
100.7	0.000	0.000	0.000	0.005
120.5	0.000	0.000	0.000	0.005
130.6	0.000	0.000	0.000	0.005

Table 21 Welded connection - loads and LVDT measurements at the joints for the second day of failure testing

LVDT Measurements at Joints - Day 2 of Testing		
Load, kips	**East Joint Deflection, in.**	**West Joint Deflection, in.**
130.4	0.022	0.022
180.4	0.099	0.099
194.0	0.161	0.157

Table 22 Welded connection - loads and LVDT measurements at the tapered webs for the second day of failure testing

LVDT Measurements at Webs - Day 2 of Testing				
Load, kips	**N.E. Web, in.**	**N.W. Web, in.**	**S.E. Web, in.**	**S.W. Web, in.**
141.0	0.000	0.000	0.000	0.000
194.0	0.001	0.005	0.000	0.000

DISCUSSIONS

Comparison to Previous Research at Virginia Tech

As has been referenced a number of times throughout this thesis, previous research was carried out by Mercer and Menkulasi at Virginia Tech. Their findings were documented in Mercer's thesis (Mercer 2012), and Menkulasi's doctoral dissertation (Menkulasi 2014). These pieces of work represent their testing objectives, methodologies, and findings. The work carried out during this phase of testing expands on the work that was carried out by these researchers.

The objective of the work carried out by these researchers was to compare the different characteristics of inverted T-beam designs; including geometries, types of connections, and deck mixes, and to come up with a design methodology for this type of bridge system. The testing of

the different characteristics of the systems was carried out by monotonic load testing in the laboratory with some subjection of the test specimens to very few cycles of repeated loading. The results of their work showed that a tapered web cross-sectional geometry was the better geometric system, and that the welded connection and no-connection connection types were the most efficient to construct and gave above adequate performance with the welded connection proving more suitable for high volume traffic bridges, and the no-connection system adequate for low volume traffic bridges.

The objective of the current phase of work is to build on this, to verify the use of the no-connection system on higher volume bridges. In addition to this the behavior of the welded connection under high volume traffic simulation was of interest. The reason for wanting to do this lies in the simpler and faster construction of the no-connection system due to the elimination of the need for field welds to form the mechanical connection between the adjacent beam units. Getting rid of the welded connection also eliminates issues associated with deterioration of the welded connection due to environmental factors, or fatigue issues with the weld. In order to carry out this verification, cyclic loading was applied to each of the test specimens equivalent to the number of axles crossing a bridge carrying 200 ADTT over a 50-year service life.

The primary difference, therefore, lies in the methodology of the testing. While the previous researchers carried out mainly monotonic load testing to failure of the specimens, and were testing multiple characteristics of the inverted T-beam system, the current phase of testing is concerned with high-cycle fatigue effects on the connection between adjacent beam units (refer to the Testing Setup section above).

Material Testing

As was described in the section on Results - Material Testing, the specified 28-day concrete compressive strength of the precast beam and C.I.P. topping concretes were 8000 psi and 4000 psi respectively, for both the no-connection and welded connection specimens. The C.I.P. topping concrete for both specimens, and the precast beam concrete for the welded connection specimen both reached their specified 28-day compressive strengths, however, the precast beam concrete for the no-connection specimen did not.

The section entitled Concrete Casting provides some insight as to why this might have occurred. In this section it is noted that the air content of the provided concrete increased

significantly - from the specified value of 5.5% to 12%. The engineering bulletin produced by the Portland Cement Association (PCA) entitled “Design and Control of Concrete Mixtures” notes in the chapter regarding “Air Entrained Concrete”, that every extra 1% of air entrainment, can reduce compressive strength by approximately 2%-6% (Kosmatka et al. 2002). In the case of this specific concrete pour, the increase in air content was 6.5%, and taking the worst-case scenario, the reduction in concrete compressive strength would be around 39%. This would reduce the 28-day strength from the 8000 psi specified value to around 4880 psi. This gives an idea as to why the concrete strength was reduced so significantly. The reasons for the additional air entrainment by Conrock is unknown.

An impact of the increased air content was a reduced the unit weight of the precast beam concrete. The unit weight decreased from the usual value of around 150 pcf, to 130 pcf. This then reduced the calculated values of Young’s Modulus - calculated using AASHTO equation 5.4.2.4-1 (AASHTO 2014) for normal weight concretes – as this equation is dependent on the unit weight.

The modulus of rupture for concrete is related to its compressive strength, and can be estimated using AASHTO (2014) 5.4.2.6. The equation given is repeated below for convenience. Using this equation, the modulus of rupture for this beam concrete reduces from 679 psi, to 511 psi. For the C.I.P. topping of the no-connection specimen, the specified 28-day concrete strength was 4000 psi, while the concrete actually attained a strength of 6200 psi. The modulus of rupture for this concrete therefore increased – using the same equation below – from 480 psi to 598 psi, higher than that of the beam concrete. The impact of this for the testing is that cracking in the precast beam occurred at a lower applied load. At service loads, based on the finite element modeling (see section on Analytical methods), the expected critical stresses in the specimen are 0.29 ksi, still well below the reduced modulus of rupture of 0.511 ksi. Therefore, cracking was still not expected during service loading and this was seen during testing. However, as was described in the section regarding the results from monotonic testing of the no-connection specimen, flexural cracking occurred in the precast beam concrete of the no-connection specimen prior to cracking occurring at the location of critical stress in the C.I.P. topping.

$$f_r = 0.24\sqrt{f_c'}\ (ksi)$$

Another impact of the reduced concrete compressive strength is the requirement for longer development lengths for reinforcement in the precast beam. This is particularly significant

because the no-connection connection specimen relies on a non-contact lap splice between adjacent reinforcement to transfer transverse bending stresses. (AASHTO 2014) section 5.11.5.3.1 requires that the length of a lap splice range from $1.0l_d$ to $1.7l_d$ depending on the class of the splice, where l_d is the development length of the bar. Equation 5.11.2.4.1-1 in AASHTO shows that the development length of a hooked bar is proportional to the inverse of the square root of compressive strength. The equation is repeated below for convenience.

$$l_{hb} = \frac{38.0 d_b}{\sqrt{f_c'}} \ (in.)$$

As can be calculated, for a No. 6 hooked reinforcing bar, the development length increases from 10 in. to 13.4 in. when the compressive strength decreases from 8000 psi to 4530 psi. The effect of this is shown in Figure 97 below. With an 8000 psi concrete, the reinforcement in the flange of the precast beam can develop within the width of the flange, before the tapered web profile forces the C.I.P. topping reinforcement away from the precast beam flange reinforcement thereby reducing the effectiveness of the non-contact lap splice. However, in the 4530 psi concrete, this does not happen. The reinforcement lap does not fit completely within the width of the flange. The inability to fully develop the reinforcement within the width of the flange is really only an issue at ultimate loads. Since the ultimate loads are over double the service loads (failure occurred at 63 kips while the service loading range was only 30 kips), and more than ¾ of the development length is reached within the flange (as can be seen in Figure 97), the lap splice will still be effective at service loading.

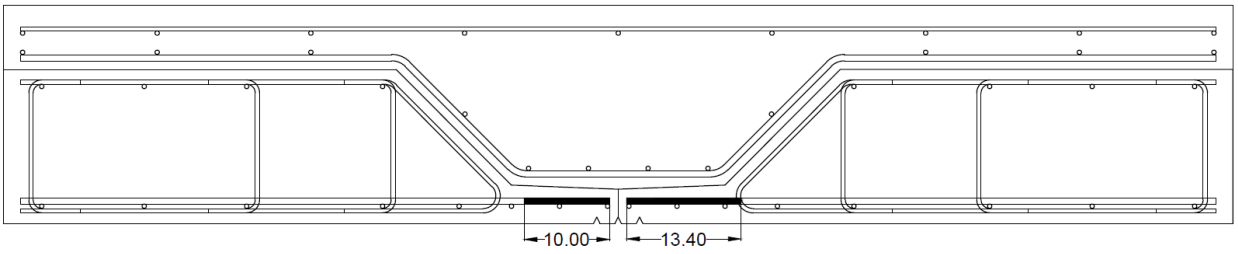

Figure 97 Lap lengths for no-connection specimen for 8000 psi concrete and 4530 psi concrete

Validation of Finite Element Model

Finite element modeling was carried out for the specimen so that the stresses that occur in a real bridge constructed using the inverted T-beams could be replicated in the laboratory using a subassemblage specimen. Finite element modeling was used to determine the load that was

needed to be applied to the subassemblage. This could not be done using traditional beam design because the subassemblage specimen geometry and location of load application (refer to Figure 18, Figure 19, and Figure 45) means that the specimen falls into the category of a deep beam (Mercer 2012). In addition to this, the full bridge has the interesting behavior due to it having a greater width than length which is atypical of bridges. During the finite element modeling, assumptions were made in order to simplify the modeling to save time and effort. Validation of these modeling assumptions can be achieved by comparing observations made during physical testing with the basis on which the assumptions were made. Individual comparisons of the experimental results with the finite element model's predictions for deflections and strains are discussed in the sections on Displacement Results and Strain Gauge Results.

The effect of longitudinal prestressing was ignored to simplify the model, and because interest was in the transverse bending behavior, and longitudinal prestressing does not contribute greatly to the transverse behavior of this bridge (Mercer 2012). In addition to this the effect of mild steel reinforcement was ignored for simplicity of the model.

Linear-elastic behavior was a significant assumption made in order to simplify the model greatly. The assumption of linear-elastic behavior allowed the effects caused by non-linearity in the system to be ignored. The concrete material could be modelled using a simple elastic material with a Young's Modulus calculated using Equation 5.4.2.4-1 in AASHTO (2014). In addition, geometric non-linearity such as the beam and concrete interface slipping or cracking during testing, did not need to be considered. During the testing it was observed from the load vs midspan deflection recordings, that the behavior of the specimen was linear. This can be seen in Figure 58 in the Results section. In addition to this, based on the visual documentation during cyclic testing, no cracking was observed during cyclic testing. Therefore, it can be inferred that the stresses in the specimen remained below the modulus of rupture of the concrete.

Another assumption made in the modeling was the use of a pin and roller support at the ends of the beam. Based on the results of the displacements along the test specimen (refer to Figure 57) it can be seen that the shape of the curve follows the deformed shape of a simply supported beam (refer to Figure 98 for an example of how the displaced shape of the no-connection and welded connection specimens follow the displaced shape of a simply supported beam subjected to concentrated forces at its quarter points; noting that the smoothness of the specimen's displaced shape is limited by the accuracy of the string pots used). In addition, the

use of rubber bearing pads in the test setup provided vertical support to the specimen but not lateral restraint. Therefore, the pin and roller support (simply supported configuration) is suitable.

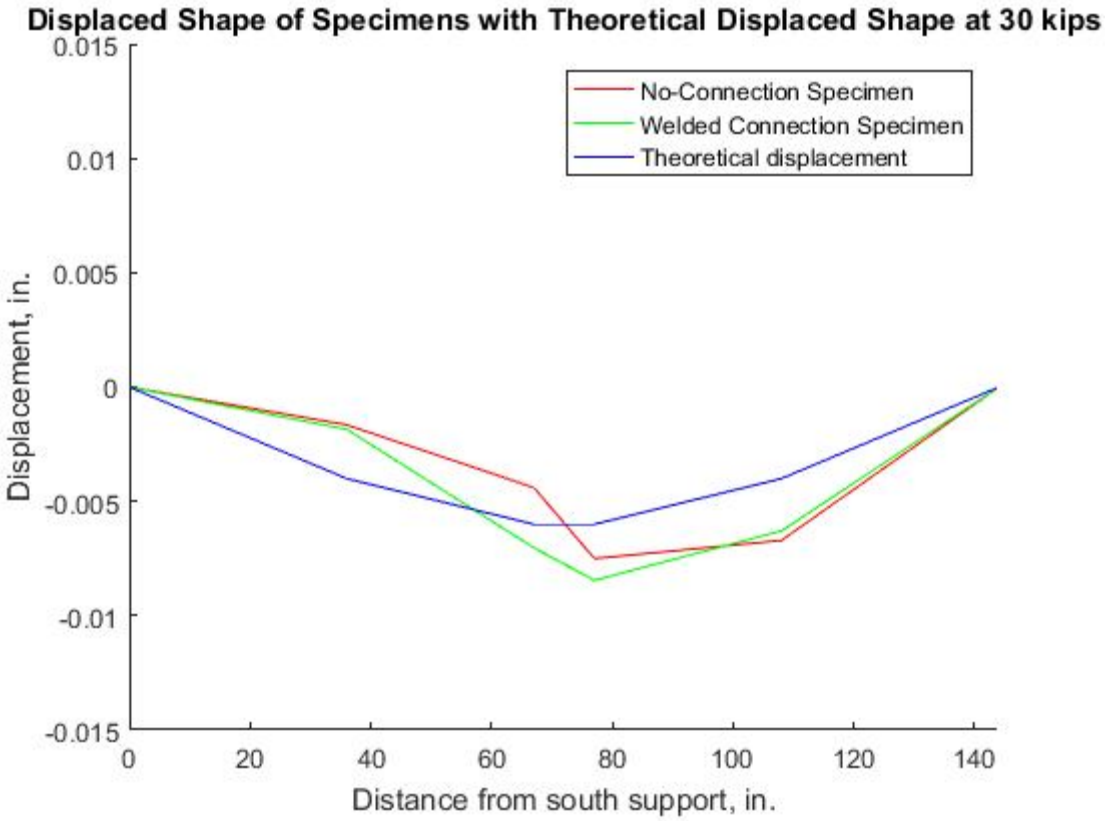

Figure 98 Displaced shape of no-connection specimen at 300000 cycles and welded connection specimen at 500000 cycles plotted against theoretical displaced shape of elastic beam

A tie constraint was used to connect the top surface of the precast beam concrete with the underside of the C.I.P. topping concrete. This carries with it an implied assumption of perfect bond between the two surfaces. During the cyclic testing the results of LVDT recordings showed that there was no slip at the surface interface between the two concretes. Additionally, no cracking or relative movement was visually observed along this surface interface. Therefore, the assumption of perfect bond appears to be well justified for service loading.

Gross section and un-cracked material properties were used during modeling. During the cyclic testing, no loss of section or cracking was visually observed, and instrumentation recordings gave no indication that this would be occurring. Therefore, this assumption holds true for this phase of testing.

It is noted that the model makes no account of the weight of the spreader beam that was placed atop the "wheel pads". Though this could have been easily included in the model as an additional concentrated force at the location of the wheel pads, it is recognized that the section used was a W12 x 50. Being approximately 8 ft long, the total weight of the beam was approximately 0.4 kips. During failure testing the spreader beam was changed to a W14 x 120 with a total weight of approximately 0.96 kips. The addition of these loads would have made only a small contribution (1.34% increase in total load during cycling, 1.5% during failure testing) and were therefore neglected to simplify the model.

It should be noted that the finite element modeling carried out during this phase of work was closely based on the modeling carried out by Virginia Tech researchers Menkulasi (2014) and Mercer (2012) but with some slight differences. Overall, the modeling for the current phase of work tried to mimic more closely, the as-built bridge characteristics for the U.S. Rte. 360 Bridge Over the Chickahominy River. The full bridge model created during previous work consisted of two 37.5 ft long spans, comprised of 19 adjacent inverted T-beams making up the 114 ft width of the bridge. Now, however, the full bridge model consists of two 43 ft long spans, made up of 18 adjacent inverted T-beams plus two edge beams to make up a 112 ft 4 in. width of bridge. Additionally, in the subassemblage model, the pin and roller support conditions were placed at the center of the bearing pads in the Testing Setup rather than at the edges of the subassemblage as they were in previously created models. This more closely represented the actual testing setup. These changes to the geometric properties of the models resulted in the need for a 27 kips actuator load, rather than the previously acquired value of 25 kips, to create stresses in the subassemblage model that matched the stresses in the full bridge model.

Failure Modes of Each Specimen

No-Connection Specimen

As described in the section on Results from Monotonic Test to Failure, failure of the no-connection specimen occurred along the tapered web surface interface between the precast beam and C.I.P. topping concrete on the southern side of the beam. The failure can be seen in Figure 68.

Interestingly, there was not a matching failure on the northern side of the beam. A possible reason for this occurring is as follows: During construction of the specimens, there was

debate as to how to roughen the interface of the tapered web and flange sections. Different methods were trialed, and eventually it was decided to use an indented wood form covered with a thin sheet of plastic. This is described more in the earlier section on Surface Roughening. However, during fabrication of these wood forms an issue arose. Since no strict guidance is currently provided by AASHTO (2014) regarding the frequency at which the undulations in the forms needed to appear, and how wide the ridges and troughs needed to be, a 1 in. wide ridge-trough formation, with these being formed at a spacing of 2 in. clear was selected. On the south side of the beam, where the specimen failed, the spacing of these formations was made as 3 in. clear rather than the specified 2 in. clear. Due to time constraints, the form could not be re-made prior to casting of the beam concrete and it was decided to proceed using this form. The fewer indentations could have potentially contributed to a reduced interlock strength between the precast beam and C.I.P. topping concrete.

Another possible reason for this type of failure occurring which is also related to the formwork indentation is this: the addition of a thin sheet of plastic over the formwork, although preventing the formwork becoming glued to the concrete and difficult to remove, caused the ridges to become less angular in their formation. As a result of this, the interlock between the precast beam and C.I.P. topping concretes may have become less effective.

The impact of this type of failure mode occurring with regards to the specimen behavior was to make the specimen fail at a much lower load than expected. During previous testing on a no-connection specimen with similar geometry and reinforcement, failure occurred via a large crack opening up in the joint above the C.I.P. topping. The actuator load required to cause failure was 240 kips (Menkulasi 2014) - almost four times the load which caused failure for the specimen in this phase of testing. The difference in magnitude of the loading at failure can be seen in Figure 99.

Another impact that the surface interface failure had on the specimen is the lack of significant ductile response. As can be seen by the load versus midspan deflection curve in Figure 100, the displacements increase linearly with increasing load, until failure occurs at which point the specimen almost immediately loses its load-carrying capability. This can be compared to the load vs midspan deflection to failure curve for the tapered web, no-connection system tested by Menkulasi (2015) – shown in Figure 99. As can be seen for Menkulasi's test, significant post-elastic response is observable prior to the specimen reaching the load at which it

fails. Note that the specimen used by Menkulasi (2015) had similar geometry and reinforcement characteristics as the ones used for cyclic testing. It is noted that the behavior of both specimens is similar up to the load at which large slips begin to occur in the no-connection system subjected to cyclic loads.

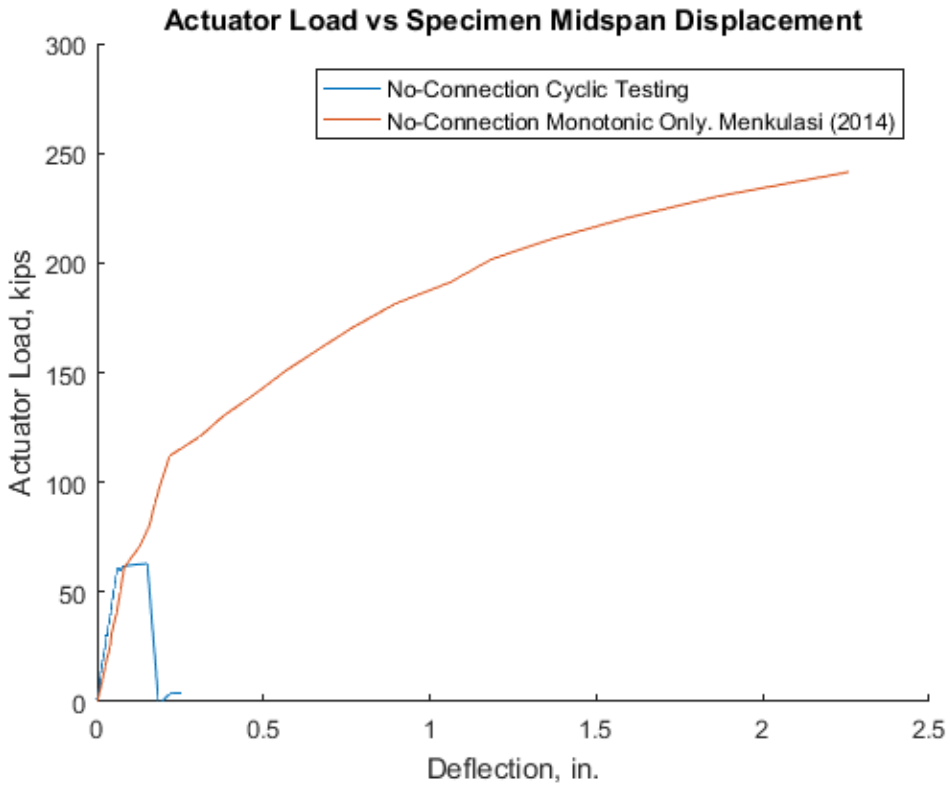

Figure 99 Load versus midspan deflection to failure for no-connection specimens during the cyclic testing regime currently being carried out (2016-2017), and Experimental Testing Phase II carried out by Menkulasi (2014)

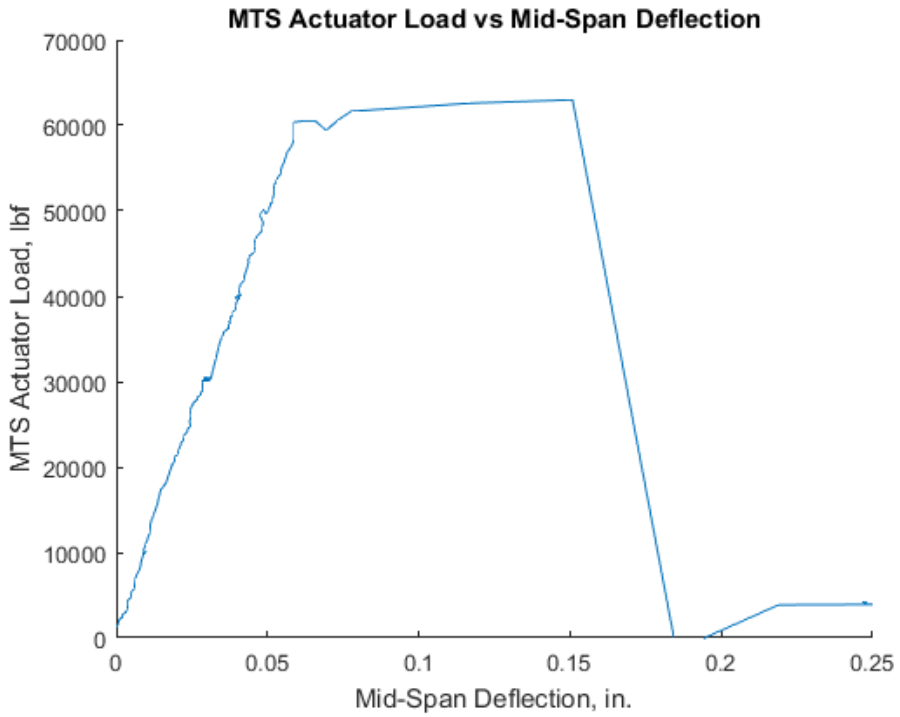

Figure 100 Plot of MTS actuator load versus midspan deflection including post-peak for no-connection specimen during current (2016-2017) phase of testing

Overall, this affects the outcomes of the testing. Firstly, behavior of the no-connection specimen during cyclic load testing was adequate. No failure or loss of performance of any type was observed over the entire 3650000 cycles. However, the failure of the specimen along the surface interface begs the question of whether it really was the formwork construction that created this failure, or whether the effect of cyclic loading was to deteriorate the interface surface such that failure occurred along this plane during the ultimate load testing. As a result, the no-connection system cannot yet be completely verified for use in high volume bridges. Additional testing may be required to determine which one of these two caused the failure. If it was the surface roughening, guidelines into this construction procedure would be needed to ensure adequate shear-friction transfer can develop at the interface between the two concretes.

Welded Connection Specimen

The Results from Monotonic Test to Failure for the Welded Connection Specimen describes that failure of this specimen occurred with a brittle fracture of the weld metal at the location near the smooth drop-in reinforcement. When this occurred, a hinge formed between the

precast beams, all load was carried on the C.I.P. topping at midspan, and this caused a large crack through the C.I.P. topping concrete directly above the joint between the two adjacent precast beams. The failure is shown in Figure 87. After failure, the specimen was able to carry a residual actuator force of 60 kips (refer to Figure 101). The hand calculations attached in (Appendix I – Calculations for Post-Failure Capacity of Welded Connection Specimen), show that this would be in accordance with the C.I.P. topping sustaining all of the load, and the bent reinforcement in the C.I.P. topping fully yielding.

The embedded plate tapered web specimens tested by Mercer (2012) and Menkulasi (2014) did not fail under the same loading conditions. Their specimen was able to reach the frame capacity of 300 kips, without failing. During their test, they observed a large crack at the interface between the precast beam and C.I.P. topping concrete. In the testing carried out by Mercer (2012) and Menkulasi (2014), they noted that the actuator load which caused first cracking was 110 kips. Although during the current phase of testing, the first hairline cracks appeared at an actuator load of 50 kips, it is observed from the displacement, strain gauge, and LVDT results that a reduction in stiffness due to cracking did not occur until 110 kips. Therefore, the initial cracks were not detrimental to the performance of the specimen, and first cracking could be considered 110 kips.

Though the welded connection specimen did fail at a load of 200 kips, it should be noted that after cycling the specimen for the equivalent of a 50 year design life, this is still over six times the service loading of 30 kips. Using the equation developed by Menkulasi (2014) to calculate the factor of safety against cracking and ultimate loads, the welded connection specimen, after being cycled at the service load 3650000 times, has a factor of safety against cracking of 4.2, and a factor of safety against ultimate loads of 7.0. It is also noted that at failure, as shown in Figure 101, the residual load capacity of 60 kips is still approximately double the service loading.

Figure 101 shows the complete load-deflection response of the specimen on the second day of testing. As can be seen, the specimen exhibits some inelastic response. However, at the point where the weld failure occurs, the drop in load-carrying capacity is sudden - the specimen during this test exhibited a brittle failure mode. Referring to the discussion on Strain Gauge Results for the Welded Connection, it should be noted that at the time of weld failure, yielding of the reinforcement in the C.I.P. topping was assumed to have occurred. Comparison of the load-

deflection behavior to that observed by Mercer and Menkulasi for the same type of connection (see Specimen 3 in Figure 102), shows that there was much less deflection able to occur at failure – 1.6 in. compared to 0.5 in. However, it should be noted that the behavior of both specimens up to an actuator load of 194 kips is similar. Mercer (2012) noted during his testing that yield of the reinforcement occurred at a load of 165 kips at the middle of the specimen. Due to a lack of available data as a result of strain gauge failures during testing, and owing to the similar behavior of the specimen up to the failure load, 165 kips is used as the load at which yield of the C.I.P. reinforcement occurs. This allows the calculation of displacement ductility to be made, as displacement ductility is the ratio of displacement at failure to displacement at first yield. For the specimen most recently tested, the displacement ductility attains a value of approximately 4, while for the specimen tested by Mercer, the displacement ductility reaches over 7.4. While the displacement ductility of the specimen is much lower than that reached during Mercer's tests, the welded connection exhibits much greater ductility when compared to the no-connection specimen tested during this round of experimentation.

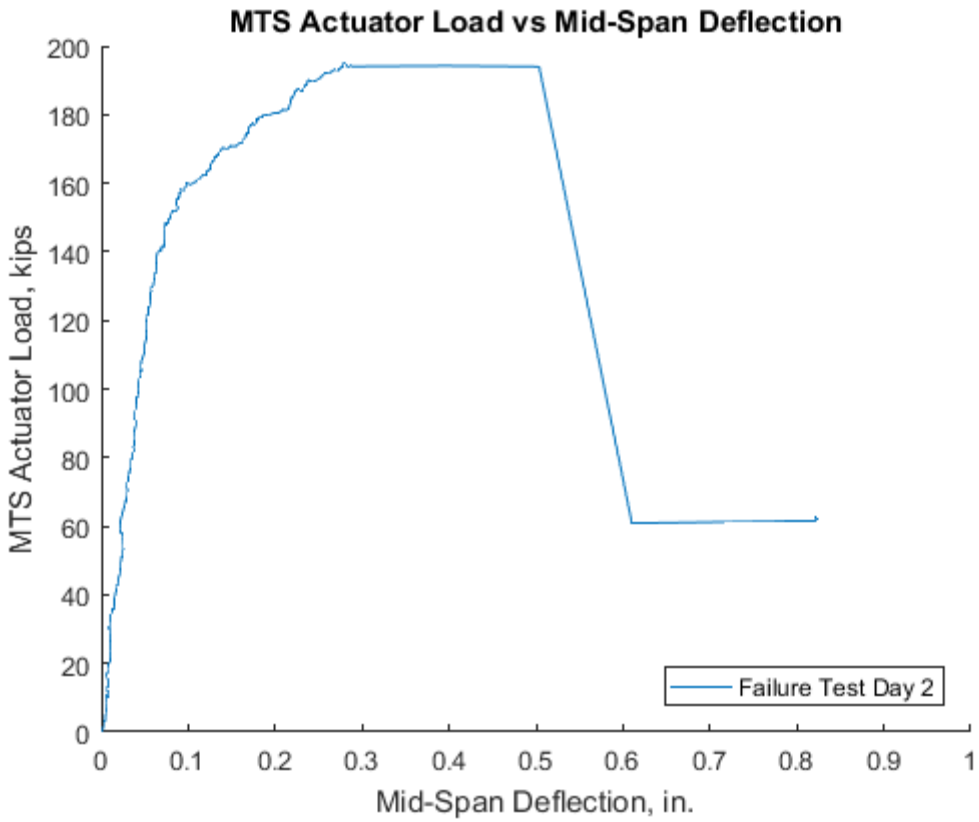

Figure 101 Welded connection failure test day 2 - load versus deflection showing full response

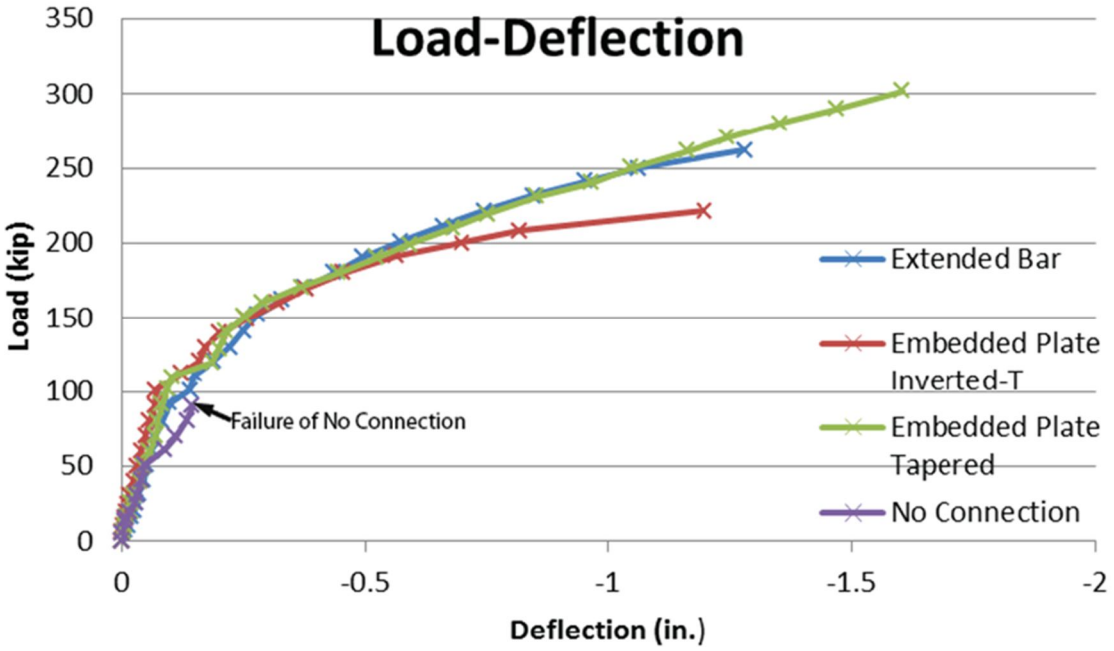

Figure 102 Load-deflection behavior of specimens tested by Mercer and Menkulasi. Obtained from Mercer (2012)

Although the weld failed near the drop-in reinforcement, the results from cyclic testing of the specimen indicates that cyclic loading was not detrimental to the behavior of the specimen and is therefore not responsible for the early failure of this connection. This is also indicated by the observed failure surface having a clean, bright appearance with no “beach marks” indicating a brittle fracture. It is thought that the weld geometry had a part to play in this. Looking at Figure 20, it is clear that the at the location where the smooth rod and embedded plate touch, there is essentially a “notch” geometry. The root pass of weld is the weld in this corner location. As the first pass is not good, this creates a weakened point of the weld, at the location of a stress concentration. In addition, under positive bending the joint is trying to open, and the notch is trying to open the first pass of weld. This created a point at which high localized stresses caused fracture initiation. The fracture then propagated vertically through the weld causing failure of the connection. The fracture surface, and build-up of impurities at the root of the weld can be seen in Figure 103 and Figure 104.

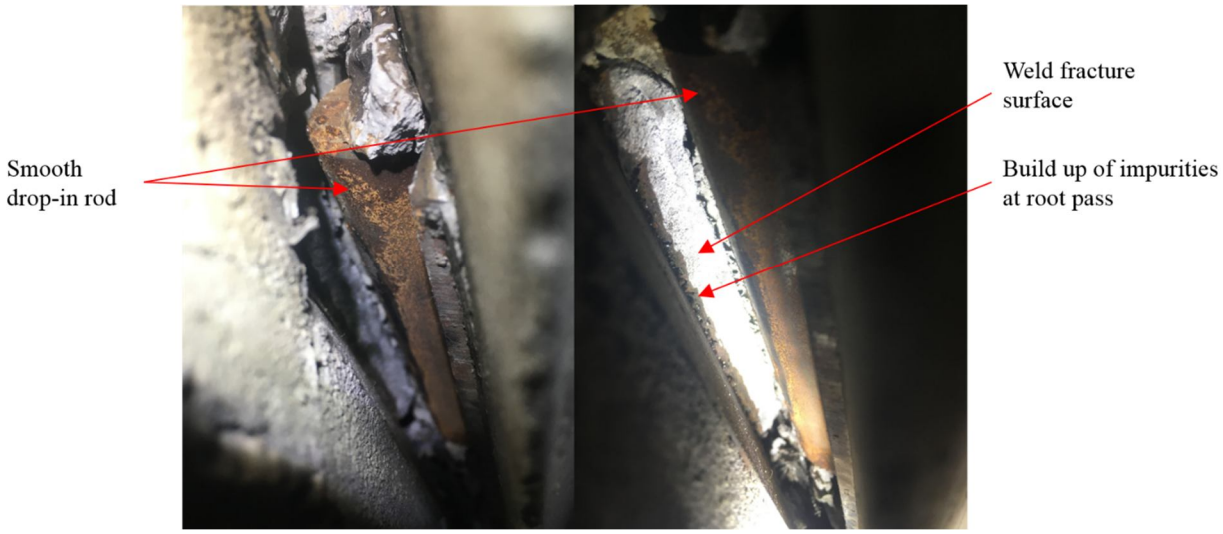

Figure 103 Welded connection failure, view looking E-W on welded connection from underneath specimen

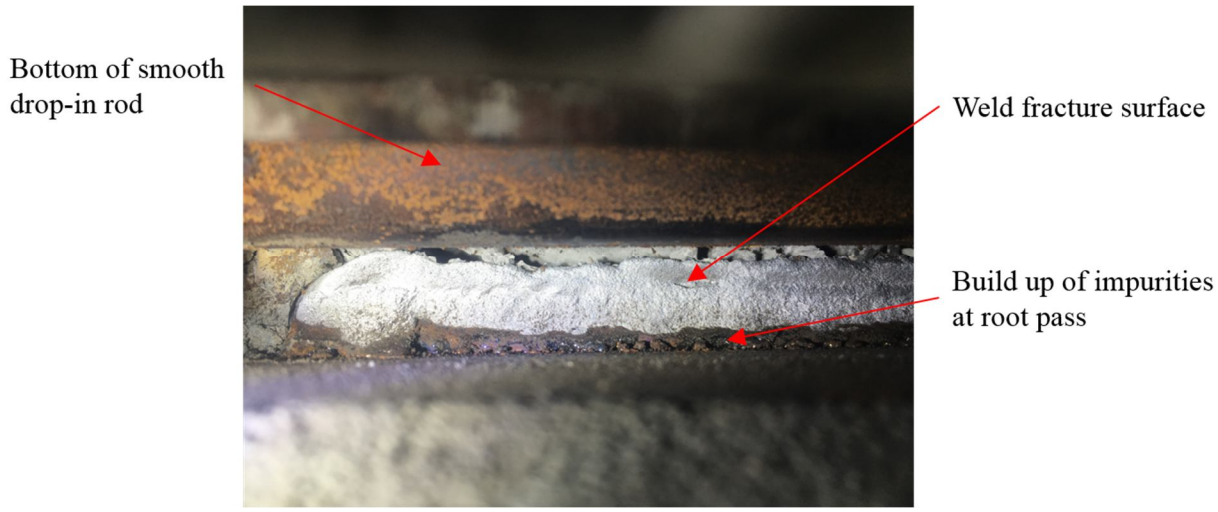

Figure 104 Welded connection failure, view looking N-S on welded connection from underneath specimen

Displacement Results

Comparison to Finite Element Analysis (FEA)

Under the 30 kip actuator loading condition, the FEA models predict a displacement of 0.0045 in. at the midspan of the sub-assemblage specimen (refer to Figure 105) due to actuator loads.

For the no-connection specimen, taking an average value of the displacements measured by the north midspan and south midspan string pots over all of the static load tests carried out, and subtracting out the displacements at the supports due to the compression of the bearing pads, the average midspan displacement measured by the string pots has a value of 0.0134 in. This is

larger than the predicted displacement from the FEA model by 0.0089 in. As is described in the following section, the string pots used for this testing are accurate to approximately 0.01 in. and therefore this difference is within an allowance for error for the instrumentation.

Doing the same for the welded connection specimen, we get an average recorded displacement over all of the static tests of 0.0057 in.; much closer to the predicted value of 0.0045 in. however slightly above it. The presence of the welded connection alters the stiffness of the real system and is not accounted for in the FEA model. However, this small difference could also be due to the limited accuracy of the string pots used as was described in the previous paragraph.

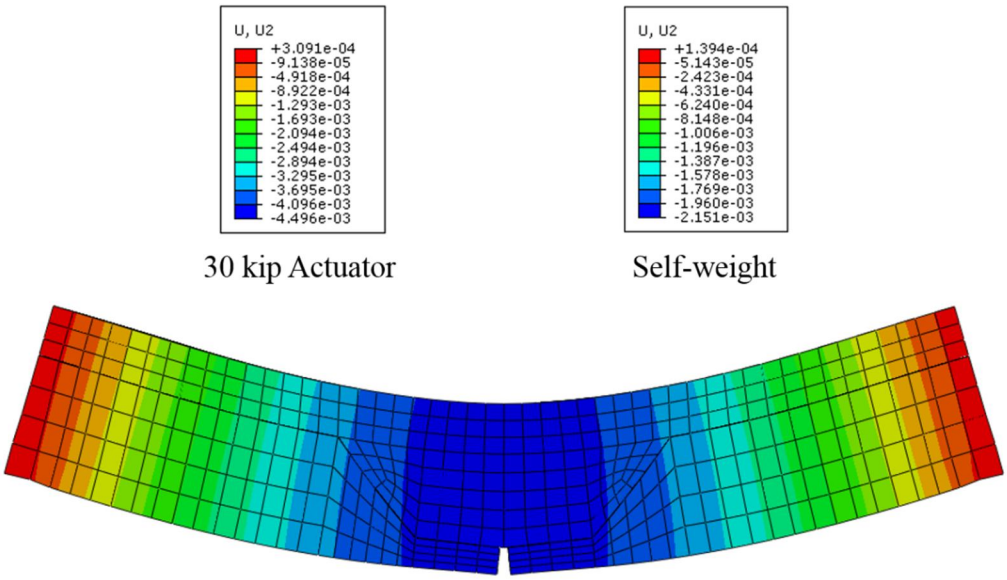

Figure 105 FEA predicted displacements for subassemblage under 30 kip actuator load and self-weight. Displacements given in units of in.

Effective Bending Stiffness Under 4 Point Bending During Cyclic Loading

For the no-connection specimen the Results section notes a decrease in the "effective bending stiffness". This effective stiffness was calculated as the load divided by the displacement for the cyclic load testing where load-displacement behavior remained linear. For the no-connection specimen, this effective stiffness decreased from 2797 kips/in. to 1956 kips/in. Looking at the table of "Displacements in Inches Along the Beam at 30 kips for Each Test" located in Appendix G – Results Tables for No-Connection Specimen, it can be seen that after 300000 cycles, there is a jump in the values of north midspan displacements being recorded. The recorded values reduce by approximately 0.01 in. The reason for this reduction is unknown,

however, it is noted that a reduction in the values of displacements being recorded at the supports would increase the value of deflections plotted in Figure 59. This explains the reduction in stiffness at the final static load test. It is unlikely that cyclic loading reduced the stiffness of the specimen because the strain readings and LVDT readings remain consistent throughout testing. Therefore, it is deduced that a malfunction to the recordings of the string pots occurred after 300000 cycles.

For the welded connection specimen, the stiffness actually increased from 2595 kips/in. to 3073 kips/in. It is noted by the string pot manufacturer that the specific string pots used have an accuracy of 0.1% of their 10 in. stroke – 0.01 in. As can be seen in Figure 76, for the initial static test, the displacement values are within 0.01 in. but the majority of values are higher, or to the right of the best fit line, thus reducing the slope of the line. Figure 77 shows the opposite for the final static test – that is, most of the string pot recordings are lower, or to the left of the best fit line, but still within the accuracy of the string pot of 0.01 in. As no visual observations could explain an increase in stiffness, and the strain gauge and LVDT results indicate that the specimen has neither gained nor lost stiffness throughout the test, it is possible that the increase in effective stiffness obtained from the load-displacement curves is due to measurement error in the string pots. As can be seen in Figure 106, all recording magnitudes fall within an order of accuracy of the string pots which could explain this apparent increase in effective stiffness.

It would be expected that the welded connection would have a higher effective stiffness than the no-connection specimen due to the presence of the embedded plates and welded connections that add to the overall stiffness of the specimen's joint region. Since the joint region is at midspan, and this "effective stiffness" is calculated based on midspan deflections, this creates a situation where the welded connection has a higher "effective stiffness".

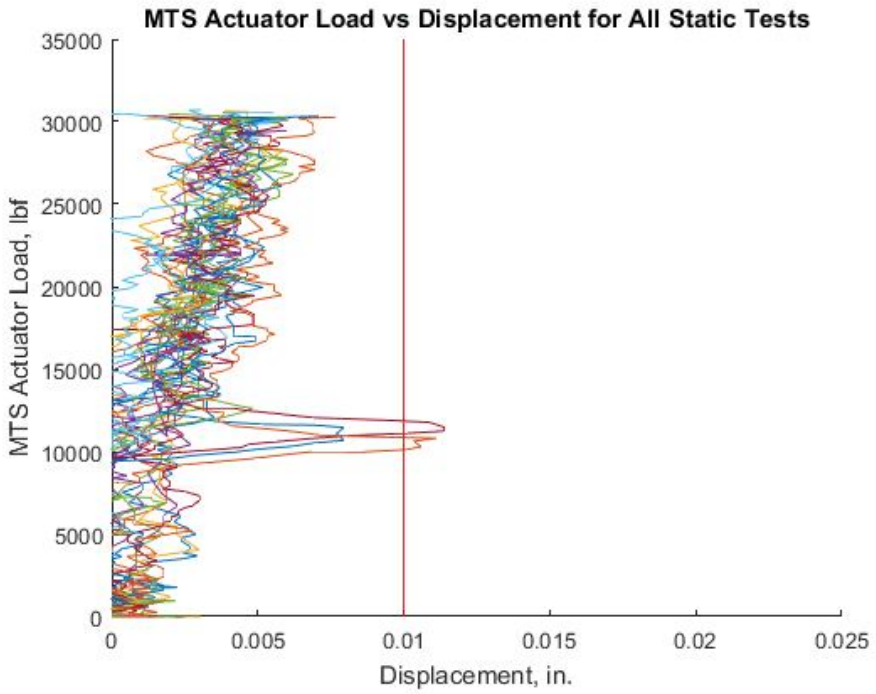

Figure 106 Plot of load versus displacement for all static load tests for the welded connection specimen.

Strain Gauge Results

No-Connection Specimen

The results section shows that five of the six attached strain gauges were giving readings. The sixth strain gauge which was attached to the C.I.P. topping bent reinforcement on the west side of the specimen did not record any values. The reason for this was unknown. Initially it was thought to be a gauge error, however, during subsequent testing of the welded connection specimen, the same gauge location was not able to read any values. As a result of this it is thought that the culprit is the System 5000 data acquisition system's memory cards.

Under cyclic loading at the service level load, Table 12 shows that the maximum strain in the bent reinforcement in the C.I.P. topping reached 44 με, and the reinforcement in the beams reached 24 με. The finite element model is in agreement with these values. Noting that the strain gauges were zeroed prior to application of the 30 kip load, and referring to Figure 43, the finite element model shows that in the region of the C.I.P. reinforcement, the stresses are approximately between 0.163 ksi and 0.187 ksi under the 30 kip actuator load. Taking an average of these values the stress in the concrete around the reinforcement is approximately 0.175 ksi. Using AASHTO (2014) to calculate the modulus of elasticity of concrete (refer to the equation

below), and noting from the Material Testing Results that the C.I.P. topping concrete reached a strength of 6200 psi, we find the modulus of elasticity of the C.I.P. topping concrete to be 4774 ksi. The strains in the concrete at the level of the reinforcement - under the assumption of linear-elastic behavior – are therefore calculated as 37 με. Using a similar approach, the strain in the beam reinforcement can be found from the finite element model. The model shows the stresses in the concrete at the level of the beam reinforcement to be approximately equal to 0.089 ksi under the effect of the 30 kip actuator load. This equates to a strain at the level of the beam reinforcement of 19 με.

$$E_c = 33000(w_c^{1.5})\sqrt{f_c'}$$

Hand calculations are attached in Appendix J – Calculations for Expected Strains During Testing to demonstrate a simple beam theory calculation of strains assuming linear-elastic behavior. The calculations show that the values of strain obtained during the 30 kip static load tests are as expected for the beam reinforcement – 19 με. However, the hand calculations underestimate the strains in the C.I.P. topping reinforcement, because they do not account for the discontinuity at the joint between the two adjacent precast beams which creates a stress concentration and increases the stresses at this location. The hand calculations predict a strain of 30 με in the C.I.P. topping reinforcement, lower than the 44 με actually attained.

It was mentioned in the Results section, that the strains remained below that which would cause cracking in the concrete. Assuming linear-elastic behavior, an assumption justified by the load-displacement behavior of the specimen and the low levels of strain recorded, the strain required to cause cracking in the concrete can be calculated as 125 με. The maximum recorded strain reaches a value of 44 με in the C.I.P. topping reinforcement. Therefore, the results of the recorded strain values are in agreement with the visual observations which indicated no cracking during service load testing.

It is also important to note that at the failure load of 63 kips, the maximum recorded strain in the C.I.P. topping reinforcement attained a value of 1075 με. The yield strain of a piece of Grade 60 mild reinforcement is equal to 2070 με. The reinforcement does not yield prior to failure of the specimen. This is in agreement with the non-ductile behavior of this specimen caused by this specific failure mechanism. Comparing this fact with the results obtained by (Mercer 2012) it can be seen that, although they were able to yield the reinforcement, this occurred at loads of 80 kips - 90 kips, much greater than the failure load for this specimen. It is

thought that if failure of the surface interface had not occurred, yielding of the reinforcement would have occurred.

Welded Connection

It was noted in the discussion regarding the strain gauge results in the no-connection system, that only five of the six strain gauges were able to record data. The sixth strain gauge, located in the C.I.P. topping bent reinforcement on the western side of the beam, was again unable to record strain information. Due to the same gauge location not reading anything for both of the tests, it was thought that this could be due to an issue with the System 5000 data acquisition system, rather than the gauge itself.

As can be seen in (Appendix H – Results Tables for Welded Connection Specimen) and in Table 16 of the Results section, between the static tests, the strain gauge results have not changed significantly. This would indicate that over the period of testing, there was no obvious diminishment in performance of the welded connection. Had the welded connection deteriorated during the cyclic testing, larger strains would have been expected to be recorded, especially in the C.I.P. topping reinforcement as the behavior of the specimen would move more towards the behavior of the no-connection specimen.

It is interesting to note that for the welded connection, the FEA model slightly over-predicts strains in the specimen, compared to what was recorded by the strain gauges in the specimen. For example, a maximum strain recording in the precast beam reinforcement of 17 με was close to the 19 με predicted by the FEA model (refer to the discussion on Strain Gauge Results in the No-Connection Specimen) but the FEA model predicted a higher value. This was the same, only accentuated in the C.I.P. topping reinforcement, where predicted strains of 37 με were higher than the actual strain recorded of 26 με. This is due to the presence of the welded connection. The presence of the welded connection adds to the overall stiffness of the section when bending in this direction. This contributes to lower displacements and consequently lower strains. The added stiffness from the welded connection was not accounted for in the modeling in order to keep the models as simple as possible.

When comparing these results to the manual calculations provided in Appendix J – Calculations for Expected Strains During Testing, we note that these simple calculations using linear-elastic engineering beam-theory give results close to what was recorded by the

instrumentation in the precast beam, however they under-predict the strains in the C.I.P. topping reinforcement. These simple calculations assume a completely monolithic section, which indicates that the behavior of the welded connection specimen over the joint is somewhere in-between a fully composite beam, and a non-composite one. In the precast beam reinforcement, hand calculations predict a strain of 18 με, almost matching the 19 με recorded. In the C.I.P. topping, the hand calculations give predicted strains of 12 με, compared to the 26 με recorded.

In the Results section, it was mentioned that none of the strains recorded exceed strains needed to initiate cracking in the concrete. Assuming linear-elastic behavior, an assumption which is justified by the low strains in the specimen and the behavior exemplified by the load-displacement curves, the strain required to cause cracking in either the precast beam or C.I.P. topping is 125 με. As can be seen from the Results, the maximum strain reaches a value of 26 με. Although this would theoretically be the strain at the level of the C.I.P. reinforcement, and the critical fiber would be below this; it is unlikely that over this 1 in. distance the strains would increase by a multiple of 5. The results from the strains pertaining to cracking under service loads are in agreement with the visual observations of no cracking during cycling under service level loads.

The results from the strain gauge recordings during the first day of monotonic testing to failure show a large jump in strain at 110k with no corresponding increase in load (Figure 91). Comparing this to the results from visual observations, and the load-deflection plots, we can see that this corresponds to cracking in the C.I.P. topping. Note that although hairline cracking began to appear at an actuator load of 50 kips, this did not have any corresponding increase in strains, or deflections – no loss of stiffness was indicated from the results. Due to this, it is inferred that the cracking occurring at 50 kips was superficial. At 120 kips, another smaller increase in strains occurred in the beam reinforcement. 120 kips is the load at which cracks that had previously formed in the C.I.P. topping widened to approximately 0.007 in., and propagated further through the section.

On the second day of monotonic testing to failure, it is observed that the strains increase linearly to 130 kips, with strains in the beam reinforcement ranging between 400-700 at this load. These are the same values of load and strain at which the testing was stopped the previous day. Hence the strains followed a “reduced, or, cracked stiffness” up to the 130 kips. The maximum strain attained by the beam reinforcement had a value equal to 2003 με. This indicates

that at the time of failure, the reinforcement in the beam flanges had not yet yielded. According to Mercer (2012), during previous testing of a similar specimen, yielding occurred at an actuator load of 165 kips. In addition, it is noted that the strains in the C.I.P. reinforcement are much higher than those in the precast beam reinforcement. This indicates that yielding of the C.I.P. reinforcement had taken place prior to failure. This correlates well to the ductile behavior (though limited) of the subassemblage described in the discussion on load-deflection behavior above.

Comparing the strain results for the welded connection specimen, to those obtained from the no-connection specimen, it can be seen that the initial stiffness of each specimen up to their respective cracking loads is very similar. However, in the no-connection specimen cracking occurs much earlier (50 kips), and due to the nature of the failure mechanism for this specimen, the strains are less than half of what the strains reach in the welded connection specimen. Although, ultimately, the failure mode of both specimens was brittle, the no-connection specimen did not exhibit any strain ductility since none of the reinforcement reached yield prior to failure of the specimen. This is undesirable as the failure was much more instantaneous compared to the welded connection specimen which did exhibit strain ductility.

LVDT Results

No-Connection Specimen

The LVDT results show the amounts of relative slip occurring between the precast beam concrete and the C.I.P. topping concrete, and opening of the joint at the flanges of the precast beams. The LVDT recordings during cyclic loading show that there is no relative slip between the precast beam concrete and the C.I.P. topping concrete. Thus during service loading, monolithic behavior was observed, and the LVDT results indicate the specimen performed as expected. Additionally, it is noted that there is little difference between the results observed during the initial testing prior to cycling, and after completion of the 3650000 cycles. This indicates that the performance of the interface did not deteriorate over the period of cyclic testing for service loading. For the same reason, it is inferred that the joint did not show deterioration over time either. Finally, it can be noted that upon unloading, during service loading, there was no residual deformation of the joint region which justifies assumptions about the elastic behavior of this region during service loading.

For the applied service loading conditions, the FEA modelling predicts a joint opening of 0.0006 in. on both sides of the specimen at the bottom of the joint. The model does not predict slip between the interfaces of the precast beam and C.I.P. topping due to the tie constraint used at these surfaces which adheres them with a perfect bond. Looking at Figure 60, the LVDT recordings show that the east joint opens to approximately 0.0005 in. for the initial test, and to about 0.001 in. for the final test. Figure 61 shows the west joint opening to almost 0.001 in. for both the initial and final static load test. These numbers are within a suitable range, though not completely accurate, for the FEA model. Differences from the real specimen's values to the model may be due to construction defects within the region of the joint.

During the failure load testing, the results show that the joint opening increases with increasing load, and then spikes at failure. The joint opening increasing largely at failure is a result of the loss of monolithic action at failure due to the debonding of the two concrete interface surfaces. When this happens, the two beams try to rotate as rigid bodies, and the joint opening at the bottom of the beam gets larger. This effect is illustrated in Figure 107.

It is interesting to note in Figure 72 to Figure 74 in the Results section for the monotonic failure testing of the no-connection specimen, that the behavior on each side of the specimen is not the same. Unusual behavior from a load of 60 kips to 63 kips was noted where the slip recorded on the southwest beam-C.I.P. interface actually decreased. It was noted that at the same time, there was significant opening of the joint on the east side of the beam, while the slip recorded at the northwest beam-C.I.P. interface increased. Two possible explanations for this behavior are presented; the first being simply due to noise in the recording equipment creating this effect as the slip values recorded were so small. The second, perhaps more interesting possibility, is that it at the same time as the southwest interface slips appeared to be reducing, the east joint opened more than the west joint. What could have happened is that once monolithic action was lost, the southern precast beam tried to twist itself in a clockwise direction, reducing the slip recording at the southwest beam-C.I.P. interface and increasing the slip recorded at the northwest beam-C.I.P. interface. This effect could have been caused by an uneven loading condition where the actuator pushed down on the east side of the beam slightly more than the west.

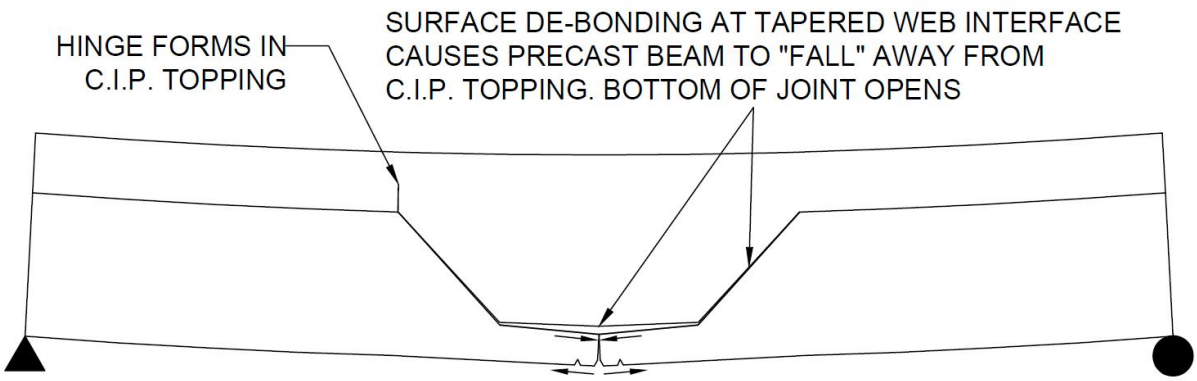

Figure 107 Diagram demonstrating tapered web surface bond failure causing joint opening

Welded Connection Specimen

During the cyclic load testing, the results from the LVDT measurements indicate that there was no slip at the interface between the precast beam concrete and the C.I.P. topping concrete. Also, Figure 78 and Figure 79 show that during service loading there was no significant opening of the joint between the adjacent precast beams. This meant that the specimen, with its two concretes cast at different times, acted as a single monolithic beam throughout the period of cyclic testing as was expected. Due to the fact that there was not a significant amount of variation between the results recorded for the initial and final static load tests, it is inferred that the performance of the interface between the two concretes did not deteriorate over the period of cyclic testing. The joint did not show deterioration over time either, as there is little difference between the initial and final joint opening data. Finally, it was shown that for all of the static load tests, during unloading, the joint “closed” itself and no residual deformation was left in the joint which means the joint region behaved in an elastic manner. This justifies the assumptions made during the modeling of the specimen, and the use of simple linear-elastic equations in calculating the cracking strains of the specimen above.

For the service level loading, Figure 78 and Figure 79 both show that the joint opening is smaller than that predicted by the FEA model. The predicted opening is 0.0006 in. while the east and west joint of the welded connection specimen have joint openings less than 0.0004 in. This would be expected, as the presence of the welded connection which ties the two adjacent girders together would reduce the amount that the joint could open under loads.

The Results from Monotonic Test to Failure for the Welded Connection Specimen indicate that slipping or cracking of the surface interface between the precast beam and C.I.P. topping concrete was limited to two locations. The first was at the interface on the southwest tapered web of the beam. Hairline cracking at the interface close to the top of the web appeared at 60 kips, indicating slippage. This crack propagated a slight amount at loads of 90 kips and 100 kips. This explains the jumps in the southwest LVDT readings at these loads on the first day of testing. The second location at which more significant slippage occurred was at the northwest tapered web interface at 190 kips. This was again indicated by a jump in the LVDT reading at this location at 190 kips, and coincides with visual observations of crack formation along the surface interface following the profile of the tapered web and flange. The results showing joint openings at the east and west joint locations show when cracking appears in the C.I.P. topping, a significant amount of opening occurs at the joint which would be expected as stresses in the concrete are relieved as the joint opens. Additionally, on the second day of testing it is clear that the joint behavior follows a reduced stiffness similar to the rest of the specimen.

Compared to the no-connection specimen during the failure test, the welded connection exhibited a much more desirable behavior with regards to the slippage at the interface locations. Small amounts of slip occurred at one location (the southwest web) at a load of 60 kips, but this stabilized at a load of 100 kips and no further slip was recorded at this location. Larger amounts of slip occurred at 190 kips prior to the specimen failing, however failure was not along the surface interface. In the no-connection specimen however, first cracking occurred along the surface interface, and these cracks widened and propagated until failure occurred along the surface interface. Failure due to slip along an interface results in a sudden loss of composite action and therefore a sudden reduction in load-carrying capacity. Therefore, this mode of failure is highly undesirable and can be prevented by adequate interface surface roughening measures.

CONCLUSIONS

The first objective of this research was to develop preliminary design tables for the inverted T-beam bridge concept, similar to those already in use by VDOT for adjacent box-beam and voided slab bridges. The preliminary design was undertaken in accordance with AASHTO (2014) allowable stresses, midspan flexural strength, and mid-span short term deflections and camber. Tables needed to cover a range of span lengths, prestressing arrangements, and include

considerations for the use of lightweight concrete. Currently the tables only cover the use of an 18 in. deep precast beam with a 7.5 in. thick C.I.P. topping.

The second major objective was to verify the use of the no-connection inverted T-beam system on high volume bridges through cyclic load tests on a subassemblage specimen. 3650000 cycles of testing - representing a bridge carrying 200 ADTT over a 50 year design life - was carried out at a frequency of 2 Hz. The results of these cyclic load tests were compared with the results of cyclic load testing on a similar subassemblage specimen using the welded connection inverted T-beam system.

Based on the work the following conclusions are drawn:

Preliminary Design Tables

- The comfortable maximum span length currently stands at 50 ft for all combinations of normal weight and lightweight concrete. Altering the concrete unit weight reduces the number of prestressing strands needed, but does not increase span length.
- Reaching spans up to 70 ft is possible, but requires time-consuming construction methods such as staged deck placement, the use of temporary midspan shoring, and/or cutting top strands in the beam prior to deck placement.

Cyclic Testing

- Both subassemblage specimens - the no-connection specimen and the welded connection specimen - exhibited satisfactory performance, with no degradation over time under cyclic load conditions.
- Monotonic loading to failure upon completion of the cyclic testing caused an unanticipated failure mode for the no-connection system. Failure occurred along the surface interface between the precast beams and the C.I.P. topping at a load much lower than anticipated. The cause of this was determined to be inadequate surface roughening of the interface.
- Monotonic loading to failure of the welded connection system also exhibited an unanticipated failure mode whereby the weld failed in a brittle manner, causing the section to lose composite action and a large crack to appear through the C.I.P. topping directly over the joint. The cause of this was thought to be poor weld quality at the root

pass, and the geometry of the welded connection creating a large localized stress at the weakest point of the weld.

- The no-connection system did not demonstrate suitable ductility or factors of safety due to its failure mode.
- In-spite of the unintended failure mode of the welded connection system, adequate subassemblage ductility was observed, and significant factors of safety against cracking and failure were calculated.

RECOMMENDATIONS

Based on the analysis of the results from the testing of the no-connection and welded connection specimens, the following recommendations are made:

- Testing of different surface roughening methods should be undertaken, and guidance provided to ensure that adequate surface roughening is provided between the precast beam and C.I.P. topping concretes. This is especially important for the no-connection system due to the nature of its transverse load path mechanism.
- Once a suitable surface roughening method has been decided on, the no-connection subassemblage specimen testing should be repeated to determine whether the cause of failure during the monotonic load test was in-fact due solely to poor surface roughening, or whether cyclic loading had an effect on the quality of this interface.
- Prior to any welding all surfaces, including those of the drop-in reinforcement must be properly cleaned to ensure a proper weld. The weld should go through proper quality control measures. A possible re-evaluation of the weld geometry may be required.

REFERENCES

AASHTO (2014). "AASHTO LRFD Bridge Design Specifications."Washington D.C.

Culmo, M. P. (2011). "Accelerated Bridge Construction - Experience in Design, Fabrication and Erection of Prefabricated Bridge Elements and Systems." FHWA, Virginia, U.S.A., 346.

FHWA "Make Every Day Count Accelerating Bridge Construction With Prefabricated Bridge Elements & Systems." FHWA, ed.

FHWA (2015). "Connection Details for PBES." Federal Highway Administration, Washington, DC.

FHWA (2017). "Accelerated Bridge Construction." <https://www.fhwa.dot.gov/bridge/abc/>. (05/16, 2017).

French, C., Shield, C., Klasesus, D., Smith, M., Eriksson, W., Ma, J. Z., and Zhu, P. (2011). "Cast-in-Place Concrete Connections for Precast Deck Systems." *Web-Only Document*, NCHRP, ed., NCHRP.

Grace, N. F., Patki, K. D., and Hanson, J. Q. (2011). "Flexural behaviour of side-by-side box-beam bridges: A comparative study." *PCI Journal*(Summer), 19.

Hällmark, R., White, H., and Collin, P. (2012). "Prefabricated Bridge Construction Across Europe and America." *Practice Periodical on Structural Design and Construction*, 17(3), 82-92.

Issa, M. A., Ribeiro do Valle, C. L., Abdalla, H. A., Islam, S., and Issa, M. A. (2003). "Performance of Transverse Joint Grout Materials in Full-Depth Precast Concrete Bridge Deck Systems." *PCI Journal*(July-August), 12.

Joyce, P. C. (2014). "Development of Improved Connection Details for Voided Slab Bridges." Master of Science Explanatory, Virginia Polytechnic Institute and State University, Blacksburg, VA.

Kosmatka, S. H., Kerkhoff, B., and Panarese, W. C. (2002). *Design and Control of Concrete Mixtures*.

Li, L., Ma, Z., Griffey, M. E., and Oesterle, R. G. (2010). "Improved Longitudinal Joint Details in Decked Bulb Tees for Accelerated Bridge Construction: Concept Development." *Journal of Bridge Engineering*, 15(3), 327-336.

Mary Lou Ralls, Ben Tang, Shrinivas Bhide, Barry Brecto, Eugene Calvert, Harry Capers, Dan Dorgan, Eric Matsumoto, Claude Napier, William Nickas, and Russell, H. (2005). "Prefabricated Bridge Elements and Systems in Japan and Europe." U.S. Department of Transportation,

Federal Highway Administration, 65.

Menkulasi, F. (2014). "The Development of a Composite Concrete Bridge System for Short-to-Medium-Span Bridges." Doctor of Philosophy, Virginia Polytechnic Institute and State University, Blacksburg, VA.

Menkulasi, F., Mercer, M., Roberts-Wollmann, C. L., and Cousins, T. (2012). "Accelerating Bridge Construction Using the Precast Inverted T-Beam Concept." *National Bridge Conference*Nashville, TN, 26.

Menkulasi, F., Roberts-Wollmann, C. L., and Cousins, T. (2015). "Implementation of a Precast Inverted T-Beam System in Virginia - Part I: Laboratory Investigations." Virginia Department of Transportation (VDOT),

Federal Highway Administration (FHWA), 67.

Menkulasi, F., Roberts-Wollmann, C. L., and Cousins, T. (2015). "Implementation of a Precast Inverted T-Beam System in Virginia - Part II: Analytic and Field Investigations." Virginia Center for Transportation Innovation and Research.

Mercer, M. S. (2012). "Transverse Sub-Assemblage Testing of the Inverted-T Bridge System." Master of Science, Virginia Polytechnic Institute and State University, Blacksburg, VA.

Piccinin, R., and Schultz, A. E. (2012). "The Minnesota inverted-tee system: Parametric studies for preliminary design." *PCI Journal*, Spring, 18.

Ralls, M. L., Tang, B., Bhidé, S., Brecto, B., Calvert, E., Capers, H., Dorgan, D., Matsumoto, E., Napier, C., Nickas, W., and Russell, H. (2005). "Prefabricated Bridge Elements and Systems in Japan and Europe." Federal Highway Administration,

U.S. Department of Transportation,

American Association of State Highway and Transportation Officials,, 64.

Roberts-Wollmann, C. L., Cousins, T., and Menkulasi, F. "Route 360 Inverted T-beams."

Roberts-Wollmann, C. L., Zickler, A. M., and Brown, M. C. (2016). "Virginia's Development of an Inverted-tee Beam Bridge Superstructure System." *ASPIRE - The Concrete Bridge Magazine*, Precast Concrete Institute (PCI), 1.

Russell, H. G. (2011). "Adjacent precast concrete box-beam bridges: State of the practice." *PCI Journal*(Winter 2011), 17.

VDOT (2015). "Prestressed and Post-Tensioned Concrete." *Prestressed Concrete Box-Beams,*

11.

VDOT (2012). "Proposed Bridge on Rte. 360 Over Chickahominy River - Henrico Co. 0.3 Mi. W. Hanover-Henrico Co. Line Proj. 0360-964-I20. B607." Department of Transportation, ed.Commonwealth of Virginia, 16.

APPENDIX A – MATLAB CODE FOR PRELIMINARY DESIGN TABLES

Design Checks

```
%THE FUNCTION CARRIES OUT THE DESIGN OF AN INVERTED T-BEAM FOR A SPECIFIC
%SPAN LENGTH

%Function has been updated as of 09/04/2016 to include the live load
%distribution factors for type a Slab-Type bridges for moments.
% This is as recommended by Fatmir Menkalusi in his dissertation.

function [CheckPSLossSup,CheckPSLossMid,CheckDeflection,CheckStrength,...
    CheckShear,fMatSup,fMatMid] = InvertedT_Design(Lpiertopier,PSrow,...
    ShapeSize)

%% Inputs
% Materials
% Concrete
fc = 8;         %Beam concrete 28-day specified compressive strength (ksi)
fci = 5;        %Beam concrete initial concrete compressive strength (ksi)
wc = 0.15;      %Beam concrete unit weight (kips per cubic foot)
fcdeck = 4;     %CIP topping 28-day specified compressive strength (ksi)
wcdeck = 0.15;  %CIP topping unit weight (kips per cubic foot)
K1 = 1.0;       %Aggregate source correction factor. 1 unless tested
% Steel
fy = 60;        %Mild steel yield stress
Es = 29000;     %Mild steel Young's Modulus
fpu = 270;      %Prestressing GUTS
Ep = 28500;     %Prestressing Young's Modulus
As = 0;         %Area of mild steel tensile reinf.
fs = 0;         %Stress in mild steel tensile reinf.
Aprimes = 0;    %Area of mild steel compression reinf.
fprimes = 0;    %Stress in mild steel compression reinf.
ds = 0;         %Depth from extreme comp. fiber to centroid of mild T steel
dprimes = 0;    %Depth from extreme comp. fiber to centroid of mild C steel
% Geometry
% Precast Concrete - refer to diagram for further explanation
if strcmp(ShapeSize,'SMALL')
    htotal = 8;
    wtotal = 72;
    hweb = 4;
    wweb = 39;
    hflange = 4;
    wflange = 12.5;
    hflangesloped = 0;
    wwebsloped = 4;
    Thetawebsloped = NaN;
    yrow = [2,4,0,6];       %[Row 1, Row 2, Row 3, Row 4]
elseif strcmp(ShapeSize,'MEDIUM')
    htotal = 18;
    wtotal = 72;
    hweb = 14;
    wweb = 20;
    hflange = 4;
    wflange = 12.5;
```

Design Checks

```
    hflangesloped = 0;
    wwebsloped = 13.5;
    Thetawebsloped = NaN;
    yrow = [2,4,6,16];      %[Row 1, Row 2, Row 3, Row 4]
elseif strcmp(ShapeSize,'LARGE')
    htotal = 24;
    wtotal = 72;
    hweb = 18;
    wweb = 20;
    hflange = 6;
    wflange = 12;
    hflangesloped = 0;
    wwebsloped = 14;
    Thetawebsloped = NaN;
    yrow = [2,4,6,22];      %[Row 1, Row 2, Row 3, Row 4]
else
    error('ShapeSize must be SMALL, MEDIUM, or LARGE')
end

% Deck CIP Concrete
tslab = 7.5;        %Thickness of the CIP topping slab over precast web
% PS Strands
Astrand = 0.217;    %Area of individual prestressing strand

% Bridge
H = 70;             %Relative humidity in location
% Geometry
Ng = 18;            %Number of girders
Nl = 6;             %Number of lanes for live load placement
Sg = 6;             %Girder spacing
Woverall = 114;     %Overall bridge width
Wcurbtocurb = 110;  %Curb-curb width
Nbarrier = 4;       %Number of barrier rows
Wmed = 16;          %Median width
Wbarrierext = 1.3;  %Shoulder barrier width
% Span
Lpiertopier = 43;   %Center of pier - center of pier span length
Endclear = 0.5;     %Clearance from edge of pier to edge of bearing pad
Loverall = Lpiertopier - Endclear;  %Center of bearing - center of bearing
Lpad = 12;          %Width of bearing pad
L = Loverall - Lpad/12; %Clear span
% Loads
% Dead Loads
qfws = 0.025;       %Future wearing surface (ksf)
wbarrier = 0.3;     %Barrier (k/ft)
wmed = 0.15;        %Median (kcf)
tmed = 0.75;        %Median thickness (in.)
% Live Loads
%HL-93
wconLL = 0.12;      %Concentrated live load (k/ft)
wlane = 0.64;       %Distributed lane load (k/ft)
```

Design Checks

```
% Construction
% Precast Concrete
tcure = 7;          %Curing information
ti = 1;             %Time at placement of girder after curing
td = 90;            %Time at deck placement
tf = 75*365;        %"Final time" = 75 years


%% Section Properties
% Non-Composite Section
% Gross
% Precast Concrete
if isnan(Thetawebsloped)
    Thetawebsloped = atan(hweb/wwebsloped)*180/pi();
end
if isnan(wwebsloped)
    wwebsloped = tan(Thetawebsloped*pi()/180);
end

%Width of web at the bottom of the web
wwebbottom = 2*wwebsloped + wweb;

%Coordinates to trace outline of precast beam shape
PCxy = [0,0; wtotal,0; wtotal,hflange; wtotal-wflange,hflange ...
    +hflangesloped; wtotal-wflange-wwebsloped,htotal; wflange+wwebsloped,...
    htotal; wflange,hflange+hflangesloped; 0,hflange; wflange,hflange; ...
    wtotal-wflange,hflange; wtotal-wflange-wwebsloped,hflange+...
    hflangesloped;wflange+wwebsloped,hflange+hflangesloped];

PCshapes = [1,2,3,8; 8,9,7,NaN; 9,10,4,7; 10,3,4,NaN; 7,12,6,NaN; ...
    12,11,5,6; 11,4,5,NaN];

%Area, centroidal location, and moment of inertia for precast section
PCshapeprop = ShapeProp(PCshapes,PCxy,1);
Agprecast = sum(PCshapeprop(4,:));
cgprecast = sum(PCshapeprop(3,:).*PCshapeprop(4,:))/Agprecast;

PCshapeI = ShapeI(PCshapeprop,PCshapes,cgprecast);
Igprecast = sum(PCshapeI);
ytprecast = htotal-cgprecast;

% Deck CIP Concrete
Deckshapes = [1,9,8,NaN; 2,3,10,NaN; 8,9,14,7; 9,13,14,NaN; 10,11,12,NaN; ...
    10,3,4,11; 7,4,5,6];

%Coordinates to trace outline of CIP
Deckxy = [0,hflange; wtotal,hflange; wtotal,hflange+hflangesloped; ...
    wtotal,htotal; wtotal,htotal+tslab; 0,htotal+tslab; 0,htotal; ...
    0,hflange+hflangesloped; wflange,hflange+hflangesloped; ...
    wtotal-wflange,hflange+hflangesloped; wtotal-wflange,htotal; ...
```

Design Checks

```
    wtotal-wflange-wwebsloped, htotal; wflange+wwebsloped,htotal; ...
    wflange,htotal];

%Area, centroidal location, moment of inertia, location of prestressing for
%CIP topping
Deckshapeprop = ShapeProp(Deckshapes,Deckxy,2);
Agdeck = sum(Deckshapeprop(4,:));
cgdeck = sum(Deckshapeprop(3,:).*Deckshapeprop(4,:))/Agdeck;
DeckshapeI = ShapeI(Deckshapeprop,Deckshapes,cgdeck);
Igdeck = sum(DeckshapeI);
egd = cgdeck - cgprecast;

% PS Steel
Apsrow = PSrow * Astrand;       %Strand area in each row
Aps = sum(Apsrow);              %Total prestressing area
cps = sum(Apsrow.*yrow)/Aps;    %Centroid of prestressing
epg = cgprecast - cps;          %Eccentricity of prestressing

% Transformed at Transfer
Eci = 33000*K1*wc^1.5*sqrt(fci);    %@ Transfer Concrete Young's Modulus
npi = Ep/Eci;                       %@ Transfer modular ratio
Apstt = Aps*(npi-1);                %Transformed steel area @ Transfer
Att = Agprecast+Apstt;              %Total area @ transfer
ctt = ((Agprecast*cgprecast)+(Apstt*cps))/Att;  %Centroid
Itt = Igprecast + Agprecast*(cgprecast-ctt)^2+Apstt*(cps-ctt)^2;  %Inertia
% Transformed at Service
Ec = 33000*K1*wc^1.5*sqrt(fc);      %@ Service Concrete Young's Modulus
np = Ep/Ec;                         %@ Service modular ratio
Apsts = Aps*(np-1);                 %Transformed steel area @ Service
Ats = Agprecast+Apsts;              %Total area @ service
cts = ((Agprecast*cgprecast)+(Apsts*cps))/Ats;  %Centroid
Its = Igprecast + Agprecast*(cgprecast-cts)^2+Apsts*(cps-cts)^2;  %Inertia
epts = cts-cps;                     %Eccentricity of prestressing

% Composite Section section properties (A, I, cg, e)
Ecdeck = 33000*K1*wcdeck^1.5*sqrt(fcdeck);
ndeck = Ecdeck/Ec;
Atrdeck = ndeck*Agdeck;
Itrdeck = ndeck*Igdeck;
Acomp = Agprecast + Atrdeck;
ccomp = ((Agprecast*cgprecast)+(Atrdeck*cgdeck))/Acomp;
Icomp = Igprecast + Agprecast*(cgprecast-ccomp)^2+Itrdeck+Atrdeck*...
    (cgdeck-ccomp)^2;
ecd = cgdeck - ccomp;
epc = ccomp - cps;
ytcomp = htotal - ccomp;

%% Loads
% Dead Loads
% PC Self Weight
wgprecast = Agprecast/(12^2)*wc;
```

Design Checks

```
Mgprecast = wgprecast*L^2/8;
% CIP Deck Self Weight
wgdeck = Agdeck/(12^2)*wcdeck;
Mgdeck = wgdeck*L^2/8;
% Dead Loads on Composite System
% FWS (future wearing surface)
wfwsg = qfws*(Wcurbtocurb/Ng);
Mfws = wfwsg*L^2/8;
% Barrier
wbarrierg = wbarrier*Nbarrier/Ng;
Mbarrier = wbarrierg*L^2/8;
% Median
wmedg = wmed*tmed*Wmed/Ng;
Mmed = wmedg*L^2/8;
wsuperdead = wfwsg+wbarrierg+wmedg;
Msuperdead = Mfws+Mbarrier+Mmed;
DC = Mgprecast+Mgdeck+Mbarrier;
DW = Mfws;

% Live Load Distribution Factor. Note: DFM = Distribution Factor for
% Moments, DFV = Distribution Factor for Shear
% Code Checks
if Ng > 4
    CheckLDF = 'OK';
else
    CheckLDF = 'NG';
end

% Beam-Slab Bridges
if and(20 <= L, L<=120)
    if and(5<=Ng, Ng<=20)
        CheckDFMint = 'OK';
    else
        CheckDFMint = 'NG';
    end
else
    CheckDFMint = 'NG';
end

Kg = ndeck^-1 * (Icomp+Acomp*ecd^2);
I_J = 0.54*(htotal/wtotal)+0.16;

% For Bending Moment in Interior Beams
% One Design Lane Loaded
kDFM = max(2.5*Ng^-0.2,1.5);
DFMintsingle = kDFM*(wtotal/(33.3*L))^0.5*(I_J)^0.25;
% Two or More Lanes Loaded
DFMintmulti = kDFM*(wtotal/305)^0.6*(wtotal/(12*L))^0.2*I_J^0.06;
DFMint = max(DFMintsingle,DFMintmulti);
% For Bending Moment in Exterior Beams
de = Wbarrierext;
```

Design Checks

```
if de <= 2
    CheckDFMext = 'OK';
else
    CheckDFMext = 'NG';
end
% One Design Lane Loaded
emsingle = max(1.125+de/30,1.0);
DFMextsingle = emsingle*DFMintsingle;
% Two or More Lanes Loaded
emmulti = max(1.04+de/25,1);
DFMextmulti = emmulti*DFMintmulti;
DFMext = max(DFMextsingle,DFMextmulti);
% For Shear in Interior Beams
if and(20 <= L, L<=120)
    if and(5<=Ng, Ng<=20)
        CheckDFVint = 'OK';
    else
        CheckDFVint = 'NG';
    end
else
    CheckDFVint = 'NG';
end
% One Design Lane Loaded
DFVintsingle = (wtotal/(130*L))^0.15*I_J^0.05;
% Two or More Lanes Loaded
b_48 = max(wtotal/48,1);
DFVintmulti = (wtotal/156)^0.4*(wtotal/(12*L))^0.1*I_J^0.05*b_48;
DFVint = max(DFVintsingle,DFVintmulti);
% For Shear in Exterior Beams
if de <= 2
    CheckDFVext = 'OK';
else
    CheckDFVext = 'NG';
end
% One Design Lane Loaded
evsingle = max(1.25+de/20,1.0);
DFVextsingle = evsingle*DFVintsingle;
% Two or More Lanes Loaded
evmulti = max(1+((de+(wtotal/12)-2)/40)^0.5,1);
DFVextmulti = evmulti*DFVintmulti*b_48^-1;
DFVext = max(DFVextsingle,DFVextmulti);

%Equivalent Strip Widths for Slab-Type Bridges
%AASHTO Table 4.6.2.3-1 => Typical cross-section a (based on
%recommendations by Fatmir Menkalusi
L1 = min(L,60);
%One design lane loaded
W1single = min(Woverall,30);
Esingle = 10 + 5*sqrt(L1*W1single);
DFMslabsingle = wtotal/Esingle;
%Two or more design lanes loaded
```

Design Checks

```
W1multi = min(Woverall,60);
Emulti = min(84 + 1.44*sqrt(L1*W1multi), (12*Woverall)/Nl);
DFMslabmulti = wtotal/Emulti;

DFMslab = max(DFMslabsingle,DFMslabmulti);

% Live Loads
DFM = max([DFMslab,DFMint,DFMext]);
DFV = max(DFVint,DFVext);
IM = 33;
MLL = wlane*L^2/8*DFM;
MLT = ((72*L/2*(L/2-4.67))/L-112)*DFM*(1+IM/100);

%% PS Losses
% Short Term Losses
% Elastic Shortening
fpy = 0.9*fpu;
fpo = 0.75*fpu;
Ppo = fpo*Aps;
fcgp = Ppo/Agprecast + Ppo*epg^2/Igprecast - Mgprecast*12*epg/Igprecast;
nps = Ep/Eci;
deltafpES = nps*fcgp;
fpi = max(fpo-deltafpES,0.55*fpy);
Pi = fpi*Aps;
% Long Term Losses
% Time of Transfer to Time of Deck Placement
% Shrinkage of Precast Girder
Perimeterprecast = wtotal + 2*hflange + 2*sqrt(hflangesloped^2+wflange^2) + ...
    2*sqrt(hweb^2+wwebsloped^2) + wweb;
VSprecast = Agprecast*(Loverall*12)/(Perimeterprecast*Loverall*12+2*Agprecast);
ks = max(1.45-0.13*VSprecast,1.0);
khs = 2-0.014*H;
kf = 5/(1+fci);
ktdid = (td-ti)/(61-4*fci+(td-ti));
ktdif = (tf-ti)/(61-4*fci+(tf-ti));
Epsilonbid = ks*khs*kf*ktdid*(0.48*10^-3);
khc = 1.56-0.008*H;
Psibif = 1.9*ks*khc*kf*ktdif*ti^-0.118;
Psibid = 1.9*ks*khc*kf*ktdid*ti^-0.118;
Kid = 1/(1+Ep/Eci*Aps/Agprecast*(1+Agprecast*epg^2/Igprecast)*(1+0.7*Psibif));
deltafpSR = Epsilonbid*Ep*Kid;
% Creep of Precast Girder
deltafpCR = Ep/Eci*fcgp*Psibid*Kid;
% Relaxation of PS Steel
Kl = 30;
deltafpR1 = (fpi/Kl)*(fpi/fpy-0.55);
% Time of Deck Placement to Final Time
ktddf = (tf-td)/(61-4*fci+(tf-td));
Epsilonbif = ks*khs*kf*ktdif*0.48*10^-3;
Epsilonbdf = Epsilonbif-Epsilonbid;
Kdf = 1/(1+(Ep/Eci)*(Aps/Acomp)*(1+Acomp*epc^2/Icomp)*(1+0.7*Psibif));
```

Design Checks

```
deltafpSD = Epsilonbdf*Ep*Kdf;
% Creep of Precast Concrete
deltafcd = -(deltafpSR+deltafpCR+deltafpR1)*(Aps/Agprecast)*(1+Agprecast* ...
    epg^2/Igprecast)-(12*Mgdeck*epts/Its+12*(Mbarrier+Mfws)*epc/Icomp);
Psibdf = 1.9*ks*khc*kf*ktddf*td^-0.118;
deltafpCD = Ep/Eci*fcgp*(Psibif-Psibid)*Kdf+Ep/Ec*deltafcd*Psibdf*Kdf;
% Relaxation of PS Steel
deltafpR2 = deltafpR1;
% Shrinkage of Deck Concrete
fcideck = 0.8*fcdeck;
Perimeterdeck = wtotal;
VSdeck = Agdeck*Loverall*12/(Perimeterdeck*Loverall*12+2*Agdeck);
ksdeck = max(1.45-0.13*VSdeck,1);
kfdeck = 5/(1+fcideck);
ktddfdeck = (tf-td)/(61-4*fcideck+(tf-td));
Epsilonddf = ksdeck*khs*kfdeck*ktddfdeck*0.48*10^-3;
Psiddf = 1.9*ksdeck*khc*kfdeck*ktddfdeck*td^-0.118;
deltafcdf = Epsilonddf*Agdeck*Ecdeck/(1+0.7*Psiddf)*(1/Acomp-epc*ecd/Icomp);
deltafpSS = Ep/Ec*deltafcdf*Kdf*(1+0.7*Psibdf);
% Total PS Losses at Transfer
% Initial Loss
Lossinitial = 100*deltafpES/fpo;
% Time-Dependent PS Loss between time of transfer and deck placement
deltafpLTid = deltafpSR+deltafpCR+deltafpR1;
% Time-Dependent PS Loss after time of deck placement
deltafpLTdf = deltafpSD+deltafpCD+deltafpR2-deltafpSS;
% Total Time-Dependent PS Losses
deltafpLT = deltafpLTid+deltafpLTdf;
% Total PS Losses at Service
deltafpT = deltafpES+deltafpLT;
% Tendons after all losses
fpe = min(fpo-deltafpT,0.8*fpy);
Pe = fpe*Aps;
% Finall Loss
Lossfinal = 100*deltafpT/fpo;

%% Stress Limit State
% Allowable Stress
% Stresses at Transfer
% At Support
sigmaiCSup = -0.6*fci;
sigmaiTSup = min(0.0948*sqrt(fci),0.2);
% At Midspan
sigmaiCMid = -0.6*fci;
sigmaiTMid = min(0.0948*sqrt(fci),0.2);
% Stresses at Deck Placement
% At Support
sigmadCSup = -0.45*fc;
sigmadTSup = 0.19*sqrt(fc);
% At Midspan
sigmadCMid = -0.6*fc;
```

Design Checks

```
sigmadCMidSus = -0.45*fc;
sigmadTMid = 0.19*sqrt(fc);
% Stresses at Service
% At Support
sigmafCSup = -0.6*fc;
sigmafCSupSus = -0.45*fc;
sigmafTSup = 0.19*sqrt(fc);
% At Midspan
sigmafCMid = -0.6*fc;
sigmafCMidSus = -0.45*fc;
sigmafTMid = 0.19*sqrt(fc);

% Calculated Stresses
% Stresses at Transfer
% At Support
ftiSup = -Pi/Agprecast+Pi*epg*ytprecast/Igprecast;
fbiSup = -Pi/Agprecast-Pi*epg*cgprecast/Igprecast;
% At Midspan
ftiMid = -Pi/Agprecast + Pi*epg*ytprecast/Igprecast - (Mgprecast*12*...
    ytprecast)/Igprecast;
fbiMid = -Pi/Agprecast - Pi*epg*cgprecast/Igprecast + (Mgprecast*12*...
    cgprecast)/Igprecast;
% Stresses at Deck Placement
MconLL = wconLL*L^2/8;
% At Support
ftdSup = -Pe/Agprecast + Pe*epg*ytprecast/Igprecast;
fbdSup = -Pe/Agprecast - Pe*epg*cgprecast/Igprecast;
% At Midspan
ftdMid = -Pe/Agprecast + Pe*epg*ytprecast/Igprecast - (Mgprecast+Mgdeck+...
    MconLL)*12*ytprecast/Igprecast;
ftdMidSus = -Pe/Agprecast + Pe*epg*ytprecast/Igprecast - (Mgprecast+...
    Mgdeck)*12*ytprecast/Igprecast;
fbdMid = -Pe/Agprecast - Pe*epg*cgprecast/Igprecast + (Mgprecast+Mgdeck+...
    MconLL)*12*cgprecast/Igprecast;
fbdMidSus = -Pe/Agprecast - Pe*epg*cgprecast/Igprecast + (Mgprecast+...
    Mgdeck)*12*cgprecast/Igprecast;
% Stresses at Service
ML = MLL+MLT;
% At Support
ftfSup = ftdSup;
fbfSup = fbdSup;
% At Midspan
ftfMid = -Pe/Agprecast + Pe*epg*ytprecast/Igprecast - (Mgprecast+...
    Mgdeck)*12*ytprecast/Igprecast - (Msuperdead+ML)*12*ytcomp/Icomp;
ftfMidSus = -Pe/Agprecast + Pe*epg*ytprecast/Igprecast - (Mgprecast+...
    Mgdeck)*12*ytprecast/Igprecast - (Msuperdead)*12*ytcomp/Icomp;
fbfMid = -Pe/Agprecast - Pe*epg*cgprecast/Igprecast + (Mgprecast+...
    Mgdeck)*12*cgprecast/Igprecast + (Msuperdead+ML)*12*ccomp/Icomp;
fbfMidSus = -Pe/Agprecast - Pe*epg*cgprecast/Igprecast + (Mgprecast+...
    Mgdeck)*12*cgprecast/Igprecast + (Msuperdead)*12*ccomp/Icomp;
```

Design Checks

```
% Stress Check
% Stresses at Transfer
% At Support
CheckbiSup = SC(fbiSup,sigmaiCSup,sigmaiTSup);
ChecktiSup = SC(ftiSup,sigmaiCSup,sigmaiTSup);
% At Midspan
CheckbiMid = SC(fbiMid,sigmaiCMid,sigmaiTMid);
ChecktiMid = SC(ftiMid,sigmaiCMid,sigmaiTMid);
% Stresses at Deck Placement
% At Support
CheckbdSup = SC(fbdSup,sigmadCSup,sigmadTSup);
ChecktdSup = SC(ftdSup,sigmadCSup,sigmadTSup);
% At Midspan
CheckbdMid = SC(fbdMid,sigmadCMid,sigmadTMid);
ChecktdMid = SC(ftdMid,sigmadCMid,sigmadTMid);
CheckbdMidSus = SC(fbdMidSus,sigmadCMidSus,sigmadTMid);
ChecktdMidSus = SC(ftdMidSus,sigmadCMidSus,sigmadTMid);
% Stresses at Service
% At Support
CheckbfSup = SC(fbfSup,sigmafCSup,sigmafTSup);
ChecktfSup = SC(ftfSup,sigmafCSup,sigmafTSup);
% At Midspan
CheckbfMid = SC(fbfMid,sigmafCMid,sigmafTMid);
ChecktfMid = SC(ftfMid,sigmafCMid,sigmafTMid);
CheckbfMidSus = SC(fbfMidSus,sigmafCMidSus,sigmafTMid);
ChecktfMidSus = SC(ftfMidSus,sigmafCMidSus,sigmafTMid);

%% Short Term Deflection and Camber
% Deflections at Transfer
% Camber due to PS force
deltapi = -Pi/(Eci*Igprecast)*(epg*(L*12)^2/8);
% Deflection due to Precast Self Weight
deltagi = 5/384*(wgprecast/12)*(L*12)^4/(Eci*Igprecast);
% Total Deflections at Transfer
deltai = deltagi+deltapi;
% Deflections at Deck Placement
% Deflection due to CIP Deck Self Weight
deltadgdeck = 5/384*((wgdeck+wconLL)/12)*(L*12)^4/(Ec*Igprecast);
% Total Deflections at Deck Placement
deltad = deltai+deltadgdeck;
% Deflections at Service
% Deflections due to live loads at service
deltafLL = 5/384*(wlane*DFM/12)*(L*12)^4/(Ec*Icomp);
P = [32,32,8];
xaxel = [-14,0,14];
aaxel = L/2 + xaxel + 2.33;
for axel = 1:3
    deltaaxel(axel) = deltaeachaxel(P(axel),aaxel(axel),L,Ec,Icomp);
end
deltatruck = sum(deltaaxel);
deltafLT = deltatruck*DFM*(1+IM/100);
```

Design Checks

```
deltafL = max(deltafLT,0.25*deltafLT+deltafLL);
deltafLallow = L*12/800;
if deltafL <= deltafLallow
    CheckdeltafL = 'OK';
else
    CheckdeltafL = 'NG';
end
% Deflection due to superimposed dead loads at service
deltafsuperdead = 5/384*(wsuperdead/12)*(L*12)^4/(Ec*Icomp);
% Total Deflections at Service
deltaf = deltad+deltafL+deltafsuperdead;

%% Strength Limit State
% Flexural Strength
Mupos = 1.25*DC + 1.5*DW + 1.75*ML;
if fpe >= 0.5*fpu
    Checkfpehalffpu = 'OK';
else
    Checkfpehalffpu = 'NG';
end
dp = htotal+tslab-cps;
k = 2*(1.04-fpy/fpu);
if fcdeck <= 4
    Beta1deck = 0.85;
elseif fcdeck >= 8
    Beta1deck = 0.65;
else
    Beta1deck = 0.85-0.05*(fcdeck-4);
end
c = (Aps*fpu+As*fs+Aprimes*fprimes)/(0.85*fcdeck*Beta1deck*wtotal+k*Aps*...
    fpu/dp);
fps = fpu*(1-k*c/dp);
a = Aps*fps/(0.85*fcdeck*wtotal);
cNA = a/Beta1deck;
dt = htotal+tslab-yrow(1);
Epsilont = 0.003/cNA*(dt-cNA);
if Epsilont <= 0.002
    phif = 0.75;
elseif Epsilont >= 0.005
    phif = 1.0;
else
    phif = 0.65+0.15*(dt/cNA-1);
end
if a <= tslab
    b = wtotal;
else
    b = wweb;
end
hf = tslab;
Mn = (Aps*fps*(dp-a/2)+As*fs*(ds-a/2)-Aprimes*fprimes*(dprimes-a/2)+...
    0.85*fcdeck*(wtotal-b)*hf*(a/2-hf/2))/12;
```

Design Checks

```
Mr = phif*Mn;
if Mr >= Mupos
    CheckMrMupos = 'OK';
else
    CheckMrMupos = 'NG';
end
% Minimum Reinforcement
fr = 0.24*sqrt(fc);
fcpe = Pe/Agprecast + Pe*epg*cgprecast/Igprecast;
Sc = Icomp/ccomp;
Snc = Igprecast/cgprecast;
Mdnc = Mgprecast + Mgdeck;
Mcr = max((Sc/12)*(fr+fcpe)-Mdnc*(Sc/Snc-1),Sc*fr/12);
Mmin = 1.2*Mcr;
if Mr >= min(Mmin,1.33*Mupos)
    CheckMpos = 'OK';
else
    CheckMpos = 'NG';
end

%% Shear Design
% Shear Strength
de = (Aps*fps*dp+As*fy*ds)/(Aps*fps+As*fy);
dv = max(de-a/2,max(0.9*de,0.72*(htotal+tslab)));
xvcritical = dv/12;
phiv = 0.9;
VLTcritical = 72*((L-xvcritical)-9.33)/L;
VLLcritical = wlane*(L-xvcritical)^2/(2*L);
VLcrit = VLTcritical*(1+IM/100)*DFV + VLLcritical*DFV;
Vgprecastcrit = wgprecast*(L-xvcritical)^2/(2*L);
Vgdeckcrit = wgdeck*(L-xvcritical)^2/(2*L);
Vsuperdeadcrit = wsuperdead*(L-xvcritical)^2/(2*L);
VDcrit = Vgprecastcrit+Vgdeckcrit+Vsuperdeadcrit;
Vucrit = 1.25*VDcrit+1.75*VLcrit;
Vp = 0;
Nu = 0;
MLTcritical = VLTcritical*xvcritical;
MLLcritical = wlane*xvcritical*(L-xvcritical)/2;
MLcritical = MLTcritical*(1+IM/100)*DFM+MLLcritical*DFM;
Mgprecastcritical = wgprecast*xvcritical*(L-xvcritical)/2;
Mgdeckcritical = wgdeck*xvcritical*(L-xvcritical)/2;
Msuperdeadcritical = wsuperdead*xvcritical*(L-xvcritical)/2;
MDcritical = Mgprecastcritical+Mgdeckcritical+Msuperdeadcritical;
Mucritical = 1.25*MDcritical+1.75*MLcritical;
bv = wtotal;
Mucrit = max(Mucritical,abs(Vucrit-Vp)*(dv/12))*12;
Act = bv*(htotal+tslab)/2;
Epsilons = (abs(Mucrit)/dv+0.5*Nu+abs(Vucrit-Vp)-Aps*fpo)/(Es*As+Ep*Aps);
if Epsilons < 0
    Epsilons = max((abs(Mucrit)/dv+0.5*Nu+abs(Vucrit-Vp)-Aps*fpo)/...
        (Es*As+Ep*Aps+Ec*Act),-0.4*10^-3);
```

Design Checks

```
else
    Epsilons = min(Epsilons,6*10^-3);
end
sx = dv;
ag = 0.5;
sxe = min(max(sx*1.38/(ag+0.63),12),80);
Betav = 4.8/(1+750*Epsilons)*51/(39+sxe);
Thetav = 29+3500*Epsilons;
Vc = 0.0316*Betav*sqrt(fcdeck)*bv*dv;
if Vucrit <= 0.5*phiv*(Vc+Vp)
    CheckVu = 'OK';
else
    CheckVu = 'NG';
end
Vs = 0;
% Longitudingal Reinforcement Shear Check
phic = 1;
if Aps*fps+As*fy >= abs(Mucrit)/(dv*phif)+0.5*Nu/phic+...
        (abs(Vucrit/phiv-Vp)-0.5*Vs)*cot(Thetav*pi()/180)
    CheckVLs = 'OK';
else
    CheckVLs = 'NG';
end
VLTsup = 72;
VLLsup = wlane*L/2;
VLsup = VLTsup*(1+IM/100)*DFV+VLLsup*DFV;
Vgprecastsup = wgprecast*L/2;
Vgdecksup = wgdeck*L/2;
Vsuperdeadsup = wsuperdead*L/2;
VDsup = Vgprecastsup+Vgdecksup+Vsuperdeadsup;
Vusup = 1.25*VDsup+1.75*VLsup;
if Aps*fps+As*fy >= (Vusup/phiv-Vp-0.5*Vs)*cot(Thetav*pi()/180)
    CheckVLssup = 'OK';
else
    CheckVLssup = 'NG';
end
%Interface Shear Design
bvi(1) = wtotal;
bvi(2) = 2*sqrt(hflangesloped^2+wflange^2)+2*sqrt(hweb^2+wwebsloped^2)+wweb;
Lvi = 12;
Acv = bvi*Lvi;
Vui = Vucrit/dv*12;
cv = 0.24;
muv = 1;
K1v = 0.25;
K2v = 1.5;
Avf = 0;
Pc = 0;
Vni(1,:) = cv*Acv+muv*(Avf*fy+Pc);
Vni(2,:) = K1v*fc*Acv;
Vni(3,:) = K2v*Acv;
```

Design Checks

```
Vni = min(min(Vni));
if Vni >= 1.33*Vui/phiv
    CheckAvf = 'OK';
    Avf = 0;
else
    CheckAvf = 'NG';
    Avf = max(0.05*Acv/fy);
end

%% Summary of Checks
CheckPSLossSup = {CheckbiSup,ChecktiSup;CheckbdSup,ChecktdSup;CheckbfSup,...
    ChecktfSup};
CheckPSLossMid = {CheckbiMid,ChecktiMid,'OK','OK';...
    CheckbdMid,ChecktdMid,CheckbdMidSus,ChecktdMidSus;...
    CheckbfMid,ChecktfMid,CheckbfMidSus,ChecktfMidSus};
% CheckLLDF = [CheckLDF,CheckDFMint,CheckDFMext,CheckDFVint,CheckDFVext];
CheckDeflection = {CheckdeltafL};
CheckStrength = {Checkfpehalffpu,CheckMrMupos,CheckMpos};
CheckShear = {CheckVu,CheckVLs,CheckVLssup,CheckAvf};

% CheckPSLoss = {CheckbiSup,ChecktiSup,CheckbiMid,ChecktiMid,'OK','OK';...
%     CheckbdSup,ChecktdSup,CheckbdMid,ChecktdMid,CheckbdMidSus,ChecktdMidSus;...
%     CheckbfSup,ChecktfSup,CheckbfMid,ChecktfMid,CheckbfMidSus,ChecktfMidSus};

% Stresses
fMatSup = [fbiSup,ftiSup;fbdSup,ftdSup;fbfSup,ftfSup];
fMatMid = [fbiMid,ftiMid,NaN,NaN';fbdMid,ftdMid,fbdMidSus,ftdMidSus;...
    fbfMid,ftfMid,fbfMidSus,ftfMidSus];

% fMat = [fbiSup,ftiSup,fbiMid,ftiMid,NaN,NaN';...
%     fbdSup,ftdSup,fbdMid,ftdMid,fbdMidSus,ftdMidSus;...
%     fbfSup,ftfSup,fbfMid,ftfMid,fbfMidSus,ftfMidSus];

end




%% Shape Properties
function ShapeMatrix = ShapeProp(Nodes,XY,h1)

[rows,cols] = size(Nodes);

for i = 1:rows
    shape = 0;
    for j = 1:cols
        if isnan(Nodes(i,j)) == 0
            x(j) = XY(Nodes(i,j),1);
            y(j) = XY(Nodes(i,j),2);
        else
            shape = 1;
```

Design Checks

```
            x(j) = NaN;
            y(j) = NaN;
        end
    end
    b(i) = max(x) - min(x);
    h(i) = max(y) - min(y);
    if shape == 0
        cy(i) = min(y) + h(i)/2;
        A(i) = b(i)*h(i);
    else
        cy(i) = min(y) + h(i)*h1/3;
        A(i) = 1/2*b(i)*h(i);
    end
end

ShapeMatrix = [b;h;cy;A];
end

%% Shape I
function Ishape = ShapeI(ShapeProp,Nodes,cg)

[rows,cols] = size(Nodes);

for i = 1:rows
    shape = 0;
    for j = 1:cols
        if isnan(Nodes(i,j))
            shape = 1;
        end
    end
    b = ShapeProp(1,:);
    h = ShapeProp(2,:);
    cy = ShapeProp(3,:);
    A = ShapeProp(4,:);

    if shape == 0
        Ishape(i) = (b(i)*h(i)^3)/12 + (cy(i)-cg)^2*A(i);
    else
        Ishape(i) = (b(i)*h(i)^3)/36 + (cy(i)-cg)^2*A(i);
    end
end
end

%% Stress Check
function Check = SC(f,sigmaC,sigmaT)

if f <= 0
    if abs(f) <= abs(sigmaC)
        Check = 'OK';
    else
        Check = 'NG';
```

Design Checks

```
    end
else
    if abs(f) <= abs(sigmaT)
        Check = 'OK';
    else
        Check = 'NG';
    end
end

end

%% Deflection due to each truck axle
function delta = deltaeachaxel(P,a,L,Ec,Ic)

x = L/2;
b = L-a;
if x <= a
    delta = P*b*x/(6*Ec*Ic*L)*(L^2-b^2-x^2)*12^3;
else
    delta = P*b/(6*Ec*Ic*L)*((x-a)^3*L/b+(L^2-b^2)*x-x^3)*12^3;
end


end
```

```
%THIS FUNCTION CARRIES OUT THE DESIGN CALCULATIONS GIVEN A SECTION AND
%PRESTRESSING ARRANGEMENT. SPECIFICALLY THIS FUNCTION WORKS WITH THE SCRIPT
%FILES TO OPTIMIZE STRAND GEOMETRY WITHOUT DEBONDING ANY STRANDS.

%This function was updated to include the distribution factors for
%slab-type bridges as of 09/04/2016, by EAE. Lines 286 - 302

function [CheckPSLossSup,CheckPSLossMid,CheckDeflection,CheckStrength,...
    CheckShear,fMatSup,fMatMid,cgprecast,sigmaiCSup,sigmaiTSup,sigmaiCMid...
    ,sigmaiTMid,Pi,Agprecast,Igprecast,ytprecast,Mgprecast]...
    = InvertedT_Design_AltStrandGeom(Lpiertopier,PSrow,ShapeSize)

%% Inputs
% Materials
% Concrete
fc = 8;
fci = 5;
wc = 0.15;
fcdeck = 4;
wcdeck = 0.15;
K1 = 1.0;
% Steel
fy = 60;
Es = 29000;
fpu = 270;
Ep = 28500;
As = 0;
fs = 0;
Aprimes = 0;
fprimes = 0;
ds = 0;
dprimes = 0;
% Geometry
% Precast Concrete
if strcmp(ShapeSize,'SMALL')
    htotal = 8;
    wtotal = 72;
    hweb = 4;
    wweb = 39;
    hflange = 4;
    wflange = 12.5;
    hflangesloped = 0;
    wwebsloped = 4;
    Thetawebsloped = NaN;
    yrow = [2,4,0,6];
elseif strcmp(ShapeSize,'MEDIUM')
    htotal = 18;
    wtotal = 72;
    hweb = 14;
    wweb = 20;
    hflange = 4;
```

```
    wflange = 12.5;
    hflangesloped = 0;
    wwebsloped = 13.5;
    Thetawebsloped = NaN;
    yrow = [2,4,6,16];
elseif strcmp(ShapeSize,'LARGE')
    htotal = 24;
    wtotal = 72;
    hweb = 18;
    wweb = 20;
    hflange = 6;
    wflange = 12;
    hflangesloped = 0;
    wwebsloped = 14;
    Thetawebsloped = NaN;
    yrow = [2,4,6,22];
else
    error('ShapeSize must be SMALL, MEDIUM, or LARGE')
end

% Deck CIP Concrete
tslab = 7.5;
% PS Strands
Astrand = 0.217;

% Bridge
H = 70;
% Geometry
Ng = 18;
Nl = 6;
Sg = 6;
Woverall = 114;
Wcurbtocurb = 110;
Nbarrier = 4;
Wmed = 16;
Wbarrierext = 1.3;
% Span
% Lpiertopier = 43;
% Lpiertopier = Linput;
Endclear = 0.5;
Loverall = Lpiertopier - Endclear;
Lpad = 12;
L = Loverall - Lpad/12;
% Loads
% Dead Loads
qfws = 0.025;
wbarrier = 0.3;
wmed = 0.15;
tmed = 0.75;
% Live Loads
%HL-93
```

```
wconLL = 0.12;
wlane = 0.64;

% Construction
% Precast Concrete
tcure = 7;
ti = 1;
td = 90;
tf = 75*365;


%% Section Properties
% Non-Composite Section
% Gross
% Precast Concrete
if isnan(Thetawebsloped)
    Thetawebsloped = atan(hweb/wwebsloped)*180/pi();
end
if isnan(wwebsloped)
    wwebsloped = tan(Thetawebsloped*pi()/180);
end

wwebbottom = 2*wwebsloped + wweb;

PCxy = [0,0; wtotal,0; wtotal,hflange; wtotal-wflange,hflange+hflangesloped; ...
    wtotal-wflange-wwebsloped,htotal; wflange+wwebsloped,htotal; ...
    wflange,hflange+hflangesloped; 0,hflange; wflange,hflange; ...
    wtotal-wflange,hflange; wtotal-wflange-wwebsloped,hflange+hflangesloped; ...
    wflange+wwebsloped,hflange+hflangesloped];

PCshapes = [1,2,3,8; 8,9,7,NaN; 9,10,4,7; 10,3,4,NaN; 7,12,6,NaN; ...
    12,11,5,6; 11,4,5,NaN];

PCshapeprop = ShapeProp(PCshapes,PCxy,1);
Agprecast = sum(PCshapeprop(4,:));
cgprecast = sum(PCshapeprop(3,:).*PCshapeprop(4,:))/Agprecast;

PCshapeI = ShapeI(PCshapeprop,PCshapes,cgprecast);
Igprecast = sum(PCshapeI);
ytprecast = htotal-cgprecast;

% Deck CIP Concrete
Deckshapes = [1,9,8,NaN; 2,3,10,NaN; 8,9,14,7; 9,13,14,NaN; 10,11,12,NaN; ...
    10,3,4,11; 7,4,5,6];
Deckxy = [0,hflange; wtotal,hflange; wtotal,hflange+hflangesloped; ...
    wtotal,htotal; wtotal,htotal+tslab; 0,htotal+tslab; 0,htotal; ...
    0,hflange+hflangesloped; wflange,hflange+hflangesloped; ...
    wtotal-wflange,hflange+hflangesloped; wtotal-wflange,htotal; ...
    wtotal-wflange-wwebsloped, htotal; wflange+wwebsloped,htotal; ...
    wflange,htotal];
```

```
Deckshapeprop = ShapeProp(Deckshapes,Deckxy,2);
Agdeck = sum(Deckshapeprop(4,:));
cgdeck = sum(Deckshapeprop(3,:).*Deckshapeprop(4,:))/Agdeck;
DeckshapeI = ShapeI(Deckshapeprop,Deckshapes,cgdeck);
Igdeck = sum(DeckshapeI);
egd = cgdeck - cgprecast;

% PS Steel
Apsrow = PSrow * Astrand;
Aps = sum(Apsrow);
cps = sum(Apsrow.*yrow)/Aps;
epg = cgprecast - cps;

% Transformed at Transfer
Eci = 33000*K1*wc^1.5*sqrt(fci);
npi = Ep/Eci;
Apstt = Aps*(npi-1);
Att = Agprecast+Apstt;
ctt = ((Agprecast*cgprecast)+(Apstt*cps))/Att;
Itt = Igprecast + Agprecast*(cgprecast-ctt)^2+Apstt*(cps-ctt)^2;
% Transformed at Service
Ec = 33000*K1*wc^1.5*sqrt(fc);
np = Ep/Ec;
Apsts = Aps*(np-1);
Ats = Agprecast+Apsts;
cts = ((Agprecast*cgprecast)+(Apsts*cps))/Ats;
Its = Igprecast + Agprecast*(cgprecast-cts)^2+Apsts*(cps-cts)^2;
epts = cts-cps;

% Composite Section
Ecdeck = 33000*K1*wcdeck^1.5*sqrt(fcdeck);
ndeck = Ecdeck/Ec;
Atrdeck = ndeck*Agdeck;
Itrdeck = ndeck*Igdeck;
Acomp = Agprecast + Atrdeck;
ccomp = ((Agprecast*cgprecast)+(Atrdeck*cgdeck))/Acomp;
Icomp = Igprecast + Agprecast*(cgprecast-ccomp)^2+Itrdeck+Atrdeck*...
    (cgdeck-ccomp)^2;
ecd = cgdeck - ccomp;
epc = ccomp - cps;
ytcomp = htotal - ccomp;

%% Loads
% Dead Loads
% PC Self Weight
wgprecast = Agprecast/(12^2)*wc;
Mgprecast = wgprecast*L^2/8;
% CIP Deck Self Weight
wgdeck = Agdeck/(12^2)*wcdeck;
Mgdeck = wgdeck*L^2/8;
% Dead Loads on Composite System
```

```
% FWS
wfwsg = qfws*(Wcurbtocurb/Ng);
Mfws = wfwsg*L^2/8;
% Barrier
wbarrierg = wbarrier*Nbarrier/Ng;
Mbarrier = wbarrierg*L^2/8;
% Median
wmedg = wmed*tmed*Wmed/Ng;
Mmed = wmedg*L^2/8;
wsuperdead = wfwsg+wbarrierg+wmedg;
Msuperdead = Mfws+Mbarrier+Mmed;
DC = Mgprecast+Mgdeck+Mbarrier;
DW = Mfws;

% Live Load Distribution Factor
% Code Checks
if Ng > 4
    CheckLDF = 'OK';
else
    CheckLDF = 'NG';
end

% Beam-Slab Bridges
if and(20 <= L, L<=120)
    if and(5<=Ng, Ng<=20)
        CheckDFMint = 'OK';
    else
        CheckDFMint = 'NG';
    end
else
    CheckDFMint = 'NG';
end

Kg = ndeck^-1 * (Icomp+Acomp*ecd^2);
I_J = 0.54*(htotal/wtotal)+0.16;

% For Bending Moment in Interior Beams
% One Design Lane Loaded
kDFM = max(2.5*Ng^-0.2,1.5);
DFMintsingle = kDFM*(wtotal/(33.3*L))^0.5*(I_J)^0.25;
% Two or More Lanes Loaded
DFMintmulti = kDFM*(wtotal/305)^0.6*(wtotal/(12*L))^0.2*I_J^0.06;
DFMint = max(DFMintsingle,DFMintmulti);
% For Bending Moment in Exterior Beams
de = Wbarrierext;
if de <= 2
    CheckDFMext = 'OK';
else
    CheckDFMext = 'NG';
end
% One Design Lane Loaded
```

```
emsingle = max(1.125+de/30,1.0);
DFMextsingle = emsingle*DFMintsingle;
% Two or More Lanes Loaded
emmulti = max(1.04+de/25,1);
DFMextmulti = emmulti*DFMintmulti;
DFMext = max(DFMextsingle,DFMextmulti);
% For Shear in Interior Beams
if and(20 <= L, L<=120)
    if and(5<=Ng, Ng<=20)
        CheckDFVint = 'OK';
    else
        CheckDFVint = 'NG';
    end
else
    CheckDFVint = 'NG';
end
% One Design Lane Loaded
DFVintsingle = (wtotal/(130*L))^0.15*I_J^0.05;
% Two or More Lanes Loaded
b_48 = max(wtotal/48,1);
DFVintmulti = (wtotal/156)^0.4*(wtotal/(12*L))^0.1*I_J^0.05*b_48;
DFVint = max(DFVintsingle,DFVintmulti);
% For Shear in Exterior Beams
if de <= 2
    CheckDFVext = 'OK';
else
    CheckDFVext = 'NG';
end
% One Design Lane Loaded
evsingle = max(1.25+de/20,1.0);
DFVextsingle = evsingle*DFVintsingle;
% Two or More Lanes Loaded
evmulti = max(1+((de+(wtotal/12)-2)/40)^0.5,1);
DFVextmulti = evmulti*DFVintmulti*b_48^-1;
DFVext = max(DFVextsingle,DFVextmulti);

%Equivalent Strip Widths for Slab-Type Bridges
%AASHTO Table 4.6.2.3-1 => Typical cross-section a (based on
%recommendations by Fatmir Menkalusi
L1 = min(L,60);
%One design lane loaded
W1single = min(Woverall,30);
Esingle = 10 + 5*sqrt(L1*W1single);
DFMslabsingle = wtotal/Esingle;
%Two or more design lanes loaded
W1multi = min(Woverall,60);
Emulti = min(84 + 1.44*sqrt(L1*W1multi), (12*Woverall)/Nl);
DFMslabmulti = wtotal/Emulti;

DFMslab = max(DFMslabsingle,DFMslabmulti);
```

```
% Live Loads
DFM = max([DFMslab,DFMint,DFMext]);
DFV = max(DFVint,DFVext);
IM = 33;
MLL = wlane*L^2/8*DFM;
MLT = ((72*L/2*(L/2-4.67))/L-112)*DFM*(1+IM/100);

%% PS Losses
% Short Term Losses
% Elastic Shortening
fpy = 0.9*fpu;
fpo = 0.75*fpu;
Ppo = fpo*Aps;
fcgp = Ppo/Agprecast + Ppo*epg^2/Igprecast - Mgprecast*12*epg/Igprecast;
nps = Ep/Eci;
deltafpES = nps*fcgp;
fpi = max(fpo-deltafpES,0.55*fpy);
Pi = fpi*Aps;
% Long Term Losses
% Time of Transfer to Time of Deck Placement
% Shrinkage of Precast Girder
Perimeterprecast = wtotal + 2*hflange + 2*sqrt(hflangesloped^2+wflange^2) + ...
    2*sqrt(hweb^2+wwebsloped^2) + wweb;
VSprecast = Agprecast*(Loverall*12)/(Perimeterprecast*Loverall*12+2*Agprecast);
ks = max(1.45-0.13*VSprecast,1.0);
khs = 2-0.014*H;
kf = 5/(1+fci);
ktdid = (td-ti)/(61-4*fci+(td-ti));
ktdif = (tf-ti)/(61-4*fci+(tf-ti));
Epsilonbid = ks*khs*kf*ktdid*(0.48*10^-3);
khc = 1.56-0.008*H;
Psibif = 1.9*ks*khc*kf*ktdif*ti^-0.118;
Psibid = 1.9*ks*khc*kf*ktdid*ti^-0.118;
Kid = 1/(1+Ep/Eci*Aps/Agprecast*(1+Agprecast*epg^2/Igprecast)*(1+0.7*Psibif));
deltafpSR = Epsilonbid*Ep*Kid;
% Creep of Precast Girder
deltafpCR = Ep/Eci*fcgp*Psibid*Kid;
% Relaxation of PS Steel
Kl = 30;
deltafpR1 = (fpi/Kl)*(fpi/fpy-0.55);
% Time of Deck Placement to Final Time
ktddf = (tf-td)/(61-4*fci+(tf-td));
Epsilonbif = ks*khs*kf*ktdif*0.48*10^-3;
Epsilonbdf = Epsilonbif-Epsilonbid;
Kdf = 1/(1+(Ep/Eci)*(Aps/Acomp)*(1+Acomp*epc^2/Icomp)*(1+0.7*Psibif));
deltafpSD = Epsilonbdf*Ep*Kdf;
% Creep of Precast Concrete
deltafcd = -(deltafpSR+deltafpCR+deltafpR1)*(Aps/Agprecast)*(1+Agprecast* ...
    epg^2/Igprecast)-(12*Mgdeck*epts/Its+12*(Mbarrier+Mfws)*epc/Icomp);
Psibdf = 1.9*ks*khc*kf*ktddf*td^-0.118;
deltafpCD = Ep/Eci*fcgp*(Psibif-Psibid)*Kdf+Ep/Ec*deltafcd*Psibdf*Kdf;
```

```
% Relaxation of PS Steel
deltafpR2 = deltafpR1;
% Shrinkage of Deck Concrete
fcideck = 0.8*fcdeck;
Perimeterdeck = wtotal;
VSdeck = Agdeck*Loverall*12/(Perimeterdeck*Loverall*12+2*Agdeck);
ksdeck = max(1.45-0.13*VSdeck,1);
kfdeck = 5/(1+fcideck);
ktddfdeck = (tf-td)/(61-4*fcideck+(tf-td));
Epsilonddf = ksdeck*khs*kfdeck*ktddfdeck*0.48*10^-3;
Psiddf = 1.9*ksdeck*khc*kfdeck*ktddfdeck*td^-0.118;
deltafcdf = Epsilonddf*Agdeck*Ecdeck/(1+0.7*Psiddf)*(1/Acomp-epc*ecd/Icomp);
deltafpSS = Ep/Ec*deltafcdf*Kdf*(1+0.7*Psibdf);
% Total PS Losses at Transfer
% Initial Loss
Lossinitial = 100*deltafpES/fpo;
% Time-Dependent PS Loss between time of transfer and deck placement
deltafpLTid = deltafpSR+deltafpCR+deltafpR1;
% Time-Dependent PS Loss after time of deck placement
deltafpLTdf = deltafpSD+deltafpCD+deltafpR2-deltafpSS;
% Total Time-Dependent PS Losses
deltafpLT = deltafpLTid+deltafpLTdf;
% Total PS Losses at Service
deltafpT = deltafpES+deltafpLT;
% Tendons after all losses
fpe = min(fpo-deltafpT,0.8*fpy);
Pe = fpe*Aps;
% Finall Loss
Lossfinal = 100*deltafpT/fpo;

%% Stress Limit State
% Allowable Stress
% Stresses at Transfer
% At Support
sigmaiCSup = -0.6*fci;
sigmaiTSup = min(0.0948*sqrt(fci),0.2);
% At Midspan
sigmaiCMid = -0.6*fci;
sigmaiTMid = min(0.0948*sqrt(fci),0.2);
% Stresses at Deck Placement
% At Support
sigmadCSup = -0.45*fc;
sigmadTSup = 0.19*sqrt(fc);
% At Midspan
sigmadCMid = -0.6*fc;
sigmadCMidSus = -0.45*fc;
sigmadTMid = 0.19*sqrt(fc);
% Stresses at Service
% At Support
sigmafCSup = -0.6*fc;
sigmafCSupSus = -0.45*fc;
```

```
sigmafTSup = 0.19*sqrt(fc);
% At Midspan
sigmafCMid = -0.6*fc;
sigmafCMidSus = -0.45*fc;
sigmafTMid = 0.19*sqrt(fc);

% Calculated Stresses
% Stresses at Transfer
% At Support
ftiSup = -Pi/Agprecast+Pi*epg*ytprecast/Igprecast;
fbiSup = -Pi/Agprecast-Pi*epg*cgprecast/Igprecast;
% At Midspan
ftiMid = -Pi/Agprecast + Pi*epg*ytprecast/Igprecast - (Mgprecast*12*ytprecast)/...
    Igprecast;
fbiMid = -Pi/Agprecast - Pi*epg*cgprecast/Igprecast + (Mgprecast*12*cgprecast)/...
    Igprecast;
% Stresses at Deck Placement
MconLL = wconLL*L^2/8;
% At Support
ftdSup = -Pe/Agprecast + Pe*epg*ytprecast/Igprecast;
fbdSup = -Pe/Agprecast - Pe*epg*cgprecast/Igprecast;
% At Midspan
ftdMid = -Pe/Agprecast + Pe*epg*ytprecast/Igprecast - (Mgprecast+Mgdeck+MconLL)*...
    12*ytprecast/Igprecast;
ftdMidSus = -Pe/Agprecast + Pe*epg*ytprecast/Igprecast - (Mgprecast+Mgdeck)*...
    12*ytprecast/Igprecast;
fbdMid = -Pe/Agprecast - Pe*epg*cgprecast/Igprecast + (Mgprecast+Mgdeck+MconLL)*...
    12*cgprecast/Igprecast;
fbdMidSus = -Pe/Agprecast - Pe*epg*cgprecast/Igprecast + (Mgprecast+Mgdeck)*...
    12*cgprecast/Igprecast;
% Stresses at Service
ML = MLL+MLT;
% At Support
ftfSup = ftdSup;
fbfSup = fbdSup;
% At Midspan
ftfMid = -Pe/Agprecast + Pe*epg*ytprecast/Igprecast - (Mgprecast+Mgdeck)*12*...
    ytprecast/Igprecast - (Msuperdead+ML)*12*ytcomp/Icomp;
ftfMidSus = -Pe/Agprecast + Pe*epg*ytprecast/Igprecast - (Mgprecast+Mgdeck)*12*...
    ytprecast/Igprecast - (Msuperdead)*12*ytcomp/Icomp;
fbfMid = -Pe/Agprecast - Pe*epg*cgprecast/Igprecast + (Mgprecast+Mgdeck)*12*...
    cgprecast/Igprecast + (Msuperdead+ML)*12*ccomp/Icomp;
fbfMidSus = -Pe/Agprecast - Pe*epg*cgprecast/Igprecast + (Mgprecast+Mgdeck)*12*...
    cgprecast/Igprecast + (Msuperdead)*12*ccomp/Icomp;

% Stress Check
% Stresses at Transfer
% At Support
CheckbiSup = SC(fbiSup,sigmaiCSup,sigmaiTSup);
ChecktiSup = SC(ftiSup,sigmaiCSup,sigmaiTSup);
% At Midspan
```

```
CheckbiMid = SC(fbiMid,sigmaiCMid,sigmaiTMid);
ChecktiMid = SC(ftiMid,sigmaiCMid,sigmaiTMid);
% Stresses at Deck Placement
% At Support
CheckbdSup = SC(fbdSup,sigmadCSup,sigmadTSup);
ChecktdSup = SC(ftdSup,sigmadCSup,sigmadTSup);
% At Midspan
CheckbdMid = SC(fbdMid,sigmadCMid,sigmadTMid);
ChecktdMid = SC(ftdMid,sigmadCMid,sigmadTMid);
CheckbdMidSus = SC(fbdMidSus,sigmadCMidSus,sigmadTMid);
ChecktdMidSus = SC(ftdMidSus,sigmadCMidSus,sigmadTMid);
% Stresses at Service
% At Support
CheckbfSup = SC(fbfSup,sigmafCSup,sigmafTSup);
ChecktfSup = SC(ftfSup,sigmafCSup,sigmafTSup);
% At Midspan
CheckbfMid = SC(fbfMid,sigmafCMid,sigmafTMid);
ChecktfMid = SC(ftfMid,sigmafCMid,sigmafTMid);
CheckbfMidSus = SC(fbfMidSus,sigmafCMidSus,sigmafTMid);
ChecktfMidSus = SC(ftfMidSus,sigmafCMidSus,sigmafTMid);

%% Deflection and Camber
% Deflections at Transfer
% Camber due to PS force
deltapi = -Pi/(Eci*Igprecast)*(epg*(L*12)^2/8);
% Deflection due to Precast Self Weight
deltagi = 5/384*(wgprecast/12)*(L*12)^4/(Eci*Igprecast);
% Total Deflections at Transfer
deltai = deltagi+deltapi;
% Deflections at Deck Placement
% Deflection due to CIP Deck Self Weight
deltadgdeck = 5/384*((wgdeck+wconLL)/12)*(L*12)^4/(Ec*Igprecast);
% Total Deflections at Deck Placement
deltad = deltai+deltadgdeck;
% Deflections at Service
% Deflections due to live loads at service
deltafLL = 5/384*(wlane*DFM/12)*(L*12)^4/(Ec*Icomp);
P = [32,32,8];
xaxel = [-14,0,14];
aaxel = L/2 + xaxel + 2.33;
for axel = 1:3
    deltaaxel(axel) = deltaeachaxel(P(axel),aaxel(axel),L,Ec,Icomp);
end
deltatruck = sum(deltaaxel);
deltafLT = deltatruck*DFM*(1+IM/100);
deltafL = max(deltafLT,0.25*deltafLT+deltafLL);
deltafLallow = L*12/800;
if deltafL <= deltafLallow
    CheckdeltafL = 'OK';
else
    CheckdeltafL = 'NG';
```

```
end
% Deflection due to superimposed dead loads at service
deltafsuperdead = 5/384*(wsuperdead/12)*(L*12)^4/(Ec*Icomp);
% Total Deflections at Service
deltaf = deltad+deltafL+deltafsuperdead;

%% Strength Limit State
% Flexural Strength
Mupos = 1.25*DC + 1.5*DW + 1.75*ML;
if fpe >= 0.5*fpu
    Checkfpehalffpu = 'OK';
else
    Checkfpehalffpu = 'NG';
end
dp = htotal+tslab-cps;
k = 2*(1.04-fpy/fpu);
if fcdeck <= 4
    Beta1deck = 0.85;
elseif fcdeck >= 8
    Beta1deck = 0.65;
else
    Beta1deck = 0.85-0.05*(fcdeck-4);
end
c = (Aps*fpu+As*fs+Aprimes*fprimes)/(0.85*fcdeck*Beta1deck*wtotal+k*Aps*fpu/dp);
fps = fpu*(1-k*c/dp);
a = Aps*fps/(0.85*fcdeck*wtotal);
cNA = a/Beta1deck;
dt = htotal+tslab-yrow(1);
Epsilont = 0.003/cNA*(dt-cNA);
if Epsilont <= 0.002
    phif = 0.75;
elseif Epsilont >= 0.005
    phif = 1.0;
else
    phif = 0.65+0.15*(dt/cNA-1);
end
if a <= tslab
    b = wtotal;
else
    b = wweb;
end
hf = tslab;
Mn = (Aps*fps*(dp-a/2)+As*fs*(ds-a/2)-Aprimes*fprimes*(dprimes-a/2)+...
    0.85*fcdeck*(wtotal-b)*hf*(a/2-hf/2))/12;
Mr = phif*Mn;
if Mr >= Mupos
    CheckMrMupos = 'OK';
else
    CheckMrMupos = 'NG';
end
% Minimum Reinforcement
```

```
fr = 0.24*sqrt(fc);
fcpe = Pe/Agprecast + Pe*epg*cgprecast/Igprecast;
Sc = Icomp/ccomp;
Snc = Igprecast/cgprecast;
Mdnc = Mgprecast + Mgdeck;
Mcr = max((Sc/12)*(fr+fcpe)-Mdnc*(Sc/Snc-1),Sc*fr/12);
Mmin = 1.2*Mcr;
if Mr >= min(Mmin,1.33*Mupos)
    CheckMpos = 'OK';
else
    CheckMpos = 'NG';
end

%% Shear Design
% Shear Strength
de = (Aps*fps*dp+As*fy*ds)/(Aps*fps+As*fy);
dv = max(de-a/2,max(0.9*de,0.72*(htotal+tslab)));
xvcritical = dv/12;
phiv = 0.9;
VLTcritical = 72*((L-xvcritical)-9.33)/L;
VLLcritical = wlane*(L-xvcritical)^2/(2*L);
VLcrit = VLTcritical*(1+IM/100)*DFV + VLLcritical*DFV;
Vgprecastcrit = wgprecast*(L-xvcritical)^2/(2*L);
Vgdeckcrit = wgdeck*(L-xvcritical)^2/(2*L);
Vsuperdeadcrit = wsuperdead*(L-xvcritical)^2/(2*L);
VDcrit = Vgprecastcrit+Vgdeckcrit+Vsuperdeadcrit;
Vucrit = 1.25*VDcrit+1.75*VLcrit;
Vp = 0;
Nu = 0;
MLTcritical = VLTcritical*xvcritical;
MLLcritical = wlane*xvcritical*(L-xvcritical)/2;
MLcritical = MLTcritical*(1+IM/100)*DFM+MLLcritical*DFM;
Mgprecastcritical = wgprecast*xvcritical*(L-xvcritical)/2;
Mgdeckcritical = wgdeck*xvcritical*(L-xvcritical)/2;
Msuperdeadcritical = wsuperdead*xvcritical*(L-xvcritical)/2;
MDcritical = Mgprecastcritical+Mgdeckcritical+Msuperdeadcritical;
Mucritical = 1.25*MDcritical+1.75*MLcritical;
bv = wtotal;
Mucrit = max(Mucritical,abs(Vucrit-Vp)*(dv/12))*12;
Act = bv*(htotal+tslab)/2;
Epsilons = (abs(Mucrit)/dv+0.5*Nu+abs(Vucrit-Vp)-Aps*fpo)/(Es*As+Ep*Aps);
if Epsilons < 0
    Epsilons = max((abs(Mucrit)/dv+0.5*Nu+abs(Vucrit-Vp)-Aps*fpo)/↙
(Es*As+Ep*Aps+Ec*Act),...
        -0.4*10^-3);
else
    Epsilons = min(Epsilons,6*10^-3);
end
sx = dv;
ag = 0.5;
sxe = min(max(sx*1.38/(ag+0.63),12),80);
```

```
Betav = 4.8/(1+750*Epsilons)*51/(39+sxe);
Thetav = 29+3500*Epsilons;
Vc = 0.0316*Betav*sqrt(fcdeck)*bv*dv;
if Vucrit <= 0.5*phiv*(Vc+Vp)
    CheckVu = 'OK';
else
    CheckVu = 'NG';
end
Vs = 0;
% Longitudingal Reinforcement Shear Check
phic = 1;
if Aps*fps+As*fy >= abs(Mucrit)/(dv*phif)+0.5*Nu/phic+(abs(Vucrit/phiv-Vp)-...
        0.5*Vs)*cot(Thetav*pi()/180)
    CheckVLs = 'OK';
else
    CheckVLs = 'NG';
end
VLTsup = 72;
VLLsup = wlane*L/2;
VLsup = VLTsup*(1+IM/100)*DFV+VLLsup*DFV;
Vgprecastsup = wgprecast*L/2;
Vgdecksup = wgdeck*L/2;
Vsuperdeadsup = wsuperdead*L/2;
VDsup = Vgprecastsup+Vgdecksup+Vsuperdeadsup;
Vusup = 1.25*VDsup+1.75*VLsup;
if Aps*fps+As*fy >= (Vusup/phiv-Vp-0.5*Vs)*cot(Thetav*pi()/180)
    CheckVLssup = 'OK';
else
    CheckVLssup = 'NG';
end
%Interface Shear Design
bvi(1) = wtotal;
bvi(2) = 2*sqrt(hflangesloped^2+wflange^2)+2*sqrt(hweb^2+wwebsloped^2)+wweb;
Lvi = 12;
Acv = bvi*Lvi;
Vui = Vucrit/dv*12;
cv = 0.24;
muv = 1;
K1v = 0.25;
K2v = 1.5;
Avf = 0;
Pc = 0;
Vni(1,:) = cv*Acv+muv*(Avf*fy+Pc);
Vni(2,:) = K1v*fc*Acv;
Vni(3,:) = K2v*Acv;
Vni = min(min(Vni));
if Vni >= 1.33*Vui/phiv
    CheckAvf = 'OK';
    Avf = 0;
else
    CheckAvf = 'NG';
```

```
    Avf = max(0.05*Acv/fy);
end

%% Summary of Checks
CheckPSLossSup = {CheckbiSup,ChecktiSup;CheckbdSup,ChecktdSup;CheckbfSup,...
    ChecktfSup};
CheckPSLossMid = {CheckbiMid,ChecktiMid,'OK','OK';...
    CheckbdMid,ChecktdMid,CheckbdMidSus,ChecktdMidSus;...
    CheckbfMid,ChecktfMid,CheckbfMidSus,ChecktfMidSus};
% CheckLLDF = [CheckLDF,CheckDFMint,CheckDFMext,CheckDFVint,CheckDFVext];
CheckDeflection = {CheckdeltafL};
CheckStrength = {Checkfpehalffpu,CheckMrMupos,CheckMpos};
CheckShear = {CheckVu,CheckVLs,CheckVLssup,CheckAvf};

% CheckPSLoss = {CheckbiSup,ChecktiSup,CheckbiMid,ChecktiMid,'OK','OK';...
%     CheckbdSup,ChecktdSup,CheckbdMid,ChecktdMid,CheckbdMidSus,ChecktdMidSus;...
%     CheckbfSup,ChecktfSup,CheckbfMid,ChecktfMid,CheckbfMidSus,ChecktfMidSus};

% Stresses
fMatSup = [fbiSup,ftiSup;fbdSup,ftdSup;fbfSup,ftfSup];
fMatMid = [fbiMid,ftiMid,NaN,NaN';fbdMid,ftdMid,fbdMidSus,ftdMidSus;...
    fbfMid,ftfMid,fbfMidSus,ftfMidSus];

% fMat = [fbiSup,ftiSup,fbiMid,ftiMid,NaN,NaN';...
%     fbdSup,ftdSup,fbdMid,ftdMid,fbdMidSus,ftdMidSus;...
%     fbfSup,ftfSup,fbfMid,ftfMid,fbfMidSus,ftfMidSus];

end




%% Shape Properties
function ShapeMatrix = ShapeProp(Nodes,XY,h1)

[rows,cols] = size(Nodes);

for i = 1:rows
    shape = 0;
    for j = 1:cols
        if isnan(Nodes(i,j)) == 0
            x(j) = XY(Nodes(i,j),1);
            y(j) = XY(Nodes(i,j),2);
        else
            shape = 1;
            x(j) = NaN;
            y(j) = NaN;
        end
    end
    b(i) = max(x) - min(x);
    h(i) = max(y) - min(y);
```

```
    if shape == 0
        cy(i) = min(y) + h(i)/2;
        A(i) = b(i)*h(i);
    else
        cy(i) = min(y) + h(i)*h1/3;
        A(i) = 1/2*b(i)*h(i);
    end
end

ShapeMatrix = [b;h;cy;A];
end

%% Shape I
function Ishape = ShapeI(ShapeProp,Nodes,cg)

[rows,cols] = size(Nodes);

for i = 1:rows
    shape = 0;
    for j = 1:cols
        if isnan(Nodes(i,j))
            shape = 1;
        end
    end
    b = ShapeProp(1,:);
    h = ShapeProp(2,:);
    cy = ShapeProp(3,:);
    A = ShapeProp(4,:);

    if shape == 0
        Ishape(i) = (b(i)*h(i)^3)/12 + (cy(i)-cg)^2*A(i);
    else
        Ishape(i) = (b(i)*h(i)^3)/36 + (cy(i)-cg)^2*A(i);
    end
end
end

%% Stress Check
function Check = SC(f,sigmaC,sigmaT)

if f <= 0
    if abs(f) <= abs(sigmaC)
        Check = 'OK';
    else
        Check = 'NG';
    end
else
    if abs(f) <= abs(sigmaT)
        Check = 'OK';
    else
        Check = 'NG';
```

```
    end
end

end

%% Deflection due to each truck axle
function delta = deltaeachaxel(P,a,L,Ec,Ic)

x = L/2;
b = L-a;
if x <= a
    delta = P*b*x/(6*Ec*Ic*L)*(L^2-b^2-x^2)*12^3;
else
    delta = P*b/(6*Ec*Ic*L)*((x-a)^3*L/b+(L^2-b^2)*x-x^3)*12^3;
end


end
```

Iteration 1

```
%THIS SCRIPT FILE DOES NOT INCLUDE DEBONDING OF THE PRESTRESSING STRANDS.
%IT WAS USED TO CREATE THE FIRST ITERATION OF THE PRELIMINARY DESIGN TABLES

function InvertedT_NoDebonding

clear all;
clc;

%Create an outer loop for the three different sizes of cross-section
for k = 1:3
    clear L
    if k == 1
        ShapeSize = 'SMALL'
    elseif k == 2
        ShapeSize = 'MEDIUM'
    else
        ShapeSize = 'LARGE'
    end
    if strcmp(ShapeSize,'SMALL')
        yrow = [2,4,0,6];
        maxPSrow = [23,21,0,17];
        PSrowinitial = [10,0,0,0];
        Linitial = 10;
        Lfinal = 40;
    elseif strcmp(ShapeSize,'MEDIUM')
        yrow = [2,4,6,16];
        maxPSrow = [23,21,19,9];
        PSrowinitial = [10,0,0,0];
        Linitial = 30;
        Lfinal = 60;
    elseif strcmp(ShapeSize,'LARGE')
        yrow = [2,4,6,22];
        maxPSrow = [23,23,21,9];
        PSrowinitial = [10,0,0,0];
        Linitial = 50;
        Lfinal = 80;
    end

    %Set how many times to loop for each size
    ifinal = (Lfinal - Linitial)/5 + 1;

    %Begin the loop for the different span lengths
    for i = 1:ifinal;

        %Set the initial number of strands in each row since this will
        %change with each iteration. Also set the span length to test.
        PSrow = PSrowinitial;
        L = Linitial + (i-1)*5;

        %Initialize the checks
        CheckAll = 'NG';
```

Iteration 1

```
%Create a loop that loops while all of these checks are 'NG'
while strcmp(CheckAll,'NG');

    %Initialize the variables
    CheckSD = 'NG';
    CheckPSMid = 'NG';
    CheckPSSup = 'NG';
    StrandAdded = 0;

    %Send all of the parameters into the InvertedT_Design.m function
    %which carries out the calculations.
    [CheckPSLossSup,CheckPSLossMid,CheckDeflection,CheckStrength,...
        ~,fMatSup,fMatMid] = InvertedT_Design(L,PSrow,ShapeSize);

    %Note that for the following statements/loops, once a strand
    %has been added for any reason, we need to re-check everything
    %else before adding more strands.

    %Find the row and column of any 'NG' values in the matrices
    %outputted by the InvertedT_Design.m function
    [rowsA,colsA] = find(strcmp(CheckDeflection,'NG'));
    [rowsB,colsB] = find(strcmp(CheckStrength,'NG'));
    [rowsC,colsC] = find(strcmp(CheckPSLossMid,'NG'));
    [rowsD,colsD] = find(strcmp(CheckPSLossSup,'NG'));

    %Check strength & deflection, add a strand to the bottom if either
    %of these checks fail.
    if isempty(rowsA) == 0 | isempty(rowsB) == 0;
        PSrow = AddPSBot(PSrow,maxPSrow);
        StrandAdded = 1;
    else
        CheckSD = 'OK';
    end

    %If there are 'NG' values in the CheckPSLossMid matrix, and
    %there were no strands previously added then:
    if isempty(rowsC) == 0;

        %Figure out whether the failing check is at the top or
        %bottom of the section
        for m = 1:length(colsC);

            if (colsC(m) == 1 | colsC(m) == 3);
                Loc = 'Bot';
            else Loc = 'Top';
            end

            %Add strands to the bottom row if the check which fails is
            %either the bottom of the section in tension or the top in
```

Iteration 1

```
            %compression and set StrandAdded = 1.
            if StrandAdded == 0;
                if (strcmp(Loc,'Bot') & fMatMid(rowsC(m),colsC(m)) >= 0)...
                        | (strcmp(Loc,'Top') & fMatMid(rowsC(m),colsC(m)) < 0)
                    PSrow = AddPSBot(PSrow,maxPSrow);
                    StrandAdded = 1;

                    %Otherwise if the failing check is the bottom in
                    %compression or the top in tension then add a strand
                    %to the top and set StrandAdded = 1.
                elseif (strcmp(Loc,'Bot') & fMatMid(rowsC(m),colsC(m)) < 0)...
                        | (strcmp(Loc,'Top') & fMatMid(rowsC(m),colsC(m)) >= 0)
                    PSrow = AddPSTop(PSrow,maxPSrow);
                    StrandAdded = 1;
                end
            end
        end
        %Otherwise if there were no 'NG' values in the matrix then:
    elseif isempty(rowsC)

        %The prestress checks at the mid-span were okay
        CheckPSMid = 'OK';
    end

    %If a strand was not added in either of the previous checks
    %the support stresses, add strands to the correct location
    %depending on the check that fails.
    if isempty(rowsD) == 0;

        %If the limit was breached at the bottom of the section
        %(col 1 of CheckPSLossSup) in tension or at the top (col 2)
        %in compression then add strands to the bottom of the
        %section
        for m = 1:length(colsD);
            if StrandAdded == 0;
                if (colsD(m) == 1 & fMatSup(rowsD(m),colsD(m)) >= 0) | ...
                        (colsD(m) == 2 & fMatSup(rowsD(m),colsD(m)) < 0);
                    PSrow = AddPSBot(PSrow,maxPSrow);
                    StrandAdded = 1;

                    %Otherwise if the limit was breached at the bottom in
                    %compression or at the top in tension, then add strands to
                    %the top of the section and set StrandAdded = 1
                elseif (colsD(m) == 1 & fMatSup(rowsD(m),colsD(m)) < 0 ) | ...
                        (colsD(m) == 2 & fMatSup(rowsD(m),colsD(m)) >= 0);
                    PSrow = AddPSTop(PSrow,maxPSrow);
                    StrandAdded = 1;
                end
            end
        end
        %Otherwise if there were no 'NG' values in the matrix then the
```

Iteration 1

```
            %prestress checks at the support were okay
        elseif isempty(rowsD)
            CheckPSSup = 'OK';
        end

        if StrandAdded == 1;
            if isnan(PSrow(1));
                if k == 1;
                    FinalTable(i,1:5) = [L,PSrow];
                elseif k == 2;
                    FinalTable(i,6:10) = [L,PSrow];
                else
                    FinalTable(i,11:15) = [L,PSrow];
                end
                break
            end
        end


        %Check the values of CheckSD, CheckPSMid, and CheckPSSup. If
        %all three are 'OK' then we can set CheckAll = 'OK' and break
        %the while-loop
        if CheckSD == 'OK' & CheckPSMid == 'OK' & CheckPSSup == 'OK'
            CheckAll = 'OK';

            %Additionally if all of the checks are okay then we can write
            %the span length and prestressing information into a final
            %table and save this to a text file later
            if k == 1;
                FinalTable(i,1:5) = [L,PSrow];
            elseif k == 2;
                FinalTable(i,6:10) = [L,PSrow];
            else
                FinalTable(i,11:15) = [L,PSrow];
            end

        else CheckAll = 'NG';
        end
    end
  end
end

%Currently the matrix FinalTable is of type double. Convert this to a
%table, and then write it to a text file.
T = array2table(FinalTable);

%Change the headers in the final table to more meaningful headings
T.Properties.VariableNames = {'L_Small_ft','PSRow1_Small',...
    'PSRow2_Small','PSRow3_Small','PSRow4_Small','L_Medium_ft',...
    'PSRow1_Medium','PSRow2_Medium','PSRow3_Medium','PSRow4_Medium',...
    'L_Large_ft','PSRow1_Large','PSRow2_Large','PSRow3_Large',...
```

Iteration 1

```
    'PSRow4_Large'};

%Change the units in the final table to meaningful units
T.Properties.VariableUnits = {'ft.','#','#','#','#','ft.','#','#','#'...
    ,'#','ft.','#','#','#','#'};

%Write the table to a text file
writetable(T,'PrelimDesign_NoDebonding.txt');

end


%% Add prestressing strands to the bottom of the section
%Check whether you have reached the maximum number of strands in that row,
%if you haven't then add a strand to that row, if you have then move to the
%next row. If all rows have the maximum number of strands, assign "NaN" to
%the rows.

function [PSrow] = AddPSBot(PSrow,maxPSrow)

if PSrow(1) < maxPSrow(1)
    PSrow(1) = PSrow(1) + 1;
elseif PSrow(2) < maxPSrow(2);
    PSrow(2) = PSrow(2) + 1;
elseif PSrow(3) < maxPSrow(3);
    PSrow(3) = PSrow(3) + 1;
else
    PSrow(1:length(PSrow)) = NaN;
end

end
%% Add prestressing strands to the top of the section
%Check whether you have reached the maximum number of strands in that row,
%if you haven't then add a strand to that row. If the row has the maximum
%number of strands, assign "NaN" to the rows.

function [PSrow] = AddPSTop(PSrow,maxPSrow)

if PSrow(4) < maxPSrow(4)
    PSrow(4) = PSrow(4) + 1;
else
    PSrow(1:length(PSrow)) = NaN;
end

end
```

Iteration 2

```
%THIS FUNCTION CHANGES THE SPAN LENGTH, GEOMETRY, AND PRESTRESSING
%ARRANGEMENT FOR AN INVERTED T-BEAM AND FEEDS THIS INFORMATION INTO THE
%"DESIGN" FUNCTION TO CARRY OUT ALL OF THE DESIGN CALCULATIONS

function InvertedT_Debonding

clear all;
clc;

%Create an outer loop for the three different sizes of cross-section
for k = 1:3
    clear L
    if k == 1
        ShapeSize = 'SMALL'
    elseif k == 2
        ShapeSize = 'MEDIUM'
    else
        ShapeSize = 'LARGE'
    end
    if strcmp(ShapeSize,'SMALL')
        yrow = [2,4,0,6];
        maxPSrow = [23,21,0,17];
        PSrowinitial = [10,0,0,0];
        Linitial = 10;
        Lfinal = 40;
    elseif strcmp(ShapeSize,'MEDIUM')
        yrow = [2,4,6,16];
        maxPSrow = [23,21,19,9];
        PSrowinitial = [10,0,0,0];
        Linitial = 30;
        Lfinal = 60;
    elseif strcmp(ShapeSize,'LARGE')
        yrow = [2,4,6,22];
        maxPSrow = [23,23,21,9];
        PSrowinitial = [10,0,0,0];
        Linitial = 50;
        Lfinal = 80;
    end

    %Set how many times to loop for each size
    ifinal = (Lfinal - Linitial)/5 + 1;

    %Begin the loop for the different span lengths
    for i = 1:ifinal;

        %Set the initial number of strands in each row since this will
        %change with each iteration. Also set the span length to test.
        PSrow = PSrowinitial;
        PSdebond = PSrowinitial;
        L = Linitial + (i-1)*5;
```

Iteration 2

```
%Initialize the checks
CheckAll = 'NG';        %Initially set all checks as no good
NumDebonded = 0;        %Initially no strands have been debonded
StrandDebonded = 0;     %Initially no strands have been debonded
DebondAgain = 0;


%Create a loop that loops while all of these checks are 'NG'
while strcmp(CheckAll,'NG');

    %Initialize the variables
    CheckSD = 'NG';     %Strength and deflection checks initially NG
    CheckPSMid = 'NG';  %Mid-span stresses initially NG
    CheckPSSup = 'NG';  %Support stresses initially NG
    StrandAdded = 0;    %No Strands added initially

    %Send all of the parameters into the InvertedT_Design.m function
    %which carries out the calculations. If we have debonded some
    %strands then the only checks which will change are the Support
    %stress checks so we will only check & change those arrays.
    if StrandDebonded == 0;
        [CheckPSLossSup,CheckPSLossMid,CheckDeflection,CheckStrength,...
            ~,fMatSup,fMatMid] = InvertedT_Design(L,PSdebond,ShapeSize);
    else
        [CheckPSLossSup,~,~,~,...
            ~,fMatSup,~] = InvertedT_Design(L,PSdebond,ShapeSize);
    end

    %Note that for the following statements/loops, once a strand
    %has been added for any reason, we need to re-check everything
    %else before adding more strands. If strands have been debonded
    %then we need to re-check the support stresses.

    %Find the row and column of any 'NG' values in the matrices
    %outputted by the InvertedT_Design.m function
    [rowsA,colsA] = find(strcmp(CheckDeflection,'NG'));
    [rowsB,colsB] = find(strcmp(CheckStrength,'NG'));
    [rowsC,colsC] = find(strcmp(CheckPSLossMid,'NG'));
    [rowsD,colsD] = find(strcmp(CheckPSLossSup,'NG'));

    %Check strength & deflection, add a strand to the bottom if either
    %of these checks fail.
    if (isempty(rowsA) == 0 | isempty(rowsB) == 0);
        PSrow = AddPSBot(PSrow,maxPSrow);
        PSdebond = AddPSBot(PSdebond,maxPSrow);
        StrandAdded = 1;
    else
        CheckSD = 'OK';
    end

    %If there are 'NG' values in the CheckPSLossMid matrix, and
```

Iteration 2

```
%there were no strands previously added then:
if isempty(rowsC) == 0;

    %Figure out whether the failing check is at the top or
    %bottom of the section
    for m = 1:length(colsC);

        if (colsC(m) == 1 | colsC(m) == 3);
            Loc = 'Bot';
        else Loc = 'Top';
        end

        %Add strands to the bottom row if the check which fails is
        %either the bottom of the section in tension or the top in
        %compression and set StrandAdded = 1.
        if StrandAdded == 0;
            if (strcmp(Loc,'Bot') & fMatMid(rowsC(m),colsC(m)) >= 0)...
                    | (strcmp(Loc,'Top') & fMatMid(rowsC(m),colsC(m)) < 0)
                PSrow = AddPSBot(PSrow,maxPSrow);
                PSdebond = AddPSBot(PSdebond,maxPSrow);
                StrandAdded = 1;

                %Otherwise if the failing check is the bottom in
                %compression or the top in tension then add a strand
                %to the top and set StrandAdded = 1.
            elseif (strcmp(Loc,'Bot') & fMatMid(rowsC(m),colsC(m)) < 0)...
                    | (strcmp(Loc,'Top') & fMatMid(rowsC(m),colsC(m)) >= 0)
                PSrow = AddPSTop(PSrow,maxPSrow);
                PSdebond = AddPSTop(PSdebond,maxPSrow);
                StrandAdded = 1;
            end
        end
    end
    %Otherwise if there were no 'NG' values in the matrix then:
elseif isempty(rowsC)

    %The prestress checks at the mid-span were okay
    CheckPSMid = 'OK';
end

%If a strand was not added in either of the previous checks
%the support stresses, add strands to the correct location
%depending on the check that fails.
if isempty(rowsD) == 0;

    %If the limit was breached at the bottom of the section
    %(col 1 of CheckPSLossSup) in tension or at the top (col 2)
    %in compression then add strands to the bottom of the
    %section
    for m = 1:length(colsD);
        if StrandAdded == 0;
```

Iteration 2

```
                    if (colsD(m) == 1 & fMatSup(rowsD(m),colsD(m)) >= 0) | ...
                            (colsD(m) == 2 & fMatSup(rowsD(m),colsD(m)) < 0);
                        PSrow = AddPSBot(PSrow,maxPSrow);
                        PSdebond = AddPSBot(PSdebond,maxPSrow);
                        StrandAdded = 1;
                        StrandDebonded = 0;

                        %Otherwise if the limit was breached at the bottom in
                        %compression or at the top in tension, then
                        %debond strands from the bottom of the section
                        %and set StrandAdded = 1
                    elseif (colsD(m) == 1 & fMatSup(rowsD(m),colsD(m)) < 0 ) | ...
                            (colsD(m) == 2 & fMatSup(rowsD(m),colsD(m)) >= 0);
                        if DebondAgain == 0;
                            PSrow = AddPSTop(PSrow,maxPSrow);
                            PSdebond = PSrow;
                            NumDebonded = 0;
                            StrandAdded = 1;
                            DebondAgain = 1;
                            StrandDebonded = 0;
                        else
                            [PSdebond,NumDebonded,DebondCount,PSrow] = Debond↙
(PSdebond,NumDebonded,PSrow);
                            StrandDebonded = 1;
                            if isnan(DebondCount)
                                DebondAgain = 0;
                                StrandDebonded = 0;
                            end
                        end
                    end
                end
            end

            %Otherwise if there were no 'NG' values in the matrix then the
            %prestress checks at the support were okay
        elseif isempty(rowsD)
            CheckPSSup = 'OK';
        end

        %If strands were either added or debonded, check that there are
        %no "NaN" values in the PSrow array. If there are then print
        %this to the table and break out of the while-loop.
        if StrandAdded == 1;
            if isnan(PSrow(1));
                if k == 1;
                    FinalTable(i,1:6) = [L,PSrow,NaN];
                elseif k == 2;
                    FinalTable(i,7:12) = [L,PSrow,NaN];
                else
                    FinalTable(i,13:18) = [L,PSrow,NaN];
                end
```

Iteration 2

```
                    break
                end
            end


            %Check the values of CheckSD, CheckPSMid, and CheckPSSup. If
            %all three are 'OK' then we can set CheckAll = 'OK' and break
            %the while-loop
            if CheckSD == 'OK' & CheckPSMid == 'OK' & CheckPSSup == 'OK'
                CheckAll = 'OK';

                %Additionally if all of the checks are okay then we can write
                %the span length and prestressing information into a final
                %table and save this to a text file later
                if k == 1;
                    FinalTable(i,1:6) = [L,PSrow,NumDebonded];
                elseif k == 2;
                    FinalTable(i,7:12) = [L,PSrow,NumDebonded];
                else
                    FinalTable(i,13:18) = [L,PSrow,NumDebonded];
                end

            else CheckAll = 'NG';
            end
        end
    end
end

%Currently the matrix FinalTable is of type double. Convert this to a
%table, and then write it to a text file.
T = array2table(FinalTable);

%Change the headers in the final table to more meaningful headings
T.Properties.VariableNames = {'L_Small_ft','PSRow1_Small',...
    'PSRow2_Small','PSRow3_Small','PSRow4_Small','Debond_Small','L_Medium_ft',...
    'PSRow1_Medium','PSRow2_Medium','PSRow3_Medium','PSRow4_Medium','Debond_Medium',...
    'L_Large_ft','PSRow1_Large','PSRow2_Large','PSRow3_Large',...
    'PSRow4_Large','Debond_Large'};

%Change the units in the final table to meaningful units
T.Properties.VariableUnits = {'ft.','#','#','#','#','#','ft.','#','#','#'...
    ,'#','#','ft.','#','#','#','#','#'};

%Write the table to a text file
writetable(T,'PrelimDesign_WithDebonding1.txt');

end


%% Add prestressing strands to the bottom of the section
%Check whether you have reached the maximum number of strands in that row,
```

Iteration 2

```
%if you haven't then add a strand to that row, if you have then move to the
%next row. If all rows have the maximum number of strands, assign "NaN" to
%the rows.

function [PSrow] = AddPSBot(PSrow,maxPSrow)

if PSrow(1) < maxPSrow(1)
    PSrow(1) = PSrow(1) + 1;
elseif PSrow(2) < maxPSrow(2);
    PSrow(2) = PSrow(2) + 1;
elseif PSrow(3) < maxPSrow(3);
    PSrow(3) = PSrow(3) + 1;
else
    PSrow(1:length(PSrow)) = NaN;
end

end
%% Add prestressing strands to the top of the section
%Check whether you have reached the maximum number of strands in that row,
%if you haven't then add a strand to that row. If the row has the maximum
%number of strands, assign "NaN" to the rows.

function [PSrow] = AddPSTop(PSrow,maxPSrow)

if PSrow(4) < maxPSrow(4)
    if PSrow(4) == 0;
        PSrow(4) = PSrow(4) + 2;
    else
        PSrow(4) = PSrow(4) + 1;
    end
else
    PSrow(1:length(PSrow)) = NaN;
end

end
%% Debond strands from the bottom of the section
%This function debonds 2 strands from the lowest possible row in the
%cross-section (since this will have the greatest eccentricity hence the
%greatest effect on the flexural stresses).

function [PSdebond,NumDebonded,DebondCount,PSrow] = Debond(PSdebond,NumDebonded,PSrow)

%Check whether you have exceeded AASHTO's limit on the total number of
%debonded strands
DebondCount = NumDebonded + 2;

if DebondCount < (sum(PSrow) * 0.25)

    %If not, check whether you have debonded the max number of strands in
    %row 1 as per AASHTO's limits. If not then debond 2 strands, if you
    %have then move to the second row and so on.
```

Iteration 2

```
    if  PSdebond(1) - 2 > 0.4*PSrow(1)
        PSdebond(1) = PSdebond(1) - 2;
        NumDebonded = NumDebonded + 2;
    elseif PSdebond(2) - 2 > 0.4*PSrow(2)
        PSdebond(2) = PSdebond(2) - 2;
        NumDebonded = NumDebonded + 2;
    elseif PSdebond(3) - 2 > 0.4*PSrow(3)
        PSdebond(3) = PSdebond(3) - 2;
        NumDebonded = NumDebonded + 2;
    else
        %If you have debonded the maximum number of strands then set the
        %number debonded to NaN
        DebondCount = NaN;
    end

else
    %If you have debonded the maximum number of strands then set the
    %number debonded to NaN
    DebondCount = NaN;
end

end
```

Iteration 2

```
%THIS FUNCTION WORKS TO OPTIMIZE THE STRAND ARRANGEMENT AND ALLOW FOR
%DEBONDING OF STRANDS. IT SELECTS THE STRAND ARRANGEMENT GIVING DUE
%CONSIDERATION TO THESE, AND THEN FEEDS THIS INTO THE FUNCTION WHICH
%CARRIES OUT ALL OF THE DESIGN CALCULATIONS


function InvertedT_Debonding_StrandGeometry

clear all;
clc;

%Create an outer loop for the three different sizes of cross-section
for k = 1:3
    clear L
    if k == 1
        ShapeSize = 'SMALL'
    elseif k == 2
        ShapeSize = 'MEDIUM'
    else
        ShapeSize = 'LARGE'
    end
    if strcmp(ShapeSize,'SMALL')
        yrow = [2,4,0,6];
        maxPSrow = [23,21,0,17];
        PSrowinitial = [10,0,0,0];
        Linitial = 10;
        Lfinal = 40;
    elseif strcmp(ShapeSize,'MEDIUM')
        yrow = [2,4,6,16];
        maxPSrow = [23,21,19,9];
        PSrowinitial = [10,0,0,0];
        Linitial = 30;
        Lfinal = 60;
    elseif strcmp(ShapeSize,'LARGE')
        yrow = [2,4,6,22];
        maxPSrow = [23,23,21,9];
        PSrowinitial = [10,0,0,0];
        Linitial = 50;
        Lfinal = 80;
    end

    %Set how many times to loop for each size
    ifinal = (Lfinal - Linitial)/5 + 1;

    %Begin the loop for the different span lengths
    for i = 1:ifinal;

        %Set the initial number of strands in each row since this will
        %change with each iteration. Also set the span length to test.
        PSrow = PSrowinitial;
        PSdebond = PSrowinitial;
```

Iteration 2

```
L = Linitial + (i-1)*5;

%Initialize the checks
CheckAll = 'NG';        %Initially set all checks as no good
NumDebonded = 0;        %Initially no strands have been debonded
StrandDebonded = 0;     %Initially no strands have been debonded
DebondAgain = 1;


%Create a loop that loops while all of these checks are 'NG'
while strcmp(CheckAll,'NG');

    %Initialize the variables
    CheckSD = 'NG';     %Strength and deflection checks initially NG
    CheckPSMid = 'NG';  %Mid-span stresses initially NG
    CheckPSSup = 'NG';  %Support stresses initially NG
    StrandAdded = 0;    %No Strands added initially

    %Send all of the parameters into the InvertedT_Design.m function
    %which carries out the calculations. If we have debonded some
    %strands then the only checks which will change are the Support
    %stress checks so we will only check & change those arrays.
    if StrandDebonded == 0;
        [CheckPSLossSup,CheckPSLossMid,CheckDeflection,CheckStrength,...
            ~,fMatSup,fMatMid,cgprecast,sigmaiCSup,sigmaiTSup...
        ,sigmaiCMid,sigmaiTMid,Pi,Agprecast,Igprecast,ytprecast,...
        Mgprecast] = InvertedT_Design_AltStrandGeom(L,PSdebond,ShapeSize);
    else
        [CheckPSLossSup,~,~,~,...
            ~,fMatSup,~,cgprecast,sigmaiCSup,sigmaiTSup...
        ,sigmaiCMid,sigmaiTMid,Pi,Agprecast,Igprecast,ytprecast,...
        Mgprecast] = InvertedT_Design_AltStrandGeom(L,PSdebond,ShapeSize);
    end

    %Note that for the following statements/loops, once a strand
    %has been added for any reason, we need to re-check everything
    %else before adding more strands. If strands have been debonded
    %then we need to re-check the support stresses.

    %Find the row and column of any 'NG' values in the matrices
    %outputted by the InvertedT_Design.m function
    [rowsA,colsA] = find(strcmp(CheckDeflection,'NG'));
    [rowsB,colsB] = find(strcmp(CheckStrength,'NG'));
    [rowsC,colsC] = find(strcmp(CheckPSLossMid,'NG'));
    [rowsD,colsD] = find(strcmp(CheckPSLossSup,'NG'));

    %Check strength & deflection, add a strand to the bottom if either
    %of these checks fail.
    if (isempty(rowsA) == 0 | isempty(rowsB) == 0);
        PSrow = AddPSBot(PSrow,maxPSrow);
        PSdebond = AddPSBot(PSdebond,maxPSrow);
```

Iteration 2

```
            StrandAdded = 1;
        else
            CheckSD = 'OK';
        end

        %If there are 'NG' values in the CheckPSLossMid matrix, and
        %there were no strands previously added then:
        if isempty(rowsC) == 0;

            %Is the failure occurring at the time of release of the
            %prestress into the concrete, and if it is can we fix this
            %issue by altering the strand geometry
            for m = 1:length(rowsC);
                if rowsC(m) == 1
                    TransferFailure = 1;
                end
            end

            %If the failure occurs at transfer only, then maybe we can
            %rearrange the strands to get it to work
            if TransferFailure == 1 & StrandAdded == 0;

                %Figure out what eccentricity we need to make it work
                et = (sigmaiTMid + Pi/Agprecast + (Mgprecast*ytprecast)/Igprecast)↙
*...
                    Igprecast/(Pi*ytprecast);
                eb = ((Mgprecast*cgprecast)/Igprecast - Pi/Agprecast - sigmaiCMid)↙
*...
                    Igprecast/(Pi*cgprecast);
                erequired = min(et,eb);

                %Rearrange the strands to get that required
                %eccentricity. If we can't then we need to just
                %continue with the rest of the code. If we rearrange
                %the strands then set StrandAdded = 1 so that we ignore
                %the remainder of the checks and go back to recalculate
                %the stresses.
                [PSrow,StrandAdded] = AlterStrandGeometry(PSrow,erequired,↙
cgprecast,StrandAdded,yrow,maxPSrow);
                [PSdebond,StrandAdded] = AlterStrandGeometry(PSdebond,erequired,↙
cgprecast,StrandAdded,yrow,maxPSrow);
            end

            %Figure out whether the failing check is at the top or
            %bottom of the section
            for m = 1:length(colsC);

                if (colsC(m) == 1 | colsC(m) == 3);
                    Loc = 'Bot';
                else Loc = 'Top';
                end
```

Iteration 2

```
            %Add strands to the bottom row if the check which fails is
            %either the bottom of the section in tension or the top in
            %compression and set StrandAdded = 1.
            if StrandAdded == 0;
                if (strcmp(Loc,'Bot') & fMatMid(rowsC(m),colsC(m)) >= 0)...
                        | (strcmp(Loc,'Top') & fMatMid(rowsC(m),colsC(m)) < 0)
                    PSrow = AddPSBot(PSrow,maxPSrow);
                    PSdebond = AddPSBot(PSdebond,maxPSrow);
                    StrandAdded = 1;

                    %Otherwise if the failing check is the bottom in
                    %compression or the top in tension then add a strand
                    %to the top and set StrandAdded = 1.
                elseif (strcmp(Loc,'Bot') & fMatMid(rowsC(m),colsC(m)) < 0)...
                        | (strcmp(Loc,'Top') & fMatMid(rowsC(m),colsC(m)) >= 0)
                    PSrow = AddPSTop(PSrow,maxPSrow);
                    PSdebond = AddPSTop(PSdebond,maxPSrow);
                    StrandAdded = 1;
                end
            end
        end
        %Otherwise if there were no 'NG' values in the matrix then:
    elseif isempty(rowsC)

        %The prestress checks at the mid-span were okay
        CheckPSMid = 'OK';
    end

    %If a strand was not added in either of the previous checks
    %the support stresses, add strands to the correct location
    %depending on the check that fails.
    if isempty(rowsD) == 0;

        %If the limit was breached at the bottom of the section
        %(col 1 of CheckPSLossSup) in tension or at the top (col 2)
        %in compression then add strands to the bottom of the
        %section
        for m = 1:length(colsD);
            if StrandAdded == 0;
                if (colsD(m) == 1 & fMatSup(rowsD(m),colsD(m)) >= 0) | ...
                        (colsD(m) == 2 & fMatSup(rowsD(m),colsD(m)) < 0);
                    PSrow = AddPSBot(PSrow,maxPSrow);
                    PSdebond = AddPSBot(PSdebond,maxPSrow);
                    StrandAdded = 1;
                    StrandDebonded = 0;

                    %Otherwise if the limit was breached at the bottom in
                    %compression or at the top in tension, then
                    %debond strands from the bottom of the section
                    %and set StrandAdded = 1
```

Iteration 2

```
                elseif (colsD(m) == 1 & fMatSup(rowsD(m),colsD(m)) < 0 ) | ...
                        (colsD(m) == 2 & fMatSup(rowsD(m),colsD(m)) >= 0);
                    if DebondAgain == 0;
                        PSrow = AddPSTop(PSrow,maxPSrow);
                        PSdebond = PSrow;
                        NumDebonded = 0;
                        StrandAdded = 1;
                        DebondAgain = 1;
                        StrandDebonded = 0;
                    else
                        [PSdebond,NumDebonded,DebondCount,PSrow] = Debond↙
(PSdebond,NumDebonded,PSrow);
                        StrandDebonded = 1;
                        if isnan(DebondCount)
                            DebondAgain = 0;
                            StrandDebonded = 0;
                        end
                        break;
                    end
                end
            end
        end

        %Otherwise if there were no 'NG' values in the matrix then the
        %prestress checks at the support were okay
    elseif isempty(rowsD)
        CheckPSSup = 'OK';
    end

    %If strands were either added or debonded, check that there are
    %no "NaN" values in the PSrow array. If there are then print
    %this to the table and break out of the while-loop.
    if StrandAdded == 1;
        if isnan(PSrow(1));
            if k == 1;
                FinalTable(i,1:6) = [L,PSrow,NaN];
            elseif k == 2;
                FinalTable(i,7:12) = [L,PSrow,NaN];
            else
                FinalTable(i,13:18) = [L,PSrow,NaN];
            end
            break
        end
    end


    %Check the values of CheckSD, CheckPSMid, and CheckPSSup. If
    %all three are 'OK' then we can set CheckAll = 'OK' and break
    %the while-loop
    if CheckSD == 'OK' & CheckPSMid == 'OK' & CheckPSSup == 'OK'
        CheckAll = 'OK';
```

Iteration 2

```
                %Additionally if all of the checks are okay then we can write
                %the span length and prestressing information into a final
                %table and save this to a text file later
                if k == 1;
                    FinalTable(i,1:6) = [L,PSrow,NumDebonded];
                elseif k == 2;
                    FinalTable(i,7:12) = [L,PSrow,NumDebonded];
                else
                    FinalTable(i,13:18) = [L,PSrow,NumDebonded];
                end

            else CheckAll = 'NG';
            end
        end
    end
end

%Currently the matrix FinalTable is of type double. Convert this to a
%table, and then write it to a text file.
T = array2table(FinalTable);

%Change the headers in the final table to more meaningful headings
T.Properties.VariableNames = {'L_Small_ft','PSRow1_Small',...
    'PSRow2_Small','PSRow3_Small','PSRow4_Small','Debond_Small','L_Medium_ft',...
    'PSRow1_Medium','PSRow2_Medium','PSRow3_Medium','PSRow4_Medium','Debond_Medium',...
    'L_Large_ft','PSRow1_Large','PSRow2_Large','PSRow3_Large',...
    'PSRow4_Large','Debond_Large'};

%Change the units in the final table to meaningful units
T.Properties.VariableUnits = {'ft.','#','#','#','#','#','ft.','#','#','#'...
    ,'#','#','ft.','#','#','#','#','#'};

%Write the table to a text file
writetable(T,'PrelimDesign_WithDebonding&StrandGeometry1.txt');

end


%% Add prestressing strands to the bottom of the section
%Check whether you have reached the maximum number of strands in that row,
%if you haven't then add a strand to that row, if you have then move to the
%next row. If all rows have the maximum number of strands, assign "NaN" to
%the rows.

function [PSrow] = AddPSBot(PSrow,maxPSrow)

if PSrow(1) < maxPSrow(1)
    PSrow(1) = PSrow(1) + 1;
elseif PSrow(2) < maxPSrow(2);
    PSrow(2) = PSrow(2) + 1;
```

Iteration 2

```
elseif PSrow(3) < maxPSrow(3);
    PSrow(3) = PSrow(3) + 1;
else
    PSrow(1:length(PSrow)) = NaN;
end

end
%% Add prestressing strands to the top of the section
%Check whether you have reached the maximum number of strands in that row,
%if you haven't then add a strand to that row. If the row has the maximum
%number of strands, assign "NaN" to the rows.

function [PSrow] = AddPSTop(PSrow,maxPSrow)

if PSrow(4) < maxPSrow(4)
    if PSrow(4) == 0;
        PSrow(4) = PSrow(4) + 2;
    else
        PSrow(4) = PSrow(4) + 1;
    end
else
    PSrow(1:length(PSrow)) = NaN;
end

end
%% Debond strands from the bottom of the section
%This function debonds 2 strands from the lowest possible row in the
%cross-section (since this will have the greatest eccentricity hence the
%greatest effect on the flexural stresses).

function [PSdebond,NumDebonded,DebondCount,PSrow] = Debond(PSdebond,NumDebonded,PSrow)

%Check whether you have exceeded AASHTO's limit on the total number of
%debonded strands
DebondCount = NumDebonded + 2;

if DebondCount < (sum(PSrow) * 0.25)

    %If not, check whether you have debonded the max number of strands in
    %row 1 as per AASHTO's limits. If not then debond 2 strands, if you
    %have then move to the second row and so on.
    if  PSdebond(1) - 2 > 0.4*PSrow(1)
        PSdebond(1) = PSdebond(1) - 2;
        NumDebonded = NumDebonded + 2;
    elseif PSdebond(2) - 2 > 0.4*PSrow(2)
        PSdebond(2) = PSdebond(2) - 2;
        NumDebonded = NumDebonded + 2;
    elseif PSdebond(3) - 2 > 0.4*PSrow(3)
        PSdebond(3) = PSdebond(3) - 2;
        NumDebonded = NumDebonded + 2;
    else
```

Iteration 2

```
        %If you have debonded the maximum number of strands then set the
        %number debonded to NaN
        DebondCount = NaN;
    end

else
    %If you have debonded the maximum number of strands then set the
    %number debonded to NaN
    DebondCount = NaN;
end

end
%% Alter the strand geometry to try and get the required eccentricity for
%the stresses to work

function [PSrow,StrandAdded] = AlterStrandGeometry(PSrow,erequired,cgprecast,↙
StrandAdded,yrow,maxPSrow)

ecalculated = cgprecast - (sum(PSrow.*yrow))/(sum(PSrow));

while ecalculated > erequired
    if (PSrow(2) == 0) & (PSrow(1) - 2 >= PSrow(2) + 2) & ...
            (PSrow(2) + 2 < maxPSrow(2))
        if rem(PSrow(1),2) == 0;
            PSrow(2) = PSrow(2) + 2;
            PSrow(1) = PSrow(1) - 2;
            StrandAdded = 1;
        else
            PSrow(2) = PSrow(2) + 1;
            StrandAdded = 1;
            break;
        end
    elseif (PSrow(2) > 0) & (PSrow(1) - 2 >= PSrow(2) + 2) & ...
            (PSrow(2) + 2 < maxPSrow(2))
        PSrow(2) = PSrow(2) + 2;
        PSrow(1) = PSrow(1) - 2;
        StrandAdded = 1;
    elseif (PSrow(3) == 0) & (PSrow(1) - 2 < PSrow(2) + 2) & ...
            (PSrow(2) - 2 >= PSrow(3) + 2) & (PSrow(3) + 2 < maxPSrow(3))
        if rem(PSrow(2),2) == 0;
            PSrow(3) = PSrow(3) + 2;
            PSrow(2) = PSrow(2) - 2;
            StrandAdded = 1;
        else
            PSrow(3) = PSrow(3) + 1;
            StrandAdded = 1;
            break;
        end
    elseif (PSrow(3) > 0) & (PSrow(1) - 2 < PSrow(2) + 2) & ...
            (PSrow(2) - 2 >= PSrow(3) + 2) & (PSrow(3) + 2 < maxPSrow(3))
        PSrow(3) = PSrow(3) + 2;
```

Iteration 2

```
        PSrow(2) = PSrow(2) - 2;
        StrandAdded = 1;
    else
%         StrandAdded = 0;
        break
    end

    ecalculated = cgprecast - (sum(PSrow.*yrow))/(sum(PSrow));

end

end
```

Iteration 3

```
%THIS SCRIPT FILE AUTOMATES THE DESIGN CALCULATIONS FOR GIVEN SPAN LENGTH,
%SECTION SIZE, AND PRESTRESSING ARRANGEMENT. IT USES LIGHTWEIGHT CONCRETE.
%THE UNIT WEIGHTS OF CONCRETE CAN BE ALTERED IN LINES 16 AND 18.

%This function was updated to include the distribution factors for
%slab-type bridges as of 09/04/2016, by EAE. Lines 286 - 302

function [CheckPSLossSup,CheckPSLossMid,CheckDeflection,CheckStrength,...
    CheckShear,fMatSup,fMatMid] = InvertedT_DesignLW(Lpiertopier,PSrow,ShapeSize)

%% Inputs
% Materials
% Concrete
fc = 8;
fci = 5;
wc = 0.125;
fcdeck = 4;
wcdeck = 0.125;
K1 = 1.0;
% Steel
fy = 60;
Es = 29000;
fpu = 270;
Ep = 28500;
As = 0;
fs = 0;
Aprimes = 0;
fprimes = 0;
ds = 0;
dprimes = 0;
% Geometry
% Precast Concrete
if strcmp(ShapeSize,'SMALL')
    htotal = 8;
    wtotal = 72;
    hweb = 4;
    wweb = 39;
    hflange = 4;
    wflange = 12.5;
    hflangesloped = 0;
    wwebsloped = 4;
    Thetawebsloped = NaN;
    yrow = [2,4,0,6];
elseif strcmp(ShapeSize,'MEDIUM')
    htotal = 18;
    wtotal = 72;
    hweb = 14;
    wweb = 20;
    hflange = 4;
    wflange = 12.5;
    hflangesloped = 0;
```

Iteration 3

```
    wwebsloped = 13.5;
    Thetawebsloped = NaN;
    yrow = [2,4,6,16];
elseif strcmp(ShapeSize,'LARGE')
    htotal = 24;
    wtotal = 72;
    hweb = 18;
    wweb = 20;
    hflange = 6;
    wflange = 12;
    hflangesloped = 0;
    wwebsloped = 14;
    Thetawebsloped = NaN;
    yrow = [2,4,6,22];
else
    error('ShapeSize must be SMALL, MEDIUM, or LARGE')
end

% Deck CIP Concrete
tslab = 7.5;
% PS Strands
Astrand = 0.217;

% Bridge
H = 70;
% Geometry
Ng = 18;
Nl = 6;
Sg = 6;
Woverall = 114;
Wcurbtocurb = 110;
Nbarrier = 4;
Wmed = 16;
Wbarrierext = 1.3;
% Span
% Lpiertopier = 43;
% Lpiertopier = Linput;
Endclear = 0.5;
Loverall = Lpiertopier - Endclear;
Lpad = 12;
L = Loverall - Lpad/12;
% Loads
% Dead Loads
qfws = 0.025;
wbarrier = 0.3;
wmed = 0.15;
tmed = 0.75;
% Live Loads
%HL-93
wconLL = 0.12;
wlane = 0.64;
```

Iteration 3

```
% Construction
% Precast Concrete
tcure = 7;
ti = 1;
td = 90;
tf = 75*365;


%% Section Properties
% Non-Composite Section
% Gross
% Precast Concrete
if isnan(Thetawebsloped)
    Thetawebsloped = atan(hweb/wwebsloped)*180/pi();
end
if isnan(wwebsloped)
    wwebsloped = tan(Thetawebsloped*pi()/180);
end

wwebbottom = 2*wwebsloped + wweb;

PCxy = [0,0; wtotal,0; wtotal,hflange; wtotal-wflange,hflange+hflangesloped; ...
    wtotal-wflange-wwebsloped,htotal; wflange+wwebsloped,htotal; ...
    wflange,hflange+hflangesloped; 0,hflange; wflange,hflange; ...
    wtotal-wflange,hflange; wtotal-wflange-wwebsloped,hflange+hflangesloped; ...
    wflange+wwebsloped,hflange+hflangesloped];

PCshapes = [1,2,3,8; 8,9,7,NaN; 9,10,4,7; 10,3,4,NaN; 7,12,6,NaN; ...
    12,11,5,6; 11,4,5,NaN];

PCshapeprop = ShapeProp(PCshapes,PCxy,1);
Agprecast = sum(PCshapeprop(4,:));
cgprecast = sum(PCshapeprop(3,:).*PCshapeprop(4,:))/Agprecast;

PCshapeI = ShapeI(PCshapeprop,PCshapes,cgprecast);
Igprecast = sum(PCshapeI);
ytprecast = htotal-cgprecast;

% Deck CIP Concrete
Deckshapes = [1,9,8,NaN; 2,3,10,NaN; 8,9,14,7; 9,13,14,NaN; 10,11,12,NaN; ...
    10,3,4,11; 7,4,5,6];
Deckxy = [0,hflange; wtotal,hflange; wtotal,hflange+hflangesloped; ...
    wtotal,htotal; wtotal,htotal+tslab; 0,htotal+tslab; 0,htotal; ...
    0,hflange+hflangesloped; wflange,hflange+hflangesloped; ...
    wtotal-wflange,hflange+hflangesloped; wtotal-wflange,htotal; ...
    wtotal-wflange-wwebsloped, htotal; wflange+wwebsloped,htotal; ...
    wflange,htotal];

Deckshapeprop = ShapeProp(Deckshapes,Deckxy,2);
Agdeck = sum(Deckshapeprop(4,:));
```

Iteration 3

```
cgdeck = sum(Deckshapeprop(3,:).*Deckshapeprop(4,:))/Agdeck;
DeckshapeI = ShapeI(Deckshapeprop,Deckshapes,cgdeck);
Igdeck = sum(DeckshapeI);
egd = cgdeck - cgprecast;

% PS Steel
Apsrow = PSrow * Astrand;
Aps = sum(Apsrow);
cps = sum(Apsrow.*yrow)/Aps;
epg = cgprecast - cps;

% Transformed at Transfer
Eci = 33000*K1*wc^1.5*sqrt(fci);
npi = Ep/Eci;
Apstt = Aps*(npi-1);
Att = Agprecast+Apstt;
ctt = ((Agprecast*cgprecast)+(Apstt*cps))/Att;
Itt = Igprecast + Agprecast*(cgprecast-ctt)^2+Apstt*(cps-ctt)^2;
% Transformed at Service
Ec = 33000*K1*wc^1.5*sqrt(fc);
np = Ep/Ec;
Apsts = Aps*(np-1);
Ats = Agprecast+Apsts;
cts = ((Agprecast*cgprecast)+(Apsts*cps))/Ats;
Its = Igprecast + Agprecast*(cgprecast-cts)^2+Apsts*(cps-cts)^2;
epts = cts-cps;

% Composite Section
Ecdeck = 33000*K1*wcdeck^1.5*sqrt(fcdeck);
ndeck = Ecdeck/Ec;
Atrdeck = ndeck*Agdeck;
Itrdeck = ndeck*Igdeck;
Acomp = Agprecast + Atrdeck;
ccomp = ((Agprecast*cgprecast)+(Atrdeck*cgdeck))/Acomp;
Icomp = Igprecast + Agprecast*(cgprecast-ccomp)^2+Itrdeck+Atrdeck*...
    (cgdeck-ccomp)^2;
ecd = cgdeck - ccomp;
epc = ccomp - cps;
ytcomp = htotal - ccomp;

%% Loads
% Dead Loads
% PC Self Weight
wgprecast = Agprecast/(12^2)*wc;
Mgprecast = wgprecast*L^2/8;
% CIP Deck Self Weight
wgdeck = Agdeck/(12^2)*wcdeck;
Mgdeck = wgdeck*L^2/8;
% Dead Loads on Composite System
% FWS
wfwsg = qfws*(Wcurbtocurb/Ng);
```

Iteration 3

```
Mfws = wfwsg*L^2/8;
% Barrier
wbarrierg = wbarrier*Nbarrier/Ng;
Mbarrier = wbarrierg*L^2/8;
% Median
wmedg = wmed*tmed*Wmed/Ng;
Mmed = wmedg*L^2/8;
wsuperdead = wfwsg+wbarrierg+wmedg;
Msuperdead = Mfws+Mbarrier+Mmed;
DC = Mgprecast+Mgdeck+Mbarrier;
DW = Mfws;

% Live Load Distribution Factor
% Code Checks
if Ng > 4
    CheckLDF = 'OK';
else
    CheckLDF = 'NG';
end

% Beam-Slab Bridges
if and(20 <= L, L<=120)
    if and(5<=Ng, Ng<=20)
        CheckDFMint = 'OK';
    else
        CheckDFMint = 'NG';
    end
else
    CheckDFMint = 'NG';
end

Kg = ndeck^-1 * (Icomp+Acomp*ecd^2);
I_J = 0.54*(htotal/wtotal)+0.16;

% For Bending Moment in Interior Beams
% One Design Lane Loaded
kDFM = max(2.5*Ng^-0.2,1.5);
DFMintsingle = kDFM*(wtotal/(33.3*L))^0.5*(I_J)^0.25;
% Two or More Lanes Loaded
DFMintmulti = kDFM*(wtotal/305)^0.6*(wtotal/(12*L))^0.2*I_J^0.06;
DFMint = max(DFMintsingle,DFMintmulti);
% For Bending Moment in Exterior Beams
de = Wbarrierext;
if de <= 2
    CheckDFMext = 'OK';
else
    CheckDFMext = 'NG';
end
% One Design Lane Loaded
emsingle = max(1.125+de/30,1.0);
DFMextsingle = emsingle*DFMintsingle;
```

Iteration 3

```
% Two or More Lanes Loaded
emmulti = max(1.04+de/25,1);
DFMextmulti = emmulti*DFMintmulti;
DFMext = max(DFMextsingle,DFMextmulti);
% For Shear in Interior Beams
if and(20 <= L, L<=120)
    if and(5<=Ng, Ng<=20)
        CheckDFVint = 'OK';
    else
        CheckDFVint = 'NG';
    end
else
    CheckDFVint = 'NG';
end
% One Design Lane Loaded
DFVintsingle = (wtotal/(130*L))^0.15*I_J^0.05;
% Two or More Lanes Loaded
b_48 = max(wtotal/48,1);
DFVintmulti = (wtotal/156)^0.4*(wtotal/(12*L))^0.1*I_J^0.05*b_48;
DFVint = max(DFVintsingle,DFVintmulti);
% For Shear in Exterior Beams
if de <= 2
    CheckDFVext = 'OK';
else
    CheckDFVext = 'NG';
end
% One Design Lane Loaded
evsingle = max(1.25+de/20,1.0);
DFVextsingle = evsingle*DFVintsingle;
% Two or More Lanes Loaded
evmulti = max(1+((de+(wtotal/12)-2)/40)^0.5,1);
DFVextmulti = evmulti*DFVintmulti*b_48^-1;
DFVext = max(DFVextsingle,DFVextmulti);

%Equivalent Strip Widths for Slab-Type Bridges
%AASHTO Table 4.6.2.3-1 => Typical cross-section a (based on
%recommendations by Fatmir Menkalusi
L1 = min(L,60);
%One design lane loaded
W1single = min(Woverall,30);
Esingle = 10 + 5*sqrt(L1*W1single);
DFMslabsingle = wtotal/Esingle;
%Two or more design lanes loaded
W1multi = min(Woverall,60);
Emulti = min(84 + 1.44*sqrt(L1*W1multi), (12*Woverall)/Nl);
DFMslabmulti = wtotal/Emulti;

DFMslab = max(DFMslabsingle,DFMslabmulti);

% Live Loads
DFM = max([DFMslab,DFMint,DFMext]);
```

Iteration 3

```
DFV = max(DFVint,DFVext);
IM = 33;
MLL = wlane*L^2/8*DFM;
MLT = ((72*L/2*(L/2-4.67))/L-112)*DFM*(1+IM/100);

%% PS Losses
% Short Term Losses
% Elastic Shortening
fpy = 0.9*fpu;
fpo = 0.75*fpu;
Ppo = fpo*Aps;
fcgp = Ppo/Agprecast + Ppo*epg^2/Igprecast - Mgprecast*12*epg/Igprecast;
nps = Ep/Eci;
deltafpES = nps*fcgp;
fpi = max(fpo-deltafpES,0.55*fpy);
Pi = fpi*Aps;
% Long Term Losses
% Time of Transfer to Time of Deck Placement
% Shrinkage of Precast Girder
Perimeterprecast = wtotal + 2*hflange + 2*sqrt(hflangesloped^2+wflange^2) + ...
    2*sqrt(hweb^2+wwebsloped^2) + wweb;
VSprecast = Agprecast*(Loverall*12)/(Perimeterprecast*Loverall*12+2*Agprecast);
ks = max(1.45-0.13*VSprecast,1.0);
khs = 2-0.014*H;
kf = 5/(1+fci);
ktdid = (td-ti)/(61-4*fci+(td-ti));
ktdif = (tf-ti)/(61-4*fci+(tf-ti));
Epsilonbid = ks*khs*kf*ktdid*(0.48*10^-3);
khc = 1.56-0.008*H;
Psibif = 1.9*ks*khc*kf*ktdif*ti^-0.118;
Psibid = 1.9*ks*khc*kf*ktdid*ti^-0.118;
Kid = 1/(1+Ep/Eci*Aps/Agprecast*(1+Agprecast*epg^2/Igprecast)*(1+0.7*Psibif));
deltafpSR = Epsilonbid*Ep*Kid;
% Creep of Precast Girder
deltafpCR = Ep/Eci*fcgp*Psibid*Kid;
% Relaxation of PS Steel
Kl = 30;
deltafpR1 = (fpi/Kl)*(fpi/fpy-0.55);
% Time of Deck Placement to Final Time
ktddf = (tf-td)/(61-4*fci+(tf-td));
Epsilonbif = ks*khs*kf*ktdif*0.48*10^-3;
Epsilonbdf = Epsilonbif-Epsilonbid;
Kdf = 1/(1+(Ep/Eci)*(Aps/Acomp)*(1+Acomp*epc^2/Icomp)*(1+0.7*Psibif));
deltafpSD = Epsilonbdf*Ep*Kdf;
% Creep of Precast Concrete
deltafcd = -(deltafpSR+deltafpCR+deltafpR1)*(Aps/Agprecast)*(1+Agprecast* ...
    epg^2/Igprecast)-(12*Mgdeck*epts/Its+12*(Mbarrier+Mfws)*epc/Icomp);
Psibdf = 1.9*ks*khc*kf*ktddf*td^-0.118;
deltafpCD = Ep/Eci*fcgp*(Psibif-Psibid)*Kdf+Ep/Ec*deltafcd*Psibdf*Kdf;
% Relaxation of PS Steel
deltafpR2 = deltafpR1;
```

Iteration 3

```
% Shrinkage of Deck Concrete
fcideck = 0.8*fcdeck;
Perimeterdeck = wtotal;
VSdeck = Agdeck*Loverall*12/(Perimeterdeck*Loverall*12+2*Agdeck);
ksdeck = max(1.45-0.13*VSdeck,1);
kfdeck = 5/(1+fcideck);
ktddfdeck = (tf-td)/(61-4*fcideck+(tf-td));
Epsilonddf = ksdeck*khs*kfdeck*ktddfdeck*0.48*10^-3;
Psiddf = 1.9*ksdeck*khc*kfdeck*ktddfdeck*td^-0.118;
deltafcdf = Epsilonddf*Agdeck*Ecdeck/(1+0.7*Psiddf)*(1/Acomp-epc*ecd/Icomp);
deltafpSS = Ep/Ec*deltafcdf*Kdf*(1+0.7*Psibdf);
% Total PS Losses at Transfer
% Initial Loss
Lossinitial = 100*deltafpES/fpo;
% Time-Dependent PS Loss between time of transfer and deck placement
deltafpLTid = deltafpSR+deltafpCR+deltafpR1;
% Time-Dependent PS Loss after time of deck placement
deltafpLTdf = deltafpSD+deltafpCD+deltafpR2-deltafpSS;
% Total Time-Dependent PS Losses
deltafpLT = deltafpLTid+deltafpLTdf;
% Total PS Losses at Service
deltafpT = deltafpES+deltafpLT;
% Tendons after all losses
fpe = min(fpo-deltafpT,0.8*fpy);
Pe = fpe*Aps;
% Finall Loss
Lossfinal = 100*deltafpT/fpo;

%% Stress Limit State
% Allowable Stress
% Stresses at Transfer
% At Support
sigmaiCSup = -0.6*fci;
sigmaiTSup = min(0.0948*sqrt(fci),0.2);
% At Midspan
sigmaiCMid = -0.6*fci;
sigmaiTMid = min(0.0948*sqrt(fci),0.2);
% Stresses at Deck Placement
% At Support
sigmadCSup = -0.45*fc;
sigmadTSup = 0.19*sqrt(fc);
% At Midspan
sigmadCMid = -0.6*fc;
sigmadCMidSus = -0.45*fc;
sigmadTMid = 0.19*sqrt(fc);
% Stresses at Service
% At Support
sigmafCSup = -0.6*fc;
sigmafCSupSus = -0.45*fc;
sigmafTSup = 0.19*sqrt(fc);
% At Midspan
```

Iteration 3

```
sigmafCMid = -0.6*fc;
sigmafCMidSus = -0.45*fc;
sigmafTMid = 0.19*sqrt(fc);

% Calculated Stresses
% Stresses at Transfer
% At Support
ftiSup = -Pi/Agprecast+Pi*epg*ytprecast/Igprecast;
fbiSup = -Pi/Agprecast-Pi*epg*cgprecast/Igprecast;
% At Midspan
ftiMid = -Pi/Agprecast + Pi*epg*ytprecast/Igprecast - (Mgprecast*12*ytprecast)/...
    Igprecast;
fbiMid = -Pi/Agprecast - Pi*epg*cgprecast/Igprecast + (Mgprecast*12*cgprecast)/...
    Igprecast;
% Stresses at Deck Placement
MconLL = wconLL*L^2/8;
% At Support
ftdSup = -Pe/Agprecast + Pe*epg*ytprecast/Igprecast;
fbdSup = -Pe/Agprecast - Pe*epg*cgprecast/Igprecast;
% At Midspan
ftdMid = -Pe/Agprecast + Pe*epg*ytprecast/Igprecast - (Mgprecast+Mgdeck+MconLL)*...
    12*ytprecast/Igprecast;
ftdMidSus = -Pe/Agprecast + Pe*epg*ytprecast/Igprecast - (Mgprecast+Mgdeck)*...
    12*ytprecast/Igprecast;
fbdMid = -Pe/Agprecast - Pe*epg*cgprecast/Igprecast + (Mgprecast+Mgdeck+MconLL)*...
    12*cgprecast/Igprecast;
fbdMidSus = -Pe/Agprecast - Pe*epg*cgprecast/Igprecast + (Mgprecast+Mgdeck)*...
    12*cgprecast/Igprecast;
% Stresses at Service
ML = MLL+MLT;
% At Support
ftfSup = ftdSup;
fbfSup = fbdSup;
% At Midspan
ftfMid = -Pe/Agprecast + Pe*epg*ytprecast/Igprecast - (Mgprecast+Mgdeck)*12*...
    ytprecast/Igprecast - (Msuperdead+ML)*12*ytcomp/Icomp;
ftfMidSus = -Pe/Agprecast + Pe*epg*ytprecast/Igprecast - (Mgprecast+Mgdeck)*12*...
    ytprecast/Igprecast - (Msuperdead)*12*ytcomp/Icomp;
fbfMid = -Pe/Agprecast - Pe*epg*cgprecast/Igprecast + (Mgprecast+Mgdeck)*12*...
    cgprecast/Igprecast + (Msuperdead+ML)*12*ccomp/Icomp;
fbfMidSus = -Pe/Agprecast - Pe*epg*cgprecast/Igprecast + (Mgprecast+Mgdeck)*12*...
    cgprecast/Igprecast + (Msuperdead)*12*ccomp/Icomp;

% Stress Check
% Stresses at Transfer
% At Support
CheckbiSup = SC(fbiSup,sigmaiCSup,sigmaiTSup);
ChecktiSup = SC(ftiSup,sigmaiCSup,sigmaiTSup);
% At Midspan
CheckbiMid = SC(fbiMid,sigmaiCMid,sigmaiTMid);
ChecktiMid = SC(ftiMid,sigmaiCMid,sigmaiTMid);
```

Iteration 3

```
% Stresses at Deck Placement
% At Support
CheckbdSup = SC(fbdSup,sigmadCSup,sigmadTSup);
ChecktdSup = SC(ftdSup,sigmadCSup,sigmadTSup);
% At Midspan
CheckbdMid = SC(fbdMid,sigmadCMid,sigmadTMid);
ChecktdMid = SC(ftdMid,sigmadCMid,sigmadTMid);
CheckbdMidSus = SC(fbdMidSus,sigmadCMidSus,sigmadTMid);
ChecktdMidSus = SC(ftdMidSus,sigmadCMidSus,sigmadTMid);
% Stresses at Service
% At Support
CheckbfSup = SC(fbfSup,sigmafCSup,sigmafTSup);
ChecktfSup = SC(ftfSup,sigmafCSup,sigmafTSup);
% At Midspan
CheckbfMid = SC(fbfMid,sigmafCMid,sigmafTMid);
ChecktfMid = SC(ftfMid,sigmafCMid,sigmafTMid);
CheckbfMidSus = SC(fbfMidSus,sigmafCMidSus,sigmafTMid);
ChecktfMidSus = SC(ftfMidSus,sigmafCMidSus,sigmafTMid);

%% Deflection and Camber
% Deflections at Transfer
% Camber due to PS force
deltapi = -Pi/(Eci*Igprecast)*(epg*(L*12)^2/8);
% Deflection due to Precast Self Weight
deltagi = 5/384*(wgprecast/12)*(L*12)^4/(Eci*Igprecast);
% Total Deflections at Transfer
deltai = deltagi+deltapi;
% Deflections at Deck Placement
% Deflection due to CIP Deck Self Weight
deltadgdeck = 5/384*((wgdeck+wconLL)/12)*(L*12)^4/(Ec*Igprecast);
% Total Deflections at Deck Placement
deltad = deltai+deltadgdeck;
% Deflections at Service
% Deflections due to live loads at service
deltafLL = 5/384*(wlane*DFM/12)*(L*12)^4/(Ec*Icomp);
P = [32,32,8];
xaxel = [-14,0,14];
aaxel = L/2 + xaxel + 2.33;
for axel = 1:3
    deltaaxel(axel) = deltaeachaxel(P(axel),aaxel(axel),L,Ec,Icomp);
end
deltatruck = sum(deltaaxel);
deltafLT = deltatruck*DFM*(1+IM/100);
deltafL = max(deltafLT,0.25*deltafLT+deltafLL);
deltafLallow = L*12/800;
if deltafL <= deltafLallow
    CheckdeltafL = 'OK';
else
    CheckdeltafL = 'NG';
end
% Deflection due to superimposed dead loads at service
```

Iteration 3

```
deltafsuperdead = 5/384*(wsuperdead/12)*(L*12)^4/(Ec*Icomp);
% Total Deflections at Service
deltaf = deltad+deltafL+deltafsuperdead;

%% Strength Limit State
% Flexural Strength
Mupos = 1.25*DC + 1.5*DW + 1.75*ML;
if fpe >= 0.5*fpu
    Checkfpehalffpu = 'OK';
else
    Checkfpehalffpu = 'NG';
end
dp = htotal+tslab-cps;
k = 2*(1.04-fpy/fpu);
if fcdeck <= 4
    Beta1deck = 0.85;
elseif fcdeck >= 8
    Beta1deck = 0.65;
else
    Beta1deck = 0.85-0.05*(fcdeck-4);
end
c = (Aps*fpu+As*fs+Aprimes*fprimes)/(0.85*fcdeck*Beta1deck*wtotal+k*Aps*fpu/dp);
fps = fpu*(1-k*c/dp);
a = Aps*fps/(0.85*fcdeck*wtotal);
cNA = a/Beta1deck;
dt = htotal+tslab-yrow(1);
Epsilont = 0.003/cNA*(dt-cNA);
if Epsilont <= 0.002
    phif = 0.75;
elseif Epsilont >= 0.005
    phif = 1.0;
else
    phif = 0.65+0.15*(dt/cNA-1);
end
if a <= tslab
    b = wtotal;
else
    b = wweb;
end
hf = tslab;
Mn = (Aps*fps*(dp-a/2)+As*fs*(ds-a/2)-Aprimes*fprimes*(dprimes-a/2)+...
    0.85*fcdeck*(wtotal-b)*hf*(a/2-hf/2))/12;
Mr = phif*Mn;
if Mr >= Mupos
    CheckMrMupos = 'OK';
else
    CheckMrMupos = 'NG';
end
% Minimum Reinforcement
fr = 0.24*sqrt(fc);
fcpe = Pe/Agprecast + Pe*epg*cgprecast/Igprecast;
```

Iteration 3

```
Sc = Icomp/ccomp;
Snc = Igprecast/cgprecast;
Mdnc = Mgprecast + Mgdeck;
Mcr = max((Sc/12)*(fr+fcpe)-Mdnc*(Sc/Snc-1),Sc*fr/12);
Mmin = 1.2*Mcr;
if Mr >= min(Mmin,1.33*Mupos)
    CheckMpos = 'OK';
else
    CheckMpos = 'NG';
end

%% Shear Design
% Shear Strength
de = (Aps*fps*dp+As*fy*ds)/(Aps*fps+As*fy);
dv = max(de-a/2,max(0.9*de,0.72*(htotal+tslab)));
xvcritical = dv/12;
phiv = 0.9;
VLTcritical = 72*((L-xvcritical)-9.33)/L;
VLLcritical = wlane*(L-xvcritical)^2/(2*L);
VLcrit = VLTcritical*(1+IM/100)*DFV + VLLcritical*DFV;
Vgprecastcrit = wgprecast*(L-xvcritical)^2/(2*L);
Vgdeckcrit = wgdeck*(L-xvcritical)^2/(2*L);
Vsuperdeadcrit = wsuperdead*(L-xvcritical)^2/(2*L);
VDcrit = Vgprecastcrit+Vgdeckcrit+Vsuperdeadcrit;
Vucrit = 1.25*VDcrit+1.75*VLcrit;
Vp = 0;
Nu = 0;
MLTcritical = VLTcritical*xvcritical;
MLLcritical = wlane*xvcritical*(L-xvcritical)/2;
MLcritical = MLTcritical*(1+IM/100)*DFM+MLLcritical*DFM;
Mgprecastcritical = wgprecast*xvcritical*(L-xvcritical)/2;
Mgdeckcritical = wgdeck*xvcritical*(L-xvcritical)/2;
Msuperdeadcritical = wsuperdead*xvcritical*(L-xvcritical)/2;
MDcritical = Mgprecastcritical+Mgdeckcritical+Msuperdeadcritical;
Mucritical = 1.25*MDcritical+1.75*MLcritical;
bv = wtotal;
Mucrit = max(Mucritical,abs(Vucrit-Vp)*(dv/12))*12;
Act = bv*(htotal+tslab)/2;
Epsilons = (abs(Mucrit)/dv+0.5*Nu+abs(Vucrit-Vp)-Aps*fpo)/(Es*As+Ep*Aps);
if Epsilons < 0
    Epsilons = max((abs(Mucrit)/dv+0.5*Nu+abs(Vucrit-Vp)-Aps*fpo)/↙
(Es*As+Ep*Aps+Ec*Act),...
        -0.4*10^-3);
else
    Epsilons = min(Epsilons,6*10^-3);
end
sx = dv;
ag = 0.5;
sxe = min(max(sx*1.38/(ag+0.63),12),80);
Betav = 4.8/(1+750*Epsilons)*51/(39+sxe);
Thetav = 29+3500*Epsilons;
```

Iteration 3

```
Vc = 0.0316*Betav*sqrt(fcdeck)*bv*dv;
if Vucrit <= 0.5*phiv*(Vc+Vp)
    CheckVu = 'OK';
else
    CheckVu = 'NG';
end
Vs = 0;
% Longitudingal Reinforcement Shear Check
phic = 1;
if Aps*fps+As*fy >= abs(Mucrit)/(dv*phif)+0.5*Nu/phic+(abs(Vucrit/phiv-Vp)-...
        0.5*Vs)*cot(Thetav*pi()/180)
    CheckVLs = 'OK';
else
    CheckVLs = 'NG';
end
VLTsup = 72;
VLLsup = wlane*L/2;
VLsup = VLTsup*(1+IM/100)*DFV+VLLsup*DFV;
Vgprecastsup = wgprecast*L/2;
Vgdecksup = wgdeck*L/2;
Vsuperdeadsup = wsuperdead*L/2;
VDsup = Vgprecastsup+Vgdecksup+Vsuperdeadsup;
Vusup = 1.25*VDsup+1.75*VLsup;
if Aps*fps+As*fy >= (Vusup/phiv-Vp-0.5*Vs)*cot(Thetav*pi()/180)
    CheckVLssup = 'OK';
else
    CheckVLssup = 'NG';
end
%Interface Shear Design
bvi(1) = wtotal;
bvi(2) = 2*sqrt(hflangesloped^2+wflange^2)+2*sqrt(hweb^2+wwebsloped^2)+wweb;
Lvi = 12;
Acv = bvi*Lvi;
Vui = Vucrit/dv*12;
cv = 0.24;
muv = 1;
K1v = 0.25;
K2v = 1.5;
Avf = 0;
Pc = 0;
Vni(1,:) = cv*Acv+muv*(Avf*fy+Pc);
Vni(2,:) = K1v*fc*Acv;
Vni(3,:) = K2v*Acv;
Vni = min(min(Vni));
if Vni >= 1.33*Vui/phiv
    CheckAvf = 'OK';
    Avf = 0;
else
    CheckAvf = 'NG';
    Avf = max(0.05*Acv/fy);
end
```

Iteration 3

```
%% Summary of Checks
CheckPSLossSup = {CheckbiSup,ChecktiSup;CheckbdSup,ChecktdSup;CheckbfSup,...
    ChecktfSup};
CheckPSLossMid = {CheckbiMid,ChecktiMid,'OK','OK';...
    CheckbdMid,ChecktdMid,CheckbdMidSus,ChecktdMidSus;...
    CheckbfMid,ChecktfMid,CheckbfMidSus,ChecktfMidSus};
% CheckLLDF = [CheckLDF,CheckDFMint,CheckDFMext,CheckDFVint,CheckDFVext];
CheckDeflection = {CheckdeltafL};
CheckStrength = {Checkfpehalffpu,CheckMrMupos,CheckMpos};
CheckShear = {CheckVu,CheckVLs,CheckVLssup,CheckAvf};

% CheckPSLoss = {CheckbiSup,ChecktiSup,CheckbiMid,ChecktiMid,'OK','OK';...
%     CheckbdSup,ChecktdSup,CheckbdMid,ChecktdMid,CheckbdMidSus,ChecktdMidSus;...
%     CheckbfSup,ChecktfSup,CheckbfMid,ChecktfMid,CheckbfMidSus,ChecktfMidSus};

% Stresses
fMatSup = [fbiSup,ftiSup;fbdSup,ftdSup;fbfSup,ftfSup];
fMatMid = [fbiMid,ftiMid,NaN,NaN';fbdMid,ftdMid,fbdMidSus,ftdMidSus;...
    fbfMid,ftfMid,fbfMidSus,ftfMidSus];

% fMat = [fbiSup,ftiSup,fbiMid,ftiMid,NaN,NaN';...
%     fbdSup,ftdSup,fbdMid,ftdMid,fbdMidSus,ftdMidSus;...
%     fbfSup,ftfSup,fbfMid,ftfMid,fbfMidSus,ftfMidSus];

end




%% Shape Properties
function ShapeMatrix = ShapeProp(Nodes,XY,h1)

[rows,cols] = size(Nodes);

for i = 1:rows
    shape = 0;
    for j = 1:cols
        if isnan(Nodes(i,j)) == 0
            x(j) = XY(Nodes(i,j),1);
            y(j) = XY(Nodes(i,j),2);
        else
            shape = 1;
            x(j) = NaN;
            y(j) = NaN;
        end
    end
    b(i) = max(x) - min(x);
    h(i) = max(y) - min(y);
    if shape == 0
        cy(i) = min(y) + h(i)/2;
```

Iteration 3

```
        A(i) = b(i)*h(i);
    else
        cy(i) = min(y) + h(i)*h1/3;
        A(i) = 1/2*b(i)*h(i);
    end
end

ShapeMatrix = [b;h;cy;A];
end

%% Shape I
function Ishape = ShapeI(ShapeProp,Nodes,cg)

[rows,cols] = size(Nodes);

for i = 1:rows
    shape = 0;
    for j = 1:cols
        if isnan(Nodes(i,j))
            shape = 1;
        end
    end
    b = ShapeProp(1,:);
    h = ShapeProp(2,:);
    cy = ShapeProp(3,:);
    A = ShapeProp(4,:);

    if shape == 0
        Ishape(i) = (b(i)*h(i)^3)/12 + (cy(i)-cg)^2*A(i);
    else
        Ishape(i) = (b(i)*h(i)^3)/36 + (cy(i)-cg)^2*A(i);
    end
end
end

%% Stress Check
function Check = SC(f,sigmaC,sigmaT)

if f <= 0
    if abs(f) <= abs(sigmaC)
        Check = 'OK';
    else
        Check = 'NG';
    end
else
    if abs(f) <= abs(sigmaT)
        Check = 'OK';
    else
        Check = 'NG';
    end
end
```

Iteration 3

```
end

%% Deflection due to each truck axle
function delta = deltaeachaxel(P,a,L,Ec,Ic)

x = L/2;
b = L-a;
if x <= a
    delta = P*b*x/(6*Ec*Ic*L)*(L^2-b^2-x^2)*12^3;
else
    delta = P*b/(6*Ec*Ic*L)*((x-a)^3*L/b+(L^2-b^2)*x-x^3)*12^3;
end


end
```

APPENDIX B – DESIGN SPREADSHEETS FOR PRELIMINARY DESIGN TABLES

STAGED DECK POUR CALCULATION SPREADHSEETS

Notes on following spreadsheet pages

Yellow highlighted cells = User input values

Blue/green highlighted cells = Output/calculated values

No highlighting = Intermediate calculation/constant values

Plots of stresses along the length of the beam and allowable stresses along the length of the beam (Inputs & Results tab) automatically update when other tabs are filled out

Span Length

L	70	ft	This should theoretically be the clear span

Beam section properties

Ag	757	in2
cg	6.99	in
Ig	19220	in4
Perimeter	152	in

Calculated properties

yt	11.01	in

Beam material properties

f'c	8	ksi	Ec	5422.453	ksi
f'ci	5	ksi	Eci	4286.826	ksi
wc	0.15	kcf			
K1	1				

Deck section properties

Ad	1079	in2
cd	16.79	in
Id	37582	in2
Perimeter	115	in

Deck material properties

f'cd	4	ksi	f'cid	3.2	ksi
K1	1		Ec	3834.254	ksi
wcd	0.15	kcf	Eci	3429.461	ksi

Composite section properties

Ac	1519.9682	in2			
cgc	11.90924	in	yt	6.09076	in
Ic	82288.361	in4	For the purposes of stress calculations at the top of the precast section		
Perimeter	80	in			

Prestressing strand

fpu	270	ksi	fpy	243	ksi
Astrand	0.217	in2/strand			
Numps1	23		Aps1	4.991	in2
Numps2	21		Aps2	4.557	in2
Numps3	19		Aps3	4.123	in2
Numps4	0		Aps4	0	in2
yps1	2	in	SumAps	13.671	in2
yps2	4	in			
yps3	6	in	cgps	3.873016	in
yps4	16	in	e	3.116984	in
Es	28500	ksi	ec	8.036224	in

Debondedps1	0	Adebondps1	0
Debondedps2	0	Adebondps2	0
Debondedps3	0	Adebondps3	0
Debondedps4	0	Adebondps4	0
DebondLength	6 ft	SumAdebondps	0

Live load distribution factors & Impact factors

DFM 0.4348

IM 1.33 Applied to truck load only

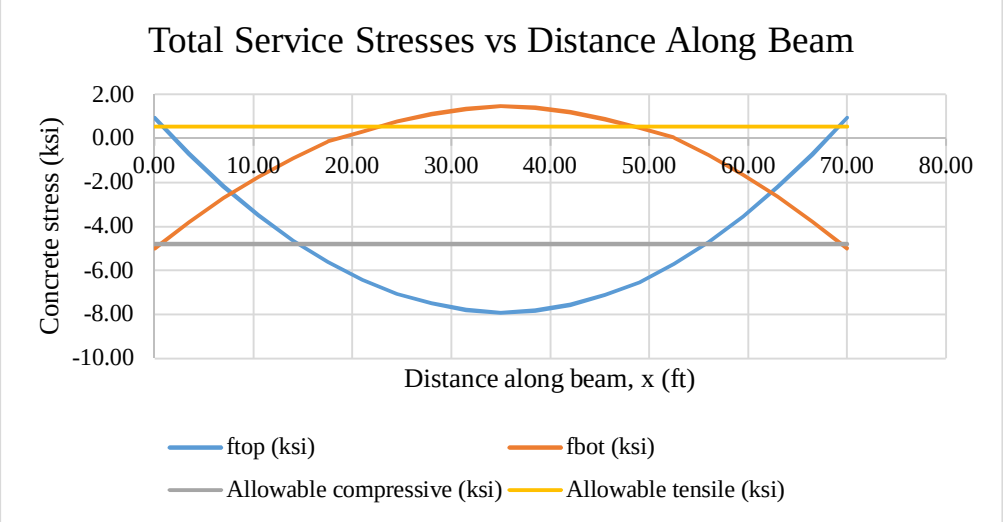

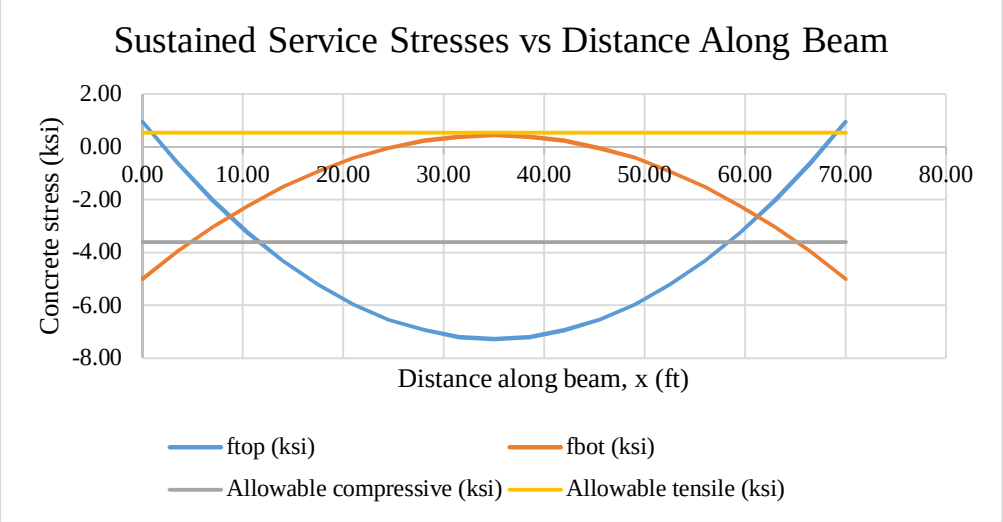

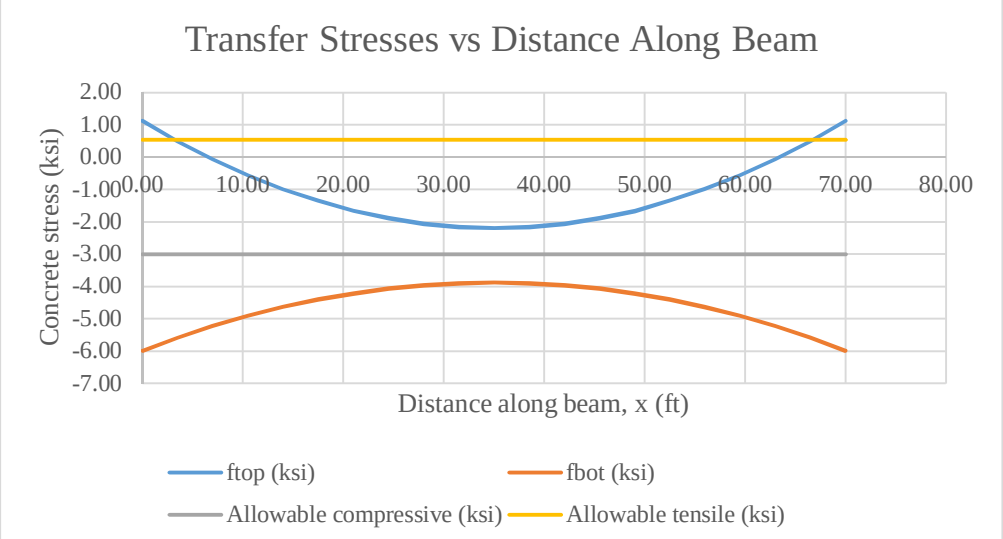

Load	**Beam SW**	**0.79**	**k/ft**
Distance along beam, x (ft)	Shear force (kips)	Bending moment (kip-ft)	Bending moment (in-k)
0	27.60	0.00	0.00
3.5	24.84	91.77	1101.20
7	22.08	173.87	2086.48
10.5	19.32	246.32	2955.85
14	16.56	309.11	3709.30
17.5	13.80	362.24	4346.84
21	11.04	405.70	4868.46
24.5	8.28	439.51	5274.16
28	5.52	463.66	5563.95
31.5	2.76	478.15	5737.82
35	0.00	482.98	5795.78
38.5	-2.76	478.15	5737.82
42	-5.52	463.66	5563.95
45.5	-8.28	439.51	5274.16
49	-11.04	405.70	4868.46
52.5	-13.80	362.24	4346.84
56	-16.56	309.11	3709.30
59.5	-19.32	246.32	2955.85
63	-22.08	173.87	2086.48
66.5	-24.84	91.77	1101.20
70	-27.60	0.00	0.00

Load	**Superimposed DL**	**0.32**	**k/ft**
Distance along beam, x (ft)	Shear force (kips)	Bending moment (kip-ft)	Bending moment (in-k)
0	11.2	0	0
3.5	10.08	37.24	446.88
7	8.96	70.56	846.72
10.5	7.84	99.96	1199.52
14	6.72	125.44	1505.28
17.5	5.6	147	1764
21	4.48	164.64	1975.68
24.5	3.36	178.36	2140.32
28	2.24	188.16	2257.92
31.5	1.12	194.04	2328.48
35	0	196	2352
38.5	-1.12	194.04	2328.48
42	-2.24	188.16	2257.92
45.5	-3.36	178.36	2140.32
49	-4.48	164.64	1975.68
52.5	-5.6	147	1764
56	-6.72	125.44	1505.28
59.5	-7.84	99.96	1199.52
63	-8.96	70.56	846.72
66.5	-10.08	37.24	446.88
70	-11.2	0	0

Load	**Live load UDL x DFM**	**0.278272**	**k/ft**
Distance along beam, x (ft)	Shear force (kips)	Bending moment (kip-ft)	Bending moment (in-k)
0	9.73952	0	0
3.5	8.765568	32.383904	388.606848
7	7.791616	61.358976	736.307712
10.5	6.817664	86.925216	1043.102592
14	5.843712	109.082624	1308.991488
17.5	4.86976	127.8312	1533.9744
21	3.895808	143.170944	1718.051328
24.5	2.921856	155.101856	1861.222272
28	1.947904	163.623936	1963.487232
31.5	0.973952	168.737184	2024.846208
35	0	170.4416	2045.2992
38.5	-0.973952	168.737184	2024.846208
42	-1.947904	163.623936	1963.487232
45.5	-2.921856	155.101856	1861.222272
49	-3.895808	143.170944	1718.051328
52.5	-4.86976	127.8312	1533.9744
56	-5.843712	109.082624	1308.991488
59.5	-6.817664	86.925216	1043.102592
63	-7.791616	61.358976	736.307712
66.5	-8.765568	32.383904	388.606848
70	-9.73952	0	0

Load	**Live load Truck x DFM x IM**	**Distance to center wheel "a"**	35	
Distance along beam, x (ft)	Shear force (kips)	Bending moment (kip-ft)	Bending moment (in-k)	Bending moment x DFM x IM
0	18.0424608	0	0	0
3.5	18.0424608	109.2	1310.4	757.7833536
7	18.0424608	218.4	2620.8	1515.566707
10.5	18.0424608	327.6	3931.2	2273.350061
14	18.0424608	436.8	5241.6	3031.133414
17.5	18.0424608	546	6552	3788.916768
21	13.4161888	655.2	7862.4	4546.700122
24.5	13.4161888	736.4	8836.8	5110.180051
28	13.4161888	817.6	9811.2	5673.659981
31.5	13.4161888	898.8	10785.6	6237.13991
35	-5.0888992	980	11760	6800.61984
38.5	-5.0888992	949.2	11390.4	6586.886074
42	-5.0888992	918.4	11020.8	6373.152307
45.5	-5.0888992	887.6	10651.2	6159.418541
49	-23.5939872	856.8	10281.6	5945.684774
52.5	-23.5939872	714	8568	4954.737312
56	-23.5939872	571.2	6854.4	3963.78985
59.5	-23.5939872	428.4	5140.8	2972.842387
63	-23.5939872	285.6	3427.2	1981.894925
66.5	-23.5939872	142.8	1713.6	990.9474624
70	-23.5939872	0	0	0

Axle 1	8	kips
Axle 2	32	kips
Axle 3	32	kips
Axle spacing 1-2	14	ft
Axle spacing 2-3	14	ft

Ra	31.2	kips
Rb	40.8	kips

Load	**Deck pour stage 1**	1.123958333	k/ft
Distance along beam, x (ft)	Shear force (kips)	Bending moment (kip-ft)	Bending moment (in-k)
0	39.34	0.00	0.00
3.5	35.40	130.80	1569.61
7	31.47	247.83	2973.99
10.5	27.54	351.10	4213.16
14	23.60	440.59	5287.10
17.5	19.67	516.32	6195.82
21	15.74	578.28	6939.32
24.5	11.80	626.47	7517.60
28	7.87	660.89	7930.65
31.5	3.93	681.54	8178.48
35	0.00	688.42	8261.09
38.5	-3.93	681.54	8178.48
42	-7.87	660.89	7930.65
45.5	-11.80	626.47	7517.60
49	-15.74	578.28	6939.32
52.5	-19.67	516.32	6195.82
56	-23.60	440.59	5287.10
59.5	-27.54	351.10	4213.16
63	-31.47	247.83	2973.99
66.5	-35.40	130.80	1569.61
70	-39.34	0.00	0.00

Length of pour, L1	70	ft
L2	0	ft

Ra	39.33854167	kips
Rb	39.33854167	kips

Load	**Deck pour stage 2**	1.123958333	k/ft
Distance along beam, x (ft)	Shear force (kips)	Bending moment (kip-ft)	Bending moment (in-k)
0	0.00	0.00	0.00
3.5	0.00	0.00	0.00
7	0.00	0.00	0.00
10.5	0.00	0.00	0.00
14	0.00	0.00	0.00
17.5	0.00	0.00	0.00
21	0.00	0.00	0.00
24.5	0.00	0.00	0.00
28	0.00	0.00	0.00
31.5	0.00	0.00	0.00
35	0.00	0.00	0.00
38.5	0.00	0.00	0.00
42	0.00	0.00	0.00
45.5	0.00	0.00	0.00
49	0.00	0.00	0.00
52.5	0.00	0.00	0.00
56	0.00	0.00	0.00
59.5	0.00	0.00	0.00
63	0.00	0.00	0.00
66.5	0.00	0.00	0.00
70	0.00	0.00	0.00

Ra	0
Rb	0

Load **Effective Prestress** Pe 2037.986799 kips

Distance along beam, x (ft)	Bending moment (in-k)
0	-6352.37
3.5	-6352.37
7	-6352.37
10.5	-6352.37
14	-6352.37
17.5	-6352.37
21	-6352.37
24.5	-6352.37
28	-6352.37
31.5	-6352.37
35	-6352.37
38.5	-6352.37
42	-6352.37
45.5	-6352.37
49	-6352.37
52.5	-6352.37
56	-6352.37
59.5	-6352.37
63	-6352.37
66.5	-6352.37
70	-6352.37

Load	Pedebond	2037.986799	kips

Distance along beam, x (ft)	Bending moment debonded (in-k)
0	-6352.372505
3.5	-6352.372505
7	-6352.372505
10.5	-6352.372505
14	-6352.372505
17.5	-6352.372505
21	-6352.372505
24.5	-6352.372505
28	-6352.372505
31.5	-6352.372505
35	-6352.372505
38.5	-6352.372505
42	-6352.372505
45.5	-6352.372505
49	-6352.372505
52.5	-6352.372505
56	-6352.372505
59.5	-6352.372505
63	-6352.372505
66.5	-6352.372505
70	-6352.372505

Load **Initial Prestress** Pi 2438.488838 kips

Distance along beam, x (ft)	Bending moment (in-k)
0	-7600.73
3.5	-7600.73
7	-7600.73
10.5	-7600.73
14	-7600.73
17.5	-7600.73
21	-7600.73
24.5	-7600.73
28	-7600.73
31.5	-7600.73
35	-7600.73
38.5	-7600.73
42	-7600.73
45.5	-7600.73
49	-7600.73
52.5	-7600.73
56	-7600.73
59.5	-7600.73
63	-7600.73
66.5	-7600.73
70	-7600.73

Load	Pidebond	2438.488838	kips

Distance along beam, x (ft)	Bending moment debonded (in-k)
0	-7600.731003
3.5	-7600.731003
7	-7600.731003
10.5	-7600.731003
14	-7600.731003
17.5	-7600.731003
21	-7600.731003
24.5	-7600.731003
28	-7600.731003
31.5	-7600.731003
35	-7600.731003
38.5	-7600.731003
42	-7600.731003
45.5	-7600.731003
49	-7600.731003
52.5	-7600.731003
56	-7600.731003
59.5	-7600.731003
63	-7600.731003
66.5	-7600.731003
70	-7600.731003

Calculate prestress forces as per AASHTO LRFD Refined Estimate Method

Note that for all loss calculations, compressive stress is taken positive while tensile stress is taken negative

fpo	202.5	ksi	Jacking stress
H	70	%	Relative humidity

Elastic shortening losses

fpi.trial	179	ksi	Iterate until fpi.trial = fpi
Pi	2447.109	kips	
fcpi	4.469639	ksi	Compressive
fg	0.939925	ksi	Tensile
fcgp	3.529714	ksi	Net
Deltafpi	23.466512	ksi	

fpi	179.03349	ksi

Beam shrinkage from transfer to deck placement

K.id 0.7408919

ΔfpSR	5.8980238	ksi

Beam creep from transfer to deck placement

ΔfpCR	18.84614	ksi

Relaxation from transfer to deck placement

K.L 30 For low-relaxation strands

ΔfpR1	1.114563	ksi

Beam shrinkage deck placement to final

K.df 0.7835506

ΔfpSD	2.8598833	ksi

Beam creep from deck placement to final

Δfcd -2.215123 ksi

ΔfpCD	0.6575376	ksi

Relaxation of prestressing strands from deck placement to final

ΔfpR2	1.114563	ksi

Shrinkage of deck concrete

Δfcdf -0.279049 ksi

ΔfpSS	-1.89705	ksi

ΔfpLT.id	25.858726	ksi
ΔfpLT.df	2.7349339	ksi
ΔfpLT	28.59366	ksi
fpe	150.43983	ksi

fpe/fpi	0.840289	
fpe/fpo	0.742913	Seems reasonable

-353.5146 kips
-0.645694 ksi
-1.569429 ksi

The above values of force and stress are negative because they indicate tensile stress changes or a reduction in the level of compression in the concrete

932.79682 1st half of Δfcdf
-0.000299 Second half (part in brackets) in Δfcdf

Beam Creep & Shrinkage Coefficients

ti	1	day	Time of release of initial loads
td	90	days	Time of deck placement
tf	27375	days	Final time - taken as 75 year service life

t.id	89		t.df	27285		t.if	27374
V	635880	in3					
Sid	127680	in2	Sdf	67200	in2	Sif	127680
						Majority of shrinkage/creep occurs before the section is composite	
ks.id	1		ks.df	1		ks.if	1
khc.id	1		khc.df	1		khc.df	1
kf.id	0.8333333		kf.df	0.8333333		kf.if	0.8333333
ktd.id	0.6846154		ktd.df	0.9984996		ktd.if	0.9985045
ψ(td,ti)	1.0839744		ψ(tf,td)	0.9296503		ψ(tf,ti)	1.5809654
khs.id	1.02		khs.id	1.02		khs.id	1.02
εsh.id	279E-06	με	εsh.df	128E-06	με	εsh.id	407E-06 με

Deck Creep & Shrinkage Coefficients

td	1	day	Deck loading applied when concrete is very young
tf	27285	days	75 years minus the age of the beam at deck placement

V	906360	in3
Sdf	96600	in2
t.df	27284	
ks.df	1	
khc.df	1	
kf.df	1.1904762	
ktd.df	0.9982365	
ψ(tf,td)	2.2579159	
khs.df	1.02	
εsh.ddf	582E-06	με

All service stresses (sustained + transient)

Distance along beam, x (ft)	ftop (ksi) Without 0.8 on LL	ftop (ksi) With 0.8 on LL
0.00	0.96	0.96
3.50	-0.69	-0.68
7.00	-2.17	-2.14
10.50	-3.49	-3.44
14.00	-4.63	-4.57
17.50	-5.61	-5.53
21.00	-6.42	-6.33
24.50	-7.05	-6.94
28.00	-7.51	-7.39
31.50	-7.80	-7.68
35.00	-7.93	-7.79
38.50	-7.83	-7.70
42.00	-7.56	-7.44
45.50	-7.12	-7.01
49.00	-6.52	-6.41
52.50	-5.69	-5.60
56.00	-4.70	-4.62
59.50	-3.54	-3.48
63.00	-2.21	-2.17
66.50	-0.71	-0.69
70.00	0.96	0.96

All service stresses (sustained + transient)

Distance along beam, x (ft)	fbot (ksi) Without 0.8 on LL	fbot (ksi) With 0.8 on LL
0.00	-5.05	-5.05
3.50	-3.85	-3.88
7.00	-2.76	-2.82
10.50	-1.79	-1.88
14.00	-0.93	-1.06
17.50	-0.19	-0.34
21.00	0.44	0.26
24.50	0.92	0.72
28.00	1.29	1.07
31.50	1.55	1.31
35.00	1.68	1.43
38.50	1.60	1.35
42.00	1.39	1.15
45.50	1.07	0.84
49.00	0.64	0.42
52.50	-0.02	-0.21
56.00	-0.80	-0.95
59.50	-1.69	-1.80
63.00	-2.69	-2.77
66.50	-3.81	-3.85
70.00	-5.05	-5.05

All service stresses (sustained + transient)

Distance along beam, x (ft)	ftop (ksi)	fbot (ksi)
0.00	0.96	-5.05
3.50	-0.69	-3.85
7.00	-2.17	-2.76
10.50	-3.49	-1.79
14.00	-4.63	-0.93
17.50	-5.61	-0.19
21.00	-6.42	0.26
24.50	-7.05	0.72
28.00	-7.51	1.07
31.50	-7.80	1.31
35.00	-7.93	1.43
38.50	-7.83	1.35
42.00	-7.56	1.15
45.50	-7.12	0.84
49.00	-6.52	0.42
52.50	-5.69	-0.02
56.00	-4.70	-0.80
59.50	-3.54	-1.69
63.00	-2.21	-2.69
66.50	-0.71	-3.81
70.00	0.96	-5.05

Sustained service stresses

Distance along beam, x (ft)	ftop (ksi)	fbot (ksi)
0.00	0.96	-5.05
3.50	-0.61	-4.01
7.00	-2.01	-3.09
10.50	-3.24	-2.27
14.00	-4.31	-1.56
17.50	-5.21	-0.96
21.00	-5.95	-0.47
24.50	-6.53	-0.09
28.00	-6.94	0.19
31.50	-7.19	0.35
35.00	-7.27	0.40
38.50	-7.19	0.35
42.00	-6.94	0.19
45.50	-6.53	-0.09
49.00	-5.95	-0.47
52.50	-5.21	-0.96
56.00	-4.31	-1.56
59.50	-3.24	-2.27
63.00	-2.01	-3.09
66.50	-0.61	-4.01
70.00	0.96	-5.05

All service stresses (sustained + transient)

Distance along beam, x (ft)	Allowable compressive (ksi)	Allowable tensile (ksi)
0.00	-4.80	0.54
3.50	-4.80	0.54
7.00	-4.80	0.54
10.50	-4.80	0.54
14.00	-4.80	0.54
17.50	-4.80	0.54
21.00	-4.80	0.54
24.50	-4.80	0.54
28.00	-4.80	0.54
31.50	-4.80	0.54
35.00	-4.80	0.54
38.50	-4.80	0.54
42.00	-4.80	0.54
45.50	-4.80	0.54
49.00	-4.80	0.54
52.50	-4.80	0.54
56.00	-4.80	0.54
59.50	-4.80	0.54
63.00	-4.80	0.54
66.50	-4.80	0.54
70.00	-4.80	0.54

Sustained service stresses

Distance along beam, x (ft)	Allowable compressive (ksi)	Allowable tensile (ksi)
0.00	-3.60	0.54
3.50	-3.60	0.54
7.00	-3.60	0.54
10.50	-3.60	0.54
14.00	-3.60	0.54
17.50	-3.60	0.54
21.00	-3.60	0.54
24.50	-3.60	0.54
28.00	-3.60	0.54
31.50	-3.60	0.54
35.00	-3.60	0.54
38.50	-3.60	0.54
42.00	-3.60	0.54
45.50	-3.60	0.54
49.00	-3.60	0.54
52.50	-3.60	0.54
56.00	-3.60	0.54
59.50	-3.60	0.54
63.00	-3.60	0.54
66.50	-3.60	0.54
70.00	-3.60	0.54

Stresses at transfer

Distance along beam, x (ft)	ftop (ksi)	fbot(ksi)	Allowable compressive (ksi)	Allowable tensile (ksi)
0.00	1.14	-6.01	-3.00	0.54
3.50	0.51	-5.61	-3.00	0.54
7.00	-0.06	-5.25	-3.00	0.54
10.50	-0.56	-4.93	-3.00	0.54
14.00	-0.99	-4.66	-3.00	0.54
17.50	-1.35	-4.43	-3.00	0.54
21.00	-1.65	-4.24	-3.00	0.54
24.50	-1.88	-4.09	-3.00	0.54
28.00	-2.05	-3.98	-3.00	0.54
31.50	-2.15	-3.92	-3.00	0.54
35.00	-2.18	-3.90	-3.00	0.54
38.50	-2.15	-3.92	-3.00	0.54
42.00	-2.05	-3.98	-3.00	0.54
45.50	-1.88	-4.09	-3.00	0.54
49.00	-1.65	-4.24	-3.00	0.54
52.50	-1.35	-4.43	-3.00	0.54
56.00	-0.99	-4.66	-3.00	0.54
59.50	-0.56	-4.93	-3.00	0.54
63.00	-0.06	-5.25	-3.00	0.54
66.50	0.51	-5.61	-3.00	0.54
70.00	1.14	-6.01	-3.00	0.54

Strength Checks

DL	=	Moment due to precast beam and cast-in-place topping self-weights
DW	=	Moment due to superimposed dead loads (barrier and future wearing surface)
ML	=	Moment due to live loads

	DL	SDL	L
M.mid (in-k)	14056.88	2352	8845.919
Load factor	1.25	1.5	1.75
Factored M (in-k)	17571.09375	3528	15480.358

Mu.mid (in-k) 36579.45207 in-k
3048.287673 k-ft

For low-lax strand	fpy/fpu	=	0.9	
	k	0.28		
Use strain compatibility as per the PCI BDM	Aps	13.671	in2	
	fpu	270	ksi	
	As	0	in2	Can add non-prestressed reinforcement for extra strength if needed
	fs	0	ksi	
	ds	0	in	
	A's	0	in2	
	f's	0	ksi	
	d's	0	in	
	dp	21.626984	in	
	f'cdeck	4	ksi	
	f'cbeam	8	ksi	
Guess for neutral axis depth	c	6.35	in	
	εps	0.0072175		
	fps	200.50543	ksi	
Guess for the average beta 1 value	β1trial	0.85		
	a	5.3975	in	
	Abeam,c	0	in2	β1deck 0.85
	Adeck,c	388.62	in2	β1beam 0.65
	β1calc	0.85		

a in beam	-2.1025	in	bw	20	in	bd (in.)	26
Ad1	388.62	in^2	yd1	2.69875	in		
Ad2	0	in^2	yd2	0	in		
Ad3	0	in^2	yd3	0	in		
Ad	388.62	in^2	yd	2.69875	in		
Ab1	0	in^2	yb1	0	in		
Ab2	0	in^2	yb2	0	in		
Ab	0	in^2	yb	0	in^2		

Check force equilibrium	T	2741.1097	kips
	Cb	0	kips
	Cd	1321.308	kips
T-Cb-Cd (should = 0)	=	1419.8017	kips

Calculate nominal moment capacity	Mn	25010.027	in-k
	phi	0.9	
	phi.Mn	22509.024	in-k
		1875.752	k-ft
Demand/Capacity Ratio		1.6251016	
		NG	

Vertical Deflection Checks

Note that negative deflections are downwards deflections, positive are upwards cambers

Prestressing	Pe	2447.566808	kips	M	7629.0269	in-k	E	5422.4533 ksi
	Ibeam	19220	in^4	L	840	in		
	Δp	6.456371704	in					
Beam self-weight	w	0.07	k/in	L	840	in	E	5422.4533 ksi
	Ibeam	19220	in^4				Ibeam	19220 in^4
	Δb	-4.087428035	in					
CIP Topping self-weight	w	0.093663194	k/in	L	840	in	E	5422.4533 ksi
	Icomp	82288.36128	in^4					
	ΔCIP	-5.826069814	in					
Superimposed DL	w	0.026666667	k/in	L	840	in	E	5422.4533 ksi
	Icomp	82288.36128	in^4					
	ΔSD	-0.387427479	in					
Live Load - UDL	w	0.023189333	k/in	L	840	in	E	5422.4533 ksi
	ΔL	-0.336906936	in					
Live Load - Truck	For a truck causing the maximum bending moment to occur at the center of the bridge							
	L	840	in	E	5422.4533	ksi	Icomp	82288.361 in4

i	Mi (in-k)	Li (in)	Ai (in2-k)	x,bi (in)	x,midi (in)
A	0				
1	4546.700122	252	572884.2153	672	252
2a	6800.61984	168	763845.6204	504	84
2b		168	189329.2563	476	56
3a	5945.684774	168	998875.0421	336	
3b		168	71814.54551	364	
B	1.05189E-12	252	749156.2816	168	

tB,A	3.020357204	in
tmid,A	0.491102502	in
Δmid	-1.0190761	in

Total Deflections	-5.200537	in	
LL deflections	-1.019076	in	AASHTO 3.6.1.3.2
Allowable deflections due to LL	1.05	in	**OK**

Checking the interface shear to find the minimum deck section that can be poured in stage 1

Need to ensure composite action when carrying out the stage 2 pour

Using the method presented in AASHTO 5.8.4

Assuming CIP concrete placed on clean surface roughened to 1/4 in amplitude

c	0.28	ksi	
μ	1		
K1	0.3		
K2	1.8	ksi	for normal weight concrete
	1.3	ksi	for lightweight concrete
bvi	20	in	Taken as the width of the web
Lvi	840	in	Length of the stage 1 deck pour
Acv	16800	in2	
Pc	78.677083	kips	Weight of the deck
Vni	4782.6771	kips	Nominal shear resistance
Vni max 1	20160	kips	Maximum allowed shear resistance
Vni max 2	30240	kips	Maximum allowed shear resistance
Vni	4782.6771	kips	
Vu	0.00	kips	
dv	12.916984	in	
vui	0	ksi	
Vui	0	kips	

I need composite action from the first deck pour, to resist the shears generated from the second deck pour (I assume the first deck pour is carried by the bare section, the second by the composite section)

dv taken from the centroid of the deck to the centroid of the prestressing steel

Demand/Capacity ratio
0 OK

Using the AASHTO alternative method provided in the commentary C5.8.4.2

Mu2	0.00	in-k
Mu1	0.00	in-k
V1	0.00	kips
Cu2	0	kips
C1	0	kips
Vh	0	kips

Demand/Capacity ratio
0 OK

TEMPORARY MIDSPAN SHORING CALCULATION SPREADSHEETS

Notes on the following spreadsheet tabs

Yellow highlighted cells = User input values

Blue/green highlighted cells = Output/calculated values

No highlighting = Intermediate calculations/constant values

Plots of stresses along length of beam and allowable stresses along length of beam (Inputs & Results tab) automatically update when other tabs are filled out

Span Length

L	68.5	ft	This should theoretically be the clear span

Beam section properties

Ag	757	in2			
cg	6.99	in	yt	11.01	in
Ig	19220	in4			
Perimeter	152	in			

Beam material properties

f'c	8	ksi	Ec	5422.453	ksi
f'ci	5	ksi	Eci	4286.826	ksi
wc	0.15	kcf			
K1	1				

Deck section properties

Ad	1079	in2			
cd	16.79	in			
Id	37582	in2			
Perimeter	115	in			

Deck material properties

f'cd	4	ksi	f'cid	3.2	ksi
K1	1		Ec	2916.815	ksi
wcd	0.125	kcf	Eci	2608.879	ksi

Composite section properties

Ac	1337.41	in2			
cgc	11.24301	in	yt	6.756992	in
Ic	70987.26	in4	For the purposes of stress calculations at the top of the precast section		
Perimeter	80	in			

Prestressing strand

fpu	270	ksi	fpy	243	ksi
Astrand	0.153	in2/strand			
Numps1	23		Aps1	3.519	in2
Numps2	21		Aps2	3.213	in2
Numps3	19		Aps3	2.907	in2
Numps4	3		Aps4	0.459	in2
yps1	2	in	SumAps	10.098	in2
yps2	4	in			
yps3	6	in	cgps	4.424242	in
yps4	16	in	e	2.565758	in
Es	28500	ksi	ec	6.818766	in

Debondedps1	9	Adebondps1	1.377	
Debondedps2	8	Adebondps2	1.224	
Debondedps3	7	Adebondps3	1.071	
Debondedps4	0	Adebondps4	0	
DebondLength	12 ft	SumAdebondps	3.672	

Live load distribution factors & Impact factors

DFM 0.4348

IM 1.33 Applied to truck load only

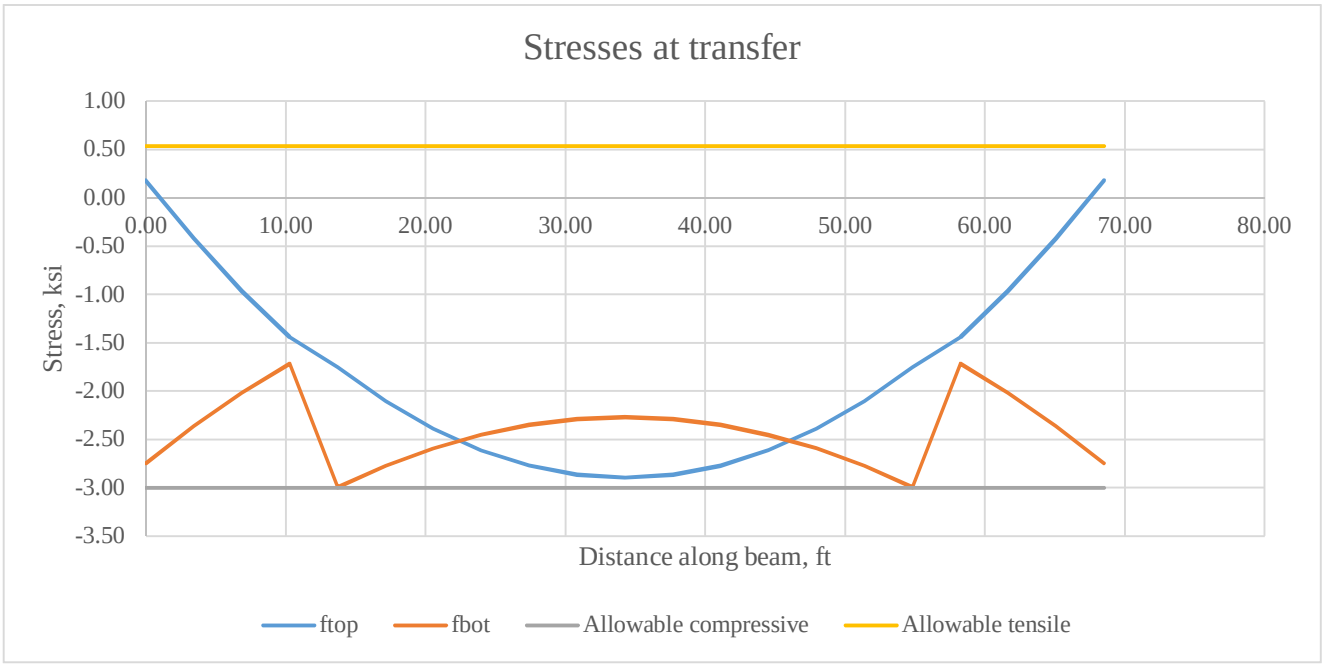

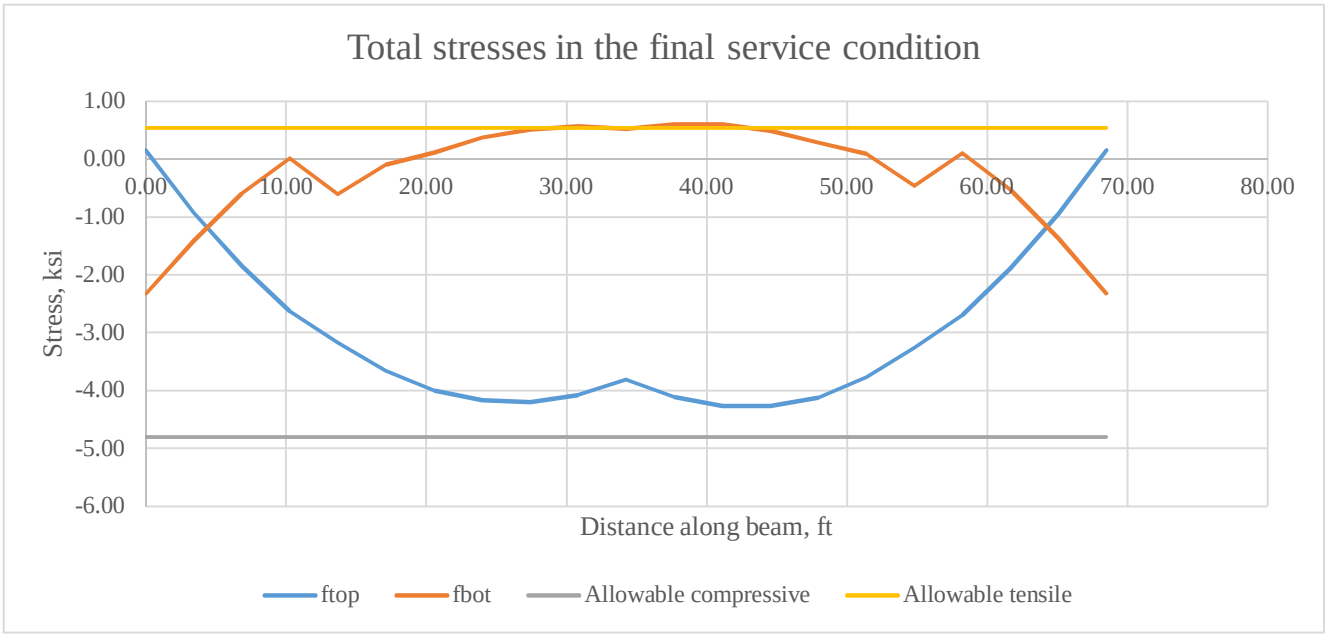

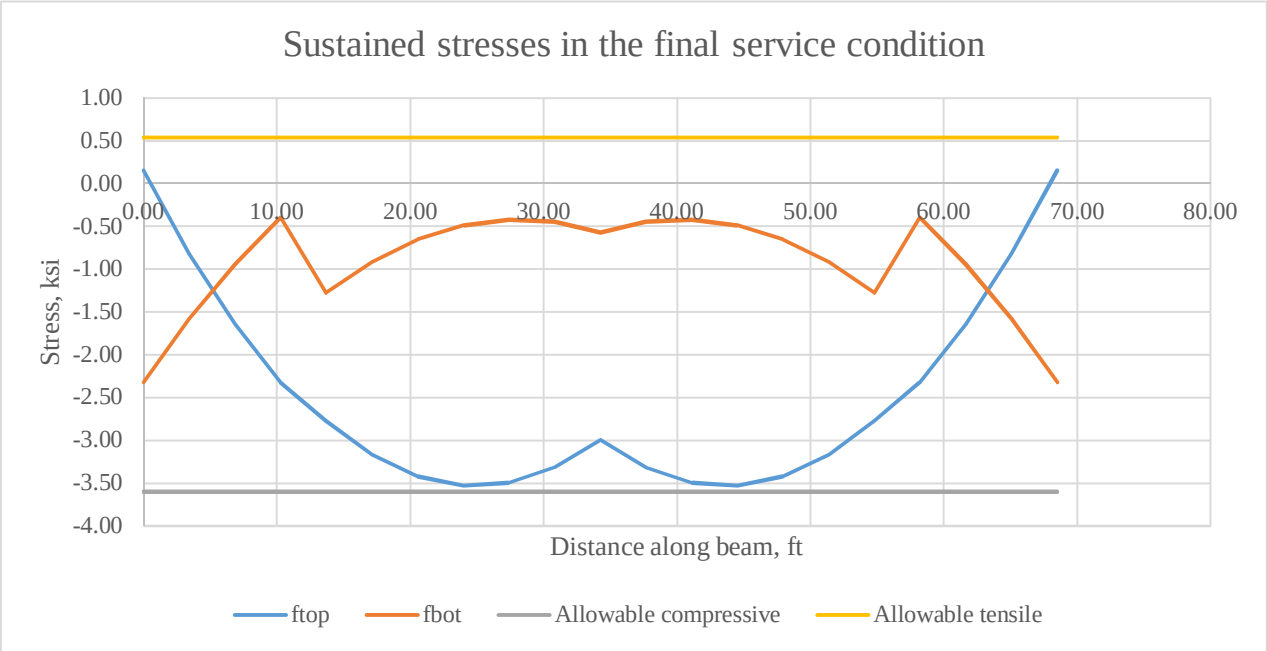
Sustained stresses in the final service condition
1.00
0.50
0.00
-0.50
-1.00
-1.50
-2.00
-2.50
-3.00
-3.50
-4.00
0.00
10.00
20.00
30.00
40.00
50.00
60.00
70.00
80.00
Stress, ksi
Distance along beam, ft
ftop
fbot
Allowable compressive
Allowable tensile

Calculate prestress forces as per AASHTO LRFD Refined Estimate Method

Note that for all calculations, compressive stress is taken positive while tensile stress is taken negative

fpo	202.5	ksi	Jacking stress
H	70	%	Relative humidity

Elastic shortening losses

fpi.trial	186	ksi	Iterate until fpi.trial = fpi
Pi	1878.228	kips	
fcpi	3.1244653	ksi	Compressive
fg	0.7408995	ksi	Tensile
fcgp	2.3835658	ksi	Net
Deltafpi	15.846603	ksi	

fpi	186.6534	ksi

Beam shrinkage from transfer to deck placement

K.id 0.8095386

ΔfpSR	6.4444999	ksi

Beam creep from transfer to deck placement

ΔfpCR	13.905696	ksi

Relaxation from transfer to deck placement

K.L 30 For low-relaxation strands

ΔfpR1	1.3571007	ksi

Beam shrinkage deck placement to final

K.df 0.8344571

ΔfpSD	3.0456869	ksi

Beam creep from deck placement to final

Δfcd -1.461031 ksi

ΔfpCD	0.6148036	ksi

Relaxation of prestressing strands from deck placement to final

ΔfpR2	1.3571007	ksi

Shrinkage of deck concrete

Δfcdf -0.137405 ksi

ΔfpSS	-0.994806	ksi

ΔfpLT.id	21.707297	ksi
ΔfpLT.df	4.0227856	ksi
ΔfpLT	25.730082	ksi
fpe	160.92331	ksi

fpe/fpi	0.8621505
fpe/fpo	0.794683

Seems reasonable

-219.2003 kips
-0.364644 ksi
-1.096388 ksi

The above values of force and stress are negative because they indicate tensile stress changes or a reduction in the level of compression in the concrete

709.60258
-0.000194 1st half of Δfcdf
Second half (part in brackets) in Δfcdf

Total stresses (sustained + transient)						
Stress checks	**Stresses due to effective prestress and self weight**		**Stresses due to deck placement (shored)**		**Stresses due to removal of shoring**	
Distance along beam, x (ft)	**ftop (ksi)**	**fbot (ksi)**	**ftop (ksi)**	**fbot (ksi)**	**ftop (ksi)**	**fbot (ksi)**
0.00	0.15	-2.33	0.00	0.00	0.00	0.00
3.43	-0.45	-1.95	-0.25	0.16	-0.08	0.13
6.85	-0.99	-1.60	-0.42	0.26	-0.16	0.26
10.28	-1.47	-1.30	-0.51	0.32	-0.24	0.39
13.70	-1.79	-2.37	-0.53	0.34	-0.31	0.52
17.13	-2.14	-2.15	-0.47	0.30	-0.39	0.65
20.55	-2.43	-1.97	-0.34	0.22	-0.47	0.78
23.98	-2.65	-1.83	-0.13	0.08	-0.55	0.91
27.40	-2.81	-1.73	0.15	-0.10	-0.63	1.04
30.83	-2.91	-1.66	0.51	-0.32	-0.71	1.17
34.25	-2.94	-1.64	0.94	-0.60	-0.78	1.31
34.25	-2.94	-1.64	0.94	-0.60	-0.78	1.31
37.68	-2.91	-1.66	0.51	-0.32	-0.71	1.17
41.10	-2.81	-1.73	0.15	-0.10	-0.63	1.04
44.53	-2.65	-1.83	-0.13	0.08	-0.55	0.91
47.95	-2.43	-1.97	-0.34	0.22	-0.47	0.78
51.38	-2.14	-2.15	-0.47	0.30	-0.39	0.65
54.80	-1.79	-2.37	-0.53	0.34	-0.31	0.52
58.23	-1.47	-1.30	-0.51	0.32	-0.24	0.39
61.65	-0.99	-1.60	-0.42	0.26	-0.16	0.26
65.08	-0.45	-1.95	-0.25	0.16	-0.08	0.13
68.50	0.15	-2.33	0.00	0.00	0.00	0.00

Total stresses (sustained + transient)			
Stresses due to additional superimposed DL and LL			
Distance along beam, x (ft)	**ftop (ksi) Without 0.8 on LL**	**ftop (ksi) With 0.8 on LL**	**fbot (ksi) Without 0.8 on LL**
0.00	0.00	0.00	0.00
3.43	-0.15	-0.13	0.24
6.85	-0.28	-0.24	0.47
10.28	-0.42	-0.35	0.69
13.70	-0.54	-0.46	0.90
17.13	-0.65	-0.55	1.09
20.55	-0.76	-0.64	1.26
23.98	-0.84	-0.71	1.39
27.40	-0.91	-0.77	1.51
30.83	-0.97	-0.82	1.62
34.25	-1.03	-0.87	1.71
34.25	-1.03	-0.87	1.71
37.68	-1.01	-0.85	1.67
41.10	-0.97	-0.82	1.62
44.53	-0.93	-0.79	1.55
47.95	-0.89	-0.74	1.47
51.38	-0.76	-0.64	1.27
54.80	-0.63	-0.53	1.04
58.23	-0.48	-0.41	0.80
61.65	-0.33	-0.28	0.55
65.08	-0.17	-0.14	0.28
68.50	0.00	0.00	0.00

Total stresses (sustained + transient)			
Final condition stresses			
Distance along beam, x (ft)	**fbot (ksi) With 0.8 on LL**	**ftop (ksi) Without 0.8 on LL**	**ftop (ksi) With 0.8 on LL**
0.00	0.00	0.15	0.15
3.43	0.21	-0.92	-0.90
6.85	0.41	-1.85	-1.81
10.28	0.59	-2.63	-2.57
13.70	0.76	-3.17	-3.09
17.13	0.92	-3.66	-3.56
20.55	1.07	-4.00	-3.88
23.98	1.18	-4.17	-4.04
27.40	1.28	-4.20	-4.06
30.83	1.37	-4.08	-3.92
34.25	1.44	-3.81	-3.64
34.25	1.44	-3.81	-3.64
37.68	1.41	-4.11	-3.95
41.10	1.36	-4.26	-4.11
44.53	1.31	-4.27	-4.12
47.95	1.24	-4.12	-3.98
51.38	1.07	-3.77	-3.65
54.80	0.88	-3.26	-3.16
58.23	0.68	-2.69	-2.62
61.65	0.46	-1.89	-1.84
65.08	0.24	-0.94	-0.92
68.50	0.00	0.15	0.15

Total stresses (sustained + transient)		
Final condition stresses		
Distance along beam, x (ft)	**fbot (ksi) Without 0.8 on LL**	**fbot (ksi) With 0.8 on LL**
0.00	-2.33	-2.33
3.43	-1.42	-1.45
6.85	-0.61	-0.67
10.28	0.10	0.00
13.70	-0.62	-0.75
17.13	-0.11	-0.28
20.55	0.29	0.10
23.98	0.56	0.35
27.40	0.74	0.50
30.83	0.81	0.55
34.25	0.78	0.50
34.25	0.78	0.50
37.68	0.86	0.60
41.10	0.84	0.59
44.53	0.73	0.48
47.95	0.50	0.27
51.38	0.07	-0.13
54.80	-0.47	-0.63
58.23	0.22	0.09
61.65	-0.53	-0.62
65.08	-1.38	-1.42
68.50	-2.33	-2.33

Total stresses (sustained + transient)				
Final condition stresses				
Distance along beam, x (ft)	**ftop (ksi)**	**fbot (ksi)**	**Allowable compressive (ksi)**	**Allowable tensile (ksi)**
0.00	0.15	-2.33	-4.80	0.54
3.43	-0.92	-1.42	-4.80	0.54
6.85	-1.85	-0.61	-4.80	0.54
10.28	-2.63	0.00	-4.80	0.54
13.70	-3.17	-0.62	-4.80	0.54
17.13	-3.66	-0.11	-4.80	0.54
20.55	-4.00	0.10	-4.80	0.54
23.98	-4.17	0.35	-4.80	0.54
27.40	-4.20	0.50	-4.80	0.54
30.83	-4.08	0.55	-4.80	0.54
34.25	-3.81	0.50	-4.80	0.54
34.25	-3.81	0.50	-4.80	0.54
37.68	-4.11	0.60	-4.80	0.54
41.10	-4.26	0.59	-4.80	0.54
44.53	-4.27	0.48	-4.80	0.54
47.95	-4.12	0.27	-4.80	0.54
51.38	-3.77	0.07	-4.80	0.54
54.80	-3.26	-0.47	-4.80	0.54
58.23	-2.69	0.09	-4.80	0.54
61.65	-1.89	-0.53	-4.80	0.54
65.08	-0.94	-1.38	-4.80	0.54
68.50	0.15	-2.33	-4.80	0.54

Sustained service stresses only						
Stress checks	**Stresses due to effective prestress and self weight**		**Stresses due to deck placement (shored)**		**Stresses due to removal of shoring**	
Distance along beam, x (ft)	**ftop (ksi)**	**fbot (ksi)**	**ftop (ksi)**	**fbot (ksi)**	**ftop (ksi)**	**fbot (ksi)**
0.00	0.15	-2.33	0.00	0.00	0.00	0.00
3.43	-0.45	-1.95	-0.25	0.16	-0.08	0.13
6.85	-0.99	-1.60	-0.42	0.26	-0.16	0.26
10.28	-1.47	-1.30	-0.51	0.32	-0.24	0.39
13.70	-1.79	-2.37	-0.53	0.34	-0.31	0.52
17.13	-2.14	-2.15	-0.47	0.30	-0.39	0.65
20.55	-2.43	-1.97	-0.34	0.22	-0.47	0.78
23.98	-2.65	-1.83	-0.13	0.08	-0.55	0.91
27.40	-2.81	-1.73	0.15	-0.10	-0.63	1.04
30.83	-2.91	-1.66	0.51	-0.32	-0.71	1.17
34.25	-2.94	-1.64	0.94	-0.60	-0.78	1.31
34.25	-2.94	-1.64	0.94	-0.60	-0.78	1.31
37.68	-2.91	-1.66	0.51	-0.32	-0.71	1.17
41.10	-2.81	-1.73	0.15	-0.10	-0.63	1.04
44.53	-2.65	-1.83	-0.13	0.08	-0.55	0.91
47.95	-2.43	-1.97	-0.34	0.22	-0.47	0.78
51.38	-2.14	-2.15	-0.47	0.30	-0.39	0.65
54.80	-1.79	-2.37	-0.53	0.34	-0.31	0.52
58.23	-1.47	-1.30	-0.51	0.32	-0.24	0.39
61.65	-0.99	-1.60	-0.42	0.26	-0.16	0.26
65.08	-0.45	-1.95	-0.25	0.16	-0.08	0.13
68.50	0.15	-2.33	0.00	0.00	0.00	0.00

Sustained service stresses only		
Stresses due to additional superimposed DL		
Distance along beam, x (ft)	**ftop (ksi)**	**fbot (ksi)**
0	0.00	0.00
3.425	-0.04	0.07
6.85	-0.08	0.13
10.275	-0.11	0.18
13.7	-0.14	0.23
17.125	-0.16	0.27
20.55	-0.18	0.30
23.975	-0.20	0.32
27.4	-0.21	0.34
30.825	-0.21	0.35
34.25	-0.21	0.36
34.25	-0.21	0.36
37.675	-0.21	0.35
41.1	-0.21	0.34
44.525	-0.20	0.32
47.95	-0.18	0.30
51.375	-0.16	0.27
54.8	-0.14	0.23
58.225	-0.11	0.18
61.65	-0.08	0.13
65.075	-0.04	0.07
68.5	0.00	0.00

Sustained service stresses only		
Final condition stresses		
Distance along beam, x (ft)	**ftop (ksi)**	**fbot (ksi)**
0.00	0.15	-2.33
3.43	-0.81	-1.59
6.85	-1.64	-0.95
10.28	-2.32	-0.40
13.70	-2.77	-1.29
17.13	-3.17	-0.93
20.55	-3.42	-0.67
23.98	-3.53	-0.50
27.40	-3.49	-0.43
30.83	-3.31	-0.46
34.25	-2.99	-0.58
34.25	-2.99	-0.58
37.68	-3.31	-0.46
41.10	-3.49	-0.43
44.53	-3.53	-0.50
47.95	-3.42	-0.67
51.38	-3.17	-0.93
54.80	-2.77	-1.29
58.23	-2.32	-0.40
61.65	-1.64	-0.95
65.08	-0.81	-1.59
68.50	0.15	-2.33

Sustained service stresses only		
Final condition stresses		
Distance along beam, x (ft)	**Allowable compressive (ksi)**	**Allowable tensile (ksi)**
0.00	-3.60	0.54
3.43	-3.60	0.54
6.85	-3.60	0.54
10.28	-3.60	0.54
13.70	-3.60	0.54
17.13	-3.60	0.54
20.55	-3.60	0.54
23.98	-3.60	0.54
27.40	-3.60	0.54
30.83	-3.60	0.54
34.25	-3.60	0.54
34.25	-3.60	0.54
37.68	-3.60	0.54
41.10	-3.60	0.54
44.53	-3.60	0.54
47.95	-3.60	0.54
51.38	-3.60	0.54
54.80	-3.60	0.54
58.23	-3.60	0.54
61.65	-3.60	0.54
65.08	-3.60	0.54
68.50	-3.60	0.54

Transfer Stresses

x (ft)	ftop (ksi)	fbot (ksi)	Allowable compressive (ksi)	Allowable tensile (ksi)
0.00	0.18	-2.69	-3.00	0.54
3.43	-0.43	-2.31	-3.00	0.54
6.85	-0.97	-1.96	-3.00	0.54
10.28	-1.44	-1.66	-3.00	0.54
13.70	-1.76	-2.94	-3.00	0.54
17.13	-2.11	-2.72	-3.00	0.54
20.55	-2.39	-2.54	-3.00	0.54
23.98	-2.61	-2.40	-3.00	0.54
27.40	-2.77	-2.30	-3.00	0.54
30.83	-2.87	-2.24	-3.00	0.54
34.25	-2.90	-2.22	-3.00	0.54
34.25	-2.90	-2.22	-3.00	0.54
37.68	-2.87	-2.24	-3.00	0.54
41.10	-2.77	-2.30	-3.00	0.54
44.53	-2.61	-2.40	-3.00	0.54
47.95	-2.39	-2.54	-3.00	0.54
51.38	-2.11	-2.72	-3.00	0.54
54.80	-1.76	-2.94	-3.00	0.54
58.23	-1.44	-1.66	-3.00	0.54
61.65	-0.97	-1.96	-3.00	0.54
65.08	-0.43	-2.31	-3.00	0.54
68.50	0.18	-2.69	-3.00	0.54

Check only at the final in-service stage for ultimate strengths and deflections - consider this to be the critical stage for preliminary design

DL	=	Moment due to precast beam and cast-in-place topping self-weights
DW	=	Moment due to superimposed dead loads (barrier and future wearing surface)
ML	=	Moment due to live loads

	DL	SDL	L
M.mid (in-k)	12142.42	2252.28	8571.84
Load factor	1.25	1.5	1.75
Factored M (in-k)	15178.02352	3378.42	15000.717

Mu.mid (in-k)	33557.16091	in-k
	2796.430076	k-ft

For low-lax strand	fpy/fpu	=	0.9		
	k		0.28		
Use strain compatibility as per the PCI BDM	Aps		10.098	in2	
	fpu		270	ksi	
	As		18	in2	Can add non-prestressed reinforcement for extra strength if needed
	fs		60	ksi	
	ds		23.5	in	
	A's		0	in2	
	f's		0	ksi	
	d's		0	in	
	dp		21.07575758	in	
	f'cdeck		4	ksi	
	f'cbeam		8	ksi	
Guess for neutral axis depth	c		9.92	in	
	εps		0.003373717		εs 0.0041069
	fps		96.14087313	ksi	
Guess for the average beta 1 value	β1trial		0.85		
	a		8.432	in	
	Abeam,c		19.47760171	in2	β1deck 0.85
	Adeck,c		564.232	in2	β1beam 0.65
	β1calc		0.837083544		

a in beam	0.932	in	bw	21.79742857	in
Ad1	540	in^2	yd1	3.75	in
Ad2	0	in^2	yd2	7.966	in
Ad3	24.232	in^2	yd3	7.810666667	in
Ad	564.232	in^2	yd	3.924392935	in
Ab1	18.64	in^2	yb1	7.966	in
Ab2	0.837601714	in^2	yb2	8.121333333	in
Ab	19.47760171	in^2	yb	7.97267985	in^2

Check force equilibrium	T	2050.830537	kips
	Cb	132.4476917	kips
	Cd	1918.3888	kips
T-Cb-Cd (should = 0)	=	-0.005954818	kips
Calculate nominal moment capacity	Mn	37256.64005	in-k

	phi	0.9	
	phi.Mn	33530.97604	in-k
		2794.248004	k-ft
Demand/Capacity Ratio		1.000780916	
		NG	

Vertical Deflection Checks

Note that negative deflections are downwards deflections, positive are upwards cambers

Prestressing	Pe	1625.003628	kips	M	4169.3654	in-k
	Δp	3.378892678	in			
	E	5422.453319	ksi	Ibeam	19220	in^4
Beam self-weight	w	0.07	k/in	L	822	in
	E	5422.453319	ksi	Ibeam	19220	in^4
	Δb	-3.748178328	in			
CIP Topping self-weight	w	0.078052662	k/in	L	822	in
	E	5422.453319	ksi	Ibeam	19220	in^4
	ΔCIP	-4.452096451	in			
Superimposed DL	w	0.026666667	k/in	L	822	in
	E	5422.453319	ksi	Icomp	70987.264	in^4
	ΔSD	-0.411830515	in			
Live Load - UDL	w	0.023189333	k/in	L	822	in
	E	5422.453319	ksi	Icomp	70987.264	in^4
	ΔL	-0.358127816	in			

Live Load - Truck: For a truck causing the maximum bending moment to occur at the center of the bridge

L	822	in	E	5422.4533	ksi
Icomp	70987.26396	in4			

i	Mi (in-k)	Li (in)	Ai (in2-k)	x,bi (in)	x,midi (in)
A	0				
1	4369.547672	243	530900.0422	660	249
2a	6613.255824	168	734084.009	495	84
2b		168	188471.4847	467	56
3a	5748.109192	168	965682.3442	327	
3b		168	72672.31712	355	
B	2.10378E-12	243	698395.2668	162	

tB,A	3.264267636	in
tmid,A	0.531042421	in
Δmid	-1.101091397	in

Total Deflections	-6.692431828	in	
LL deflections	-1.101091397	in	AASHTO 3.6.1.3.2
Allowable deflections due to LL	1.0275	in	NG

Load	**Beam SW**	**0.79 k/ft**	
Distance along beam, x (ft)	Shear force (kips)	Bending moment (kip-ft)	Bending moment (in-k)
0	27.01	0.00	0.00
3.425	24.31	87.88	1054.51
6.85	21.61	166.50	1998.02
10.275	18.91	235.88	2830.53
13.7	16.20	296.00	3552.03
17.125	13.50	346.88	4162.54
20.55	10.80	388.50	4662.04
23.975	8.10	420.88	5050.55
27.4	5.40	444.00	5328.05
30.825	2.70	457.88	5494.55
34.25	0.00	462.50	5550.05
34.25	0.00	462.50	5550.05
37.675	-2.70	457.88	5494.55
41.1	-5.40	444.00	5328.05
44.525	-8.10	420.88	5050.55
47.95	-10.80	388.50	4662.04
51.375	-13.50	346.88	4162.54
54.8	-16.20	296.00	3552.03
58.225	-18.91	235.88	2830.53
61.65	-21.61	166.50	1998.02
65.075	-24.31	87.88	1054.51
68.5	-27.01	0.00	0.00

Load	**Superimposed DL**	**0.32 k/ft**	
Distance along beam, x (ft)	Shear force (kips)	Bending moment (kip-ft)	Bending moment (in-k)
0	10.96	0	0
3.425	9.864	35.6611	427.9332
6.85	8.768	67.5684	810.8208
10.275	7.672	95.7219	1148.6628
13.7	6.576	120.1216	1441.4592
17.125	5.48	140.7675	1689.21
20.55	4.384	157.6596	1891.9152
23.975	3.288	170.7979	2049.5748
27.4	2.192	180.1824	2162.1888
30.825	1.096	185.8131	2229.7572
34.25	0	187.69	2252.28
34.25	0	187.69	2252.28
37.675	-1.096	185.8131	2229.7572
41.1	-2.192	180.1824	2162.1888
44.525	-3.288	170.7979	2049.5748
47.95	-4.384	157.6596	1891.9152
51.375	-5.48	140.7675	1689.21
54.8	-6.576	120.1216	1441.4592
58.225	-7.672	95.7219	1148.6628
61.65	-8.768	67.5684	810.8208
65.075	-9.864	35.6611	427.9332
68.5	-10.96	0	0

Load	**Live load UDL x DFM**	**0.278272 k/ft**	
Distance along beam, x (ft)	Shear force (kips)	Bending moment (kip-ft)	Bending moment (in-k)
0	9.530816	0	0
3.425	8.5777344	31.01089256	372.1307107
6.85	7.6246528	58.75748064	705.0897677
10.275	6.6715712	83.23976424	998.8771709
13.7	5.7184896	104.4577434	1253.49292
17.125	4.765408	122.411418	1468.937016
20.55	3.8123264	137.1007882	1645.209458
23.975	2.8592448	148.5258538	1782.310246
27.4	1.9061632	156.686615	1880.23938
30.825	0.9530816	161.5830718	1938.996861
34.25	0	163.215224	1958.582688
34.25	0	163.215224	1958.582688
37.675	-0.9530816	161.5830718	1938.996861
41.1	-1.9061632	156.686615	1880.23938
44.525	-2.8592448	148.5258538	1782.310246
47.95	-3.8123264	137.1007882	1645.209458
51.375	-4.765408	122.411418	1468.937016
54.8	-5.7184896	104.4577434	1253.49292
58.225	-6.6715712	83.23976424	998.8771709
61.65	-7.6246528	58.75748064	705.0897677
65.075	-8.5777344	31.01089256	372.1307107
68.5	-9.530816	0	0

Load	**Live load Truck x DFM x IM**	**Distance to center wheel "a"**	34.25
Distance along beam, x (ft)	Shear force (kips)	Full Bending moment (kip-ft)	Bending moment (in-k)
0	17.98	0.00	0.00
3.425	17.98	106.50	739.05
6.85	17.98	213.00	1478.09
10.275	17.98	319.50	2217.14
13.7	17.98	426.00	2956.19
17.125	17.98	532.50	3695.23
20.55	13.36	636.60	4417.63
23.975	13.36	715.70	4966.53
27.4	13.36	794.80	5515.44
30.825	13.36	873.90	6064.35
34.25	-5.15	953.00	6613.26
34.25	-5.15	953.00	6613.26
37.675	-5.15	922.50	6401.60
41.1	-5.15	892.00	6189.95
44.525	-5.15	861.50	5978.30
47.95	-5.15	831.00	5766.65
51.375	-23.65	700.50	4861.06
54.8	-23.65	560.40	3888.84
58.225	-23.65	420.30	2916.63
61.65	-23.65	280.20	1944.42
65.075	-23.65	140.10	972.21
68.5	-23.65	0.00	0.00

Axle 1	8	kips
Axle 2	32	kips
Axle 3	32	kips
Axle spacing 1-2	14	ft
Axle spacing 2-3	14	ft

Ra	31.09489051	kips
Rb	40.90510949	kips

Deck pour stage 1	0.936631944	k/ft
Shear force (kips)	Bending moment (kip-ft)	Bending moment (in-k)
32.08	0.00	0.00
28.87	104.38	1252.55
25.66	197.77	2373.25
22.46	280.18	3362.11
19.25	351.59	4219.11
16.04	412.02	4944.28
12.83	461.47	5537.59
9.62	499.92	5999.05
6.42	527.39	6328.67
3.21	543.87	6526.44
0.00	549.36	6592.37
0.00	549.36	6592.37
-3.21	543.87	6526.44
-6.42	527.39	6328.67
-9.62	499.92	5999.05
-12.83	461.47	5537.59
-16.04	412.02	4944.28
-19.25	351.59	4219.11
-22.46	280.18	3362.11
-25.66	197.77	2373.25
-28.87	104.38	1252.55
-32.08	0.00	0.00
Length of pour, L1	68.5	ft
L2	0	ft
		NOT USED IN THIS SPREA
Ra	32.0796441	kips
Rb	32.0796441	kips

Deck pour stage 2	0.936631944	k/ft
Shear force (kips)	Bending moment (kip-ft)	Bending moment (in-k)
0.00	0.00	0.00
0.00	0.00	0.00
0.00	0.00	0.00
0.00	0.00	0.00
0.00	0.00	0.00
0.00	0.00	0.00
0.00	0.00	0.00
0.00	0.00	0.00
0.00	0.00	0.00
0.00	0.00	0.00
0.00	0.00	0.00
0.00	0.00	0.00
0.00	0.00	0.00
0.00	0.00	0.00
0.00	0.00	0.00
0.00	0.00	0.00
0.00	0.00	0.00
0.00	0.00	0.00
0.00	0.00	0.00
0.00	0.00	0.00
0.00	0.00	0.00
0.00	0.00	0.00

DSHEET

Ra	0	
Rb	0	

Load	**Effective Prestress**	Pe	1625.0036	kips
Distance along beam, x (ft)	Bending moment (in-k)			
0	-4169.37			
3.425	-4169.37			
6.85	-4169.37			
10.275	-4169.37			
13.7	-4169.37			
17.125	-4169.37			
20.55	-4169.37			
23.975	-4169.37			
27.4	-4169.37			
30.825	-4169.37			
34.25	-4169.37			
34.25	-4169.37			
37.675	-4169.37			
41.1	-4169.37			
44.525	-4169.37			
47.95	-4169.37			
51.375	-4169.37			
54.8	-4169.37			
58.225	-4169.37			
61.65	-4169.37			
65.075	-4169.37			
68.5	-4169.37			

Load	**Initial Prestress**	Pi	1878.228	kips
Distance along beam, x (ft)	Bending moment (in-k)			
0	-4819.08			
3.425	-4819.08			
6.85	-4819.08			
10.275	-4819.08			
13.7	-4819.08			
17.125	-4819.08			
20.55	-4819.08			
23.975	-4819.08			
27.4	-4819.08			
30.825	-4819.08			
34.25	-4819.08			
34.25	-4819.08			
37.675	-4819.08			
41.1	-4819.08			
44.525	-4819.08			
47.95	-4819.08			
51.375	-4819.08			
54.8	-4819.08			
58.225	-4819.08			
61.65	-4819.08			
65.075	-4819.08			
68.5	-4819.08			

Load	**Removal of shores**	R.shore	40.09955512 kips
Distance along beam, x (ft)	Shear force (kips)	Bending moment (kip-ft)	Bending moment (in-k)
0	20.05	0.00	0.00
3.425	20.05	68.67	824.05
6.85	20.05	137.34	1648.09
10.275	20.05	206.01	2472.14
13.7	20.05	274.68	3296.18
17.125	20.05	343.35	4120.23
20.55	20.05	412.02	4944.28
23.975	20.05	480.69	5768.32
27.4	20.05	549.36	6592.37
30.825	20.05	618.03	7416.41
34.25	-20.05	686.70	8240.46
34.25	-20.05	686.70	8240.46
37.675	-20.05	618.03	7416.41
41.1	-20.05	549.36	6592.37
44.525	-20.05	480.69	5768.32
47.95	-20.05	412.02	4944.28
51.375	-20.05	343.35	4120.23
54.8	-20.05	274.68	3296.18
58.225	-20.05	206.01	2472.14
61.65	-20.05	137.34	1648.09
65.075	-20.05	68.67	824.05
68.5	-20.05	0.00	0.00

Ra	20.05	kips
Rb	20.05	kips

Load	**Deck SW**	**0.94**	**k/ft**
Distance along beam, x (ft)	Shear forces (kips)	Bending moments (k-ft)	Bending moments (k-in)
0.00	12.03	0.00	0.00
3.43	8.82	35.71	428.50
6.85	5.61	60.43	725.16
10.28	2.41	74.16	889.97
13.70	-0.80	76.91	922.93
17.13	-4.01	68.67	824.05
20.55	-7.22	49.44	593.31
23.98	-10.43	19.23	230.73
27.40	-13.63	-21.97	-263.69
30.83	-16.84	-74.16	-889.97
34.25	-20.05	-137.34	-1648.09
34.25	20.05	-137.34	-1648.09
37.68	16.84	-74.16	-889.97
41.10	13.63	-21.97	-263.69
44.53	10.43	19.23	230.73
47.95	7.22	49.44	593.31
51.38	4.01	68.67	824.05
54.80	0.80	76.91	922.93
58.23	-2.41	74.16	889.97
61.65	-5.61	60.43	725.16
65.08	-8.82	35.71	428.50
68.50	-12.03	0.00	0.00

Ra	12.02986654
Rb	40.09955512
Rc	12.02986654
Check ΣFv	0
Check ΣM(a)	0

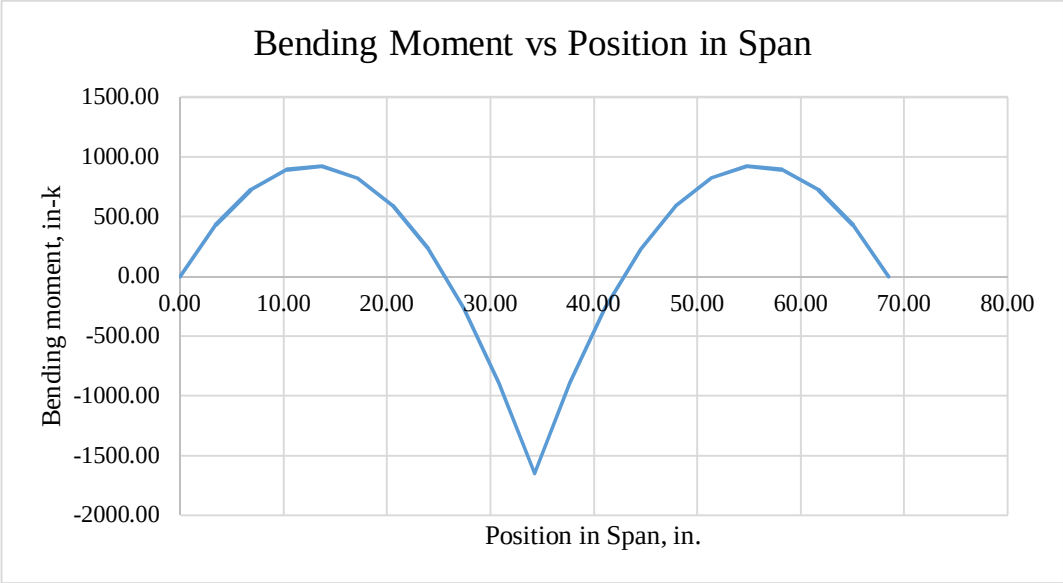
Bending Moment vs Position in Span
1500.00
1000.00
500.00
0.00
-500.00
-1000.00
-1500.00
-2000.00
Bending moment, in-k
0.00
10.00
20.00
30.00
40.00
50.00
60.00
70.00
80.00
Position in Span, in.

Beam Creep & Shrinkage Coefficients

ti	1	day	Time of release of initial loads
td	90	days	Time of deck placement
tf	27375	days	Final time - taken as 75 year service life

t.id	89		t.df	27285		t.if	27374
V	622254	in3					
Sid	124944	in2	Sdf	65760	in2	Sif	124944
						Majority of shrinkage/creep occurs before the section is composite	
ks.id	1		ks.df	1		ks.if	1
khc.id	1		khc.df	1		khc.df	1
kf.id	0.8333333		kf.df	0.8333333		kf.if	0.8333333
ktd.id	0.6846154		ktd.df	0.9984996		ktd.if	0.9985045
ψ(td,ti)	1.0839744		ψ(tf,td)	0.9296503		ψ(tf,ti)	1.5809654
khs.id	1.02		khs.id	1.02		khs.id	1.02
εsh.id	279E-06	με	εsh.df	128E-06	με	εsh.id	407E-06 με

Deck Creep & Shrinkage Coefficients

td	1	day	The loads being applied to the deck are being applied when the deck concrete is very young
tf	27285	days	75 years minus the age of the beam at deck placement
V	886938	in3	
Sdf	94530	in2	
t.df	27284		
ks.df	1		
khc.df	1		
kf.df	1.1904762		
ktd.df	0.9982365		
ψ(tf,td)	2.2579159		
khs.df	1.02		
εsh.ddf	582E-06	με	

Checking the interface shear to find the minimum deck section that can be poured in stage 1

Need to ensure composite action when carrying out the stage 2 pour

Using the method presented in AASHTO 5.8.4

Assuming CIP concrete placed on clean surface roughened to 1/4 in amplitude

c	0.28	ksi	
μ	1		
K1	0.3		
K2	1.8	ksi	for normal weight concrete
	1.3	ksi	for lightweight concrete
bvi	20	in	Taken as the width of the web
Lvi	822	in	Length of the stage 1 deck pour
Acv	16440	in2	
Pc	64.159288	kips	Weight of the deck
Vni	4667.3593	kips	Nominal shear resistance
Vni max 1	19728	kips	Maximum allowed shear resistance
Vni max 2	29592	kips	Maximum allowed shear resistance
Vni	4667.3593	kips	
Vu	0.00	kips	I need composite action from the first deck pour, to resist the shears generated from the second deck pour (I assume the first deck pour is carried by the bare section, the second by the composite section)
dv	12.365758	in	Taken from the centroid of the deck to the centroid of the prestressing steel
vui	0	ksi	
Vui	0	kips	

Demand/Capacity ratio
0 OK

Using the AASHTO alternative method provided in the commentary C5.8.4.2

Mu2	0.00	in-k
Mu1	0.00	in-k
V1	0.00	kips
Cu2	0	kips
C1	0	kips
Vh	0	kips

Demand/Capacity ratio
0 OK

APPENDIX C – REINFORCEMENT DETAILS AND SCHEDULE OF QUANTITIES

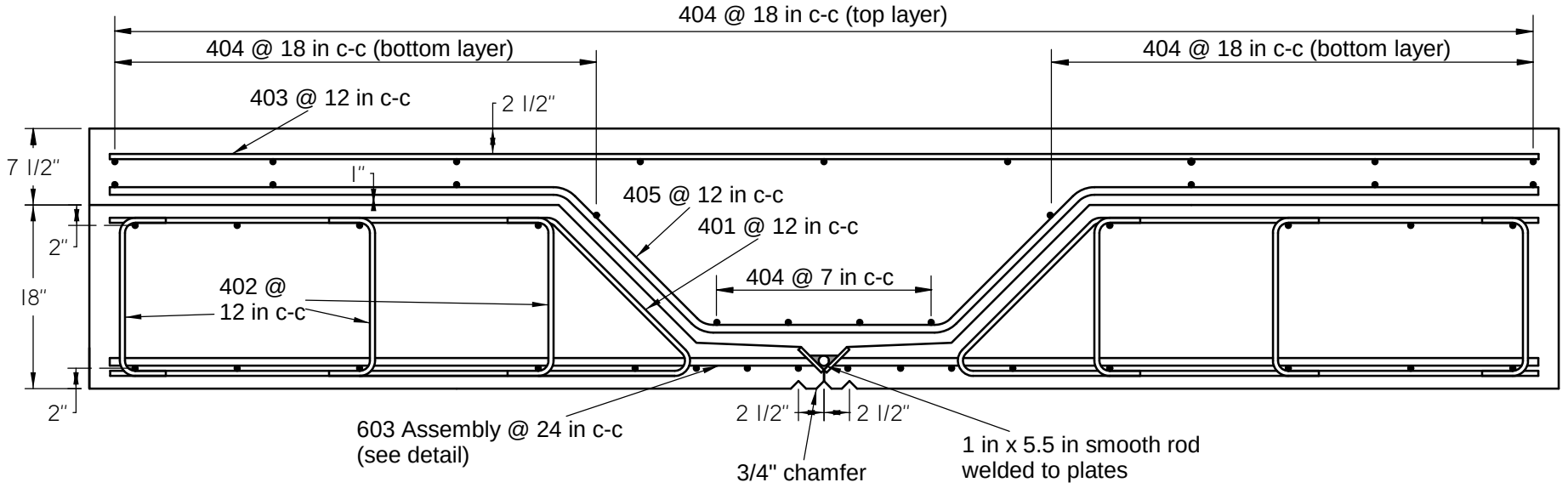

Welded Connection

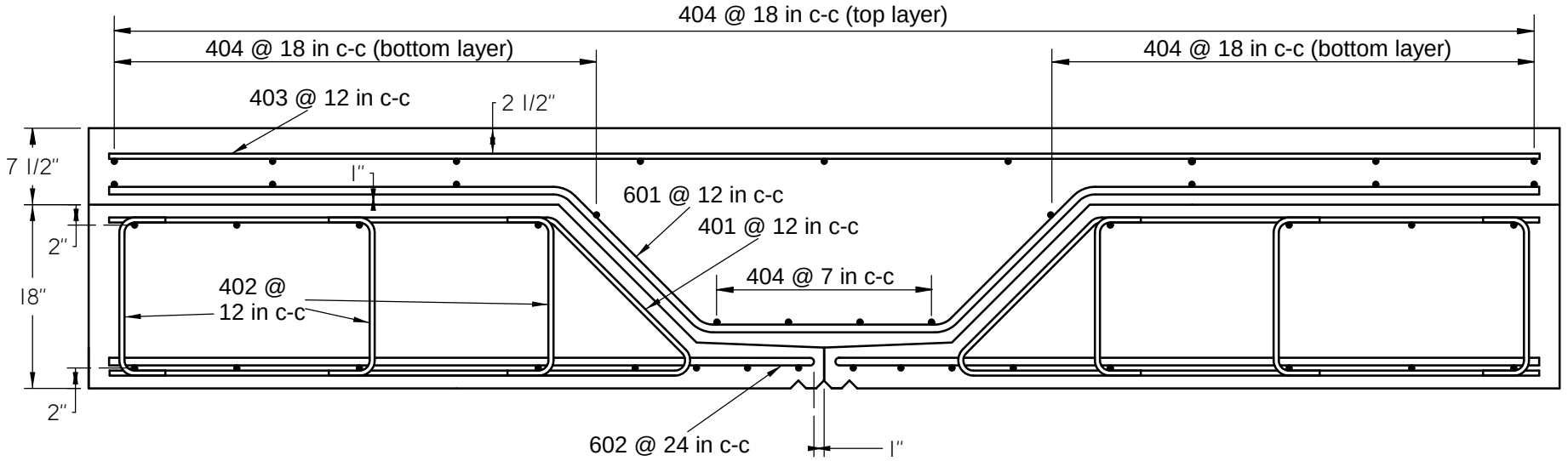

No Connection Connection

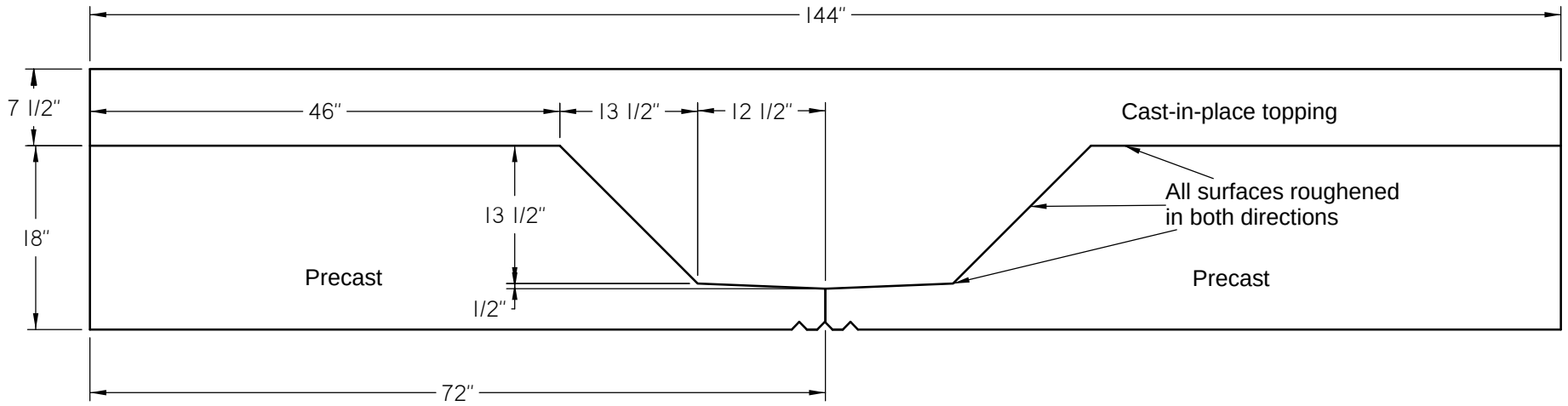

Dimensions of Specimen

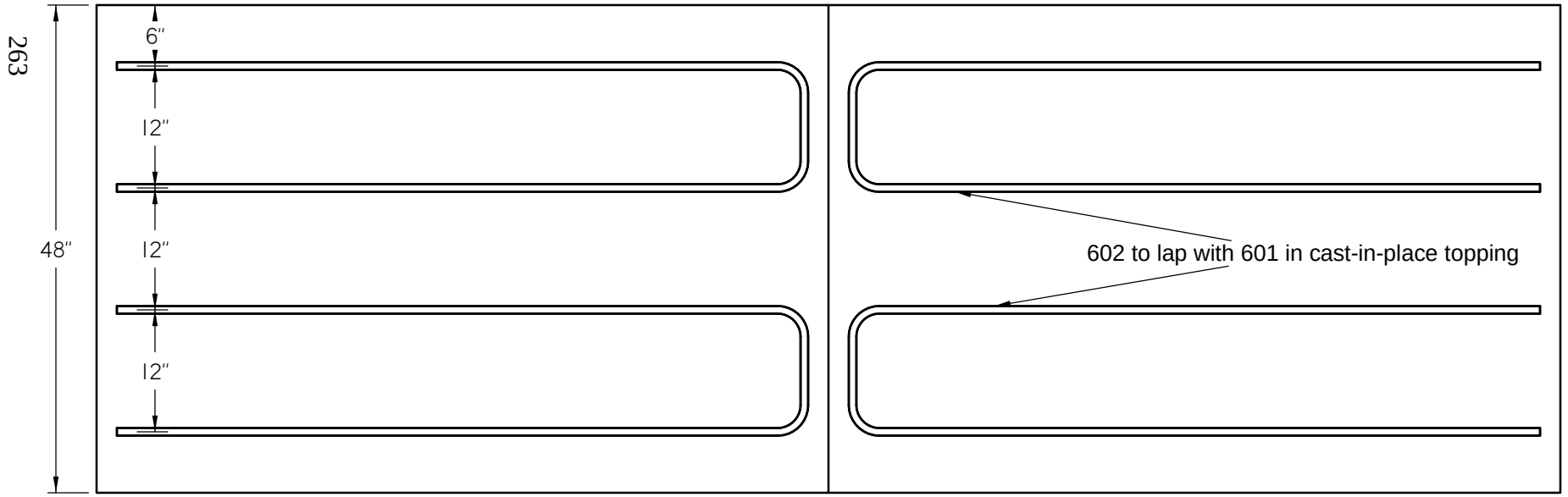

Plan View of Layout of Bottom Reinforcement for No Connection Connection

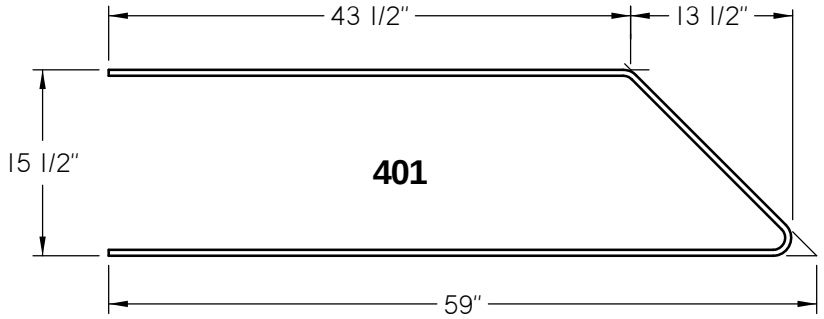

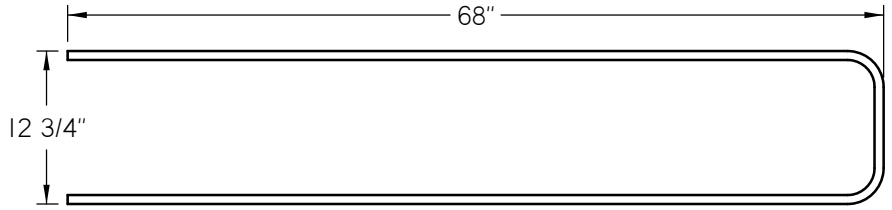

602

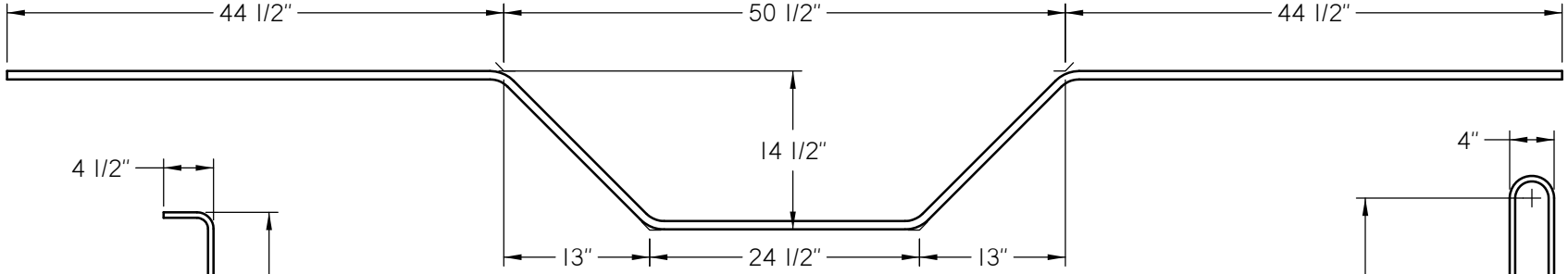

601 and 405

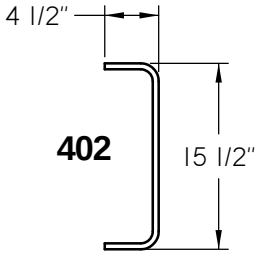

402

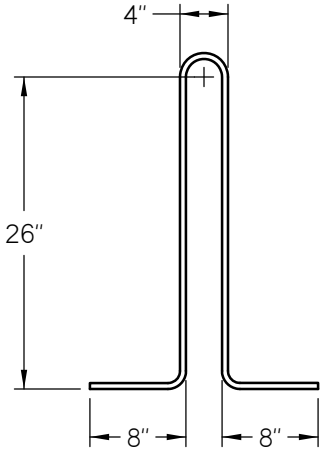

406

Bar Bend Diagrams

Mark	Size	Bend	Length	Wt. each, lbs	No. Required	Total Wt., lbs	Type
601	#6	601	12'-10.5"	19.34	4	77.4	A615 Gr60
602	#6	602	12'-5"	18.65	5	93.2	A615 Gr60
603	#6	STR	5'-8.5"	8.57	10	85.7	A706 Gr60
401	#4	401	9'-8"	6.46	16	103.3	A615 Gr60
402	#4	402	2'-0.5"	1.36	50	68.2	A615 Gr60
403	#4	STR	11'-8"	7.79	8	62.3	A615 Gr60
404	#4	STR	3'-8"	2.45	100	244.9	A615 Gr60
405	#4	405	12'-10.5"	8.60	4	34.4	A615 Gr60
406	#4	406	6'-8.5"	4.48	12	53.8	A615 Gr60
				Total Weight		823	lbs

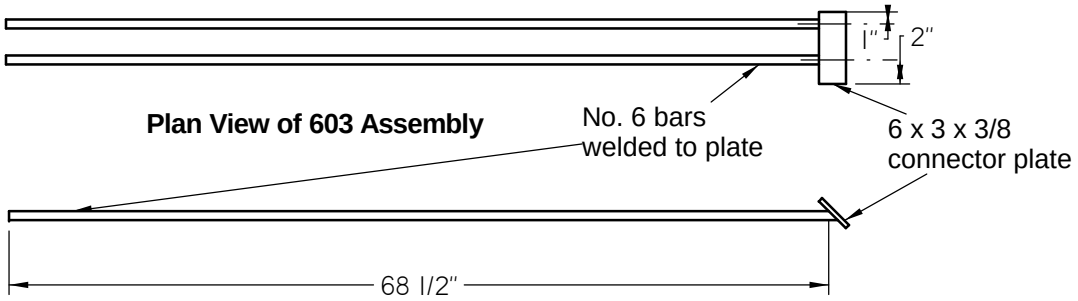

Plan View of 603 Assembly

Elevation of 603 Assembly

Note that bars must be A706 Steel (weldable)

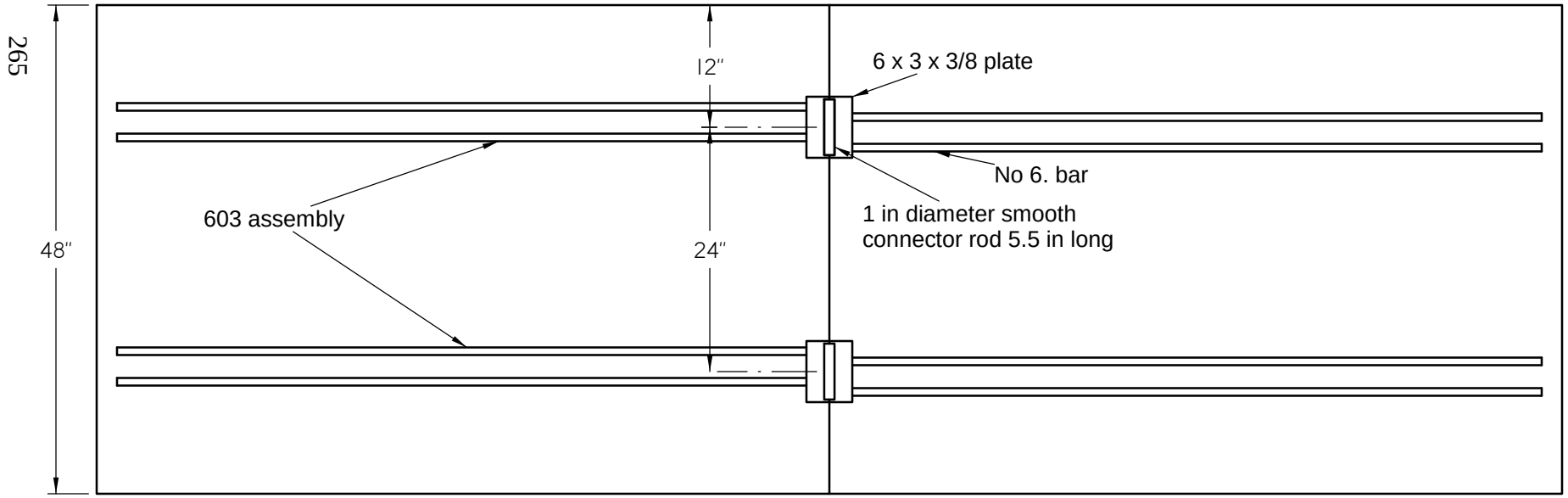

Plan View of Layout of Bottom Reinforcement for Welded Connection

APPENDIX D – FORMWORK AUTOCAD AND GOOGLE SKETCHUP DRAWINGS

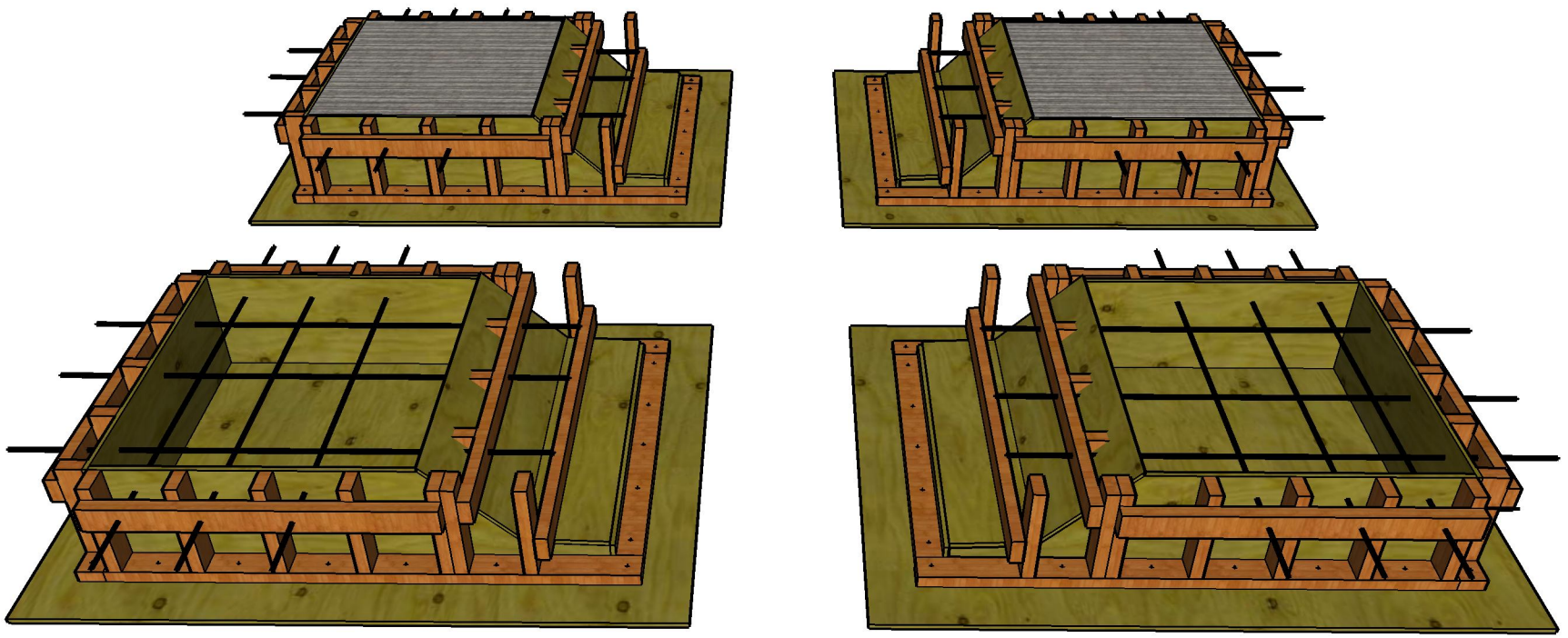

INVERTED T-BEAMS FORMWORK
SIDE-ANGLED VIEW ON BEAMS

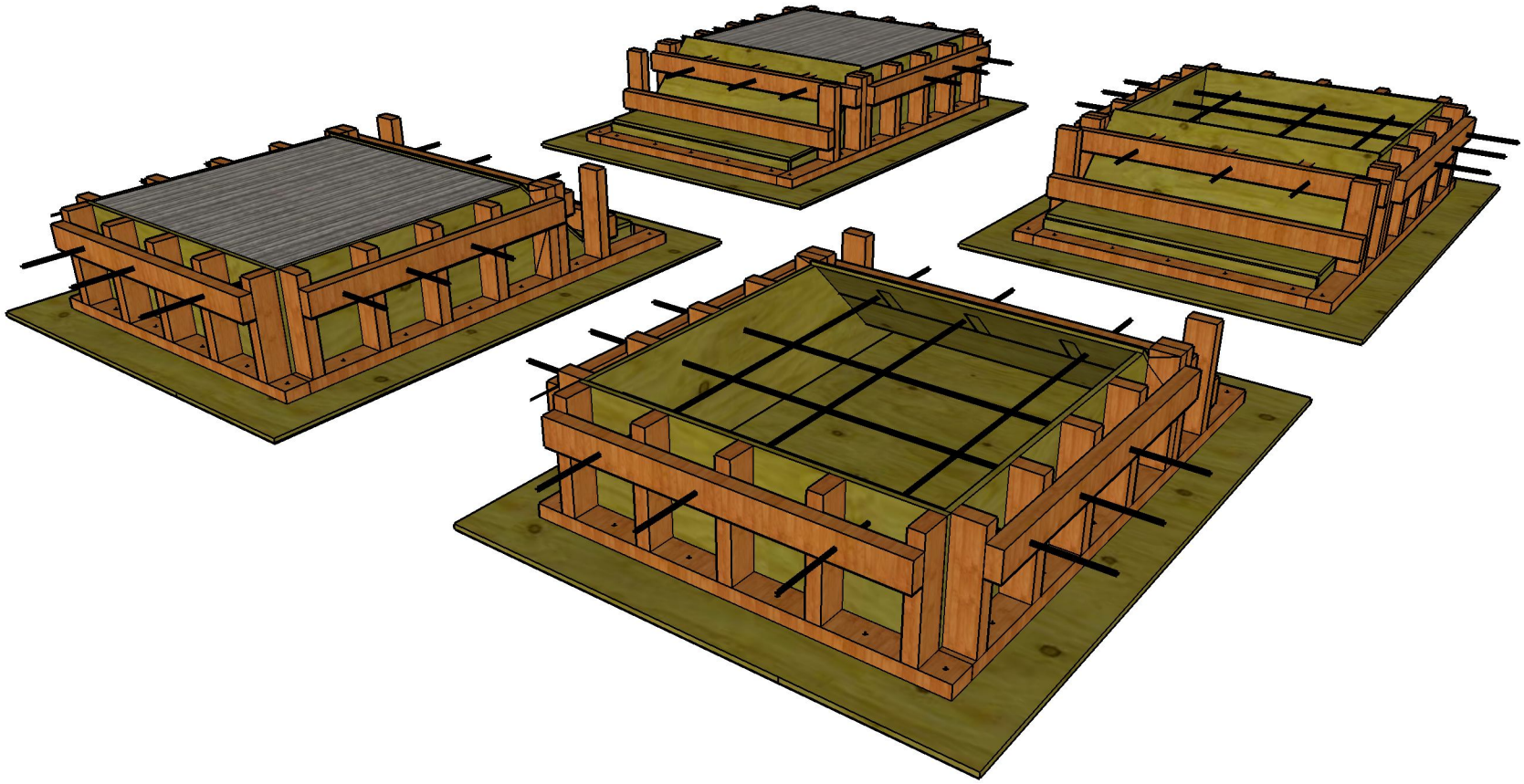

INVERTED T-BEAMS FORMWORK
ANGLED VIEW ON BEAMS

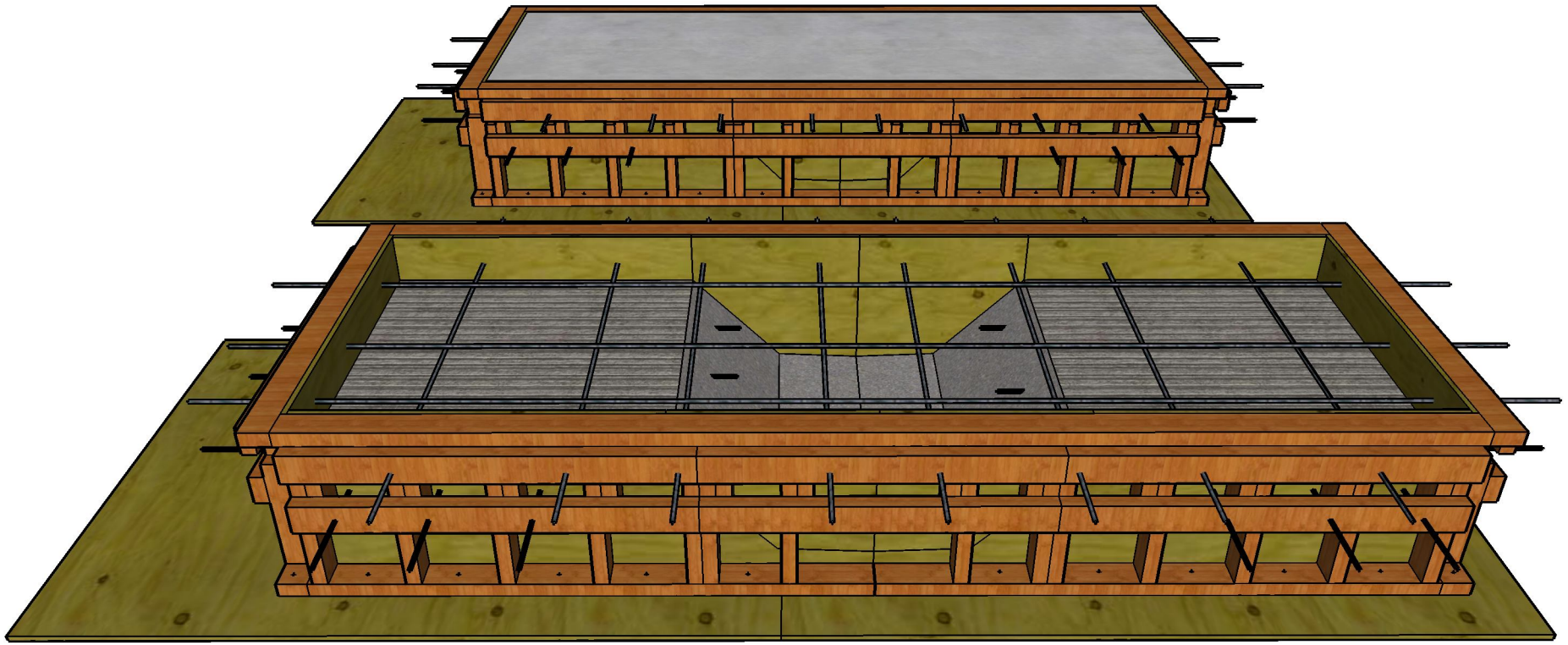

INVERTED T-BEAMS FORMWORK
SIDE-ANGLED VIEW ON C.I.P. TOPPING

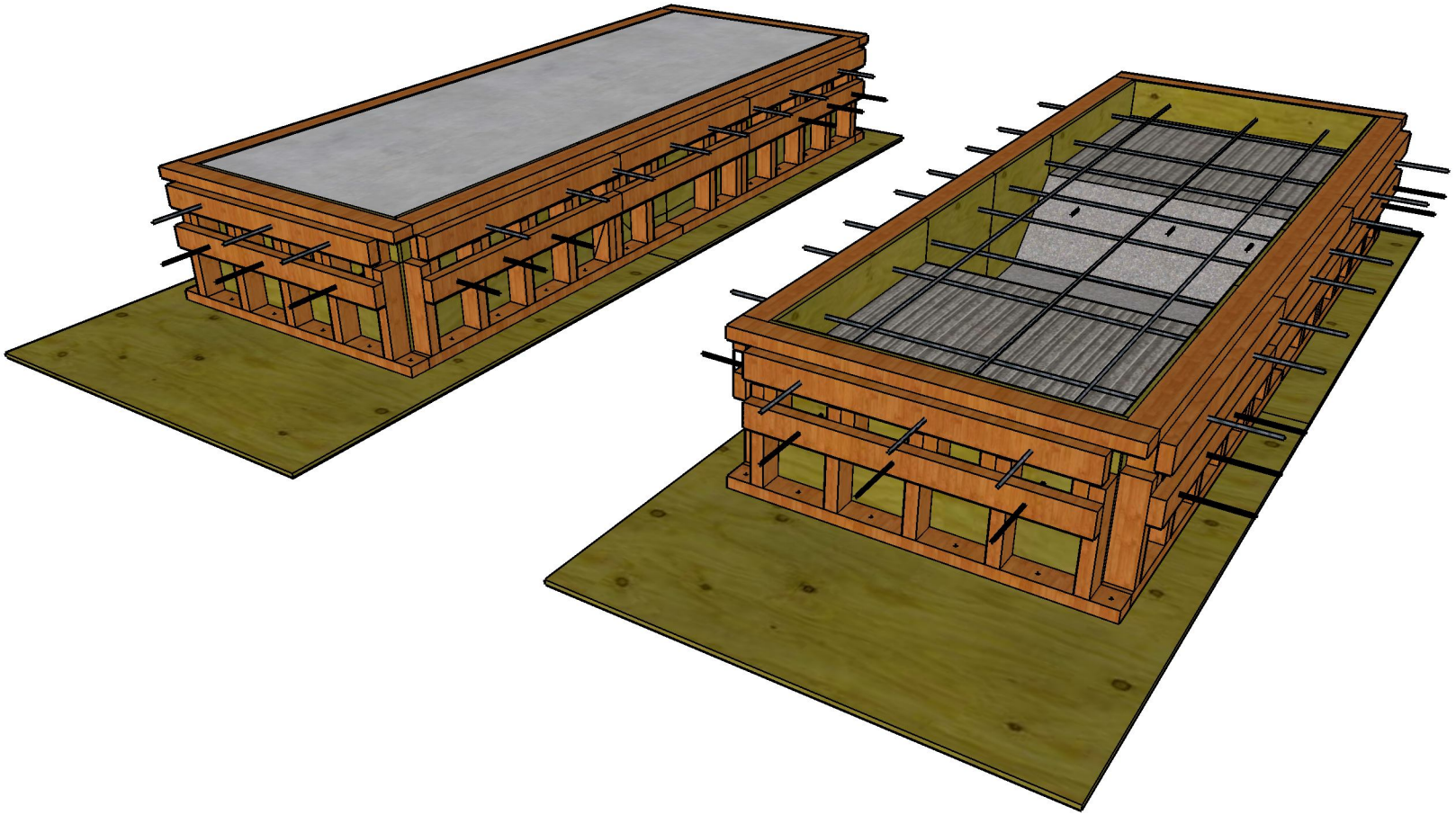

INVERTED T-BEAMS FORMWORK
ANGLED VIEW ON C.I.P. TOPPING

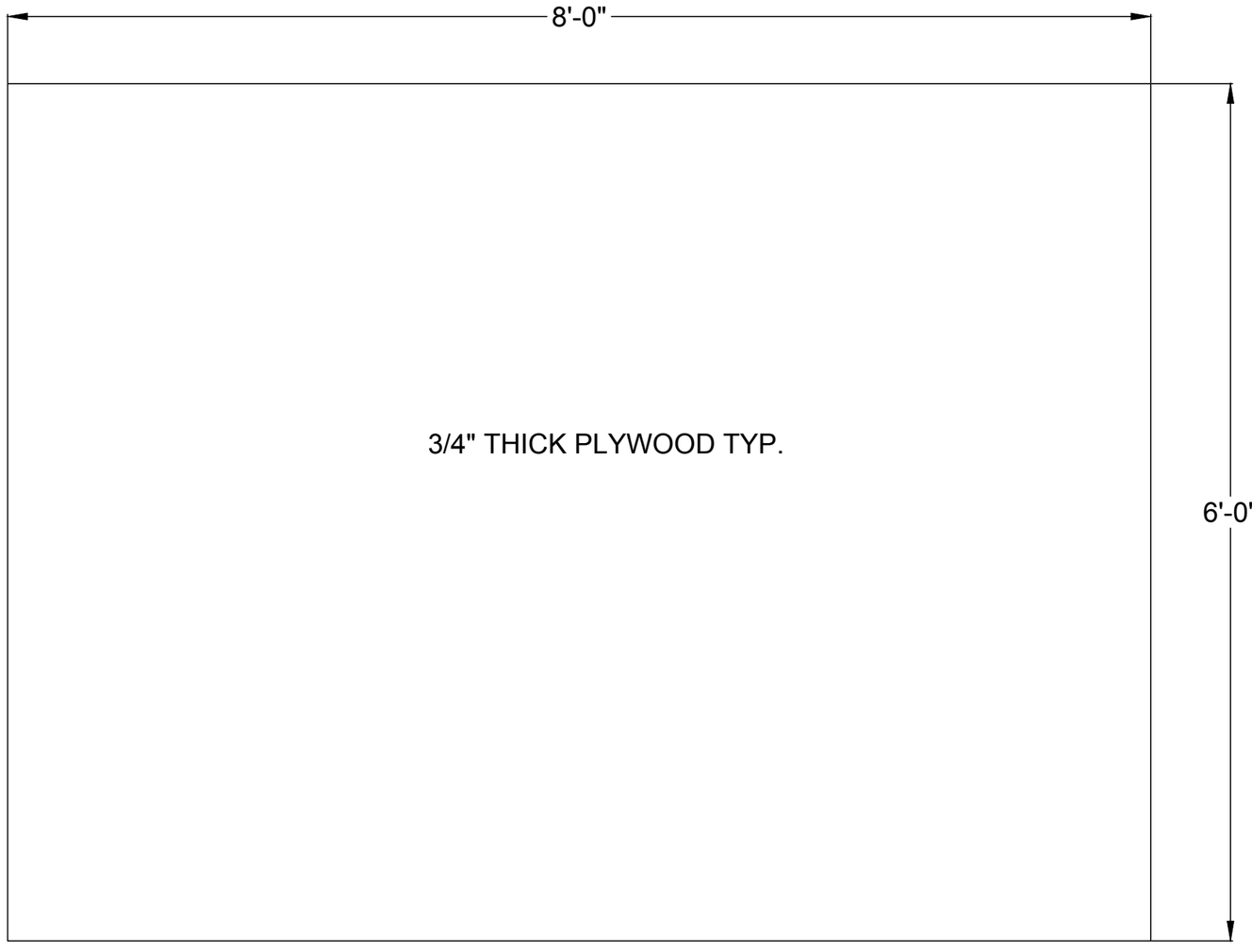

PLAN VIEW ON BASE
SCALE: 1" = 1'-0"

No.	Revision	By	Chk	Appd	Date
1					

Original Scale (11"x17") **AS SHOWN**

Design			
Drawn			
Dsg Verifier			
Drg Check			

* Refer to Revision 1 for Original Signature

VirginiaTech
Invent the Future

Subject: INVERTED T-BEAM FORMWORK

Title: PLAN - BASE

Discipline: Structural

Drawing No.

Rev. A

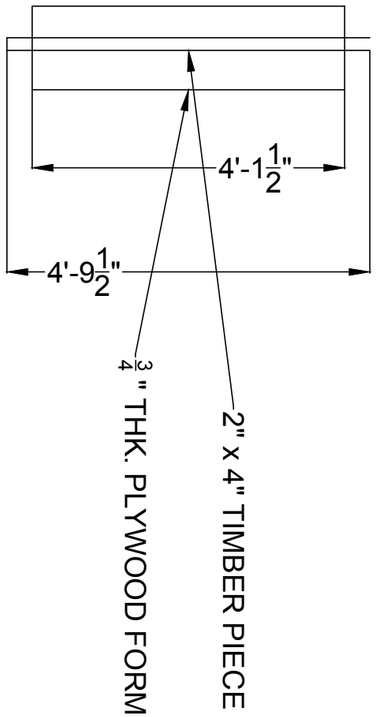

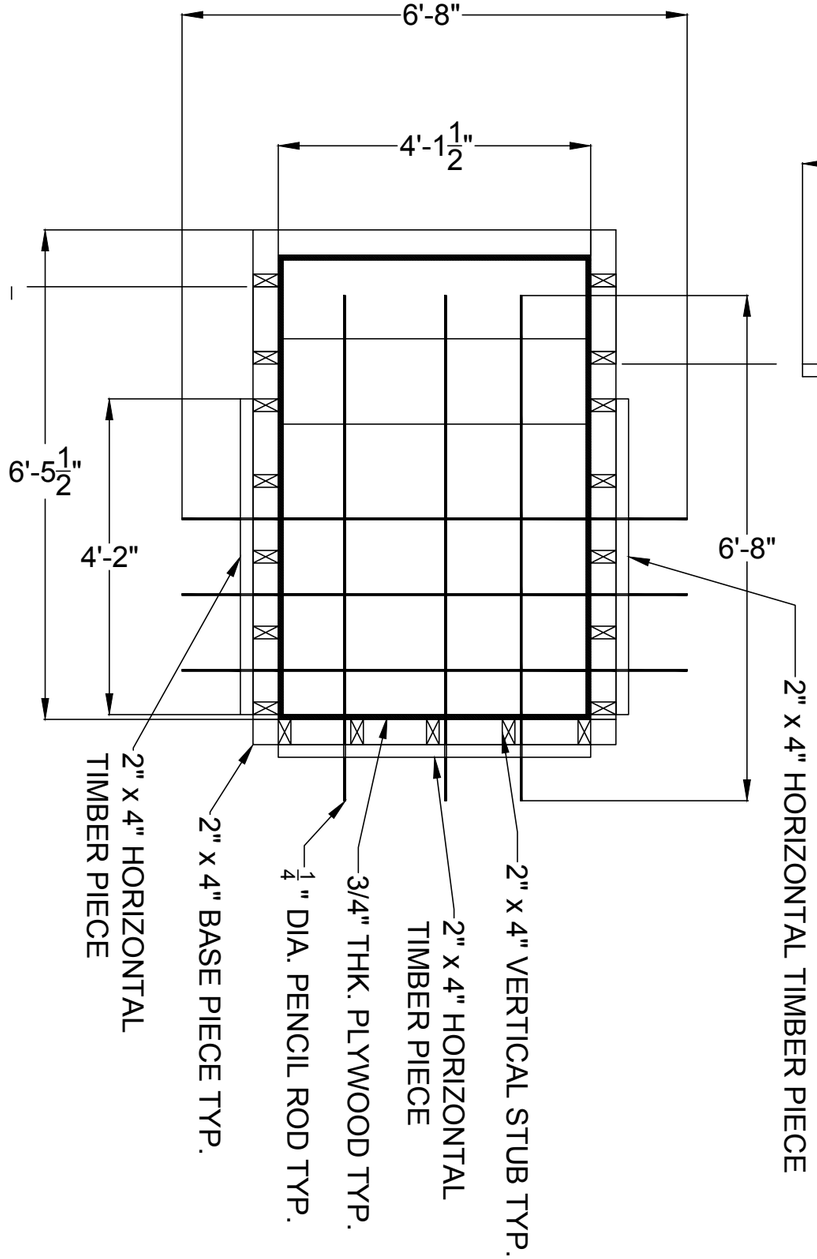

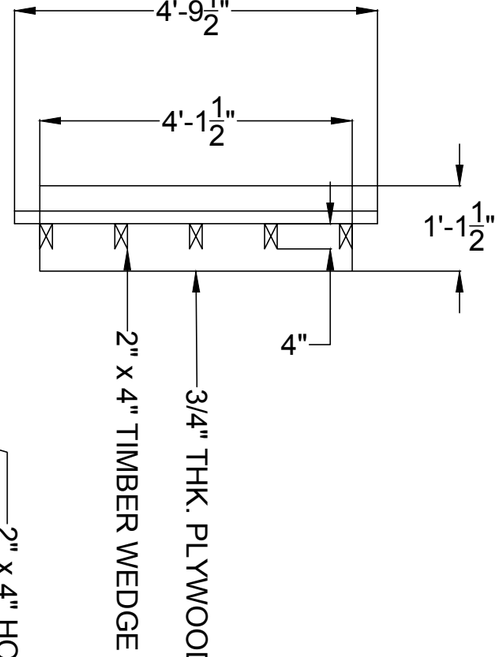

PLAN VIEW ON BEAM FORMWORK
SCALE: 1/2" = 1'-0"

No.	Revision	By	Chk	Appd	Date
1					

Original Scale (11"x17") **AS SHOWN**

Design			
Drawn			
Dsg Verifier			
Drg Check			

* Refer to Revision 1 for Original Signature

VirginiaTech
Invent the Future

Subject: INVERTED T-BEAM FORMWORK

Title: PLAN - BEAM FORMS

Discipline: Structural

Drawing No.

Rev. A

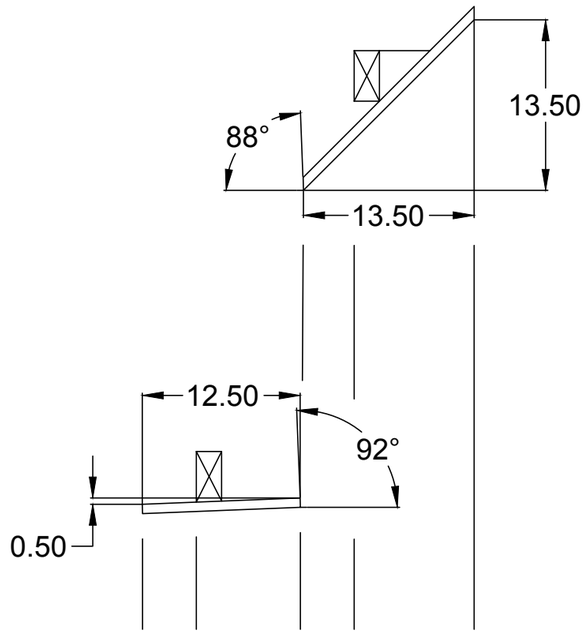

ELEVATION ON BEAM FORMWORK
PENCIL ROD NOT SHOWN FOR CLARITY
SCALE: 1" = 1'-0"

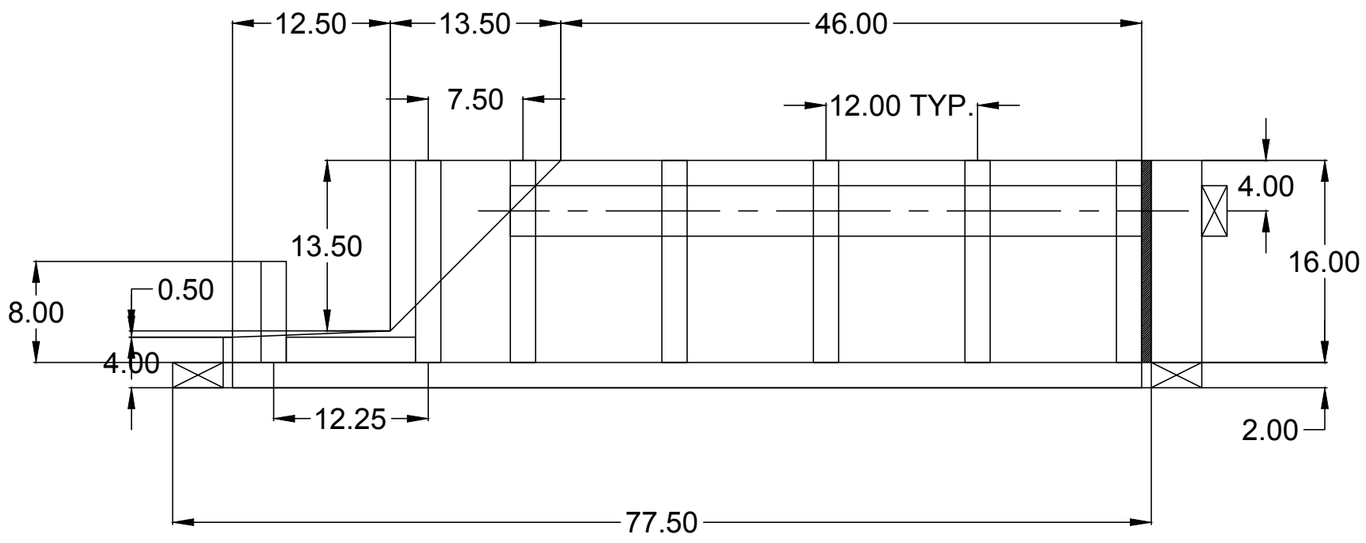

No.	Revision	By	Chk	Appd	Date
1					

Original Scale (11"x17") **AS SHOWN**

Design			
Drawn			
Dsg Verifier			
Drg Check			

* Refer to Revision 1 for Original Signature

VirginiaTech
Invent the Future

Subject: INVERTED T-BEAM FORMWORK

Title: ELEVATION - BEAM FORMS

Discipline: Structural

Drawing No.

Rev. A

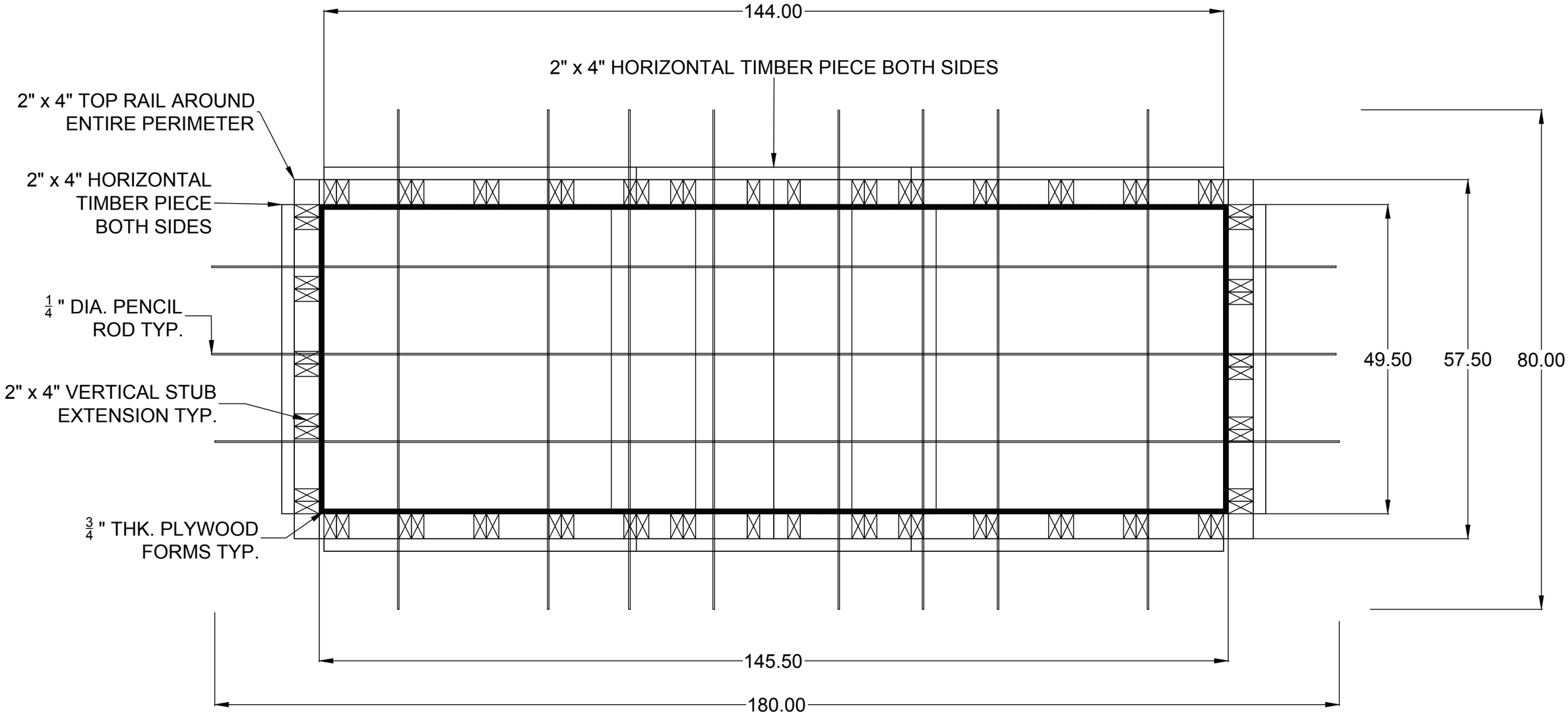

CIP FORMWORK OVERLAID ON BEAM FORMWORK
SCALE: 3/4" = 1'-0"

No.	Revision	By	Chk	Appd	Date
1					

Original Scale (11"x17") **AS SHOWN**

Design			
Drawn			
Dsg Verifier			
Drg Check			

* Refer to Revision 1 for Original Signature

VirginiaTech 1872 *Invent the Future*

Subject: INVERTED T-BEAM FORMWORK

Title: PLAN - C.I.P. FORMS

Discipline: Structural

Drawing No.

Rev. A

PENCIL ROD NOT SHOWN FOR CLARITY (REFER TO PLAN)

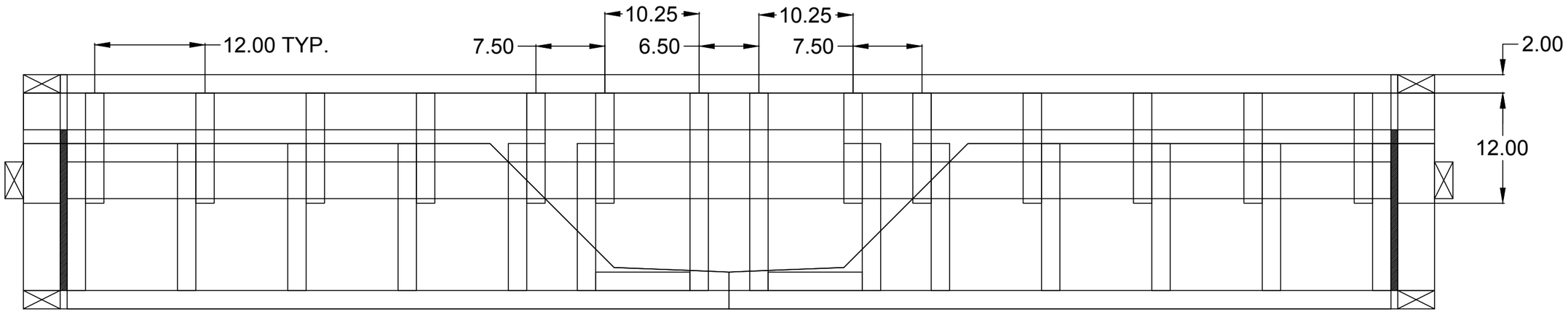

ELEVATION ON CIP FORMWORK
OVERLAID ON BEAM FORMWORK
SCALE: 1" = 1'-0"

No.	Revision	By	Chk	Appd	Date
1					

Original Scale (11"x17") **AS SHOWN**

Design			
Drawn			
Dsg Verifier			
Drg Check			

* Refer to Revision 1 for Original Signature

VirginiaTech
Invent the Future

Subject: INVERTED T-BEAM FORMWORK

Title: ELEVATION - C.I.P. FORMS

Discipline: Structural

Drawing No.

Rev. A

APPENDIX E – U.S. ROUTE 360 BRIDGE OVER THE CHICKAHOMINY RIVER DRAWINGS

12/12/2012

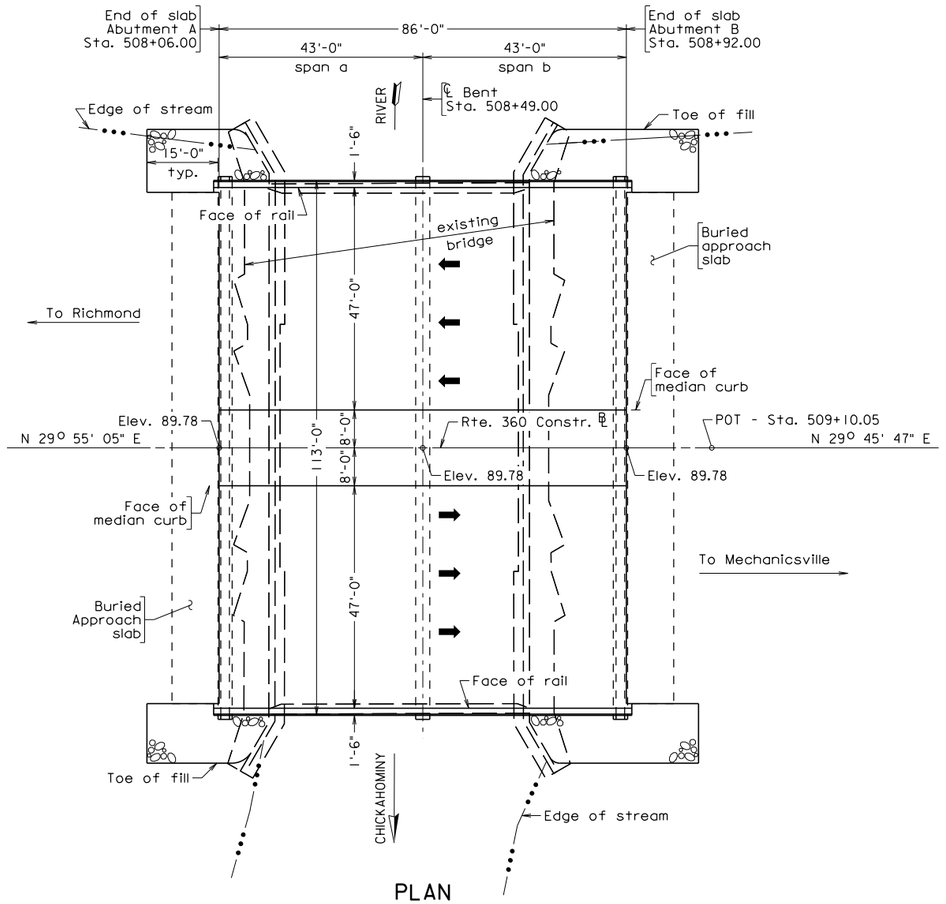

PLAN

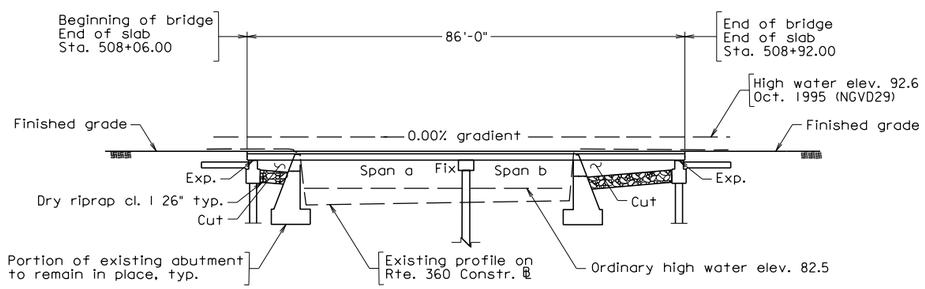

ABUTMENT A BENT ABUTMENT B

DEVELOPED SECTION ALONG ℄

b28916001.dgn

STATE	FEDERAL AID		STATE		SHEET NO.
	ROUTE	PROJECT	ROUTE	PROJECT	
VA.	—	BR-5A27(172)	360	0360-964-120, B607	1
NBIS Number: 000000000028898			UPC No. 17959		
Federal Oversight Code: NFO			FHWA Construction and Scour Code: X080-S5		

DESIGN EXCEPTION(S):

None

GENERAL NOTES:

The original approved sheet, including original signatures, is filed in the VDOT Central Office. Any misuse of electronic files, including scanned signatures is illegal. Violators will be prosecuted to the full extent of the applicable laws.

Width: 47' Roadway, 16' median, 47' Roadway.
Overall width 110'-0" face-to-face of rails.

Span layout: 2 - 43'-0" Prestressed concrete slab units (18" depth).

Capacity: HL-93 loading.

Drainage area: 72.5 sq. mi.

Specifications:

Construction: Virginia Department of Transportation Road and Bridge Specifications, 2007.

Design: AASHTO LRFD Bridge Design Specifications, 5th Edition, 2010; 2010 Interim Specifications; and VDOT Modifications.

Standards: Virginia Department of Transportation Road and Bridge Standards, 2008.

These plans are incomplete unless accompanied by the Supplemental Specifications and Special Provisions included in the contract documents.

Design loading includes 10 psf allowance for construction tolerances and construction methods.

Concrete in prestressed beam units shall be Class A5. Concrete in superstructure including terminal walls, median, and rails shall be Class A4; in substructure, Class A3.

Low permeability concrete shall be used in this project.

Prestressed concrete in prestressed beam units shall be Class A5 having a minimum compressive cylinder strength at 28 days equal to 6,000 psi and a minimum compressive cylinder strength at time of release of strands equal to 5,000 psi.

All reinforcing steel shall be deformed and shall conform to ASTM A615, Grade 60 except for reinforcing steels noted as CRR (corrosion resistant reinforcing) which shall conform to applicable specifications noted in the special provision. All reinforcing bar dimensions on the detailed drawings are to centers of bars except where otherwise noted and are subject to fabrication and construction tolerances.

General Notes continued on Sheet 2.

VDOT

COMMONWEALTH OF VIRGINIA
DEPARTMENT OF TRANSPORTATION
PROPOSED BRIDGE ON

RTE. 360
OVER CHICKAHOMINY RIVER - HENRICO CO.
0.3 MI. W. HANOVER-HENRICO CO. LINE
PROJ. 0360-964-120, B607

Recommended for Approval: Kendal R. Walus — State Structure and Bridge Engineer — 10-10-2012 Date

Approved: Malcolm T. Kerley — Chief Engineer — 10-11-2012 Date

ORIGINAL SIGNATURES ON TITLE SHEET OF ROAD PLANS

Date: July 19, 2012

289-16

VDOT S&B DIVISION
RICHMOND, VA
STRUCTURAL ENGINEER

PLANS BY:	Central Office
COORDINATED:	Christopher M. Lowe
SUPERVISED:	Jeffrey C. Hill
DESIGNED:	Christopher M. Lowe
DRAWN:	Alan M. Johnson
CHECKED:	Jeffrey C. Hill

No.	Description	Date
	REVISIONS	
	For Table of Revisions, see Sheet 2.	

Scale: 1/16" = 1'-0"

12/12/2012

STATE	FEDERAL AID		STATE		SHEET NO.
	ROUTE	PROJECT	ROUTE	PROJECT	
VA.	—	BR-5A27(172)	360	0360-964-120, B607	2

ESTIMATED QUANTITIES - SUBSTRUCTURE ONLY

		Concrete Class A3	Reinforcing Steel	Corrosion Resistant Reinf. steel Low Carbon/ Chromium	Prestressed Concrete Piles		Driving test for Prestressed Concrete Piles		Dynamic pile test (Friction piles)	Structre Excavation	Dry Riprap Class I 26"	Select Material Type I Min. CBR-30	Temp-orary sheet piling	Turbidity Curtain, Pervious
					LF		LF							
		CY	LB	LB	18"	24"	18"	24"	EA	CY ⊗	TON	TON	SF	LF
Abutment A	Neat	15.8	———	1,520	882	———	63	———	1	492	528	502	2,220	———
	Footing	37.1	4,430	———	———	———	———	———	———	———	———	———	———	———
Bent		43.4	4,400	———	———	910	———	65	1	———	———	———	———	280
Abutment B	Neat	15.8	———	1,520	945	———	———	———	———	492	859	502	2,820	———
	Footing	37.1	4,430	———	———	———	———	———	———	———	———	———	———	———
Total		149.2	13,260	3,040	1,827	910	63	65	2	984	1,387	1,004	5,040	280

⊗ Denotes items to be paid for on the basis of plan quantities in accordance with current Road and Bridge Specifications.

LUMP SUM BID ITEMS

Mobilization	LS
Construction Surveying	LS
Dismantle and Remove Existing Structure Number 1018	LS

ESTIMATED QUANTITIES - SUPERSTRUCTURE ONLY

Item	Units	Quantity
Concrete Class A4	CY	435.6
Corrosion Resistant Reinf. Steel, Low Carbon/Chromium steel ⊗	LB	43,260
Railing, Kansas Corral 32", w/out curb ⊗	LF	172
NS Prestressed Concrete Beam Inverted T-Beam	EA	36
NS Prestressed Concrete Beam Rectangular Beam	EA	4
Bridge Deck Grooving ⊗	SY	1,052
Concrete Class A4 - Bridge Approach Slab ⊗	CY	100.9
Reinforcing Steel - Bridge Approach Slab ⊗	LB	17,470

⊗ Denotes items to be paid for on the basis of plan quantities in accordance with current Road and Bridge Specifications.

GENERAL NOTES: Continued

Corrosion resistant reinforcing (CRR) steels shall conform to one or more of the three types (low carbon/chromium, stainless clad and solid stainless) listed in the special provision. The minimum yield strength shall be: 100 ksi for low carbon/chromium and 60 ksi for stainless clad steel and solid stainless steel. The type(s) of CRR steel(s) required on this project is/are noted on the plan sheets and in the reinforcing steel schedule.

Prestressing strands shall be uncoated, seven-wire, low-relaxation steel strands conforming to ASTM A416 Grade 270.

Prestressed Concrete piles were designed using a factored axial resistance of 192 tons per pile. The nominal axial resistance as measured during driving shall be at least 295 tons per pile.

The driving test pile and dynamic pile testing at Abutment A and the Bent shall be performed prior to submission of the pile order list for the entire bridge.

All piles shall be driven to a minimum tip elevation of EL. 25.0.

Bridge No. of existing bridge is 1018 Plan No. is 212-06 dated 1968, 086-11 dated 1941, and 019-23 dated 1923.

Deck shall be waterproofed in accordance with the requirements of Sec. 405 and Sec. 416 of the Specifications.

Structural approach slabs are included in the bridge contract.

B.M.: Refer to roadway sheet 1e.

See Sheet 8 and 9 for NS Prestressed Concrete Inverted T-Beam details.

See Sheet 8 and 9 for NS Prestressed Concrete Rectangular Beam details.

INDEX OF SHEETS

b28916002.dgn

VDOT S&B DIVISION
RICHMOND, VA
STRUCTURAL ENGINEER

Rev. No.	Sheets Revised	Date

TABLE OF REVISIONS

No.	Description	Date

Revisions

COMMONWEALTH OF VIRGINIA
DEPARTMENT OF TRANSPORTATION

STRUCTURE AND BRIDGE DIVISION

ESTIMATED QUANTITIES INDEX OF SHEETS

Designed: CML	Date	Plan No.	Sheet No.
Drawn: AMJ	July 2012	289-16	2 of 16
Checked: JCH			

12/12/2012

STATE	FEDERAL AID		STATE		SHEET NO.
	ROUTE	PROJECT	ROUTE	PROJECT	
VA.	—		360	0360-964-120, B607	3

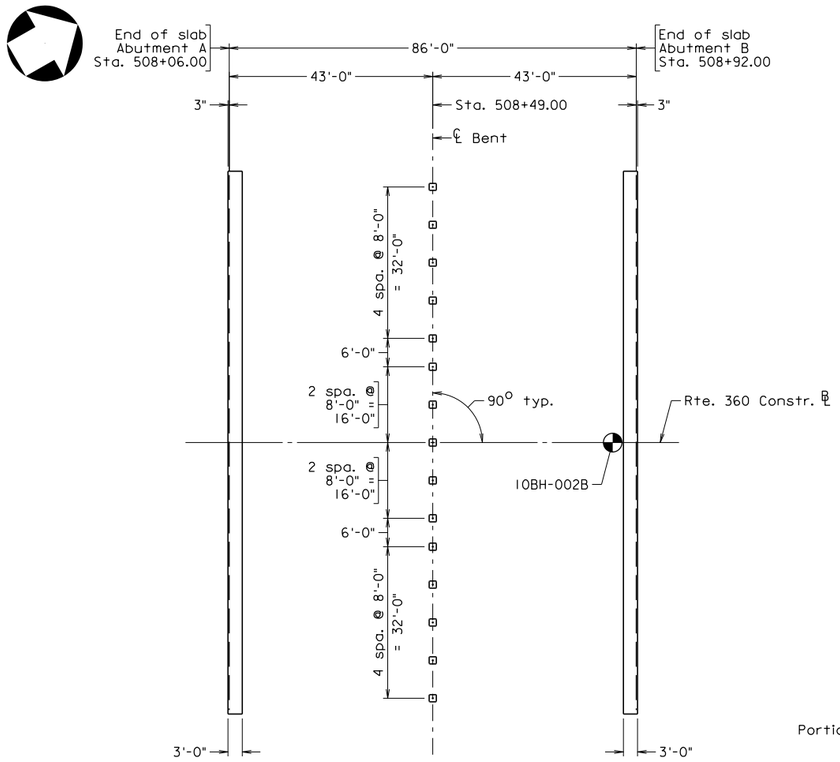

SUBSTRUCTURE LAYOUT

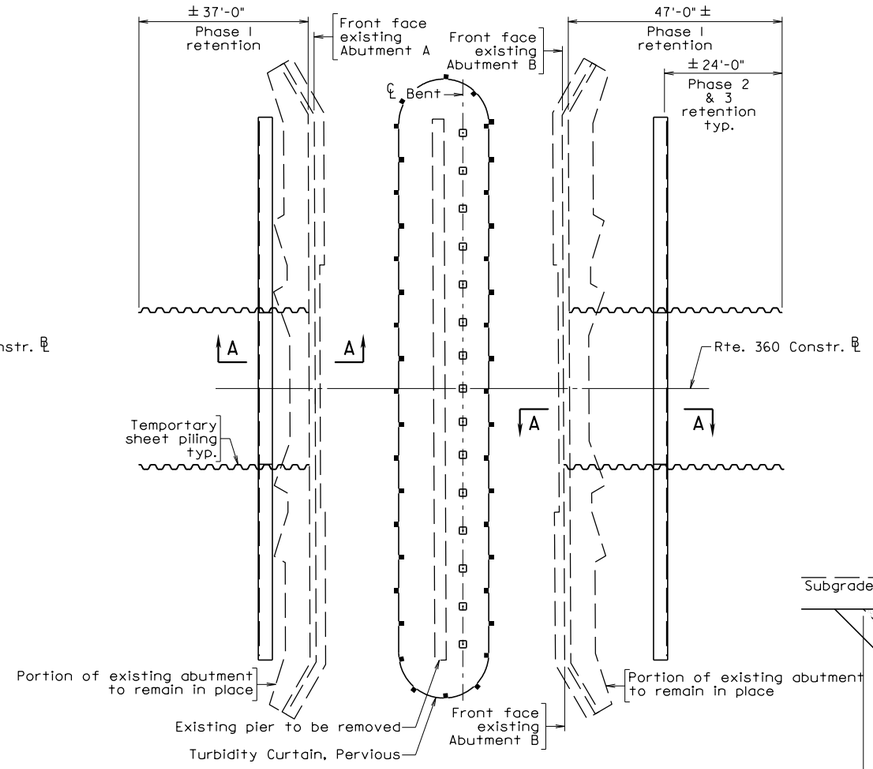

DEMOLITION AND SOIL RETENTION SYSTEM PLAN

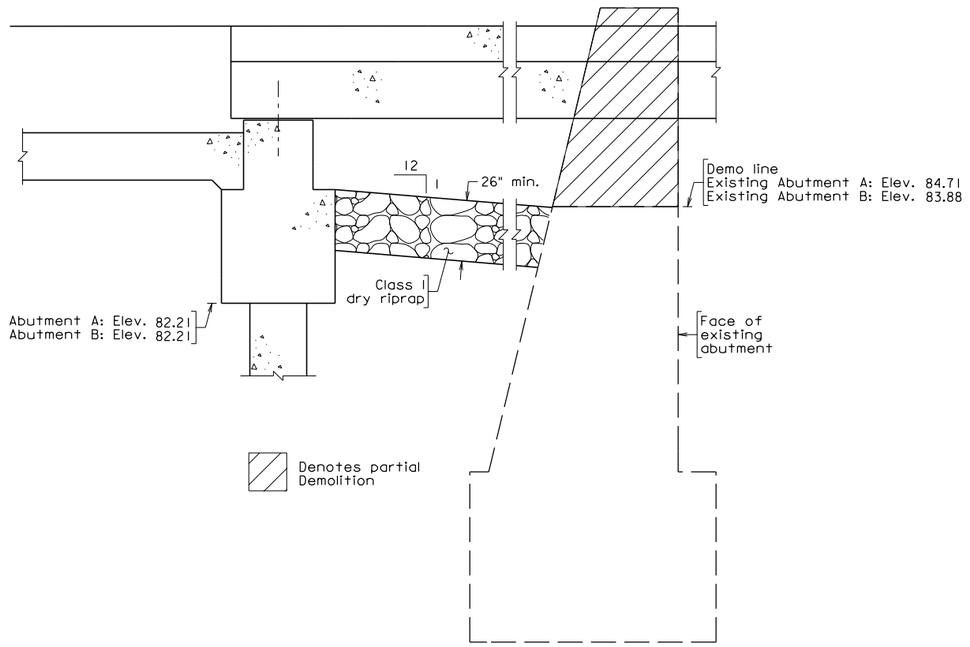

SECTION A-A
Not to scale

Notes:

Material in the abutment select backfill zone shall be Select Material Type I, minimum CBR 30 and shall be compacted in accordance with Sections 303 and 305 of the Specifications.

In cut situations, material with strength characteristics greater than the select backfill may be left in place.

The final depth of the embankment side slopes shall be regular embankment material placed and finished as required.

Denotes approximate boring locations. For details, see sheet 15.

This substructure layout is to be used only for the purpose of locating abutment footings. For abutment and bent details see sheets 5, 6 and 7.

Partial demolition of existing abutments shall be in accordance with section 413.02(b) of the specifications.

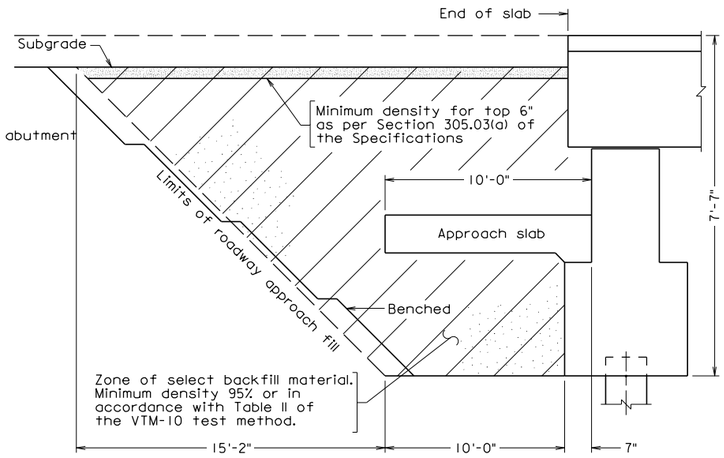

SECTION THROUGH ABUTMENT - CUT SECTION
Abutment drainage not shown
Not to scale

b28916003.dgn

VDOT S&B DIVISION
RICHMOND, VA
STRUCTURAL ENGINEER

No.	Description	Date
	Revisions	

COMMONWEALTH OF VIRGINIA
DEPARTMENT OF TRANSPORTATION

STRUCTURE AND BRIDGE DIVISION

SUBSTRUCTURE LAYOUT, DEMO., SOIL RETENTION, RIPRAP DETAILS AND SELECT BACKFILL

Designed: CEB	Date	Plan No.	Sheet No.
Drawn: AMJ	July 2012	289-16	3 of 16
Checked: JCH			

12/12/2012

STATE	FEDERAL AID		STATE		SHEET NO.
	ROUTE	PROJECT	ROUTE	PROJECT	
VA.	—		360	0360-964-120, B607	4

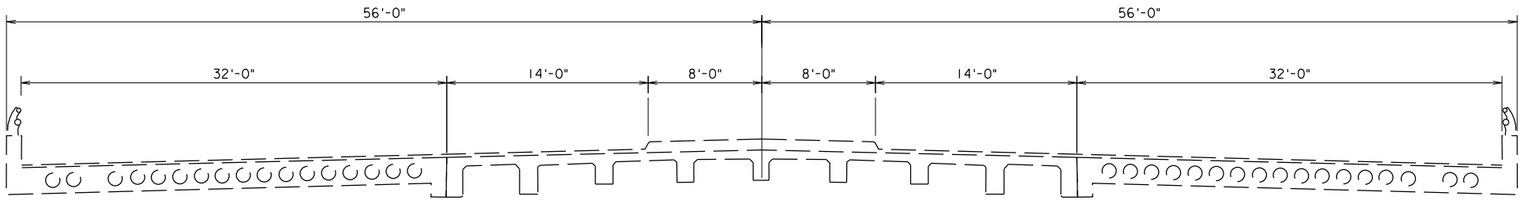

EXISTING TRANSVERSE SECTION

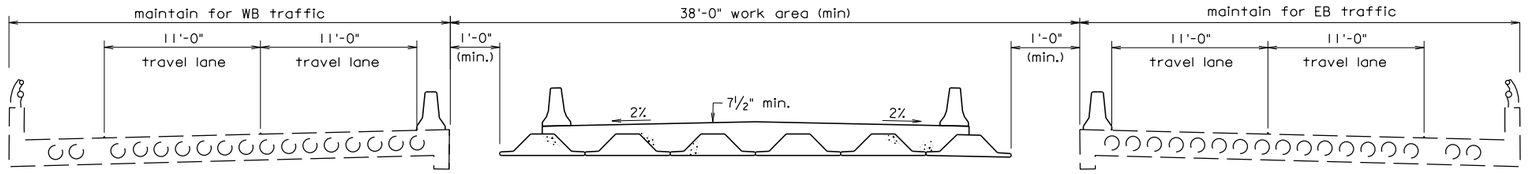

BRIDGE PHASE 1

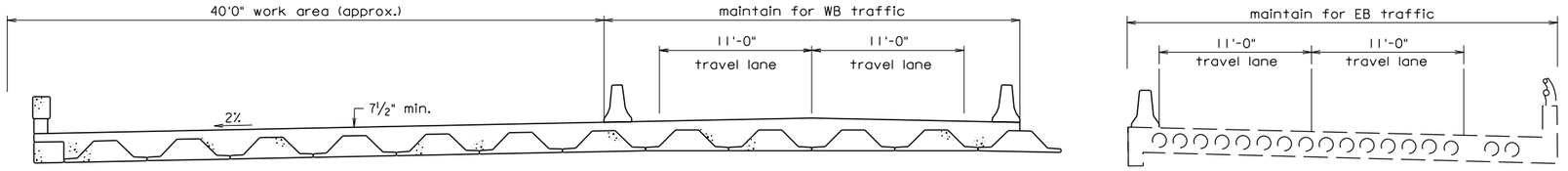

BRIDGE PHASE 2

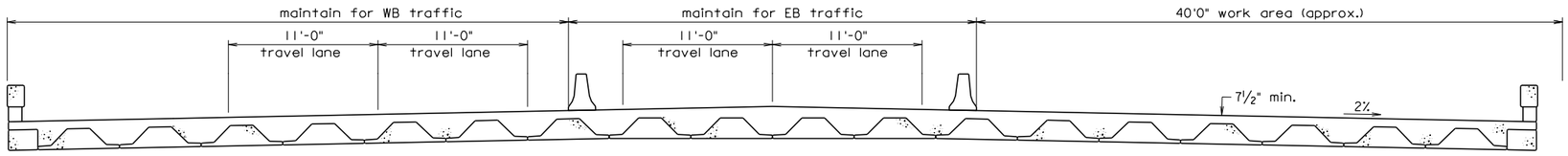

BRIDGE PHASE 3

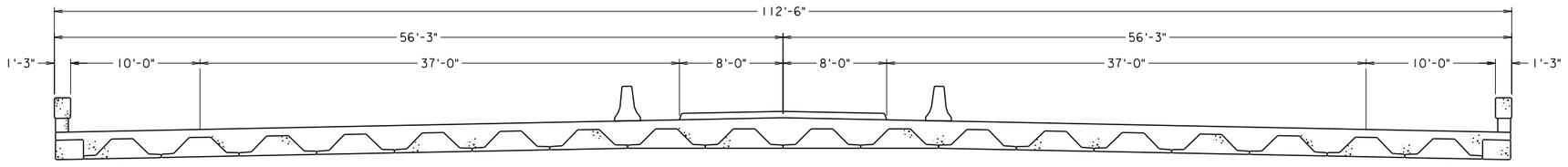

BRIDGE PHASE 4

Notes:

The contractor shall coordinate the construction sequence of the bridge with the construction sequence of the roadway.

Existing superstructure and substructure shall be removed in accordance with this construction sequence, in accordance with the roadway construction sequence, and as necessary to maintain traffic while accommodating construction of the proposed structure.

See Sheet 8 for detailed Transverse Section.

Cost of Traffic Barrier Service Concrete Parapets (Double Face) MB-11A is included in the road plans.

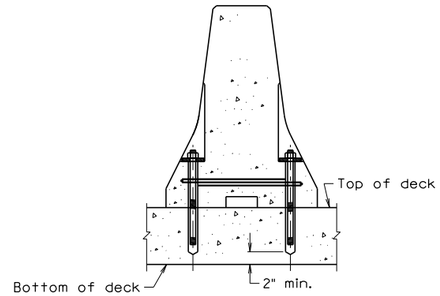

TRAFFIC BARRIER SERVICE CONRETE PARAPET (DOUBLE FACE)

NOTES:

1. Bolt down side adjacent to traffic.
2. For details not shown, see VDOT Road and Bridge Standards MB-11A.
3. After removing Temporary barrier, cut ⅞" ø bolt or threaded rod as low as practical below roadway surface and fill recess with epoxy bonding compound EP-4.
4. Anchor system shall be tested to provide a minimum pullout of 32,000 lbs. and installed according to manufacturer's recommendations.

b289160004.dgn

VDOT S&B DIVISION
RICHMOND, VA
STRUCTURAL ENGINEER

Scale ⅜"=1'-0" unless otherwise shown

No.	Description	Date
	Revisions	

COMMONWEALTH OF VIRGINIA
DEPARTMENT OF TRANSPORTATION

STRUCTURE AND BRIDGE DIVISION

SEQUENCE OF CONSTRUCTION

Designed: CML	Date	Plan No.	Sheet No.
Drawn: AMJ/BCH	July 2012	289-16	4 of 16
Checked: JCH			

12/12/2012

STATE	FEDERAL AID		STATE		SHEET NO.
	ROUTE	PROJECT	ROUTE	PROJECT	
VA.	——		360	0360-964-120, B607	5

ABUTMENT A

ABUTMENT B

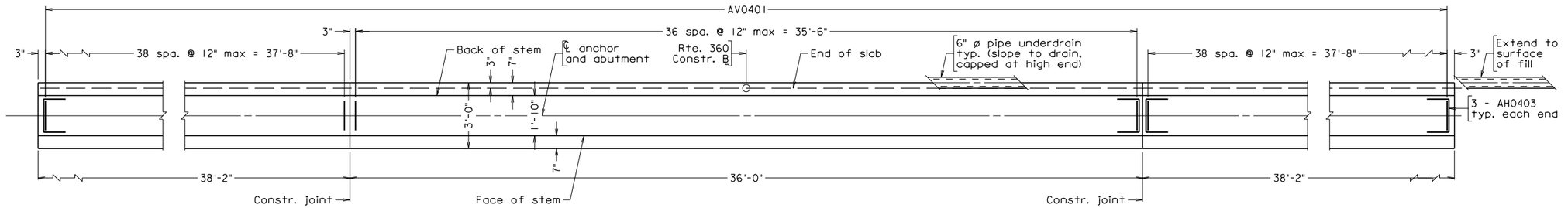

PLAN

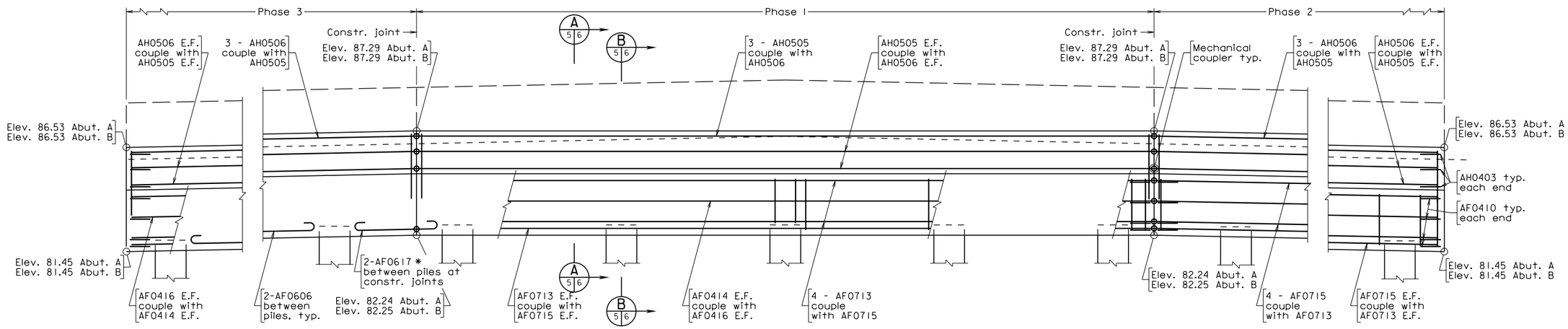

ELEVATION

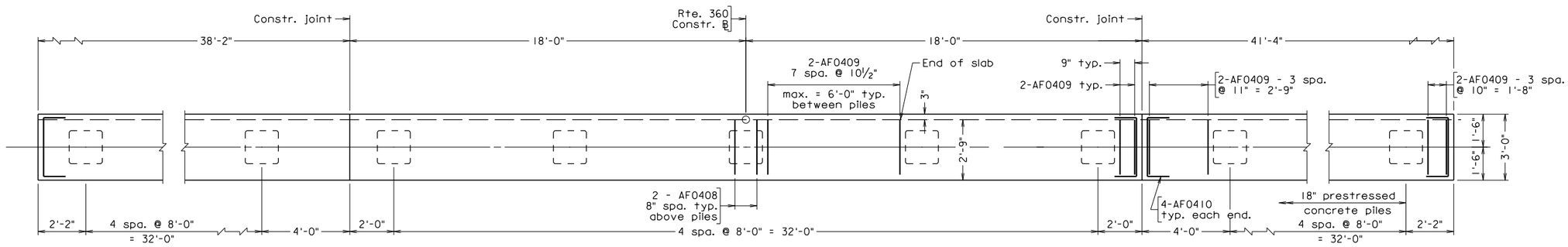

FOOTING PLAN

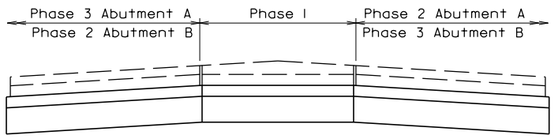

ABUTMENT KEY
Not to scale

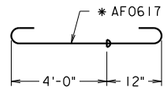

MECHANICAL COUPLER DIAGRAM

Notes:

Abutment A shown, Abutment B similar and symmetric about Constr. ℄.

Scale: ⅜" = 1'-0" unless otherwise noted

VDOT S&B DIVISION
RICHMOND, VA
STRUCTURAL ENGINEER

No.	Description	Date
	Revisions	

COMMONWEALTH OF VIRGINIA
DEPARTMENT OF TRANSPORTATION

STRUCTURE AND BRIDGE DIVISION

ABUTMENT A AND B PLAN AND ELEVATION

Designed: JCH	Date	Plan No.	Sheet No.
Drawn: AMJ	July 2012	289-16	5 of 16
Checked: CML			

b28916005.dgn

12/12/2012

STATE	FEDERAL AID		STATE		SHEET NO.
	ROUTE	PROJECT	ROUTE	PROJECT	
VA.	—		360	0360-964-120, B607	6

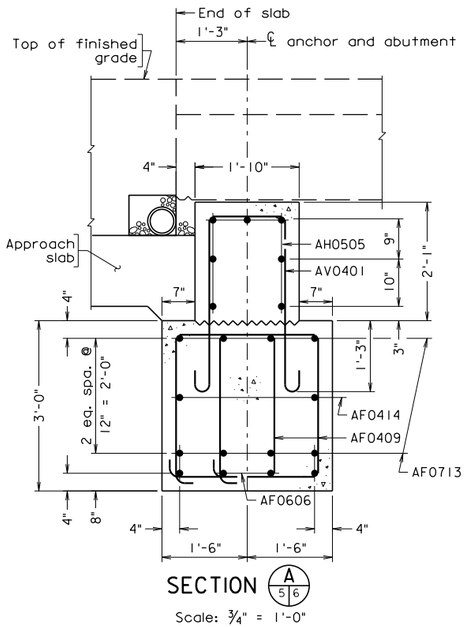

SECTION A (5 | 6)

Scale: 3/4" = 1'-0"

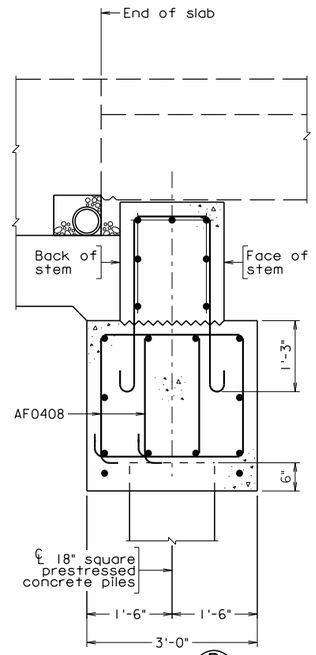

SECTION B (5 | 6)

For items shown but not detailed see SECTION A-A.

Scale: 3/4" = 1'-0"

b28916006.dgn

VDOT S&B DIVISION
RICHMOND, VA
STRUCTURAL ENGINEER

No.	Description	Date
	Revisions	

COMMONWEALTH OF VIRGINIA
DEPARTMENT OF TRANSPORTATION

STRUCTURE AND BRIDGE DIVISION

ABUTMENT A AND B DETAILS

Designed: JCH	Date	Plan No.	Sheet No.
Drawn: AMJ	July 2012	289-16	6 of 16
Checked: CML			

12/12/2012

STATE	FEDERAL AID		STATE		SHEET NO.
	ROUTE	PROJECT	ROUTE	PROJECT	
VA.	—		360	0360-964-120, B607	7

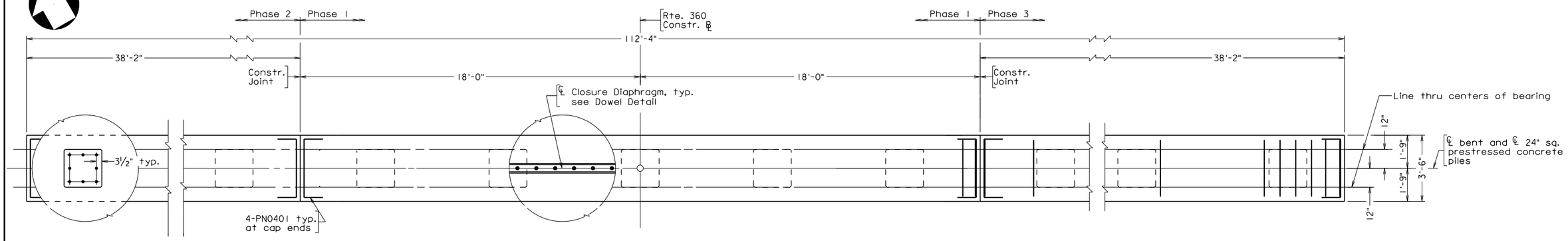

PLAN

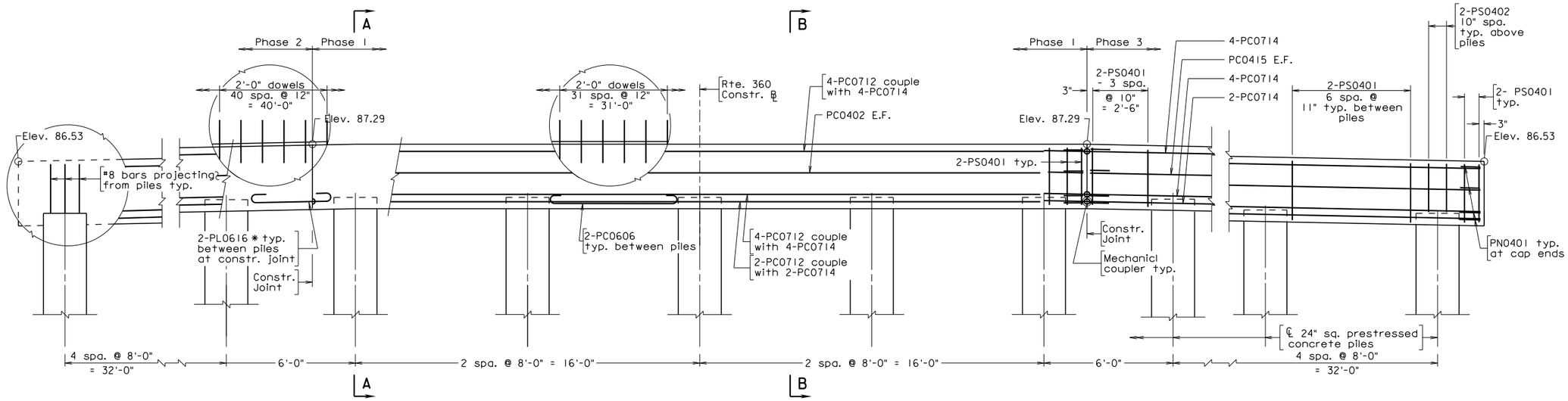

ELEVATION

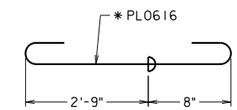

MECHANICAL COUPLER DIAGRAM

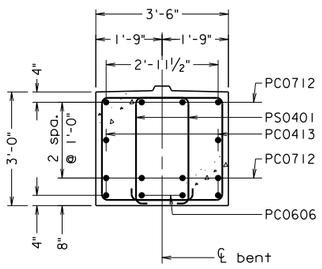

SECTION B-B
Scale: ½" = 1'-0"

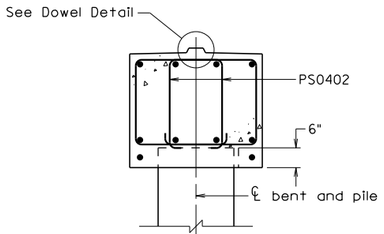

SECTION A-A
Scale: ½" = 1'-0"

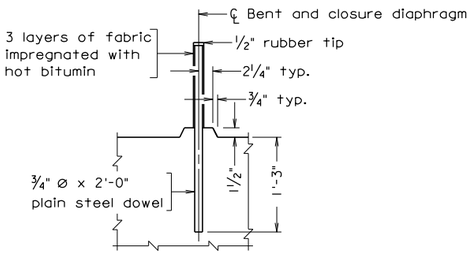

DOWEL DETAIL
Not to scale

Scale: ⅜" = 1'-0" unless otherwise noted

b28916007.dgn

VDOT S&B DIVISION
RICHMOND, VA
STRUCTURAL ENGINEER

No.	Description	Date
Revisions		

COMMONWEALTH OF VIRGINIA
DEPARTMENT OF TRANSPORTATION
STRUCTURE AND BRIDGE DIVISION

BENT

Designed: JCH	Date	Plan No.	Sheet No.
Drawn: CML	July 2012	289-16	7 of 16
Checked: CML			

12/12/2012

STATE	FEDERAL AID		STATE		SHEET
	ROUTE	PROJECT	ROUTE	PROJECT	NO.
VA.	—		360	0360-964-120, B607	8

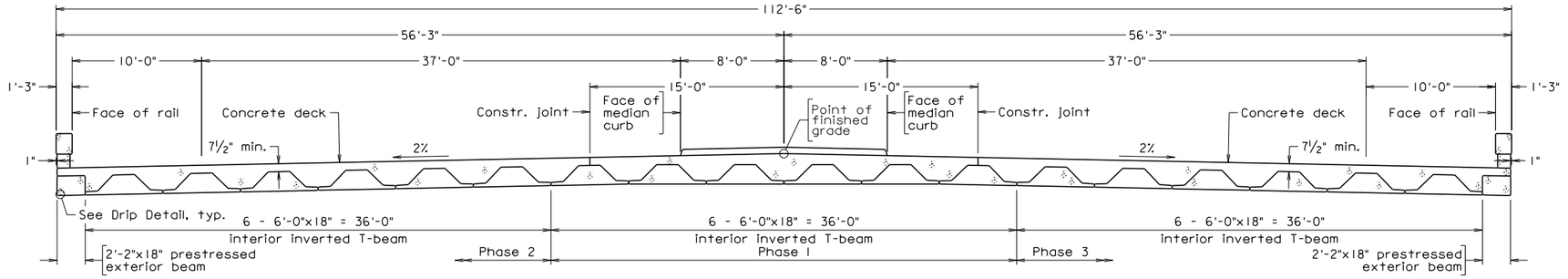

TRANSVERSE SECTION

NOTES:

All keyway surfaces shall be cleaned of all dirt, laitance and loose aggregate by means of sandblasting and pre-wetted prior to the grouting of shear keys.

All grouting of shear keys shall be done in one continuous operation without interruption for each span. Care shall be taken to prevent leakage of grout into precast holes for transverse tendons or from bottoms of shear keys.

The grout in the shear keys shall be a non-shrink grout in accordance with Section 218.03(d) of the Specifications having a minimum compressive strength of 5000 psi within 24 hours.

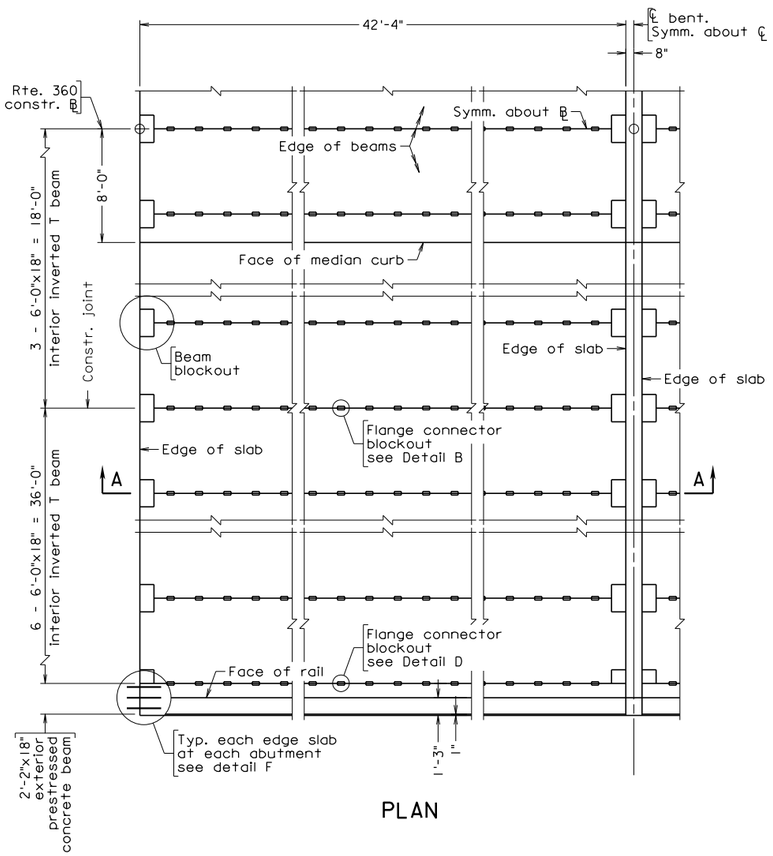

PLAN

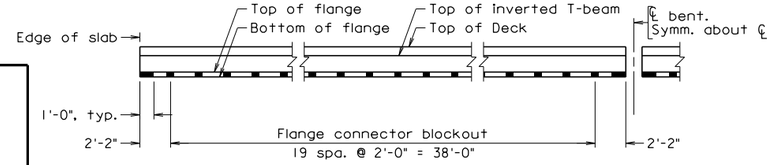

SECTION A-A

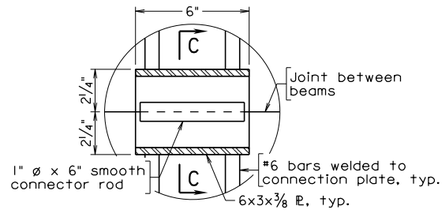

DETAIL B

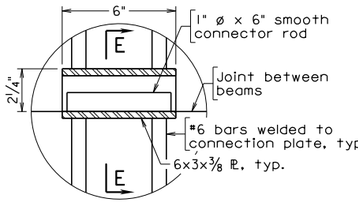

DETAIL D

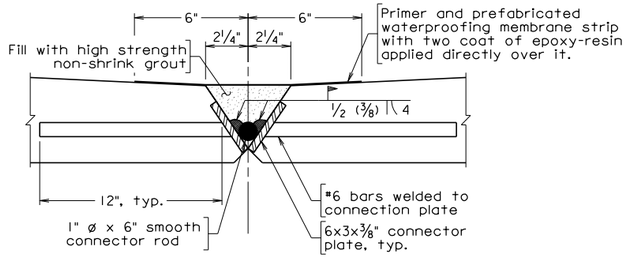

SECTION C-C

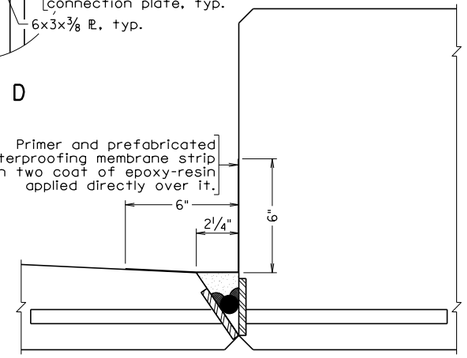

SECTION E-E

For items shown but not detailed, see Section C-C

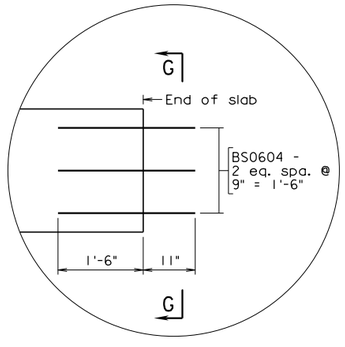

DETAIL F

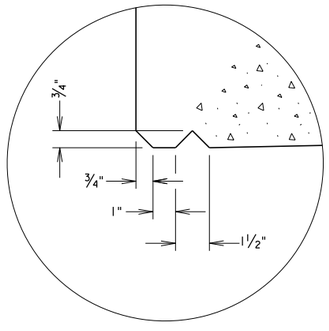

DRIP DETAIL

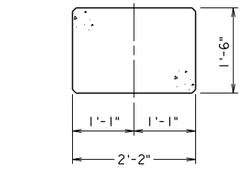

PRESTRESSED CONCRETE BEAM 2'-2" X 18"

Drip notch not shown for clarity

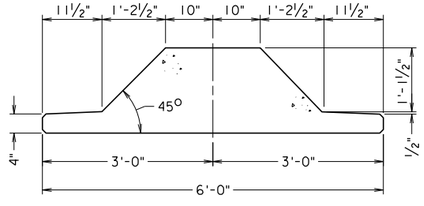

PRESTRESSED CONCRETE INVERTED T-BEAM 6'-0" X 18"

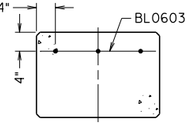

VIEW G-G

VDOT S&B DIVISION
RICHMOND, VA
STRUCTURAL ENGINEER

No.	Description	Date
	Revisions	

COMMONWEALTH OF VIRGINIA
DEPARTMENT OF TRANSPORTATION

STRUCTURE AND BRIDGE DIVISION

TRANSVERSE SECTION PRESTRESSED BEAM PLAN AND ELEVATION

Designed: CML	Date	Plan No.	Sheet No.
Drawn: AMJ	July 2012	289-16	8 of 16
Checked: JCH			

b28916008.dgn

12/12/2012

STATE	FEDERAL AID		STATE		SHEET
	ROUTE	PROJECT	ROUTE	PROJECT	NO.
VA.	—		360	0360-964-120, B607	9

Notes:

In lieu of splicing several reinforcing bars to form each stirrup, the stirrup may be made from one single bar.

All reinforcing bars shall be corrosion resistant reinforcing low carbon/chromium steel.

Slab corners damaged during construction shall be restored to their shape as shown on the plans by an approved epoxy mortar.

The Contractor shall submit prestressing strand pattern to the Engineer for approval.

Due to construction tolerances, adjustment to the bridge seat elevations may be needed. It is the Contractor's responsibility to make such adjustment as directed by the Engineer to insure the full bearing of the slab on all the pads. Cost of adjustment shall be included in other bid items.

Slab ends shall be finished in accordance with Section 405 of the Specifications.

4 - 1/2 " ø strands stressed to 1.000 lbs. may be substituted for 4 - BL05 series bars.

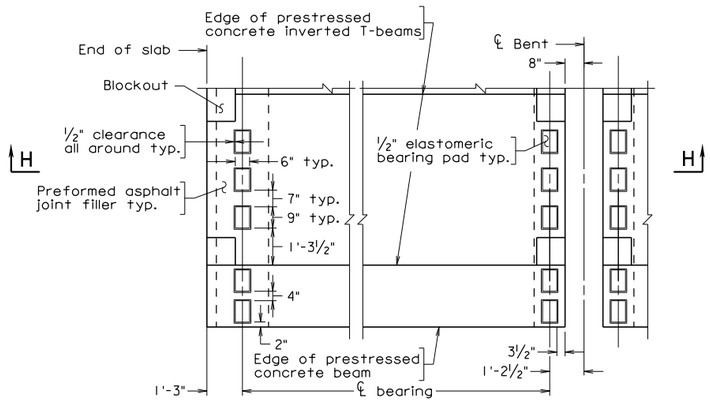

PLAN

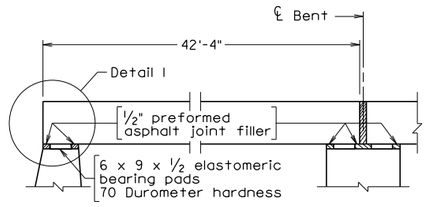

SECTION H-H

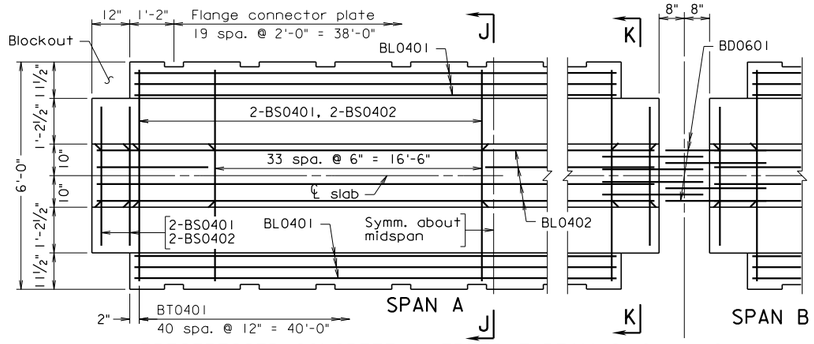

PRESTRESSED CONCRETE INVERTED T-BEAM 6'-0" X 18"

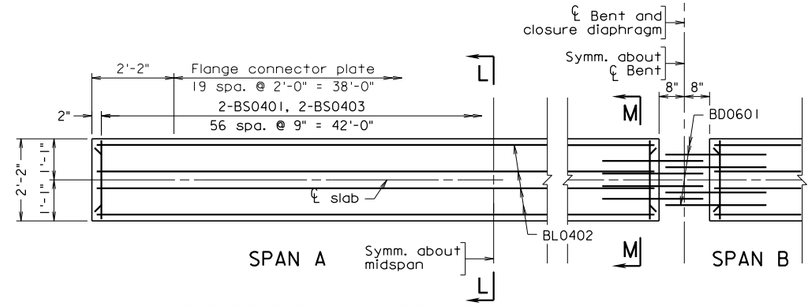

PRESTRESSED CONCRETE BEAM 2'-2" X 18"

PART PLAN OF MEMBER

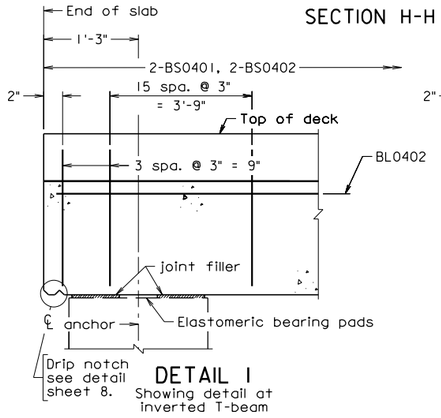

DETAIL I
Showing detail at inverted T-beam

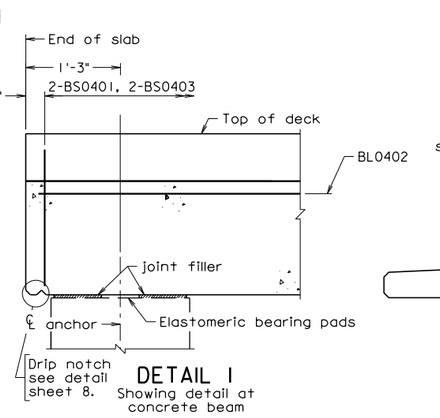

DETAIL I
Showing detail at concrete beam

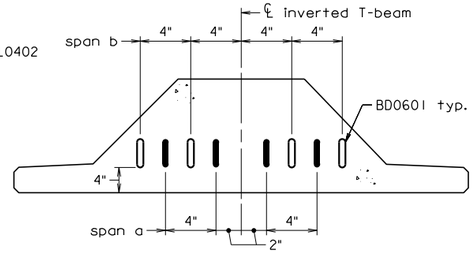

SECTION K-K

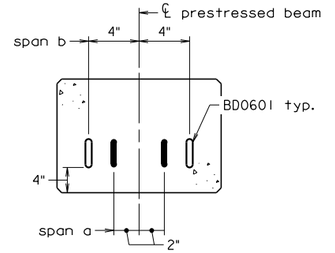

SECTION M-M

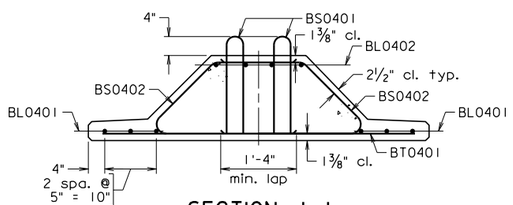

SECTION J-J
Showing location of reinforcing steel

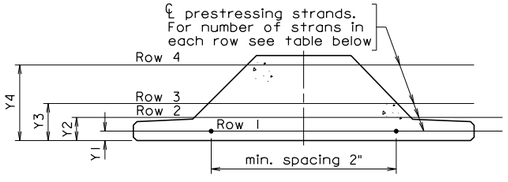

SECTION J-J
Showing location of prestressing strands

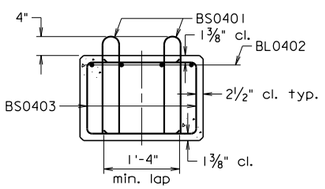

SECTION L-L
Showing location of reinforcing steel

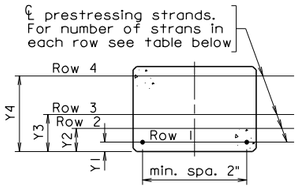

SECTION L-L
Showing location of prestressing strands

REINFORCING STEEL SCHEDULE

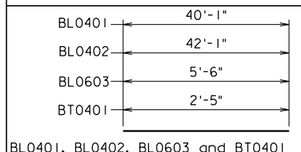

BL0401, BL0402, BL0603 and BT0401

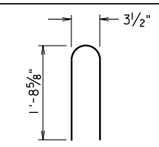

BS0401

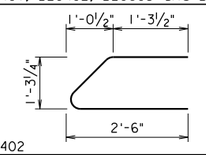

BS0402

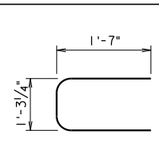

BS0403

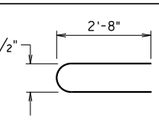

SD0601

Slab Size	Mark	No.	Size	Pin ø	Length	Location
6'-0" X 18" prestressed T-beam	BL0401	6	#4	——	40'-1"	Top longitudinal
	BL0402	4	#4	——	42'-1"	Top longitudinal
	BS0401	208	#4	3½"		Transverse
	BS0402	208	#4	2"		Transverse
	BT0401	41	#4	——	5'-6"	Transverse
	BD0601	4	#6	4½"		Longitudinal, end
2'-2" X 18" prestressed concrete beam	BL0402	4	#4	——	42'-1"	Top longitudinal
	BL0603	3	#6	——	2'-5"	Longitudinal, end
	BS0401	114	#4	3½"		Transverse
	BS0403	114	#4	2"		Transverse
	BT0401	41	#4	——	5'-6"	Transverse
	BD0601	4	#6	4½"		Longitudinal, end

No. of bars shown is for one beam.

PRESTRESSING STEEL DATA TABLE

Strand Type	Prestress Concrete Beam	No. of Strands Row 1	Row 2	Row 3	Row 4	Y1 in.	Y2 in.	Y3 in.	Y4 in.	Total number of strands per slab	Prestressing force per strand-lbs.	Net camber N in.
0.6 ø Low - Relaxation Strands	inverted T-beam 6'-0"x18"	12	12		2	2	4		16	26	43,940	½
	concrete beam 2'-2"x18"	11			4	2			16	15	43,940	½

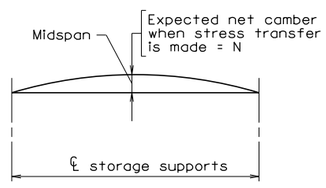

CAMBER DIAGRAM

VDOT S&B DIVISION
RICHMOND, VA
STRUCTURAL ENGINEER

No.	Description	Date
	Revisions	

COMMONWEALTH OF VIRGINIA
DEPARTMENT OF TRANSPORTATION
STRUCTURE AND BRIDGE DIVISION

PRESTRESSED BEAM DETAILS

Designed: CML	Date	Plan No.	Sheet No.
Drawn: AMJ	July 2012	289-16	9 of 16
Checked: JCH			

b28916009.dgn

12/12/2012

STATE	FEDERAL AID		STATE		SHEET NO.
	ROUTE	PROJECT	ROUTE	PROJECT	
VA.	—		360	0360-964-120, B607	10

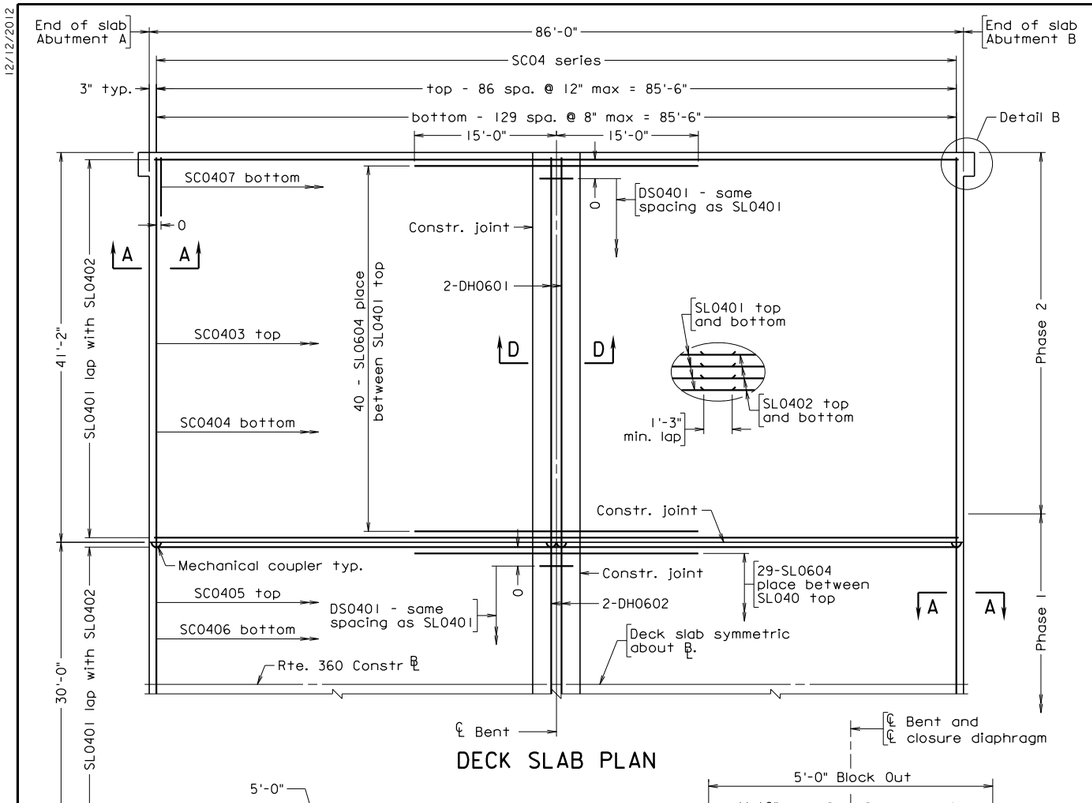

DECK SLAB PLAN

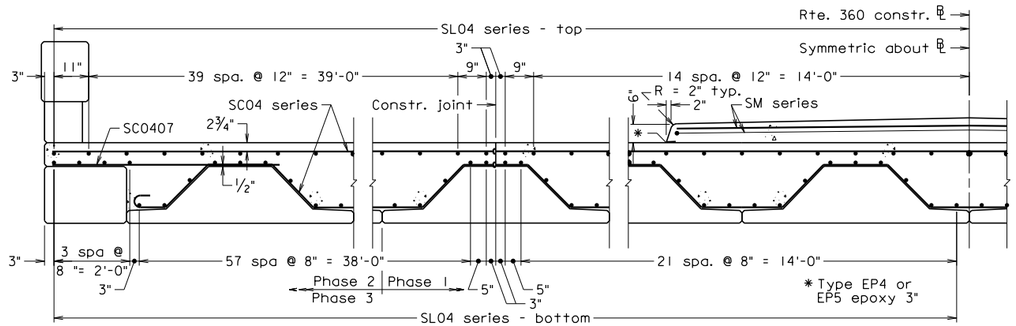

SLAB EDGE CONSTR. JOINT MEDIAN

PART SECTIONS
Not to scale

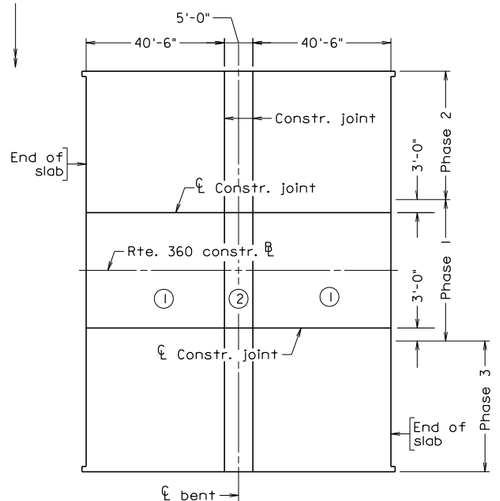

CONCRETE PLACEMENT SCHEDULE
Not to scale

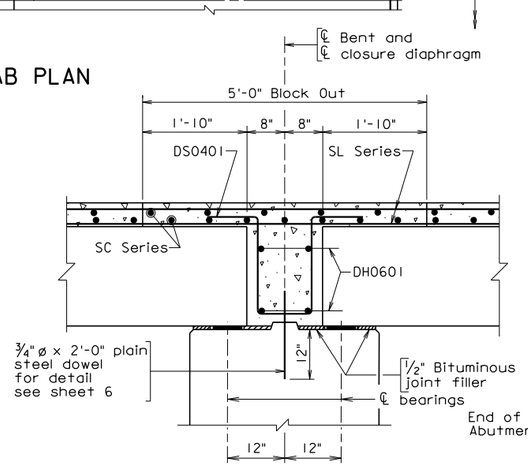

SECTION D-D
Scale: ¾" = 1'-0"

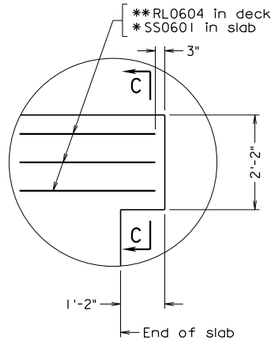

DETAIL B
Scale: ½" = 1'-0"

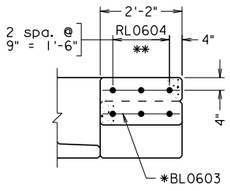

SECTION C-C
Scale: ½" = 1'-0"

* Bars are included in the prestressed slab units. See Superstructure sheets for details and quantities.

** Bars are included in the Kansas Corral Railing. See Railing sheets for details and quantities.

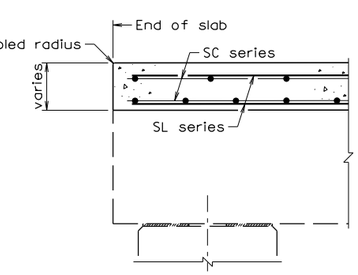

SECTION A-A
Not to scale

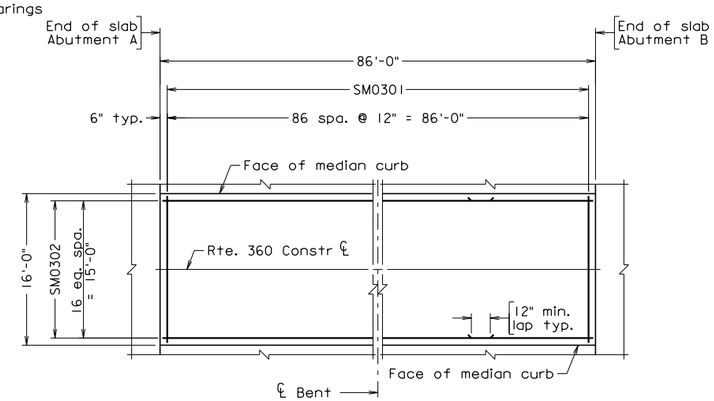

MEDIAN SLAB PLAN

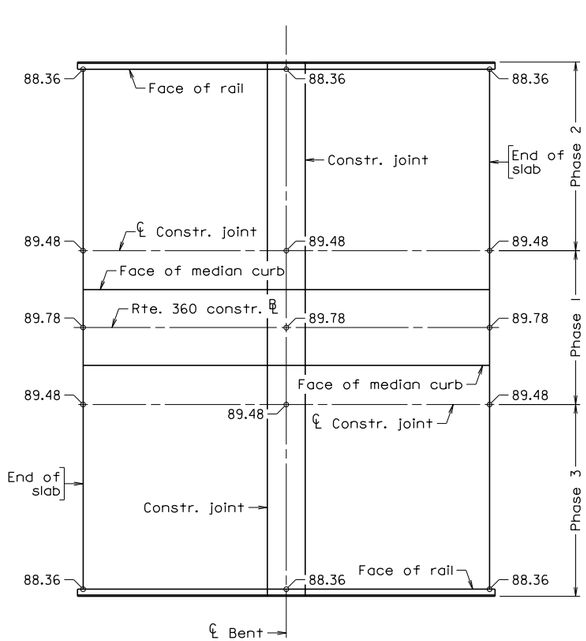

DECK SLAB ELEVATION
Not to scale

b28916010.dgn

VDOT S&B DIVISION
RICHMOND, VA
STRUCTURAL ENGINEER

Scale 2:0 = 1'-0" unless otherwise noted

No.	Description	Date
	Revisions	

COMMONWEALTH OF VIRGINIA
DEPARTMENT OF TRANSPORTATION

STRUCTURE AND BRIDGE DIVISION

DECK SLAB PLAN AND ELEVATION

Designed: CML	Date	Plan No.	Sheet No.
Drawn: AMJ	July 2012	289-16	10 of 16
Checked: JCH			

12/12/2012

STATE	FEDERAL AID		STATE		SHEET NO.
	ROUTE	PROJECT	ROUTE	PROJECT	
VA.	—		360	0360-964-120, B607	11

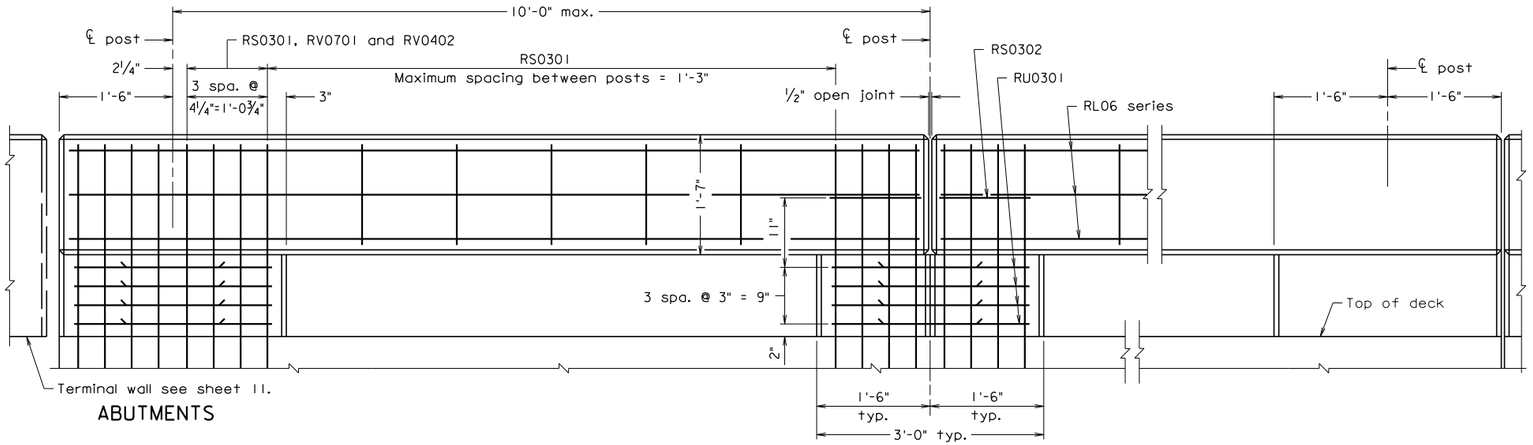

ABUTMENTS

TYPICAL ELEVATION

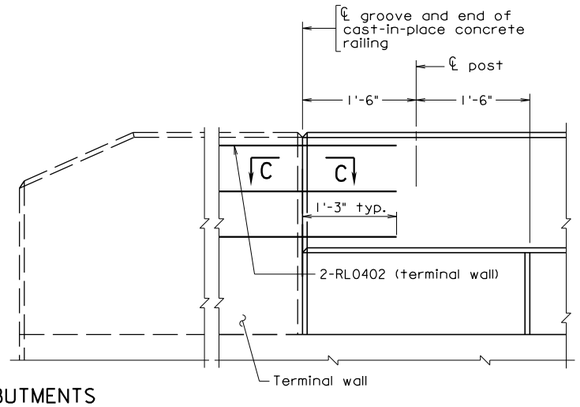

ABUTMENTS

PART ELEVATION
Terminal Wall
on Superstructure

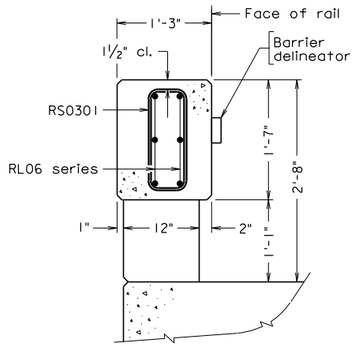

TYPICAL SECTION
BETWEEN POSTS
Reinforcing steel on deck not shown

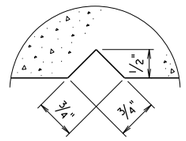

SECTION C-C
both sides of post
Not to scale
Groove detail for
or joint

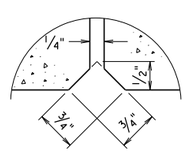

SECTION D-D
Not to scale
Deflection joint detail
for both sides of rail
and post

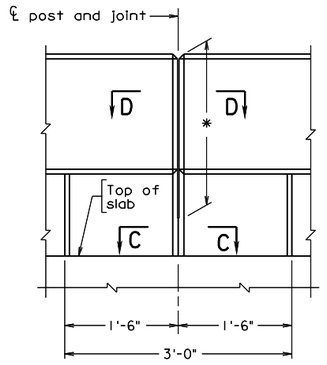

BENTS
Slab continuous over bent
* Open deflection joint
2"-2" deep

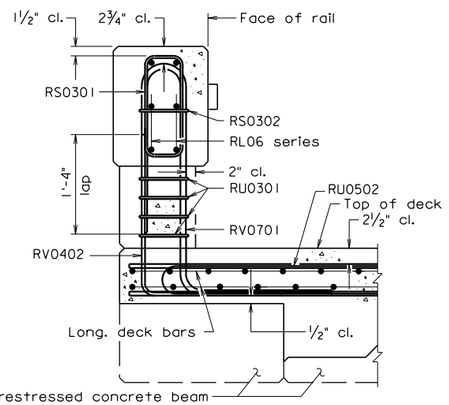

DECK WITH PRESTRESSED
CONCRETE UNITS

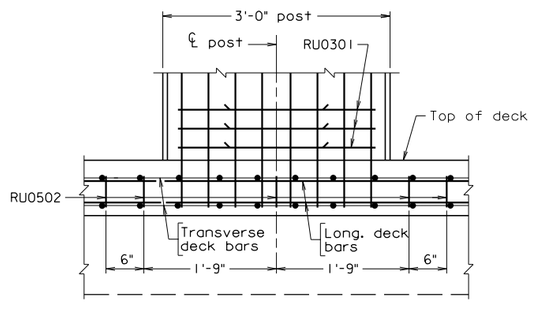

ELEVATION SHOWING RU0502 PLACEMENT
IN DECK

Notes:

All reinforcing bars shall be corrosion resistant reinforcing low carbon/ chromium steel.

Barrier delineator size, color, and spacing to be in accordance with the Specifications. Cost of delineator to be included in the price bid for railing. Reflective surface of barrier delineator, in all instances, to be facing oncoming traffic.

The Contractor shall determine all dimensions and details on this sheet and terminal wall sheet necessary for installation.

All bevels for concrete on this sheet and on terminal wall sheet shall be ¾". Rounded edges with 1" radius may be used in lieu of bevels along top of railing and terminal walls.

All concrete, including terminal walls shall be Class A4.

Bid item for railing and terminal walls shall include concrete noted in plans and reinforcing steel indicated in Reinforcing Steel Schedule.

Plan dimensions shown on this sheet and terminal wall sheet are measured in the respective horizontal and vertical planes. The reinforcing shown has been detailed based on standard 1/4" per foot horizontal slope. The Contractor shall adjust the reinforcing steel as required for the plan horizontal slope and vertical gradient.

12

For details and reinforcing steel schedule of terminal wall, see sheet 11.

REINFORCING STEEL SCHEDULE

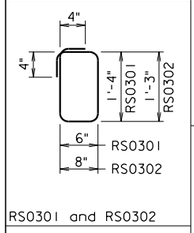

RS0301 and RS0302

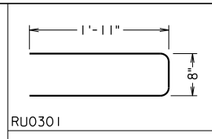

RU0301

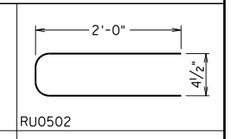

RU0502

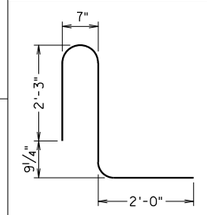

RV0701

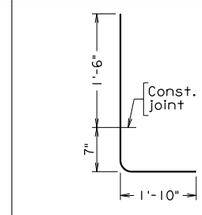

RV0402

Mark	No.	Size	Pin ø	Length	Location
RS0301		#3	2¼"	3'-11"	Rail
RS0302		#3	2¼"	4'-1"	Posts
RU0301		#3	2¼"	4'-4"	Posts
RU0502		#5	3¾"	4'-2"	Slab at posts (Deck Slabs)
RV0701		#7	5¼"	7'-5"	Posts
RV0402		#4	3"	3'-10"	Posts

Dimensions in bending diagram are out-to-out of bars, except as shown.

Gross concrete quantities above roadway slab :
Railing : C.Y. = Lin. Ft. x 0.085

BCR-4 MOD. 04-06-2012

b28916011.dgn

VDOT S&B DIVISION
RICHMOND, VA
STRUCTURAL ENGINEER

No.	Description	Date
	Revisions	

COMMONWEALTH OF VIRGINIA
DEPARTMENT OF TRANSPORTATION

STRUCTURE AND BRIDGE DIVISION

CAST-IN-PLACE CONCRETE RAILING 32" KANSAS CORRAL W/O CURB

Designed: CMJ	Date	Plan No.	Sheet No.
Drawn: AMJ	July 2012	289-16	11 of 16
Checked: JCH			

Scale: 1" = 1'-0", unless otherwise shown.

12/12/2012

STATE	FEDERAL AID		STATE		SHEET NO.
	ROUTE	PROJECT	ROUTE	PROJECT	
VA.	—		360	0360-964-120, B607	12

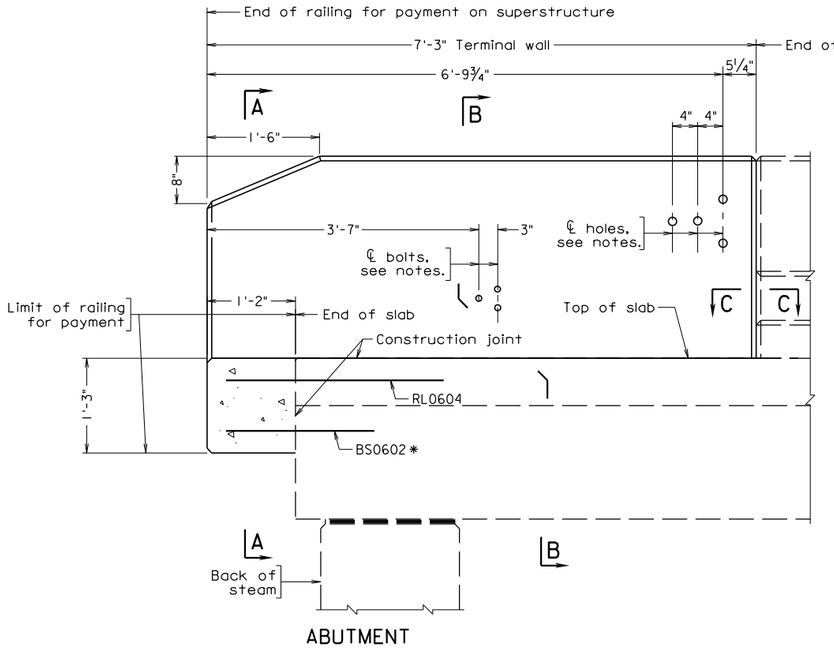

ABUTMENT

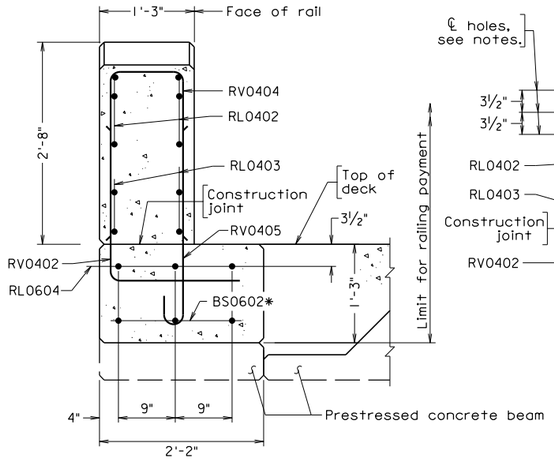

SECTION A-A

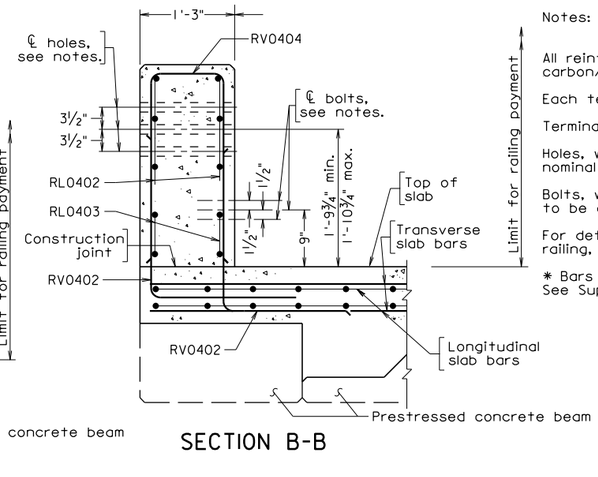

SECTION B-B

Notes:

All reinforcing bars shall be corrosion resistant reinforcing low carbon/chromium steel.

Each terminal wall shall be cast as one piece.

Terminal walls are detailed to take guardrail attachment GR-FOA-1.

Holes, where shown, shall be formed with sleeves of 1½" diameter nominal pipe.

Bolts, where shown, shall be ⅝" dia. expansion anchor bolts, 6" long to be drilled and installed when rub rail is attached.

For details and reinforcing steel schedule of cast-in-place concrete railing, see sheet 10.

* Bars are included in the prestressed concrete units. See Superstructure sheets for details and quantities.

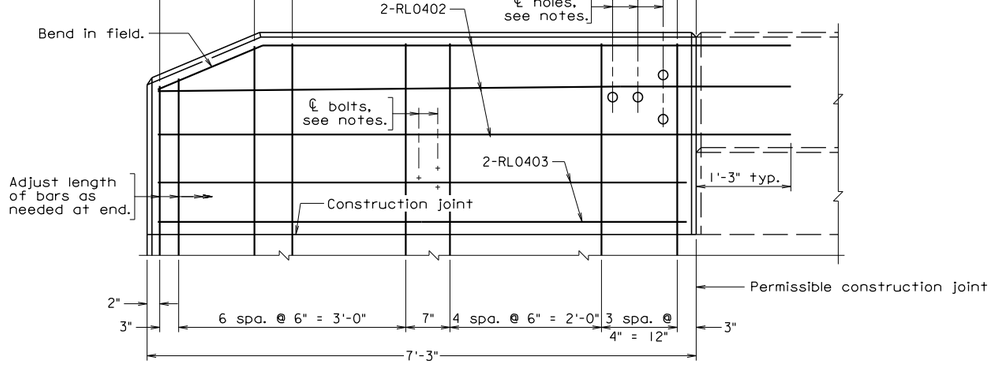

ELEVATION - TERMINAL WALL

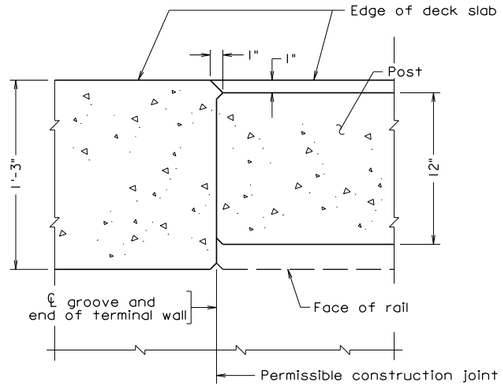

SECTION C-C
Scale: 2" = 1'-0"

REINFORCING STEEL SCHEDULE

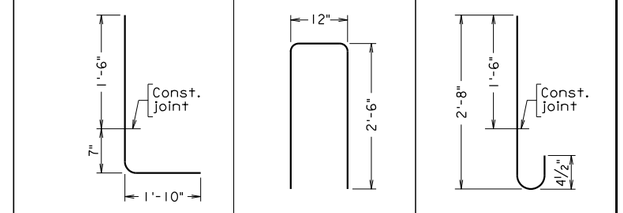

RV0402 RV0404 RV0405

Mark	No.	Size	Pin ø	Length	Location
RL0402		#4	—	8'-4"	Terminal wall
RL0403		#4	—	6'-11"	Terminal wall
RL0604		#6	—	4'-0"	Terminal wall end support
RV0402		#4	3"	3'-10"	Terminal wall
RV0404		#4	3"	5'-10"	Terminal wall
RV0405		#4	3"	3'-2"	Terminal wall

Dimensions in bending diagram are out-to-out of bars, except as shown.

04-06-2012

b28916012.dgn

BCR-9 MOD.

VDOT S&B DIVISION
RICHMOND, VA
STRUCTURAL ENGINEER

No.	Description	Date
	Revisions	

COMMONWEALTH OF VIRGINIA
DEPARTMENT OF TRANSPORTATION

STRUCTURE AND BRIDGE DIVISION

CAST-IN-PLACE TERMINAL WALL 32" KANSAS CORRAL

Designed: CMJ	Date	Plan No.	Sheet No.
Drawn: AMJ	July 2012	289-16	12 of 16
Checked: JCH			

12/12/2012

STATE	FEDERAL AID		STATE		SHEET NO.
	ROUTE	PROJECT	ROUTE	PROJECT	
VA.	—		360	0360-964-120, B607	13

POINTS	PICK UP POINTS
1	0.292L — 0.708L; L
2	0.207L — 0.586L — 0.207L; L
3	0.145L — 0.355L — 0.355L — 0.145L; L
4	0.107L — 0.262L — 0.262L — 0.262L — 0.107L; L

Unless special lifting devices are attached for pick-up, pick-up points shall be plainly marked on all piles after removal of the forms. The pile shall be supported only at the indicated pick-up points while in storage or while being handled.

The use of proper rigging is required to insure that the pick-up points remain in a straight line during lifting and when positioning the pile for driving.

The use of special embedded or attached lifting devices, the employment of other pick-up points or any other method of pick-up shall be subject to approval by the Engineer.

PILE PICK-UP DATA

Pile size W (in.)	Approx. Wt. per LF	Maximum lengths for various pick-up systems			
		1-Point	2-Point	3-Point	4-Point
W	Lbs.	L	L	L	L
10"	140	47'	66'	95'	129'
12"	150	51'	73'	104'	141'
14"	204	55'	78'	112'	152'
16"	267	62'	88'	126'	171'
18"	338	64'	90'	129'	175'
20"	417	69'	97'	138'	188'
24"	600	72'	102'	146'	198'

Maximum lengths are determined from impact loads. L is the maximum pick-up length based on a concrete compressive strength of 5000 psi. If piles are picked up when concrete strength is less than 5000 psi, the maximum pick-up length shall be the tabulated length reduced by 1% for every 250 psi below 5000 psi.

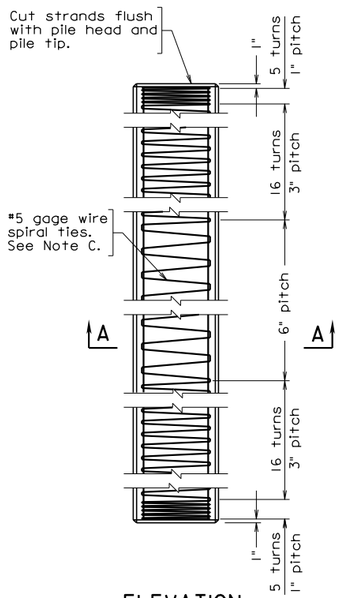

ELEVATION

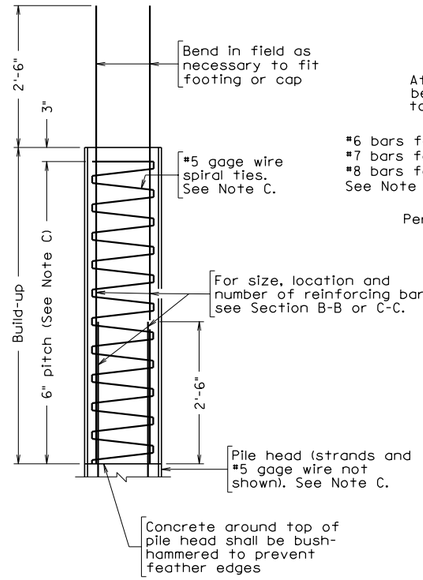

BUILD-UP WITHOUT DRIVING
See Note B

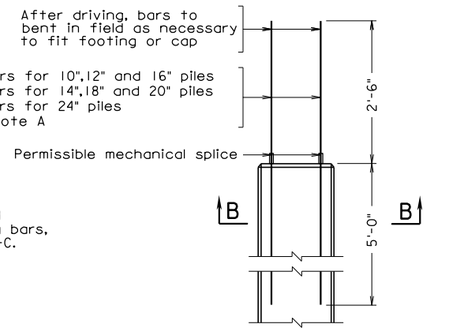

ELEVATION
Strands and #5 gage wire not shown

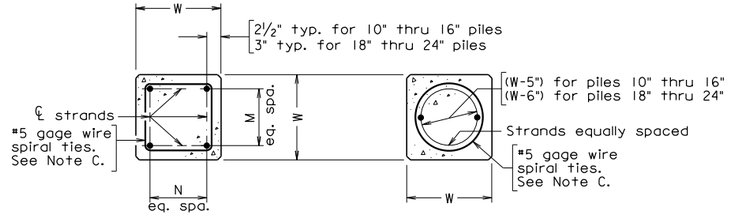

SQUARE CIRCULAR

SECTION A-A: STRAND PATTERN FOR PILE

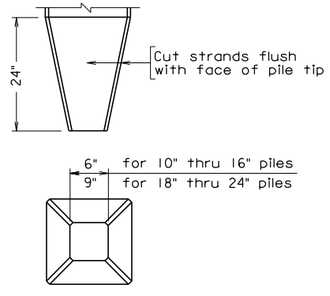

PILE TIP

Pile tip(s) shall be used only when specified. Strands not shown.

PILE DATA

Pile size W (in.)	Strand pattern	Total no. of strands in pile	Diameter of strands in.	Strand spacings M	Strand spacings N	Prestressing force per strand pounds	Effective prestress after losses psi
10"	Square	4	½	4	4	28,910	966
	Circular	4	½	—	—	28,910	966
12"	Square	4	½	4	4	30,970	751
	Circular	4	½	—	—	30,970	751
14"	Square	6	½	2	4	30,970	820
	Circular	6	½	—	—	30,970	820
16"	Square	8	½	2	2	30,970	836
	Circular	8	½	—	—	30,970	836
18"	Square	10	½	3	2	30,970	826
	Circular	10	½	—	—	30,970	826
20"	Square	12	½	3	3	30,970	805
	Circular	12	½	—	—	30,970	805
24"	Square	16	½	4	4	30,970	751
	Circular	16	½	—	—	30,970	751

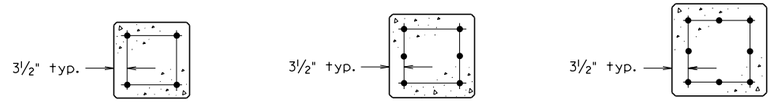

10", 12" and 14" PILES 16" and 18" PILES 20" and 24" PILES

SECTION B-B: PILE HEAD
See Note B

Note:

All concrete shall be Class A5 having a minimum compressive cylinder strength at 28 days equal to 5000 psi and a minimum compressive cylinder strength at time of release of strands equal to 3500 psi.

All strands shall be low relaxation and shall have an ultimate strength of 270 ksi.

Deformed reinforcing bars shall conform to ASTM A615, Grade 60.

One splice will be permitted where the length of pile required is greater than the maximum for 2-point pick-up unless specifically prohibited.

Build-ups shall be used only with written permission by the Engineer and then only after driving is complete.

Subject to approval by the Engineer, the bars projecting from the pile head may be cut prior to driving and rewelded upon completion of driving. The method of welding used shall develop the tensile strength of the bar.

Mechanical splices for reinforcing bars shall be in accordance with Section 406.03(e) of the Specifications. The Contractor shall provide adequate shielding to protect the ends of the reinforcing bars until the pile is driven and the bars are spliced.

When pile cut-off is greater than 2'-6" at least 30 inches of all the strands shall project into the cap or footing to serve for anchorage.

Where piles are exposed in bridges over tidal water such as in pile bents and in footings constructed above Mean High Tide elevation, the spiral ties and all other reinforcing bars in the pile shall be hot dip galvanized.

Note A:
In lieu of the reinforcing bars projecting from the head:
1. The pile may be cast 2'-6" longer than required. After driving the concrete pile, remove the concrete from the added length to expose the strands. The strands must be thoroughly cleaned before casting the footing or cap; or
2. 1⅜" ø preformed plain holes or 2" ø holes formed with galvanized corrugated metal may be used. After driving the pile and cleaning out the holes, the #6, #7 or #8 reinforcing bars shall be installed and the holes shall be filled with approved non-shrink grout.

Note B:
If alternate circular strand arrangement is used, bar extension must be placed to fit.

Note C:
For Seismic Performance Category B bridges (structures), #4/0 gage wire or #3 bars shall be used and the pitch shall be 3".

b28916013.dgn

06-14-2010

BPP-1

Sealed and Signed by:
Julius F.J. Volgyi Jr.
Lic. No. 010487
On the date of
June 14, 2010

A copy of the original sealed and signed standard drawing is on file in the Central Office.

VDOT S&B DIVISION
RICHMOND, VA
STRUCTURAL ENGINEER

No.	Description	Date
	Revisions	

COMMONWEALTH OF VIRGINIA
DEPARTMENT OF TRANSPORTATION
STRUCTURE AND BRIDGE DIVISION

PRESTRESSED CONCRETE PILES SQUARE: 10" THRU 24"

Designed: S&B...DIV	Date	Plan No.	Sheet No.
Drawn: ....S&B...DIV	July 2012	289-16	13 of 16
Checked: S&B...DIV			

Not to scale

12/12/2012

STATE	FEDERAL AID		STATE		SHEET NO.
	ROUTE	PROJECT	ROUTE	PROJECT	
VA.	—		360	0360-964-120, B607	14

REINFORCING STEEL SCHEDULE

MARK	NO.	BAR SIZE	PIN DIA. FT-IN	LENGTH FT-IN	WEIGHT (LBS.)	LOCATION
				SUPERSTRUCTURE CORROSION RESISTANT REINFORCING - LOW CARBON/CHROMIUM STEEL		
SC0403	174	4		40-11	4756	DECK
SC0404	260	4	3	45-05	7800	DECK
SC0405	87	4		30-00	1743	DECK
SC0406	130	4	3	34-08	2990	DECK
SC0407	174	4		6-00	697	DECK
SL0401	572	4		40-00	15284	DECK
SL0402	286	4		8-00	1528	DECK
SL0604	143	6		30-00	6444	DECK
SM0301	87	3		15-06	507	MEDIAN
SM0302	34	3		29-02	373	MEDIAN
DH0601	8	6		40-11	492	CLOSURE DIAPHRAGM
DH0602	4	6		30-00	180	CLOSURE DIAPHRAGM
DS0401	116	4	2	5-11	458	CLOSURE DIAPHRAGM
TOTAL WEIGHT IN PRECEDING GROUP OF BARS					433252	
				APPROACH SLAB		
AS0701	470	7		9-08	9286	APPROACH SLAB
AS0502	238	5		9-08	2400	APPROACH SLAB
AS0505	144	5		38-06	5782	APPROACH SLAB
TOTAL WEIGHT IN PRECEDING GROUP OF BARS					49930	
				BENT		
PC0606	24	6	4 1/2	6-11	248	CAP
PC0712	10	7		36-00	736	CAP
PC0413	2	4		35-06	47	CAP
PC0714	20	7		37-11	1550	CAP
PC0415	4	4		37-06	100	CAP
PC0616	4	6	4 1/2	4-10	29	CAP
PS0401	200	4	2	9-05	1253	CAP
PS0402	60	4	2	8-10	352	CAP
PN0401	24	4	3	4-10	77	CAP
TOTAL WEIGHT IN PRECEDING GROUP OF BARS					4392	
				ABUTMENT A NEAT		
				CORROSION RESISTANT REINFORCING - LOW CARBON/CHROMIUM STEEL		
AH0403	18	4	3	3-03	39	STEM
AH0505	7	5		36-00	263	STEM
AH0506	14	5		37-11	554	STEM
AV0401	115	4	2	8-07	658	STEM
TOTAL WEIGHT IN PRECEDING GROUP OF BARS					1513	
				FOOTING		
AF0606	24	6	4 1/2	7-05	266	FOOTING
AF0408	60	4	2	8-00	320	FOOTING
AF0409	224	4	2	8-08	1294	FOOTING
AF0410	24	4	3	4-03	67	FOOTING
AF0713	10	7		36-00	736	FOOTING
AF0414	2	4		36-00	48	FOOTING
AF0715	20	7		37-11	1550	FOOTING
AF0416	4	4		37-11	101	FOOTING
AF0617	4	6	4 1/2	6-05	38	FOOTING
TOTAL WEIGHT IN PRECEDING GROUP OF BARS					4421	
				ABUTMENT B NEAT		
				CORROSION RESISTANT REINFORCING - LOW CARBON/CHROMIUM STEEL		
AH0403	18	4	3	3-03	39	STEM
AH0505	7	5		36-00	263	STEM
AH0506	14	5		37-11	554	STEM
AV0401	115	4	2	8-07	658	STEM
TOTAL WEIGHT IN PRECEDING GROUP OF BARS					1513	
				FOOTING		
AF0606	24	6	4 1/2	7-05	266	FOOTING
AF0408	60	4	2	8-00	320	FOOTING
AF0409	224	4	2	8-08	1294	FOOTING
AF0410	24	4	3	4-03	67	FOOTING
AF0713	10	7		36-00	736	FOOTING
AF0414	2	4		36-00	48	FOOTING
AF0715	20	7		37-11	1550	FOOTING
AF0416	4	4		37-11	101	FOOTING
AF0617	4	6	4 1/2	6-05	38	FOOTING
TOTAL WEIGHT IN PRECEDING GROUP OF BARS					4421	

DIMENSION TABLE

MARK	TYPE	A FT-IN	B FT-IN	C FT-IN	D FT-IN	E P FT-IN	F Q FT-IN	G R FT-IN	H FT-IN	I S FT-IN	J T FT-IN	K U FT-IN	L FT-IN	V FT-IN	N
SC0403	1	40-11													
SC0404	100	1-08 3/8	1-01	2-01 1/2	11 1/4	10 1/4			4 1/2	1-01 1/2	1-06 3/4"		39-03 1/2		5
SC0405	1	30-00													
SC0406	110	1-08 3/8	1-01	2-01 1/2		10 1/4				1-01 1/2	1-06 3/4"		30-00		4
SC0407	1	6-00													
SL0401	1	40-00													
SL0402	1	8-00													
SL0604	1	30-00													
SM0301	1	15-06													
SM0302	1	29-02													
DH0601	1	40-11													
DH0602	1	30-00													
DS0401	17		1-03	1-04	1-01										
AS0701	1	9-08													
AS0502	1	9-08													
AS0505	1	38-06													
PC0606	25	5-06							6						
PC0712	1	36-00													
PC0413	1	35-06													
PC0714	1	37-11													
PC0415	1	37-05													
PC0616	25	3-05							6						
PS0401	51		2-01	2-05 3/8					4 1/2						
PS0402	51		2-01	2-01 3/4					4 1/2						
PN0401	7		3-00	1-00	1-00										
AF0606	25	6-00							6						
AF0408	51		1-08	2-02					4 1/2						
AF0409	51		1-08	2-06					4 1/2						
AF0410	7		2-05	1-00	1-00										
AF0713	1	36-00													
AF0414	1	36-00													
AF0715	1	37-11													
AF0416	1	37-11													
AF0617	25	5-00							6						
AH0403	7		1-05	1-00	1-00										
AH0505	1	36-00													
AH0506	1	37-11													
AV0401	40		1-05	3-03	3-03				4						
AF0606	25	6-00							6						
AF0408	51		1-08	2-02					4 1/2						
AF0409	51		1-08	2-06					4 1/2						
AF0410	7		2-05	1-00	1-00										
AF0713	1	36-00													
AF0414	1	36-00													
AF0715	1	37-11													
AF0416	1	37-11													
AF0617	25	5-00							6						

DIMENSION VARIATION TABLE

MARK	NO. EA. LEN.	DIMEN-SION	FROM FT-IN	TO FT-IN	VARY BY FT-IN	DIMEN-SION	FROM FT-IN	TO FT-IN	VARY BY FT-IN

BENDING DIAGRAM

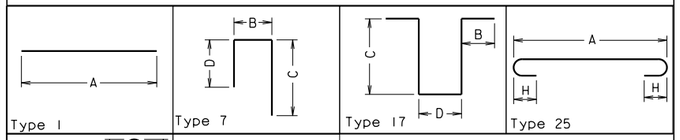

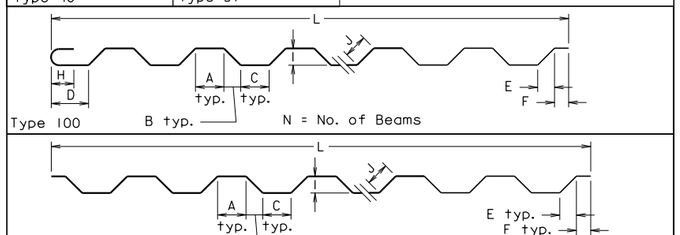

NOTES:

Dimensions in Bending Diagram are out-to-out of bars.

Weights in schedule are based on density of 490 lb/ft.^{3}

VDOT S&B DIVISION
RICHMOND, VA
STRUCTURAL ENGINEER

No.	Description	Date
	Revisions	

COMMONWEALTH OF VIRGINIA
DEPARTMENT OF TRANSPORTATION
STRUCTURE AND BRIDGE DIVISION

REINFORCING STEEL SCHEDULE

Designed: JCH/CML	Date	Plan No.	Sheet No.
Drawn: AMJ	July 2012	289-16	14 of 16
Checked: CML/JCH			

b28916014.dgn

12/12/2012

STATE	FEDERAL AID		STATE		SHEET NO.
	ROUTE	PROJECT	ROUTE	PROJECT	
VA.	—		360	0360-964-120, B607	15

10BH-002B — BRIDGE 607

STATION: 508+87 OFFSET: CL
LATITUDE: 37.593000° N LONGITUDE: 77.384611° W
SURFACE ELEVATION: 89.78 ft COORD. DATUM: NAD 83

Date(s) Drilled: 7-16-10 - 7-19-10
Drilling Method(s): Mud Rotary
SPT Method: Automatic Hammer
Other Test(s):
Driller: Wayne
Logger: Dwayne

GROUND WATER
▽ FIRST ENCOUNTERED AT 13.0 ft DEPTH
NO LONG TERM MEASUREMENTS TAKEN

DEPTH (ft)	ELEVATION (ft)	STANDARD PENETRATION TEST HAMMER BLOWS	SOIL RECOVERY (%)	SAMPLE LEGEND	SAMPLE INTERVAL	CORE RECOVERY (%)	ROCK QUALITY DESIGNATION	DIP ° STRATA	DIP ° JOINTS	STRATA LEGEND	FIELD DESCRIPTION OF STRATA	LAB DATA LL	LAB DATA PI	LAB DATA MOISTURE CONTENT (%)
0	90	5 10 26			0						0.0 / 89.78 TOPSOIL with a hard layer TOPS			
2					1.5						1.0 / 88.78 FILL - Brown clayey fine to coarse SAND FL			
4	85	2 2 5			3.5									
6					5									
8					8.5									
10	80	2 1 2			10									
12														
14		1 2 4			13.5									
16	75				15						15.0 / 74.78 Gray clayey GRAVEL GC			
18					18.5									
20	70	3 3 5			20						20.0 / 69.78 Gray silty CLAY CH			
22														
24	65	2 3 3			23.5									
26					25									
28		3 3 4			28.5									
30	60				30							70	44	54.0
32					33.5									
34	55	2 3 3			35						35.0 / 54.78 Gray sandy CLAY CH			
36														
38					38.5									
40	50	2 2 3												

REMARKS: RIG TYPE: Track Mounted.

PAGE 1 OF 3

10BH-002B — BRIDGE 607

STATION: 508+87 OFFSET: CL
LATITUDE: 37.593000° N LONGITUDE: 77.384611° W
SURFACE ELEVATION: 89.78 ft COORD. DATUM: NAD 83

Date(s) Drilled: 7-16-10 - 7-19-10
Drilling Method(s): Mud Rotary
SPT Method: Automatic Hammer
Other Test(s):
Driller: Wayne
Logger: Dwayne

GROUND WATER
▽ FIRST ENCOUNTERED AT 13.0 ft DEPTH
NO LONG TERM MEASUREMENTS TAKEN

DEPTH (ft)	ELEVATION (ft)	STANDARD PENETRATION TEST HAMMER BLOWS	SOIL RECOVERY (%)	SAMPLE LEGEND	SAMPLE INTERVAL	CORE RECOVERY (%)	ROCK QUALITY DESIGNATION	DIP ° STRATA	DIP ° JOINTS	STRATA LEGEND	FIELD DESCRIPTION OF STRATA	LAB DATA LL	LAB DATA PI	LAB DATA MOISTURE CONTENT (%)
40					40									
42														
44	45	3 3 5			43.5									
46					45							66	44	45.0
48														
50	40	3 4 4			48.5									
52					50									
54	35	8 7 7			53.5									
56					55									
58														
60	30	3 4 4			58.5									
62					60						60.0 / 29.78 Gray clayey SILT MH			
64		3 5 7			63.5									
66	25				65						65.0 / 24.78 Brown sandy CLAY CH			
68					68.5									
70	20	3 6 8			70							77	47	44.0
72					73.5									
74	15	4 5 7			75						75.0 / 14.78 Gray silty SAND SM			
76														
78					78.5									
80	10	3 3 6												

REMARKS: RIG TYPE: Track Mounted.

PAGE 2 OF 3

10BH-002B — BRIDGE 607

STATION: 508+87 OFFSET: CL
LATITUDE: 37.593000° N LONGITUDE: 77.384611° W
SURFACE ELEVATION: 89.78 ft COORD. DATUM: NAD 83

Date(s) Drilled: 7-16-10 - 7-19-10
Drilling Method(s): Mud Rotary
SPT Method: Automatic Hammer
Other Test(s):
Driller: Wayne
Logger: Dwayne

GROUND WATER
▽ FIRST ENCOUNTERED AT 13.0 ft DEPTH
NO LONG TERM MEASUREMENTS TAKEN

DEPTH (ft)	ELEVATION (ft)	STANDARD PENETRATION TEST HAMMER BLOWS	SOIL RECOVERY (%)	SAMPLE LEGEND	SAMPLE INTERVAL	CORE RECOVERY (%)	ROCK QUALITY DESIGNATION	DIP ° STRATA	DIP ° JOINTS	STRATA LEGEND	FIELD DESCRIPTION OF STRATA	LAB DATA LL	LAB DATA PI	LAB DATA MOISTURE CONTENT (%)
80					80									
82														
84	5	3 5 8			83.5									
86					85									
88														
90	0	3 6 9			88.5							NP	NP	27.0
92					90									
94	-5	3 6 8			93.5									
96					95									
98														
100	-10	3 8 12			98.5									
					100						100.0 / -10.22 Borehole Terminated			

REMARKS: RIG TYPE: Track Mounted.

PAGE 3 OF 3

Note: See Material and Sample Symbols List

17959

The subsurface information shown on the boring logs in these plans was obtained with reasonable care and recorded in good faith solely for use by the Department in establishing design controls for the project. The Department has no reason to suspect that such information is not reasonably accurate as an approximate indication of the subsurface conditions at the sites where the borings were taken. The Department does not in any way warrant or guarantee that such data can be projected as indicative of conditions beyond the limits of the borings shown; and any such projections by bidders are purely interpretive and altogether speculative. Further, the Department does not in any way guarantee, either expressly or by implication, the sufficiency of the information for bid purposes.

The boring logs are made available to bidders in order that they may have access to subsurface data identical to that which is possessed by the Department, and are not intended as a substitute for personal investigation, interpretation and judgment by the bidders.

A copy of the original signed geotechnical submittal is on file in the District Office.

No.	Description	Date
	Revisions	

COMMONWEALTH OF VIRGINIA
DEPARTMENT OF TRANSPORTATION
STRUCTURE AND BRIDGE DIVISION

0360-042-120
ENGINEERING GEOLOGY

Designed:	Date	Plan No.	Sheet No.
Drawn: SSJ	July 2012	289-16	15 of 16
Checked:			

b28916015.dgn

12/12/2012

STATE	FEDERAL AID		STATE		SHEET NO.
	ROUTE	PROJECT	ROUTE	PROJECT	
VA.	—		360	0360-964-120, B607	16

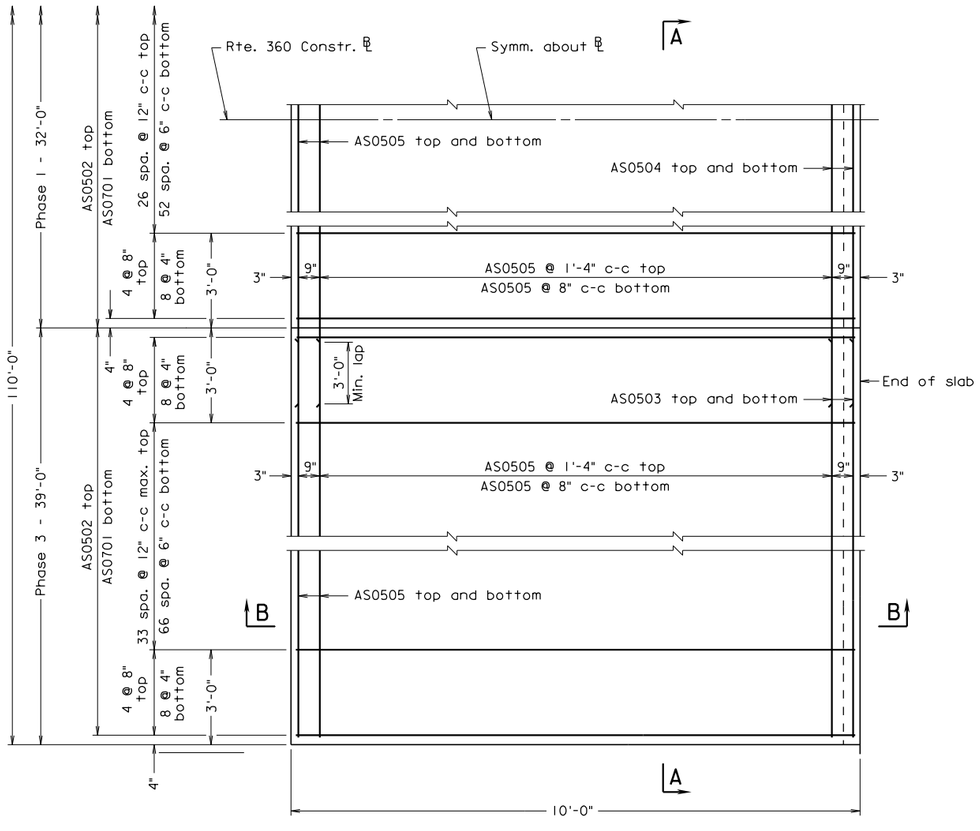

PLAN
(Abutment A shown, Abutment B opposite hand)
Not to Scale

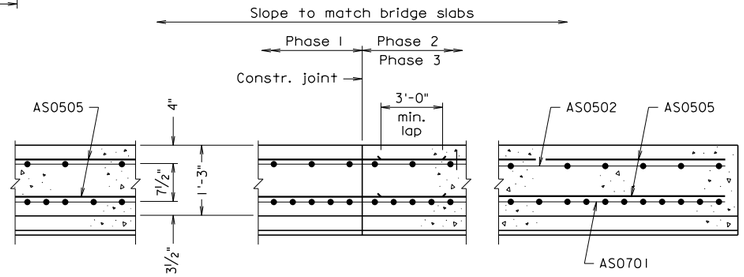

SECTION A-A
Scale: ¾" = 1'-0"

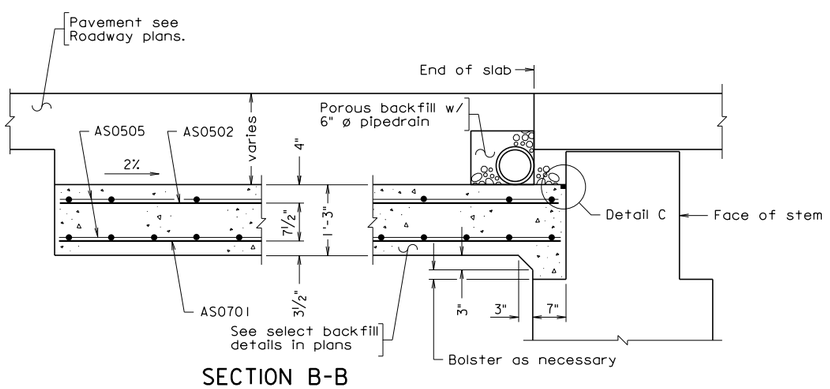

SECTION B-B
Scale: ¾" = 1'-0"

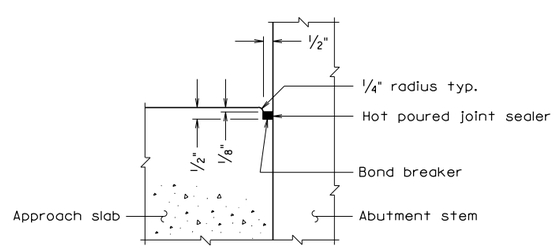

Detail C
Scale: 3" = 1'-0"

Notes:

All joints that are to be sealed shall be free of cracked and spalled areas and their faces shall be free of all foreign matter, curing compound, oils, greases and dirt. All faces must be sandblasted or brushed with a mechanical rotary wire brush. Just prior to sealing, the joint shall be blown out with oil-free compressed air.

Deformed reinforcing bars shall conform to ASTM A615, Grade 60 and shall have a yield strength of 60,000 psi.

All reinforcing bar dimensions except for bending diagram are to centers of bars.

The cost for the porous backfill w/ 6" ø pipe underdrain will be included in the price bid for concrete for the approach slab.

Prime select material with 0.35 gal. per sq. yd. Liquid Asphalt Material Type RC-70, RC-250 or MC-250 if aggregate base is exposed for more than 2 weeks.

The approach slab shall be wet cured in conformance with the specifications.

b28916016.dgn

BAS-11 MOD. 06-14-2010

VDOT S&B DIVISION
RICHMOND, VA
STRUCTURAL ENGINEER

No.	Description	Date
	Revisions	

COMMONWEALTH OF VIRGINIA
DEPARTMENT OF TRANSPORTATION
STRUCTURE AND BRIDGE DIVISION

APPROACH SLABS

Designed: CMI	Date	Plan No.	Sheet No.
Drawn: AMJ	July 2012	289-16	16 of 16
Checked: JCH			

Scale as noted

APPENDIX F – TESTING FRAME CAPACITY CALCULATIONS

TEST FRAME CAPACITY CALCULATIONS

0. Steel Properties for Sections Used

$F_y := 50$ ksi $E := 29000$ ksi $pi := 3.14159$

---

1. Actuator Mount

The actuator mount is a W21 stub-section that has been heavily stiffened (see image below). It spans between the two crossheads.

Span length: $L := 21$ in

At this span length, bending is not an issue with the stub section.

a. Stub Section Shear (AISC 360-10 Section G2.1.)

Conservative check assuming an unstiffened web - web thickness of the stub section was measured as 1"

$t_w := 1$ in $d := 21$ in $k := 0.95$ in

AISC G2.1.a: Rolled I-shaped section with: $h/t_w := 53.6$ in $<$ $2.24 \cdot \sqrt{\frac{E}{F_y}} = 53.95$

Therefore: $\phi_v := 1.00$ $C_v := 1.0$

$A_w := d \cdot t_w = 21$ in^2

$V_n := 0.6 \cdot F_y \cdot A_w \cdot C_v = 630$ kips

$\phi_v \cdot V_n = 630$ kips

The shear force in the stub section is equal to half of the actuator load

$P_{actuator.1a} := 2 \cdot \phi_v \cdot V_n$ $P_{actuator.1a} = 1260$ kips

---

2. Connection Stub Section - Crossbeam

a. Stub section - bolt hole bearing (AISC 360-10 Section J3.10.)

b. Stub section - shear yield/rupture (AISC 360-10 Section J4.2.)

c. Stub section - block shear (AISC 360-10 Section J4.3.)

It is noted that the stub section has been used for previous tests with loading over 300 kips. So this section is assumed to be okay.

d. Bolts - shear capacity (AISC 360-10 Section J3.6.)

Bolts used are a total of 8 No. 7/8" A325 Bolts acting in single shear per connection (2 connections per stub section)

AISC Table J3.2: $F_{nv} := 54$ ksi $A_b := \frac{pi \cdot \left(\frac{7}{8}\right)^2}{4} = 0.6$ $\frac{in^2}{bolt}$

AISC J3.6.: $\phi := 0.75$ $R_{nv} := F_{nv} \cdot A_b = 32.47$ $\frac{kips}{bolt}$

$\phi \cdot R_{nv} \cdot 8 = 194.83$ $\frac{kips}{connection}$

Each connection takes half of the load in the stub section, and the load in the stub section is equal to the actuator force

$P_{actuator.2d} := \phi \cdot R_{nv} \cdot 8 \cdot 2$ $P_{actuator.2d} = 389.66$ kips

e. Crossbeam - bolt hole bearing (AISC 360-10 Section J3.10.)

AISC J3.10: $\phi := 0.75$

Bolt diameter $d := \frac{7}{8}$ in $d_{hole} := 1 + \frac{1}{16} = 1.06$ in

Crossbeam is a W21 x 62: $l_c := 3 - d_{hole} = 1.94$ in $t := 0.400$ in $F_u := 65$ ksi

AISC J3.10.(a).(i): $R_n := 1.2 \cdot l_c \cdot t \cdot F_u = 60.45$ $\frac{kips}{bolt}$ > $2.4 \cdot d \cdot t \cdot F_u = 54.6$ $\frac{kips}{bolt}$

$R_n := 2.4 \cdot d \cdot t \cdot F_u = 54.6$ $\frac{kips}{bolt}$

$\phi \cdot R_n = 40.95$ $\frac{kips}{bolt}$

$\phi \cdot R_n \cdot 8 = 327.6$ $\frac{kips}{connection}$

Each crossbeam-stub section connection takes half of the load in the stub section which is equal to the load in the actuator

$P_{actuator.2e} := \phi \cdot R_n \cdot 8 \cdot 2$ $P_{actuator.2e} = 655.2$ kips

f. Crossbeam - shear yield/rupture (AISC 360-10 Section J4.2.)

W21 x 62: $F_y = 50$ ksi $F_u = 65$ ksi $d := 21.0$ in $t_w := 0.400$ in

AISC J4.10.2.(a): $A_{gv} := d \cdot t_w = 8.4$ in^2

$\phi_y := 1.00$

$R_{n.yield} := 0.60 \cdot F_y \cdot A_{gv} = 252$ $\frac{kips}{connection}$

AISC J4.10.2.(b): $d_{hole} = 1.06$ $\frac{in}{hole}$

$A_{nv} := d \cdot t_w - d_{hole} \cdot t_w \cdot 6 = 5.85$ in^2

$\phi_r := 0.75$

$R_{n.rupture} := 0.60 \cdot F_u \cdot A_{nv} = 228.15$ $\frac{kips}{connection}$

$\phi R_n := \min(\phi_y \cdot R_{n.yield}, \phi_r \cdot R_{n.rupture}) = 171.11$ $\frac{kips}{connection}$

Each connection takes half of the load in the stub section which is equal to the load in the actuator

$P_{actuator.2f} := 2 \cdot \phi R_n$ $P_{actuator.2f} = 342.22$ kips

g. Crossbeam - block shear strength (AISC 360-10 Section J4.3.)

W21 x 62: $d := 21.0$ in $t_w := 0.400$ in $d_{hole} = 1.06$ in

AISC J4.10.3: $F_u = 65$ ksi $A_{nv} := 2 \cdot t_w \cdot (d - 3 - 5.5 \cdot d_{hole}) = 9.73$ in^2

$U_{bs} := 1$ $A_{nt} := (5.5 - d_{hole}) \cdot t_w = 1.78$ in^2

$F_y = 50$ ksi $A_{gv} := d \cdot t_w = 8.4$ in^2

$\phi := 0.75$

$R_n := \min(0.60 \cdot F_u \cdot A_{nv} + U_{bs} \cdot F_u \cdot A_{nt}, 0.60 \cdot F_y \cdot A_{gv} + U_{bs} \cdot F_u \cdot A_{nt}) = 367.38$ $\frac{kips}{connection}$

Each connection takes half of the load in the stub section, the stub section is loaded with the full actuator force

$P_{actuator.2g} := 2 \cdot \phi \cdot R_n$ $P_{actuator.2g} = 551.06$ kips

3. W21 x 62 Crossbeam

a. Strength in bending (AISC 360-10 Section F2.)

Span length: $L := 95 \quad in$

Stub sections connecting to the crossbeam mean there is a "point load" applied at mid-span due to the actuator. The force in this point load is equal to half of the actuator load since there are two crossbeams in total transferring the load into the column.

Assuming the crossbeam is unbraced along its entire length

For a W21 x 62: $L_p := 6.25 \cdot 12 = 75 \quad in \quad < \quad L = 95 \quad in$

$C_b := 1.32$ AISC 360-10 Table 3-1

$\phi_b := 0.90$ For bending. See AISC 360-10 page 3-9

The following values are obtained from Eq. 3-4a, and Table 3-2 in AISC 360-10

$$M_{px} := \frac{540}{\phi_b} = 600 \quad k-ft \qquad BF := \frac{17.5}{\phi_b} = 19.44 \quad k$$

$$M_n := C_b \cdot \left[\phi_b \cdot M_{px} - \phi_b \cdot BF \cdot \left(\frac{L - L_p}{12} \right) \right] = 674.3 \quad k-ft \quad \text{Eq. 3-4a}$$

$\phi_b \cdot M_n = 606.87 \quad k-ft \quad > \quad \phi_b \cdot M_{px} = 540 \quad k-ft$

$$P_{actuator.3a} := 2 \cdot \frac{4 \cdot \phi_b \cdot M_{px} \cdot 12}{L}$$

$P_{actuator.3a} = 545.68$ kips

Section is compact for flexure

b. Strength in shear (AISC 360-10 Section G2.1.)

For a W21 x 62: $E = 29000 \quad ksi \qquad F_y = 50 \quad ksi$

$h/t_w := 46.9 \quad < \quad 2.24 \cdot \sqrt{\frac{E}{F_y}} = 53.95$

$\phi_v = 1$ AISC 360-10 G.2.1.(a)

$V_{nx} := \frac{252}{\phi_v} = 252 \quad kips$ AISC 360-10 Table 3-2

Each crossbeam is simply supported at each end - the maximum shear force at each end is half the actuator load. The load going into each crossbeam is half of the actuator load since there are two crossbeams.

$$P_{actuator.3b} := \phi_v \cdot V_{nx} \cdot 2 \cdot 2$$

$P_{actuator.3b} = 1008$ kips

4. Connection Crossbeam - Column

The connection between the crossbeam and the column is checked as a simple shear connection using 6 No. 7/8 inch A325 bolts to connect the two elements.

a. Crossbeam - bolt hole bearing (AISC 360-10 Section J3.10.)

$d_{hole} := 1$ in Measured

$l_c := 3 - d_{hole} = 2$ in Clear distance between holes (distance to edge of material doesn't govern)

$t := 0.400$ in Web thickness

$F_u = 65$ ksi

$d := \frac{7}{8} = 0.88$ in

$R_n := \min\left(1.2 \cdot l_c \cdot t \cdot F_u, 2.4 \cdot d \cdot t \cdot F_u\right) = 54.6$ $\frac{k}{bolt}$ Assume that at the actuators full force we don't want deformation at the bolt hole

$\phi := 0.75$

$\phi \cdot R_n \cdot 6 = 245.7$ $\frac{kips}{connection}$

Each connection takes half of the load in the crossbeam, and each crossbeam takes half of the load in the actuator

$P_{actuator.4a} := \phi \cdot R_n \cdot 6 \cdot 2 \cdot 2$ $P_{actuator.4a} = 982.8$ kips

b. Crossbeam - shear yield/rupture (AISC 360-10 Section J4.2.)

$F_y := 50$ ksi $d := 21.0$ in $t_w := 0.400$ in

$A_{gv} := d \cdot t_w = 8.4$ in^2

$R_{n.yield} := 0.60 \cdot F_y \cdot A_{gv} = 252$ kips

$\phi_y := 1.00$ For shear yielding

$\phi_y \cdot R_{n.yield} = 252$ kips

$F_u := 65$ ksi $d_{hole} := 1$ in

$A_{nv} := A_{gv} - 6 \cdot d_{hole} \cdot t_w = 6$ in^2 6 bolt holes along a shear failure plane

$R_{n.rupture} := 0.60 \cdot F_u \cdot A_{nv} = 234$ kips

$\phi_r := 0.75$ For shear rupture

$\phi_r \cdot R_{n.rupture} = 175.5$ kips

$\phi R_n := \min(\phi_y \cdot R_{n.yield}, \phi_r \cdot R_{n.rupture}) = 175.5$ $\frac{\text{kips}}{\text{connection}}$

Each connection takes half of the force in the crossbeam, and each crossbeam takes half of the load in the actuator

$P_{actuator.4b} := 4 \cdot \phi R_n$ $P_{actuator.4b} = 702$ kips

c. Crossbeam - block shear (AISC 360-10 Section J4.3.)

$F_u := 65$ ksi $d_{hole} := 1 + \frac{1}{16} = 1.06$ in $s_{hole} := 5.5$ in $t_w := 0.400$ in $d = 21$ in

$A_{nv} := d \cdot t_w - 6 \cdot d_{hole} \cdot t_w = 5.85$

$A_{nt} := (s_{hole} - d_{hole}) \cdot t_w = 1.78$ in^2

$U_{bs} := 1.0$

$R_{n.rupture} := 0.60 \cdot F_u \cdot A_{nv} + U_{bs} \cdot F_u \cdot A_{nt} = 343.52$ kips

$F_y := 50$ ksi $A_{gv} := d \cdot t_w = 8.4$ in^2 $U_{bs} = 1$ $F_u = 65$ ksi $A_{nt} = 1.78$ in^2

$R_{n.yield} := 0.60 \cdot F_y \cdot A_{gv} + U_{bs} \cdot F_u \cdot A_{nt} = 367.38$ $\frac{\text{kips}}{\text{connection}}$

$R_n := \min(R_{n.rupture}, R_{n.yield}) = 343.52$ $\frac{\text{kips}}{\text{connection}}$

$\phi := 0.75$

$\phi \cdot R_n = 257.64$ $\frac{\text{kips}}{\text{connection}}$

Each connection takes half of the total load applied to the crossbeam, each crossbeam takes half of the total load being applied by the actuator.

$P_{actuator.4c} := \phi \cdot R_n \cdot 2 \cdot 2$ $P_{actuator.4c} = 1030.57$ kips

d. Bolt - shear capacity (AISC 360-10 Section J3.6.)

$F_{nv} := 54$ ksi $\quad d_{bolt} := \frac{7}{8}$ in $\quad A_{bolt} := \frac{pi \cdot d_{bolt}^2}{4} = 0.6$ in^2

$R_{n.bolt} := F_{nv} \cdot A_{bolt} = 32.47$ $\frac{kips}{bolt}$

$\phi := 0.75$

$\phi \cdot R_{n.bolt} \cdot 6 = 146.12$ $\frac{kips}{connection}$

Each connection takes half of the load applied to the crossbeam, which is half of the load applied by the actuator

$P_{actuator.4d} := \phi \cdot R_{n.bolt} \cdot 6 \cdot 2 \cdot 2$ $P_{actuator.4d} = 584.48$ kips

e. Column - bolt hole bearing (AISC 360-10 Section J3.10.)

For the W21 x 62 column: $F_u = 65$ ksi $\quad F_y = 50$ ksi $\quad t_w := 0.400$ in $\quad d_{bolt} := \frac{7}{8}$ in

$d_{hole} := 1$ in

$l_c := 6 - d_{hole} = 5$ in

$R_{n.bolt} := \min\left(1.2 \cdot l_c \cdot t_w \cdot F_u, 2.4 \cdot d_{bolt} \cdot t_w \cdot F_u\right) = 54.6$ $\frac{kips}{bolt}$

$R_{n.connection} := 6 \cdot R_{n.bolt} = 327.6$ $\frac{kips}{connection}$ Each connection has 6 bolts

$\phi := 0.75$

Each connection carries half the applied load in the crossbeam which is half of the applied load from the actuator. Each connection therefore carries 1/4 of the actuator load.

$P_{actuator.4e} := 4 \cdot \phi \cdot R_{n.connection}$ $P_{actuator.4e} = 982.8$ kips

f. Column - tension yield/rupture (AISC 360-10 Section J4.1.)

For the W21 x 62 column: $F_y = 50$ ksi $\quad d := 21.0$ in $\quad t_w := 0.400$ in

$A_g := d \cdot t_w = 8.4$ in^2

$R_{n.yield} := F_y \cdot A_g = 420$ kips

$\phi_y := 0.90$

$d_{hole} := 1 + \frac{1}{16} = 1.06$ in

$A_e := d \cdot t_w - d_{hole} \cdot 2 \cdot t_w = 7.55 \quad in^2$

$R_{n.rupture} := F_u \cdot A_e = 490.75 \quad kips$

$\phi_r := 0.75$

$\phi R_n := \min\left(\phi_y \cdot R_{n.yield}, \phi_r \cdot R_{n.rupture}\right) = 368.06 \quad \frac{kips}{connection}$

Each connection takes half of the load in the crossbeam which is half of the load applied by the actuator

$P_{actuator.4f} := 4 \cdot \phi R_n$ $P_{actuator.4f} = 1472.25$ kips

g. Column - block shear strength (AISC 360-10 Section J4.3.)

Assume conservatively that the top-most bolt in the column is in the last bolt hole which has an edge distance of 3 inches

$s_{hole.vert} := 6 \quad in \qquad s_{hole.horiz} := 5.5 \quad in$

$d_{hole} := 1 + \frac{1}{16} = 1.06 \quad in \qquad t_w := 0.400 \quad in$

$A_{nv} := \left(3 + s_{hole.vert} \cdot 2 - d_{hole} \cdot 2.5\right) \cdot t_w = 4.94 \quad in^2$

$A_{nt} := \left(s_{hole.horiz} - d_{hole}\right) \cdot t_w = 1.78 \quad in^2$

$F_u = 65 \quad ksi$

$U_{bs} = 1$

$R_{n.rupture} := 0.60 \cdot F_u \cdot A_{nv} + U_{bs} \cdot F_u \cdot A_{nt} = 307.94 \quad \frac{kips}{connection}$

$F_y = 50 \quad ksi$

$A_{gv} := \left(s_{hole.vert} \cdot 2 + 3\right) \cdot t_w = 6 \quad in^2$

$R_{n.yield} := 0.60 \cdot F_y \cdot A_{gv} + U_{bs} \cdot F_u \cdot A_{nt} = 295.38 \quad \frac{kips}{connection}$

$\phi := 0.75$

$\phi R_{n.connection} := \min\left(\phi \cdot R_{n.rupture}, \phi \cdot R_{n.yield}\right) = 221.53 \quad \frac{kips}{connection}$

Each connection takes half the load applied to the crossbeam which is equal to half the load applied by the actuator => each connection takes 1/4 of the load applied by the actuator.

$P_{actuator.4g} := 4 \cdot \phi R_{n.connection}$ $P_{actuator.4g} = 886.13$ kips

5. Column

a. Tension capacity (AISC 360-10 D2.)

For the W21 x 62 column: $A_g := 18.3 \ in^2$ $F_y = 50 \ ksi$ $F_u = 65 \ ksi$

$d_{hole} := 1 + \frac{1}{16} + \frac{1}{16} = 1.13 \ in$ $t_w := 0.400 \ in$

$A_n := A_g - 2 \cdot d_{hole} \cdot t_w = 17.4 \ in^2$ $U := 1 - \left(\frac{t_w}{2} + t_w \right) \cdot \frac{1}{6} = 0.9$

$P_{n.yield} := F_y \cdot A_g = 915 \ kips$ $\phi_y := 0.90$

$P_{n.rupture} := F_u \cdot A_n \cdot U = 1017.9 \ kips$ $\phi_r := 0.75$

$\phi P_n := \min\left(\phi_y \cdot P_{n.yield}, \phi_r \cdot P_{n.rupture}\right) = 763.43 \ kips$

Each column takes half the total load applied by the actuator

$P_{actuator.5a} := 2 \cdot \phi P_n$ $P_{actuator.5a} = 1526.85 \ kips$

---

6. Connection - Column to Strong Floor

a. Bolts - Tensile capacity (AISC 360-10 Section J3.6.)

$F_{nt} := 90 \ ksi$ $d_{bolt} := 1 \ in$

$A_{bolt} := pi \cdot d_{bolt}^2 \cdot \frac{1}{4} = 0.79 \ in^2$

$\phi := 0.75$

$R_{n.bolt} := F_{nt} \cdot A_{bolt} = 70.69 \ \frac{kips}{bolt}$

$\phi R_{n.connection} := \phi \cdot R_{n.bolt} \cdot 4 = 212.06 \ \frac{kips}{connection}$

There are 2 connections in total carrying the total load applied by the actuator

$P_{actuator.6a} := \phi R_{n.connection} \cdot 2$ $P_{actuator.6a} = 424.11 \ kips$

b. Baseplate - Yieldline analysis

Tensile load is applied concentrically through the column. Column baseplate assumed to be okay at least up to 300 kips due to the same columns being used in previous testing with these loads

---

7. W12 x 50 Spreader Beam

a. Bearing of actuator on flange of spreader (AISC J7-1a)

$\phi := 0.75$

$F_y = 50$ ksi

$A_{pb} := 18 \cdot 12 = 216$ in^2

$R_n := 1.8 \cdot F_y \cdot A_{pb} = 19440$ kips

$P_{actuator.7a} := \phi \cdot R_n = 14580$ kips $\quad P_{actuator.7a} = 14580$ kips

b. Compression buckling strength of stiffener (AISC J4.4)

$K := 0.65$ For the stiffener welded to the top and bottom flanges, and the web

$L := 12 - 2 \cdot \left(\frac{5}{8}\right) = 10.75$ in

For a single, 1/2 inch thick stiffener:

$b_f := 12$ in $\quad t_w := \frac{3}{8}$ in $\quad b_{stiffener} := \frac{b_f - t_w}{2} = 5.81$ in

$t_{stiffener} := 0.5$ in

$I_{stiffener} := b_{stiffener} \cdot t_{stiffener}^3 \cdot \frac{1}{12} = 0.06$ in^4 $\quad A_{stiffener} := b_{stiffener} \cdot t_{stiffener} = 2.91$ in^2

$r_{stiffener} := \sqrt{\frac{I_{stiffener}}{A_{stiffener}}} = 0.14$

$\frac{K \cdot L}{r_{stiffener}} = 48.41 > 25$ Follow the provisions of Chapter E in AISC 360-10

Is the stiffener slender, non-compact or compact for compression in accordance with AISC 360-10 Table B4.1.b?

The stiffener is supported along its top and bottom edges, and therefore could be considered similar to a web element

$L = 10.75$ in $t_{stiffener} = 0.5$ in $E = 29000$ ksi $F_y = 50$ ksi

$\frac{L}{t_{stiffener}} = 21.5 < 3.76 \cdot \sqrt{\frac{E}{F_y}} = 90.55$

Stiffener is compact for compression

$K = 0.65$ $L = 10.75$ in $r_{stiffener} = 0.14$ in

$\frac{K \cdot L}{r_{stiffener}} = 48.41 < 4.71 \cdot \sqrt{\frac{E}{F_y}} = 113.43$

$F_e := \frac{pi^2 \cdot E}{\left(\frac{K \cdot L}{r_{stiffener}}\right)^2} = 122.13$ kips

$F_{cr} := 0.658^{\frac{F_y}{F_e}} \cdot F_y = 42.13$ ksi

$P_n := F_{cr} \cdot A_{stiffener} = 122.43$

$\phi := 0.90$

$P_{actuator.7b} := 2 \cdot P_n \cdot \phi$ $P_{actuator.7b} = 220.37$ kips

c. Compression yielding strength of stiffener

$A_{stiffener} = 2.91$ in^2 For a single stiffener

$\phi := 0.90$ $F_y = 50$ ksi

$P_{actuator.7c} := \phi \cdot A_{stiffener} \cdot 2 \cdot F_y$ $P_{actuator.7c} = 261.56$ kips

d. Bending of spreader beam (AISC F2)

Yielding: $F_y = 50$ ksi $Z_x := 71.9$ in^3

$M_p := F_y \cdot Z_x = 3595$ in − kips

Lateral-Torsional Buckling: $L_p := 6.92 \cdot 12 = 83.04$ in $L_r := 23.8 \cdot 12 = 285.6$ in

$L := 72$ in

$L < L_p$

Lateral-torsional buckling will not govern the flexural capacity

Actuator load to cause flexural yielding: $L = 72$ in

$\phi := 0.90$

$$P_{actuator.7d} := \frac{4 \cdot \phi \cdot M_p}{L} = 179.75 \text{ kips}$$

e. Shear capacity of spreader beam (AISC G)

Critical location for shear is at support where stiffeners do not pass within the critical section for shear so all shear is carried solely by the web of the section

$\phi := 0.90$ $F_y = 50$ ksi $A_w := \frac{3}{8} \cdot 12 = 4.5$ in^2 $E = 29000$ ksi

For this section: $h/tw := 26.8 < 2.24 \cdot \sqrt{\frac{E}{F_y}} = 53.95$

$\phi_v := 1.00$ $C_v := 1.00$

$V_n := 0.6 \cdot F_y \cdot A_w \cdot C_v = 135$ kips

$$P_{actuator.7e} := 2 \cdot \phi_v \cdot V_n = 270 \text{ kips}$$

f. Local web yielding at the supports (AISC J10.2)

Yielding: $\phi := 1.00$ $F_{yw} := 50$ ksi $t_w := \frac{3}{8}$ in $k := 1.14$ $l_b := 18$ in

$R_n := F_{yw} \cdot t_w \cdot (5 \cdot k + l_b) = 444.38$ kips

$$P_{actuator.7f} := 2 \cdot \phi \cdot R_n = 888.75 \text{ kips}$$

g. Local web crippling at the supports (AISC J10.3)

Crippling: $\phi := 0.75$ $t_f := \frac{5}{8}$ in $d := 12$ in $E = 29000$ ksi

$$R_n := 0.80 \cdot t_w^2 \cdot \left[1 + 3 \cdot \left(\frac{l_b}{d}\right) \cdot \left(\frac{t_w}{t_f}\right)^{1.5}\right] \cdot \sqrt{\frac{E \cdot F_{yw} \cdot t_f}{t_w}} = 540.65 \text{ kips}$$

$P_{actuator.7g} := 2 \cdot \phi \cdot R_n = 810.98$ kips

h. Local web sidesway buckling (AISC J10.4)

Sidesway buckling: $\phi := 0.85$

Compression flange not restrained against rotation

$h/tw = 26.8$ $L_b := 72$ in $b_f = 12$ in

$$\frac{h/tw}{\frac{L_b}{b_f}} = 4.47 \quad > \quad 1.7$$

As per AISC J10.4.b.ii, the limit of web sidesway buckling does not apply

i. Displacement of the beam is limited by the clearance between the bottom of the beam and the top surface of the specimen

$\delta_{max} := 2.5$ in $L = 72$ in $E = 29000$ ksi $I_x := 391$ in^4

$$P_{actuator.7i} := \frac{\delta_{max} \cdot 48 \cdot E \cdot I_x}{L^3} = 3645.51$$

$SpreaderLimit := \min(P_{actuator.7a}, P_{actuator.7b}, P_{actuator.7c}, P_{actuator.7d}, P_{actuator.7e}, P_{actuator.7f}, P_{actuator.7g}, I$

SpreaderLimit = 179.75 kips

WILL NEED A DEEPER SECTION WHEN TRYING TO PUSH IT TO FAILURE

SPREADER BEAM

Option 1: Blue beam in yard - 95" Long W14x120

Simply supported on bearing pads spaced at 6ft center-center

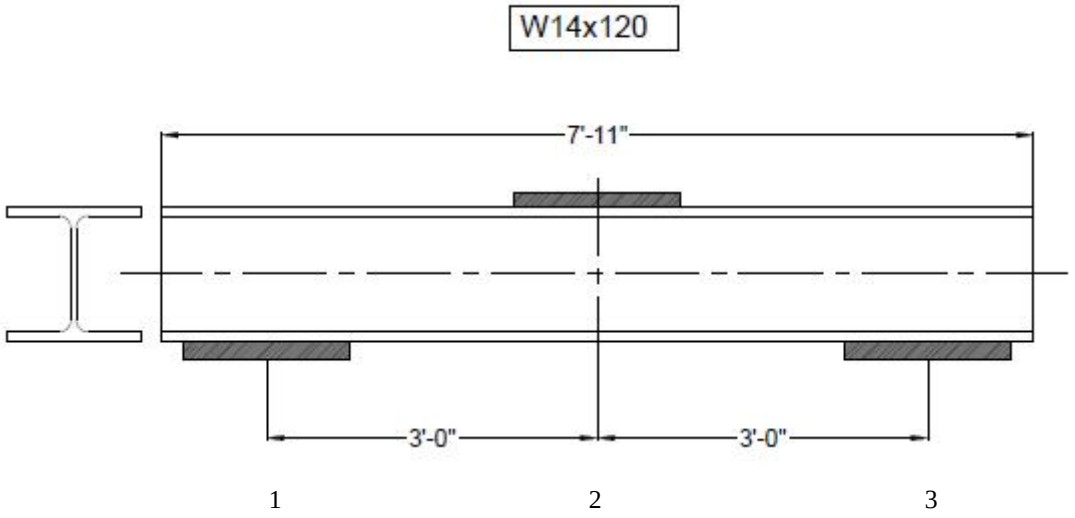

Flexural capacity ASCE 360-10 Section F2.

$\phi_b := 0.90$

$M_{px} := \frac{795}{\phi_b} = 883.33 \quad k - ft$

$L_p := 13.2 \quad ft \quad > \quad L := 6 \quad ft$ Section will fully reach plastic moment prior to lateral-torsional buckling

$P_{flexure} := \frac{4 \cdot \phi_b \cdot M_{px}}{L} = 530$ kips

Shear capacity ASCE 360-10 Section G2.1.

$\phi_v := 1.00$

$V_{nx} := \frac{257}{\phi_v} = 257 \quad kips$

$P_{shear} := 2 \cdot \phi_v \cdot V_{nx} = 514$ kips

Bearing - Actuator on Spreader ASCE 360-10 Section J7.

$A_{pb} := 18 \cdot 12 = 216$ in^2 Actuator area - conservative

$F_y := 50$ ksi

$\phi_{brg} := 0.75$

$\phi R_{n.brg} := \phi_{brg} \cdot 1.8 \cdot F_y \cdot A_{pb} = 14580$ kips

$P_{brg} := \phi R_{n.brg} = 14580$ kips

Web Local Yielding (WLY) ASCE 360-10 Section J10.2.

$\phi_{WLY} := 1.00$

$d := 14.5$ in > $dist_{R.end} := 11.5$ in

$F_{yw} := 50$ ksi

$t_w := 0.590$ in

$k := 1.54$ in

$l_b := 18$ in

$\phi R_{n.WLY.1.3} := \phi_{WLY} \cdot F_{yw} \cdot t_w \cdot (2.5 \cdot k + l_b) = 644.58$ kips At the supports

$\phi R_{n.WLY.2} := \phi_{WLY} \cdot F_{yw} \cdot t_w \cdot (5 \cdot k + l_b) = 758.15$ kips At the actuator

$P_{WLY} := \min(2 \cdot \phi R_{n.WLY.1.3}, \phi R_{n.WLY.2}) = 758.15$ kips

Web Local Crippling (WLC) ASCE 360-10 Section J10.3.

$\phi_{WLC} := 0.75$

$t_w = 0.59$ in

$l_b = 18$ in

$d = 14.5$ in

$t_f := 0.940$ in

$E := 29000$ ksi

$F_{yw} = 50$ ksi

$\frac{d}{2} = 7.25$ in < $dist_{R.end} = 11.5$ in Support reaction is applied at distance from end greater than d/2

$$\phi R_{n.WLC.1.2.3} := 0.80 \cdot t_w^2 \cdot \left[1 + 3 \cdot \frac{l_b}{d} \cdot \left(\frac{t_w}{t_f}\right)^{1.5}\right] \cdot \sqrt{\frac{E \cdot F_{yw} \cdot t_f}{t_w}} = 1207.11 \text{ kips}$$

$P_{WLC} := \min\left(2 \cdot \phi R_{n.WLC.1.2.3}, \phi R_{n.WLC.1.2.3}\right) = 1207.11$ kips

Web Sidesway Buckling (WSB) ASCE 360-10 Section J10.4.

$\phi_{WSB} := 0.85$

$d = 14.5$ in

$k = 1.54$ in

$h := d - 2 \cdot k = 11.42$ in

$t_w = 0.59$ in

$b_f := 14.7$ in

$\frac{h}{t_w} \cdot \frac{L}{b_f} = 7.9$ > 1.7 Limit does not apply

Maximum actuator load the beam can carry

$P_{max} := \min\left(P_{flexure}, P_{shear}, P_{brg}, P_{WLY}, P_{WLC}\right) = 514$ kips

APPENDIX G – RESULTS TABLES FOR NO-CONNECTION SPECIMEN

NO-CONNECTION CONNECTION: RESULTS COMPARISON TABLES

INSTRUMENTATION NAMES

String Potentiometers

Measuring displacements in inches

North Support	=	N. Sup.	South Support	=	S. Sup.
North Quarter Point	=	N. Qtr.	South Quarter Point	=	S. Qtr.
North Midspan	=	N. Mid.	South Midspan	=	S. Mid.

LVDT's

Measures relative slip between precast beam and cast-in-place topping interface in inches

South-East Web	=	S.E. Web		
East Midspan	=	E. Mid.	=	E. Web (Mistake in descriptor name in system 5000)
North-East Web	=	N.E. Web		
South-West Web	=	S.W. Web		
West Midspan	=	W. Mid.	=	W. Web (Mistake in descriptor name in system 5000)
North-West Web	=	N.W. Web		

Strain Gauges

Measuring strain in rebar in precast beam and in cast-in-place topping in microstrain

Cast In Place East	=	C.I.P. E.	Cast In Place West	=	C.I.P. W.
Beam North-East	=	Beam N.E.	Beam South-East	=	Beam S.E.
Beam North-West	=	Beam N.W.	Beam South-West	=	Beam S.W.

Static Load Test After No. of Cycles (No. Shown Below)	MTS Load (lb)	Displacement Range [in]					
	Load Cell	North Support	North Quarter	North Midspan	South Support	South Midspan	South Quarter
0 (Test 1)	30350	0.045	0.046	0.048	0.038	0.044	0.044
0 (Test 2)	30479	0.042	0.047	0.050	0.037	0.044	0.041
14	31494	0.042	0.047	0.050	0.037	0.045	0.041
100	30290	0.042	0.046	0.051	0.037	0.045	0.040
1000	30286	0.042	0.046	0.047	0.034	0.045	0.045
10000	30326	0.045	0.046	0.046	0.035	0.042	0.042
100001	30274	0.045	0.045	0.046	0.034	0.042	0.039
300000	30568	0.043	0.047	0.046	0.035	0.045	0.035
500000	30515	1.061	0.037	0.040	0.034	0.036	0.032
700000	30588	0.085	0.037	0.038	0.032	0.037	0.032
900001	30652	0.073	0.036	0.037	0.030	0.037	0.027
1100000	30717	0.021	0.036	0.036	0.033	0.037	0.028
1300000	30584	0.023	0.036	0.036	0.032	0.036	0.025
1500000	30407	0.017	0.036	0.035	0.030	0.034	0.022
1700000	30612	0.075	0.034	0.038	0.030	0.036	0.032
1900000	30515	0.023	0.034	0.036	0.030	0.036	0.029
2100000	30523	0.025	0.033	0.037	0.032	0.035	0.025
2300000	30556	0.045	0.035	0.036	0.029	0.037	0.024
2500000	30459	0.031	0.033	0.035	0.032	0.035	0.022
2700000	30539	0.070	0.033	0.037	0.030	0.036	0.024
2900000	30415	0.109	0.034	0.036	0.029	0.035	0.027
3100000	30580	0.020	0.034	0.037	0.030	0.036	0.026
3312073	30592	0.019	0.034	0.035	0.030	0.036	0.025
3500000	30402	0.019	0.034	0.037	0.029	0.035	0.021
3650000	31309	0.019	0.035	0.037	0.032	0.035	0.018

Max values	31494	1.061	0.047	0.051	0.038	0.045	0.045
Min values	30274	0.017	0.033	0.035	0.029	0.034	0.018
Range of values	1221	1.043	0.014	0.016	0.009	0.011	0.027

Difference between N&S midspan	0.005	in	
Accuracy of string potentiometer	0.01	in	0.1% of the full stroke of the string potentiometer. Refer to http://www.te.com/usa-en/product-CAT-CAPS0014.html
Fatmir/Matt Midspan Deflection (in.)	0.038	For the no-connection specimen	
Difference from my deflection range (in.)	0.004	->	0.013 See "accuracy of string potentiometer"

DEFLECTIONS MAKE SENSE EXCEPT FOR NORTH SUPPORT

The support beam at the north support location was moving significantly during testing

Values shown in red are outliers caused by string pot malfunctions

Static Load Test After No. of Cycles (No. Shown Below)	MTS Load (lb)	Strain Range (με)				
	Load Cell	Beam NW	CIP East	Beam SW	Beam NE	Beam SE
0 (Test 1)	30350	24	44	22	24	20
0 (Test 2)	30479	25	44	22	25	20
14	31494	26	45	22	25	21
100	30290	24	44	22	24	19
1000	30286	25	43	22	24	19
10000	30326	25	43	22	25	19
100001	30274	25	45	22	25	19
300000	30568	24	45	22	25	19
500000	30515	25	45	23	26	20
700000	30588	25	45	22	26	21
900001	30652	25	45	22	26	20
1100000	30717	25	46	23	26	21
1300000	30584	25	46	22	26	21
1500000	30407	25	45	22	26	20
1700000	30612	25	46	22	26	20
1900000	30515	24	45	21	26	19
2100000	30523	25	46	22	26	20
2300000	30556	25	46	22	26	20
2500000	30459	25	46	22	25	20
2700000	30539	26	47	23	26	21
2900000	30415	25	48	22	26	20
3100000	30580	25	48	23	26	20
3312073	30592	25	47	22	26	20
3500000	30402	25	46	22	25	20
3650000	31309	26	49	22	26	21

Max values	31494	26	49	23	26	21
Min values	30274	24	43	21	24	19
Range of values	1221	2	6	2	2	2

STRAINS MAKE SENSE & CONSISTENT

Static Load Test After No. of Cycles (No. Shown Below)	MTS Load (lb)	LVDT Measuring Interface Slip Range (in)					
	Load Cell	NE Web	East Mid	NW Web	SE Web	West Mid	SW Web
0 (Test 1)	30350	0.000	0.001	0.000	0.000	0.001	0.000
0 (Test 2)	30479	0.000	0.001	0.000	0.000	0.001	0.000
14	31494	0.000	0.001	0.000	0.000	0.001	0.000
100	30290	0.000	0.001	0.000	0.000	0.001	0.000
1000	30286	0.000	0.001	0.000	0.000	0.001	0.000
10000	30326	0.000	0.001	0.000	0.000	0.001	0.000
100001	30274	0.000	0.001	0.000	0.000	0.001	0.000
300000	30568	0.000	0.001	0.000	0.000	0.001	0.000
500000	30515	0.000	0.001	0.000	0.000	0.001	0.000
700000	30588	0.000	0.001	0.000	0.000	0.001	0.000
900001	30652	0.000	0.001	0.000	0.000	0.001	0.000
1100000	30717	0.000	0.001	0.000	0.000	0.001	0.000
1300000	30584	0.000	0.001	0.000	0.000	0.001	0.000
1500000	30407	0.000	0.001	0.000	0.000	0.001	0.000
1700000	30612	0.000	0.001	0.000	0.000	0.001	0.000
1900000	30515	0.000	0.001	0.000	0.000	0.001	0.000
2100000	30523	0.000	0.001	0.000	0.000	0.001	0.000
2300000	30556	0.000	0.001	0.000	0.000	0.001	0.000
2500000	30459	0.000	0.001	0.000	0.000	0.001	0.000
2700000	30539	0.000	0.001	0.000	0.000	0.001	0.000
2900000	30415	0.000	0.001	0.000	0.000	0.001	0.000
3100000	30580	0.000	0.001	0.000	0.000	0.001	0.000
3312073	30592	0.000	0.001	0.000	0.000	0.001	0.000
3500000	30402	0.000	0.001	0.000	0.000	0.001	0.000
3650000	31309	0.000	0.001	0.000	0.000	0.001	0.000

Max values	31494	0.000	0.001	0.000	0.000	0.001	0.000
Min values	30274	0.000	0.001	0.000	0.000	0.001	0.000
Range of values	1221	0.000	0.001	0.000	0.000	0.000	0.000

LVDT's SHOW NO SLIP ALONG ANY INTERFACE

DISPLACEMENT IN INCHES, ALONG BEAM AT 30 KIPS FOR EACH TEST						
Number of cycles	**Position along beam**					
	S. Sup	S. Qtr	S. Mid	N. Mid	N. Qtr	N. Sup
	0	**36**	**67**	**77**	**108**	**144**
0	-0.031	-0.037	-0.041	-0.047	-0.040	-0.036
14	-0.032	-0.038	-0.042	-0.044	-0.041	-0.040
100	-0.031	-0.036	-0.042	-0.048	-0.043	-0.037
1000	-0.029	-0.033	-0.040	-0.044	-0.042	-0.037
10000	-0.030	-0.037	-0.040	-0.043	-0.040	-0.040
100001	-0.029	-0.035	-0.039	-0.043	-0.042	-0.040
300000	-0.029	-0.033	-0.038	-0.042	-0.043	-0.039
500000	-0.029	-0.028	-0.034	-0.033	-0.034	-0.026
700000	-0.029	-0.026	-0.032	-0.036	-0.033	-0.026
900000	-0.026	-0.025	-0.033	-0.033	-0.032	-0.023
1100000	-0.028	-0.022	-0.033	-0.029	-0.033	-0.016
1300000	-0.028	-0.022	-0.033	-0.034	-0.031	-0.017
1500000	-0.027	-0.017	-0.032	-0.032	-0.033	-0.006
1700000	-0.027	-0.023	-0.031	-0.033	-0.032	-0.015
1900000	-0.026	-0.023	-0.029	-0.031	-0.027	-0.003
2100000	-0.025	-0.019	-0.032	-0.033	-0.029	-0.019
2300000	-0.027	-0.020	-0.033	-0.032	-0.032	-0.001
2500000	-0.025	-0.018	-0.032	-0.031	-0.028	-0.026
2700000	-0.026	-0.016	-0.028	-0.034	-0.029	0.026
2900000	-0.026	-0.015	-0.031	-0.031	-0.027	0.082
3100000	-0.024	-0.015	-0.031	-0.031	-0.030	-0.008
3312073	-0.025	-0.015	-0.031	-0.032	-0.028	-0.008
3500000	-0.026	-0.013	-0.030	-0.034	-0.031	-0.011
3650000	-0.028	-0.015	-0.033	-0.035	-0.031	-0.011

Max	-0.024	-0.013	-0.028	-0.029	-0.027	0.082
Min	-0.032	-0.038	-0.042	-0.048	-0.043	-0.040
Range	0.008	0.025	0.013	0.018	0.016	0.122

LVDT SLIP IN INCHES, ALL LOCATIONS AT 30 KIPS FOR EACH TEST						
Number of cycles	**LVDT Slip**					
	NE Web	East Web	NW Web	SE Web	West Web	SW Web
0	0.0016	0.0117	0.0036	0.0036	0.7498	0.0019
14	0.0016	0.0115	0.0036	0.0036	0.7499	0.0021
100	0.0016	0.0115	0.0036	0.0036	0.7499	0.0020
1000	0.0015	0.0116	0.0035	0.0036	0.7499	0.0020
10000	0.0016	0.0116	0.0035	0.0036	0.7499	0.0021
100001	0.0015	0.0115	0.0036	0.0035	0.7499	0.0020
300000	0.0016	0.0116	0.0035	0.0036	0.7497	0.0021
500000	0.0016	0.0115	0.0035	0.0036	0.7499	0.0022
700000	0.0016	0.0114	0.0036	0.0035	0.7498	0.0024
900000	0.0016	0.0113	0.0036	0.0036	0.7497	0.0022
1100000	0.0017	0.0113	0.0035	0.0036	0.7499	0.0022
1300000	0.0016	0.0114	0.0036	0.0036	0.7501	0.0023
1500000	0.0016	0.0115	0.0036	0.0034	0.7500	0.0023
1700000	0.0017	0.0112	0.0035	0.0035	0.7499	0.0022
1900000	0.0015	0.0114	0.0036	0.0034	0.7499	0.0022
2100000	0.0016	0.0113	0.0036	0.0034	0.7499	0.0022
2300000	0.0016	0.0114	0.0035	0.0034	0.7499	0.0023
2500000	0.0016	0.0115	0.0036	0.0035	0.7499	0.0022
2700000	0.0016	0.0113	0.0035	0.0035	0.7499	0.0020
2900000	0.0016	0.0120	0.0036	0.0036	0.7498	0.0023
3100000	0.0016	0.0112	0.0036	0.0036	0.7499	0.0022
3312073	0.0017	0.0114	0.0036	0.0036	0.7498	0.0022
3500000	0.0016	0.0114	0.0036	0.0036	0.7499	0.0022
3650000	0.0016	0.0113	0.0035	0.0035	0.7498	0.0022

LVDT Reading in.						
	Northeast Web	**East Web**	**Southeast Web**	**Northwest Web**	**West Web**	**Southwest Web**
Maximum	0.00	0.01	0.00	0.00	0.75	0.00
Minimum	0.00	0.01	0.00	0.00	0.75	0.00
Range	0.00	0.00	0.00	0.00	0.00	0.00

STRAINS IN MICROSTRAIN, ALL LOCATIONS AT 30 KIPS FOR EACH TEST					
Number of cycles	**Strain, με**				
	NE Beam	C.I.P. East	SE Beam	NW Beam	SW Beam
0	23	43	21	24	18
14	24	44	20	23	18
100	22	42	20	22	17
1000	22	42	21	23	17
10000	22	42	19	22	18
100001	23	41	20	22	18
300000	23	42	20	21	18
500000	23	42	20	20	17
700000	23	42	19	21	19
900000	23	39	19	20	18
1100000	23	42	20	21	18
1300000	23	40	20	21	18
1500000	22	41	21	20	16
1700000	23	42	21	22	18
1900000	23	42	20	20	18
2100000	22	41	21	21	17
2300000	22	43	21	21	17
2500000	22	41	20	21	19
2700000	23	43	20	21	19
2900000	23	43	20	21	17
3100000	23	43	21	21	17
3312073	22	44	21	21	17
3500000	24	43	20	21	17
3650000	21	43	21	20	18

Strains, με					
	Northeast Beam	**C.I.P. East**	**Southeast Beam**	**Northwest Beam**	**Southwest Beam**
Maximum	24	44	21	24	19
Minimum	21	39	19	20	16
Range	3	5	2	4	3

APPENDIX H – RESULTS TABLES FOR WELDED CONNECTION SPECIMEN

WELDED CONNECTION: RESULTS COMPARISON TABLES

String Potentiometers

Measuring displacements in inches

North Support	=	N. Sup.	South Support	=	S. Sup.
North Quarter Point	=	N. Qtr.	South Quarter Point	=	S. Qtr.
North Midspan	=	N. Mid.	South Midspan	=	S. Mid.

LVDT's

Measures relative slip between precast beam and cast-in-place topping interface in inches

South-East Web	=	S.E. Web		
East Midspan	=	E. Mid.	=	E. Web (Mistake in descriptor name in system 5000)
North-East Web	=	N.E. Web		
South-West Web	=	S.W. Web		
West Midspan	=	W. Mid.	=	W. Web (Mistake in descriptor name in system 5000)
North-West Web	=	N.W. Web		

Strain Gauges

Measuring strain in rebar in precast beam and in cast-in-place topping in microstrain

Cast In Place East	=	C.I.P. E.	Cast In Place West	=	C.I.P. W.
Beam North-East	=	Beam N.E.	Beam South-East	=	Beam S.E.
Beam North-West	=	Beam N.W.	Beam South-West	=	Beam S.W.

Static Load Test After No. of Cycles (No. Shown Below)	MTS Load (lb)	Displacement Range [in]					
	Load Cell	North Support	North Quarter	North Midspan	South Support	South Midspan	South Quarter
0	30245	0.030	0.036	0.038	0.034	0.035	0.034
10	30580	0.026	0.036	0.037	0.032	0.036	0.034
100	30668	0.026	0.036	0.036	0.033	0.035	0.033
1000	30415	0.027	0.036	0.037	0.032	0.036	0.034
10000	30487	0.027	0.034	0.036	0.032	0.035	0.037
100000	30765	0.027	0.034	0.035	0.033	0.035	0.035
300000	30326	0.028	0.033	0.036	0.032	0.034	0.032
500000	30370	1.019	0.033	0.035	0.033	0.036	0.032
702330	30334	0.115	0.031	0.036	0.029	0.034	0.028
902117	30278	0.062	0.031	0.036	0.030	0.035	0.029
1100000	30362	0.037	0.033	0.035	0.030	0.035	0.031
1300000	30310	0.062	0.034	0.036	0.032	0.035	0.032
1500000	30181	0.103	0.034	0.037	0.032	0.035	0.032
1700000	30620	0.030	0.034	0.037	0.032	0.035	0.031
1900000	30330	0.028	0.034	0.036	0.030	0.035	0.032
2100001	30314	0.026	0.033	0.034	0.029	0.034	0.075
2301873	30443	0.087	0.031	0.035	0.032	0.034	0.071
2500000	30261	0.025	0.034	0.034	0.032	0.034	0.029
2700000	30374	0.204	0.033	0.034	0.029	0.034	0.086
2900000	30294	0.027	0.031	0.034	0.029	0.034	0.031
3100000	30487	0.459	0.031	0.034	0.032	0.035	0.068
3300000	30314	0.172	0.030	0.145	0.026	0.034	0.026
3500000	30366	0.743	0.031	0.264	0.026	0.035	0.026
3650000	30282	0.291	0.033	0.036	0.028	0.031	0.026

Max values	30765	1.019	0.036	0.264	0.034	0.036	0.086
Min values	30181	0.025	0.030	0.034	0.026	0.031	0.026
Range of values	584	0.994	0.006	0.231	0.008	0.005	0.060

Difference between N&S midspan in

Accuracy of string potentiometer 0.01 in 0.1% of the full stroke of the string potentiometer. Refer to http://www.te.com/usa-en/product-CAT-CAPS0014.html

Fatmir/Matt Midspan Deflection 0.038 e no-connection specimen

Difference from my deflection range 0.007 -> 0.226 racy of string potentiometer"

DEFLECTIONS MAKE SENSE EXCEPT FOR NORTH SUPPORT

Values in red indicate outliers caused by string pot malfunctions

Static Load Test After No. of Cycles (No. Shown Below)	MTS Load (lb)	Strain Range (με)				
	Load Cell	Beam NW	CIP East	Beam SW	Beam NE	Beam SE
0	30245	17	25	16	17	17
10	30580	17	21	16	17	17
100	30668	18	19	16	17	18
1000	30415	17	26	16	17	18
10000	30487	17	28	16	17	17
100000	30765	17	19	16	18	17
300000	30326	17	23	16	19	17
500000	30370	17	27	16	19	17
702330	30334	17	23	16	18	17
902117	30278	17	22	16	18	17
1100000	30362	17	19	16	17	18
1300000	30310	19	18	17	17	18
1500000	30181	18	20	16	18	17
1700000	30620	17	19	16	17	18
1900000	30330	17	24	16	18	17
2100001	30314	18	27	16	18	18
2301873	30443	17	23	16	18	19
2500000	30261	19	34	16	17	18
2700000	30374	18	27	16	16	18
2900000	30294	17	20	15	16	17
3100000	30487	18	29	17	17	19
3300000	30314	17	30	15	16	18
3500000	30366	18	33	16	17	19
3650000	30282	16	21	16	17	17

Max values	30765	19	34	17	19	19
Min values	30181	16	18	15	16	17
Range of values	584	2	16	1	2	2

STRAINS MAKE SENSE & CONSISTENT

Static Load Test After No. of Cycles (No. Shown Below)	MTS Load (lb)	LVDT Measuring Interface Slip Range (in)					
	Load Cell	NE Web	East Mid	NW Web	SE Web	West Mid	SW Web
0	30245	0.000	0.001	0.000	0.000	0.000	0.000
10	30580	0.000	0.000	0.000	0.000	0.000	0.000
100	30668	0.000	0.000	0.000	0.000	0.000	0.000
1000	30415	0.000	0.000	0.000	0.000	0.000	0.000
10000	30487	0.000	0.000	0.000	0.000	0.000	0.000
100000	30765	0.000	0.001	0.000	0.000	0.000	0.000
300000	30326	0.000	0.001	0.000	0.000	0.000	0.000
500000	30370	0.000	0.000	0.000	0.000	0.000	0.000
702330	30334	0.000	0.000	0.000	0.000	0.000	0.000
902117	30278	0.000	0.000	0.000	0.000	0.000	0.000
1100000	30362	0.000	0.000	0.000	0.000	0.000	0.000
1300000	30310	0.000	0.001	0.000	0.000	0.000	0.000
1500000	30181	0.000	0.000	0.000	0.000	0.001	0.000
1700000	30620	0.000	0.001	0.000	0.000	0.000	0.000
1900000	30330	0.000	0.000	0.000	0.000	0.000	0.000
2100001	30314	0.000	0.000	0.000	0.000	0.001	0.000
2301873	30443	0.000	0.000	0.000	0.000	0.000	0.000
2500000	30261	0.000	0.000	0.000	0.000	0.001	0.000
2700000	30374	0.000	0.000	0.000	0.000	0.000	0.000
2900000	30294	0.000	0.000	0.000	0.000	0.000	0.000
3100000	30487	0.000	0.000	0.000	0.000	0.001	0.000
3300000	30314	0.000	0.000	0.000	0.000	0.000	0.000
3500000	30366	0.000	0.000	0.000	0.000	0.000	0.000
3650000	30282	0.000	0.000	0.000	0.000	0.001	0.000

Max values	30765	0.000	0.001	0.000	0.000	0.001	0.000
Min values	30181	0.000	0.000	0.000	0.000	0.000	0.000
Range of values	584	0.000	0.001	0.000	0.000	0.000	0.000

LVDT's SHOW NO SLIP ALONG ANY INTERFACE

DISPLACEMENT IN INCHES, ALONG BEAM AT 30 KIPS FOR EACH TEST						
Number of cycles	**Position along beam**					
	S. Sup	S. Qtr	S. Mid	N. Mid	N. Qtr	N. Sup
	0	**36**	**67**	**77**	**108**	**144**
0	-0.031	-0.031	-0.029	-0.033	-0.029	-0.022
10	-0.029	-0.030	-0.031	-0.033	-0.029	-0.019
100	-0.028	-0.031	-0.032	-0.031	-0.031	-0.020
1000	-0.027	-0.031	-0.030	-0.031	-0.032	-0.022
10000	-0.028	-0.029	-0.030	-0.030	-0.031	-0.023
100000	-0.028	-0.031	-0.030	-0.031	-0.029	-0.023
300001	-0.026	-0.028	-0.031	-0.030	-0.028	-0.022
500000	-0.025	-0.026	-0.031	-0.032	-0.029	-0.022
702330	-0.025	-0.026	-0.028	-0.028	-0.029	-0.022
902117	-0.026	-0.027	-0.029	-0.031	-0.028	-0.024
1100000	-0.025	-0.026	-0.030	-0.030	-0.028	-0.022
1300000	-0.025	-0.029	-0.030	-0.030	-0.029	-0.023
1500001	-0.026	-0.025	-0.031	-0.030	-0.028	-0.026
1700000	-0.024	-0.026	-0.031	-0.029	-0.026	-0.025
1900000	-0.027	-0.025	-0.030	-0.028	-0.027	-0.024
2100001	-0.026	-0.024	-0.028	-0.032	-0.026	-0.020
2301873	-0.027	-0.025	-0.028	-0.028	-0.027	-0.018
2503868	-0.028	-0.022	-0.031	-0.029	-0.028	-0.021
2700129	-0.025	-0.023	-0.030	-0.030	-0.029	-0.020
2900000	-0.024	-0.024	-0.029	-0.030	-0.025	-0.022
3101200	-0.030	-0.024	-0.028	-0.028	-0.027	-0.023
3300001	-0.024	-0.023	-0.029	-0.026	-0.027	-0.020
3500001	-0.023	-0.021	-0.031	-0.027	-0.027	-0.020
3650001	-0.022	-0.021	-0.028	-0.030	-0.027	-0.021

Max	-0.022	-0.021	-0.028	-0.026	-0.025	-0.018
Min	-0.031	-0.031	-0.032	-0.033	-0.032	-0.026
Range	0.009	0.010	0.005	0.007	0.007	0.008

LVDT SLIP IN INCHES, ALL LOCATIONS AT 30 KIPS FOR EACH TEST						
Number of cycles	**LVDT Slip**					
	NE Web	East Web	NW Web	SE Web	West Web	SW Web
0	0.002	0.012	0.004	0.004	0.751	0.002
10	0.002	0.012	0.004	0.004	0.751	0.002
100	0.002	0.012	0.004	0.004	0.751	0.002
1000	0.002	0.012	0.004	0.004	0.751	0.002
10000	0.002	0.012	0.004	0.004	0.751	0.002
100000	0.002	0.012	0.004	0.004	0.751	0.002
300000	0.002	0.012	0.004	0.004	0.751	0.002
500000	0.002	0.012	0.004	0.004	0.751	0.002
702330	0.002	0.012	0.004	0.004	0.751	0.002
902117	0.002	0.012	0.004	0.004	0.751	0.002
1100000	0.002	0.012	0.004	0.004	0.751	0.002
1300000	0.002	0.012	0.004	0.004	0.751	0.002
1500001	0.002	0.012	0.004	0.004	0.751	0.002
1700000	0.002	0.012	0.004	0.004	0.751	0.002
1900000	0.002	0.012	0.004	0.004	0.751	0.002
2100001	0.002	0.012	0.004	0.004	0.751	0.002
2301873	0.002	0.012	0.004	0.004	0.751	0.002
2500000	0.002	0.012	0.004	0.004	0.751	0.002
2700000	0.002	0.012	0.004	0.004	0.751	0.002
2900000	0.002	0.012	0.004	0.004	0.751	0.002
3101200	0.002	0.012	0.004	0.004	0.751	0.002
3300001	0.002	0.012	0.004	0.004	0.750	0.002
3500000	0.002	0.012	0.004	0.004	0.751	0.002
3650000	0.002	0.012	0.004	0.004	0.751	0.002

Max	0.002	0.012	0.004	0.004	0.751	0.002
Min	0.002	0.012	0.004	0.004	0.750	0.002
Range	0.000	0.000	0.000	0.000	0.000	0.000

STRAINS IN MICROSTRAIN, ALL LOCATIONS AT 30 KIPS FOR EACH TEST					
Number of cycles	**Strain, με**				
	NE Beam	**C.I.P. East**	**SE Beam**	**NW Beam**	**SW Beam**
0	15	17	14	15	16
10	15	16	14	14	16
100	15	17	15	15	15
1000	16	16	14	15	15
10000	15	17	15	15	16
100000	16	17	14	14	15
300000	16	20	15	14	16
500000	15	17	14	13	15
702330	16	20	15	14	15
902117	15	19	15	13	16
1100000	16	16	14	14	15
1300000	13	16	14	13	15
1500001	15	16	14	13	15
1700000	15	14	14	14	16
1900000	15	15	15	12	15
2100001	16	22	14	13	17
2301873	15	19	14	13	17
2500000	16	19	14	13	16
2700000	16	22	15	13	16
2900000	15	18	13	12	16
3101200	16	24	15	13	17
3300001	16	24	14	13	17
3500000	16	26	14	12	17
3650000	15	18	14	13	16

Max	16	26	15	15	17
Min	13	14	13	12	15
Range	3	11	2	3	3

APPENDIX I – CALCULATIONS FOR POST-FAILURE CAPACITY OF WELDED CONNECTION SPECIMEN

RESIDUAL CAPACITY OF WELDED CONNECTION SPECIMEN AFTER CONNECTION FAILURE

After failure of the welded connection all of the midspan bending is taken on the C.I.P. topping section at this location. Note the following calculation is conservative and is based on beam-theory (not quite accurate for this "deep beam" but should be in the ball-park:

$f'_c := 4$ ksi

$E_s := 29000$ ksi

$h := 21.5$ in

$b := 48$ in

$cover := 1.5$ in

$dia_s := 0.5$ in

$A_s := 4 \cdot 0.20 = 0.8$ in^2

$A'_s := 4 \cdot 0.2 = 0.8$ in^2

$d' := 2.5 + \frac{dia_s}{2} = 2.75$ in

$d := h - cover - \frac{dia_s}{2} = 19.75$ in

$c := 0.35$ in

$\beta_1 := 0.85$

$a := \beta_1 \cdot c = 0.297$ in

$\varepsilon'_s := \begin{cases} c > d' \text{ if } \frac{0.003}{c} \cdot (c - d') \\ 0 \text{ otherwise} \end{cases}$

$\varepsilon_s := \frac{0.003}{c} \cdot (d - c) = 0.166$

$\varepsilon'_s = 0$

$f'_s := \min(E_s \cdot \varepsilon'_s, 60) = 0$ ksi

$f_s := \min(E_s \cdot \varepsilon_s, 60) = 60$ ksi

$C_c := 0.85 \cdot f'_c \cdot a \cdot b = 48.552$ kips

$C_s := f'_s \cdot A'_s = 0$ kips

$T := f_s \cdot A_s = 48$ kips

Check force equilibrium: $C_c + C_s - T = 0.552$ kips OKAY

$$M_n := \left[C_c \cdot (d - d') + C_s \cdot \left(d - \frac{a}{2} \right) \right] \cdot \frac{1}{12} = 68.782 \quad \text{kip} - \text{ft}$$

$$P_{actuator} := \frac{2}{3} \cdot M_n = 45.855 \quad \text{kips}$$

APPENDIX J – CALCULATIONS FOR EXPECTED STRAINS DURING TESTING

EXPECTED STRAINS UNDER SERVICE LOADING BASED ON BEAM-THEORY

Note that the following calculations will not be accurate due to the nature of the beam under consideration falling into the category of a "deep beam", however we expect them to be in the correct order of magnitude.

$P_{actuator} := 30$ kips

$V_{beam} := \frac{P_{actuator}}{2} = 15$ kips

$M_{beam} := V_{beam} \cdot 3 = 45$ kip − ft

NO-CONNECTION SPECIMEN

Assuming the section is fully composite:

Note that for the no-connection specimen the beam concrete reached 4 ksi, while the C.I.P. topping concrete reached approximately 6.3 ksi

$f'_{c.beam} := 4$ ksi $E_{c.beam} := 33000 \cdot \left(0.15^{1.5}\right) \cdot \sqrt{f'_{c.beam}} = 3834.25$ ksi

$f'_{c.C.I.P.} := 6.3$ ksi $E_{c.C.I.P.} := 33000 \cdot \left(0.15^{1.5}\right) \cdot \sqrt{f'_{c.C.I.P.}} = 4811.95$ ksi

Convert the beam concrete into an equivalent C.I.P. concrete

$$\eta := \frac{E_{c.beam}}{E_{c.C.I.P.}} = 0.8$$

$b_{C.I.P.} := 48$ in $h_{C.I.P.} := 21.5$ in

$b_{beam} := b_{C.I.P.} \cdot \eta = 38.25$ in $h_{beam} := 4$ in

$A_{C.I.P.} := b_{C.I.P.} \cdot h_{C.I.P.} = 1032$ in^2 $I_{C.I.P.} := \frac{b_{C.I.P.} \cdot h_{C.I.P.}^3}{12} = 39753.5$ in^4

$A_{beam} := b_{beam} \cdot h_{beam} = 152.99$ in^2 $I_{beam} := \frac{b_{beam} \cdot h_{beam}^3}{12} = 203.99$ in^4

$$cg := \frac{A_{C.I.P.} \cdot \left(h_{beam} + \frac{h_{C.I.P.}}{2}\right) + A_{beam} \cdot \left(\frac{h_{beam}}{2}\right)}{A_{C.I.P.} + A_{beam}} = 13.1 \text{ in}$$ Above beam soffit

$$I := I_{C.I.P.} + A_{C.I.P.}\cdot\left(h_{beam} + \frac{h_{C.I.P.}}{2} - cg\right)^2 + I_{beam} + A_{beam}\cdot\left(\frac{h_{beam}}{2} - cg\right)^2 = 61616.89 \quad in^4$$

At the level of the reinforcement in the beam concrete the strains are:

$$y := cg - \left(2 + \frac{0.5}{2} + \frac{0.75}{2}\right) = 10.48 \quad in$$

$$\sigma_{beam.reinforcement} := \frac{M_{beam}\cdot 12\cdot y}{I}\cdot\eta = 0.07$$

$$\varepsilon_{beam.reinforcement} := \frac{\sigma_{beam.reinforcement}}{E_{c.beam}}\cdot 1\cdot 10^6 = 19.08 \quad \mu\varepsilon$$

At the level of the C.I.P. topping reinforcement:

$$y := \frac{h_{C.I.P.}}{2} = 10.75 \quad in$$

$$\sigma_{C.I.P..reinforcement} := \frac{M_{beam}\cdot 12\cdot y}{I_{C.I.P.}} = 0.15$$

$$\varepsilon_{C.I.P..reinforcement} := \frac{\sigma_{C.I.P..reinforcement}}{E_{c.C.I.P.}}\cdot 1\cdot 10^6 = 30.35 \quad \mu\varepsilon$$

WELDED CONNECTION SPECIMEN

Assuming the section is fully composite:

Note that for the welded-connection specimen the beam concrete reached 8 ksi, while the C.I.P. topping concrete reached 4 ksi

$f'_{c.beam} := 8$ ksi $\quad E_{c.beam} := 33000\cdot\left(0.15^{1.5}\right)\cdot\sqrt{f'_{c.beam}} = 5422.45$ ksi

$f'_{c.C.I.P.} := 4$ ksi $\quad E_{c.C.I.P.} := 33000\cdot\left(0.15^{1.5}\right)\cdot\sqrt{f'_{c.C.I.P.}} = 3834.25$ ksi

Convert the beam concrete into an equivalent C.I.P. concrete

$$\eta := \frac{E_{c.beam}}{E_{c.C.I.P.}} = 1.41$$

$b_{C.I.P.} := 48$ in $\quad h_{C.I.P.} := 21.5$ in

$b_{beam} := b_{C.I.P.} \cdot \eta = 67.88$ in $\quad h_{beam} := 4$ in

$A_{C.I.P.} := b_{C.I.P.} \cdot h_{C.I.P.} = 1032$ in^2 $\quad I_{C.I.P.} := \frac{b_{C.I.P.} \cdot h_{C.I.P.}^3}{12} = 39753.5$ in^4

$A_{beam} := b_{beam} \cdot h_{beam} = 271.53$ in^2 $\quad I_{beam} := \frac{b_{beam} \cdot h_{beam}^3}{12} = 362.04$ in^4

$$cg := \frac{A_{C.I.P.} \cdot \left(h_{beam} + \frac{h_{C.I.P.}}{2} \right) + A_{beam} \cdot \left(\frac{h_{beam}}{2} \right)}{A_{C.I.P.} + A_{beam}} = 12.09 \text{ in}$$ Above beam soffit

$$I := I_{C.I.P.} + A_{C.I.P.} \cdot \left(h_{beam} + \frac{h_{C.I.P.}}{2} - cg \right)^2 + I_{beam} + A_{beam} \cdot \left(\frac{h_{beam}}{2} - cg \right)^2 = 75061.39 \quad in^4$$

At the level of the reinforcement in the beam concrete the strains are:

$y := cg - \left(2 + \frac{0.5}{2} + \frac{0.75}{2} \right) = 9.47$ in

$\sigma_{beam.reinforcement} := \frac{M_{beam} \cdot 12 \cdot y}{I} \cdot \eta = 0.1$

$\varepsilon_{beam.reinforcement} := \frac{\sigma_{beam.reinforcement}}{E_{c.beam}} \cdot 1 \cdot 10^6 = 17.77$ $\mu\varepsilon$

At the level of the C.I.P. topping reinforcement - assumes fully composite at midspan:

$y := cg - 4 - 1.5 - \frac{0.5}{2} = 6.34$ in

$\sigma_{C.I.P..reinforcement} := \frac{M_{beam} \cdot 12 \cdot y}{I} = 0.05$

$\varepsilon_{C.I.P..reinforcement} := \frac{\sigma_{C.I.P..reinforcement}}{E_{c.C.I.P.}} \cdot 1 \cdot 10^6 = 11.9$ $\mu\varepsilon$